

**Towards an enhanced process  
understanding for a continuous  
pharmaceutical manufacturing process  
of tablets based on twin-screw wet  
granulation**

**Alexander Ryckaert**

Thesis submitted in fulfilment of the requirements for the degree of  
Doctor in Pharmaceutical Sciences – 2021

Promoter: Prof. dr. Thomas De Beer



**Towards an enhanced process  
understanding for a continuous  
pharmaceutical manufacturing process  
of tablets based on twin-screw wet  
granulation**

**Alexander Ryckaert**

Thesis submitted in fulfilment of the requirements for the degree of  
Doctor in Pharmaceutical Sciences – 2021

Promoter: Prof. dr. Thomas De Beer



The author and the promoter give the authorisation to consult and to copy part of this thesis for personal use only. Any other use is limited by the Laws of Copyright, especially concerning the obligation to refer to the source whenever results are cited from this thesis.

Ghent, January 5<sup>th</sup>, 2021

The Promoter

Prof. Dr. Thomas De Beer

The Author

Alexander Ryckaert

Please refer to this work as follows:

Alexander Ryckaert (2021). Towards an enhanced process understanding for a continuous pharmaceutical manufacturing process of tablets based on twin-screw wet granulation, PhD Thesis, Laboratory of Pharmaceutical Process Analytical Technology, Ghent University, Ghent, Belgium.

# Thank you!

Eerst en vooral zou ik graag Prof. Thomas De Beer willen bedanken. Niet enkel om mij de kans te geven om aan het doctoraat te beginnen, maar ook voor de vele interessante en leerrijke vergaderingen, discussies en brainstormsessies. Ik apprecieer het dat ik steeds te pas en te onpas kon passeren om zaken te bespreken of om raad te vragen. Verder waren de werkreizen naar het zonnige Wuppertal steeds zeer aangenaam.

I would also like to thank my promoters from Bayer AG. Thank you Dejan and Adrian for all the support during the last 4 years. Thank you for the corrections of several abstracts and papers. Although our meetings were often very heavy, the discussions were very interesting. I also like the fact that the several work packages allowed me to learn about a lot of different aspects of continuous manufacturing. Further, I also really appreciated that you gave me the trust and freedom to let me investigate topics that were initially not intended to be performed.

I also would like to thank other colleagues of Bayer AG such as Eva for giving their input during the meetings.

Dank u Prof. Chris Vervaet voor de verschillende verbeteringen van mijn papers. Maar ook dat uw deur steeds open stond om de nodige support te geven. Ook bedankt om de nodige figuurlijke schop onder mijn gat te geven indien mijn wanordelijke nonchalance naar boven kwam. Daarin ben ik al wat verbeterd.

Katharine en Ilse, bedankt voor alle administratieve steun. Aangezien dit nog een werkpuntje is van mij, hebben jullie me zeker het werk lichter gemaakt. Tania, bedankt voor al uw hulp bij de experimenten. Jij hebt me voor verschillende studies serieus wat werk bespaard. Christine, jij ook bedankt voor de ondersteuning, alsook de gezellige babbels.

Ook een woord van dank aan het adres van de Vuilen Hoek. Nils, Maxim, Wouter, Pieter-Jan en Jens, bedankt voor de hoogstaande gesprekken tijdens onze dagelijkse lunches in de resto van het UZ. Alsook de gezellige doch interessante intermezzo's tijdens de fruitpauzes.

De gezellige lunches gingen later dan verder met een nieuwe lichte doctoraatstudenten. Shana, Laure, Silke, Michiel, Michael, Gust en Brecht, bedankt voor de dagelijkse strijd tegen voedselverspilling.

Bedankt Laure, Nathan, Silke, Shana en Saar voor de ontspannende teambuilding op Rock Werchter.

Bedankt bureauleden voor de gezellige babbels in voorbije jaren. Bedankt Valérie, Jeroen, Aseel, Silke, Severien en Laure.

Thank you Fanny for the nice collaboration and for sharing knowledge, tips and tricks (..and jokes)!

Ik had ook genoeg om enkele werkgerelateerde reizen te maken. Bij toeval waren dit af en toe ook nog eens mooie bestemmingen. Christoph, Lise, Aseel, Joris, Elien, Valérie, Daan, Maxim bedankt voor de leuke tijd in Granada en Sheffield.

Thomas, Ingmar, Daan, Michiel, Shana en Michael wil ik ook nog bedanken voor de onvergetelijke werkreis naar Florida. Voor alle gezellige avonden die we hadden na de lange dagen op het congres.

Mijn buurman Michael (dezelfde man als in vorige paragraaf), bedankt voor de dagelijkse terraspauzes tijdens de lockdown. Op die manier kon een thuiswerkende mens niet vereenzamen.

Een doctoraat is geen one-man job want het onderzoek wordt beter met hulp van elkaar. Daarom zou ik het bijzonder nog even Daan, Michael, Christoph, Michiel, Maxim, Fanny en Jens willen bedanken voor het teamwork tijdens de verschillende studies in dit doctoraat.

Bedankt aan alle zatte Danny's (Thibault, Rave, Jelle, Arthur, Jolan, Peter-An en Gilles) voor de nodige ontspanning tijdens reizen, de matches van de Buffalo's of op café. Bedankt voor mij te tolereren toen ik op sommige momenten nog meer dan anders derderangs BV's en VTM op de korrel nam. Waarschijnlijk waren dat werkgerelateerde frustraties die er uit moesten.

Bedankt vriendjes van Gand Saint Germain.

En ook Jelle, Capi, Andy, coach en .. van den Excelsior.

Bedankt aan mijn Mama, Papa, Christopher, Julie, Vincent en Marraine. Bedankt aan Patricia, Stefaan, Hans, Mieke, Wout, Lien, Mathias, Lize, Auph lie en Margaux voor jullie steun en interesse. Ik weet dat jullie na al die jaren nog steeds niet weten wat ik eigenlijk doe, maar ik voelde toch jullie steun.

Last but not least zou ik mijn allerliefste Saar willen bedanken. The wife of my life, mon amour pour toujours! Jij stond op de eerste rij om op momenten mijn stress te voelen tijdens dit doctoraat. Bij jou kon ik dan eens goed ventileren. En toch slaagde je er in om mij op die momenten niet alleen te motiveren maar ook te laten relativeren. Bedankt ook voor de oprechte interesse in mijn werk... zelden gezien. Maar ook gewoon bedankt om zo leuk, lief en mooi te zijn!



# Table of contents

<b>List of abbreviations</b>		1
<b>List of symbols</b>		5
<b>Chapter 1</b>	Introduction	9
<b>Chapter 2</b>	Objectives and outlines	27
<b>Chapter 3</b>	Heat transfer evaluation during twin-screw wet granulation in view of detailed process understanding	30
<b>Chapter 4</b>	In-line temperature measurement to improve the understanding of the wetting phase in twin-screw wet granulation and its use in process development	55
<b>Chapter 5</b>	Evaluation of torque as an in-process control for granule size during twin-screw wet granulation	77
<b>Chapter 6</b>	TPLS as predictive platform for twin-screw granulation process and formulation development	107
<b>Chapter 7</b>	The influence of equipment design and process parameters on granule breakage in a semi-continuous fluid bed dryer after continuous twin-screw granulation	157
<b>Chapter 8</b>	Investigating the cell-to-cell variability in a semi-continuous fluid bed dryer	180
<b>Chapter 9</b>	Comparison a Partial Least Squares (PLS) model with a moving F-test to monitor blend uniformity in a tablet press	195
<b>Chapter 10</b>	Broader international context, relevance and future perspectives	223
<b>Chapter 11</b>	Summary and general conclusions	233
<b>Samenvatting</b>		239
<b>Acknowledgement</b>		246
<b>Curriculum vitae</b>		247



# List of abbreviations

100SD	Pearlitol 100SD mannitol
11SD	Subertab 11SD lactose
160C	Pearlitol 160C mannitol
200M	Pharmatose 200M lactose
AoR	Angle of repose
BET	Brunauer–Emmett–Teller
BU	Blend uniformity
C_p	Caffeine powder
C1	ConsiGma™-1 system
C25	ConsiGma™-25 system
CDC	Continuous direct compression
Cel	Celecoxib
CFD	Computational fluid dynamics
CM	Continuous manufacturing
CPP	Critical process parameters
CQA	Critical quality attribute
C-SOPS	Center of Structured Organic Particulate Systems
DC	Direct compression
DEM	Discrete-element method
DoE	Designs of experiments
DVS	Dynamic vapour sorption
E5	Methocel E5 hydroxypropyl methylcellulose
ECCPM	European Consortium for Continuous Pharmaceutical Manufacturing

## ABBREVIATIONS

---

EMA	European Medicine Agency
F	Friction forces
FDA	Food and Drug Administration
GFR	Granule feed rate
GSD	Granule size distribution
HCT	Hydrochlorothiazide
HPMC	Hydroxypropyl methylcellulose
Ibu	Ibuprofen
ICH	International Council for Harmonisation
IPC	In-process control
K30	Kollidon 30 polyvinylpyrrolidone
KEF	Klucel EF hydroxypropyl cellulose
L/D	Length-to-diameter
L/S	Liquid-to-solid
LIW	Loss-in-weight
LFR	Liquid feed rate
LV	Latent variable
M_f	Metformin fine
MLR	Multiple linear regression
M_r	Metformin regular
MCC	Microcrystalline cellulose
MFR	Mass feed rate
MPT_μ	Metoprolol tartrate
MVA	Multivariate data analysis
Nap	Naproxen
NIR	Near Infrared

P <sub>μ</sub>	Paracetamol micronized
PAT	Process analytical technology
PBM	Population balance model
PCA	Principal component analysis
Pgel	Unmodified maize starch
PH101	Avicel PH101 microcrystalline cellulose
PH105	Avicel PH105 microcrystalline cellulose
PH301	Avicel PH301 microcrystalline cellulose
PLS	Partial Least Squares
PVP	Polyvinylpyrrolidone
QBD	Quality by design
R	Matrix including blend ratio's
RCPE	Research Centre Pharmaceutical Engineering
RMSEcv	Root mean square error of cross validation
RSD	Relative standard deviation
RTD	Residence time distribution
Scr	Screw speed
SEM	Scanning electron microscopy
SNV	Standard normal variate
SSA	Specific surface area
ST	Surface tension
T <sub>μ</sub>	Theophylline Micronized
T <sub>A_200</sub>	Theophylline Anh. Powder 200
T <sub>A_200M</sub>	Theophylline Anh. Powder 200M
T80	Tablettose T80 lactose
TPLS	T-shaped Partial Least Squares

## ABBREVIATIONS

---

TSG	Twin-screw wet granulation
VIP	Variable importance for the projection
WBC	Water binding capacity
WoC	Work of compression
X	Matrix including the raw material properties
Y	Matrix including quality attributes
Z	Matrix including process settings

# List of symbols

$\bar{x}_{i,j}$	Average spectral value within a block
$\hat{y}_i$	Concentration of a spectrum that is estimated by cross-validation
$\rho_b$	Bulk density
$\rho_t$	Tapped density
$C_{sens}$	Sensitivity factor
$R_x^2$	Goodness of fit X data
$R_y^2$	Goodness of fit Y data
$S_{API}^2$	API-induced spectral variance
$S_{noise}^2$	Noise-induced spectral variance
$y_i$	Theoretical concentration corresponding to a spectrum
$\Delta E_{granules}$	Increase of thermal energy
$\Delta p$	Pressure across the fluid interface
$\Delta T$	Temperature increase
$\Delta \text{Torque}$	Increase in torque
AE40	Flow energy at 40 mm/s
AR40	Ratio of the flow energy at 40 mm/s and at 0 mm/s
$B_{arb}$	Arbitrary block size
BFE	Basic Flow Energy
CA1	Contact angle was measured after 1 s
CA30	Contact angle was measured after 30 s
CA60	Contact angle was measured after 60 s
CAb1	Hydrophilic contact angle after 1 s

## LIST OF SYMBOLS

---

CAb30	Hydrophilic contact angle after 30 s
CAb60	Hydrophilic contact angle after 60 s
CD	Charge density
Com	Compressibility
$C_{p,g}$	Granules specific heat capacity
$c_p$	Specific heat capacity
d10	10 % cumulative undersize fraction of volumetric particle size distribution
D40	Moisture content in desorption mode at 40 % RH
d50	50% cumulative undersize fraction of volumetric particle size distribution
D60	Moisture content in desorption mode at 60 % RH
D80	Moisture content in desorption mode at 80 % RH
d90	90 % cumulative undersize fraction of volumetric particle size distribution
d99	99 % cumulative undersize fraction of volumetric particle size distribution
DR1	Fraction powder dissolved after 1 min
DR10	Fraction powder dissolved after 10 min
DR20	Fraction powder dissolved after 20 min
DR3	Fraction powder dissolved after 3 min
DR30	Fraction powder dissolved after 30 min
DR5	Fraction powder dissolved after 5 min
DR60	Fraction powder dissolved after 60 min
$E_{granules}$	Energy transferred to the granules
$E_{jacket}$	Energy transferred to the granulator jacket
Elas	Elastic recovery
$E_{motor}$	Energy given by the granulator motor
$E_{motor}$	Mechanical energy given by the motor
$E_{screws}$	Energy used to move the granulator screws



$F_{API}$	Ratio of the total spectral variance and the noise spectral variance
$ffc$	Flow function coefficient
$ffp$	Bulk density-weighted flow
$ffrho$	Consolidated density-weighted flow
FRI	Flow Rate Index
$F_w$	Final weight
H40	Hysteresis values 40 % RH
H60	Hysteresis values 60 % RH
$h_i$	Specific heat of wetting of component i
$H_{wetting}$	Enthalpy of wetting
$l_w$	Initial weight
k	Amount of wavelengths
m	Mass
$m_{wetted,i}$	Wetted mass of component i
n	Block size
$Q^2$	Goodness of prediction
r	Radii of curvature
RH	Relative humidity
S40	Moisture content in sorption mode at 40 % RH
S60	Moisture content in sorption mode at 60 % RH
S80	Moisture content in sorption mode at 80 % RH
$S_{true}$	Maximal solubility
$T_g$	Granule temperature
$T_{p,0}$	Temperature of the dry powder
$V_b$	Bulk volume

## LIST OF SYMBOLS

---

$\text{Vis}$	Dynamic viscosity
$V_t$	Tapped volume
$x_{i,j}$	Spectral value for the $i^{\text{th}}$ block and $j^{\text{th}}$ wavelength
$\epsilon$	Porosity
$\rho_{\text{true}}$	True density
$\sigma$	Surface tension
$\sigma_1$	Major principal stress
$\sigma_c$	Unconfined yield strength
$\tau_c$	Powder cohesivity

# 1 INTRODUCTION

## 1.1 CONVENTIONAL BATCH MANUFACTURING

For decades, the manufacturing of pharmaceutical solid-dosage forms relied on batch-wise processes (1). This conventional manufacturing approach consists of multiple disconnected unit-operations whereby raw materials are processed into an intermediate or a finished product (Figure 1.1 – top). At the start of each unit-operation, the entire batch of materials is brought into the system and, subsequently, the batch is removed once the process is considered as finished. Before the intermediate product is transferred to the next process step, it is stored for off-line quality testing which is time-consuming, destructive and labour-intensive. At the end of the process, the finished pharmaceutical product is another time extensively tested. In case the quality of the intermediate or finished product does not achieve the required demands, the entire batch is discarded (2). An optimal combination of process parameters is typically chosen and kept constant during manufacturing of batch processes. However, changing input material properties, deviating process parameters or varying environmental conditions might disturb the process (3). And, as there is a lag time between the moment of production of the quality testing of the intermediate or finished product, the process is not able to anticipate for these disturbances, bringing the complete batch at risk. Therefore, batch processes are black boxes which are not fully understood, causing a varying product quality (4,5) (Figure 1.1 – bottom).

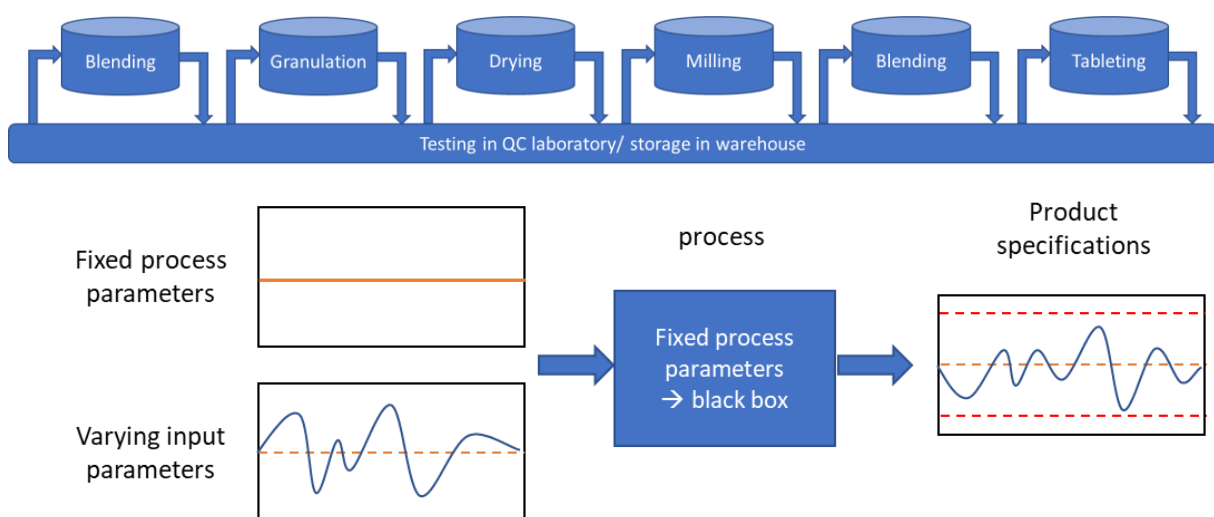


Figure 1.1: Schematic overview of the production of tablets via batch manufacturing (top). Schematic illustration of conventional batch manufacturing leading to a high variability in product quality (bottom).

Although this conventional approach is already used for many years, it may not be sufficient anymore to meet the profit targets (6). Increasing competition of generic products, expiration of blockbuster (i.e., drugs giving a yearly revenue of minimum US \$1 billion (7)) patents, the decrease in the number of new drug molecules, the overall reduction of health care budgets, the increasing socio-economic pressure to limit the drug prices, the economic loss when batches are rejected and the increasing development time and cost to manufacture new drug products has forced to switch to a more efficient and economical manufacturing (6,8–10). Therefore, the switch towards continuous manufacturing has been started almost twenty years ago.

## 1.2 CONTINUOUS MANUFACTURING

The introduction of starting materials, the processing of these materials and the collection of finished drug products occurs simultaneously during continuous manufacturing. In contrast to batch manufacturing, all unit operations are connected to form an integrated manufacturing line, whereby intermediate products are transferred from one unit operation towards another (Figure 1.2 – top). Consequently, the overall processing time is significantly decreased compared to conventional batch manufacturing (4,11).

In 2004, the pharmaceutical industry was encouraged by the US Food and Drug Administration (FDA) to implement the concept of Process Analytical Technology (PAT) (12). This initiative aims at improving the process understanding for obtaining an optimal manufacturing control, which leads to proper quality assurance. This makes the initiative also indispensable in the current switch from traditional batch manufacturing towards continuous manufacturing. By monitoring the process via PAT tools, real-time information of the product quality is provided. In addition, control systems can be used to adjust process parameters to anticipate for perturbations caused by raw or intermediate material variability, environmental conditions or process variability (2). Consequently, a consistent product quality with a lower variability compared to conventional batch manufacturing can be obtained (Figure 1.2 – bottom). This leads to a process for which the quality is built-in into the process, which is in accordance with the Quality by Design (QbD) concept, introduced by the International Council for Harmonisation (ICH) (13).

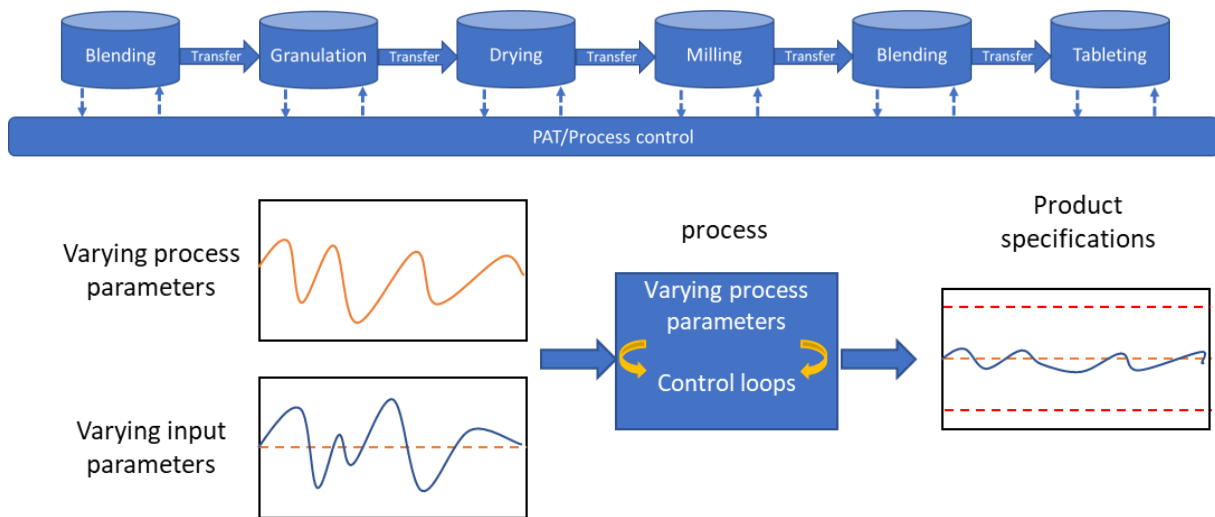


Figure 1.2: Schematic overview of the production of tablets via continuous manufacturing (top). Schematic illustration of continuous manufacturing using PAT and a control strategy to consistently result in the desired product quality (bottom).

Although continuous manufacturing has already successfully been adopted for many years in the food, consumer, automotive and petrochemical industry, the switch in the pharmaceutical industry is rather slow (7). The transition was hindered by the rigid regulatory system by stifling any post-approval changes to drug products. Therefore, innovative manufacturing was challenging for the industry and batch manufacturing was the only acceptable way forward (5). In 2003, the Wall Street Journal even reported that the manufacturing techniques of new drugs was lagging behind the techniques used for the production of potato-chips (14). However, the mindset has changed and regulatory authorities such as European Medicine Agency (EMA) and the Food and Drug Administration (FDA) encourage the switch towards continuous manufacturing as it offers plenty of other advantages besides the aforementioned economic advantages:

- As the production volume does not depend on the dimension of the equipment but rather on the processing time, the same equipment can be used for R&D trials and continuous manufacturing, making continuous manufacturing far more flexible. Hence, the time and the consumption of valuable API is also much reduced during process development, as scale-up studies are not needed. Moreover, continuous manufacturing also allows a faster response to the market in case of drug shortage (for example during a pandemic) (7). And, in addition, the flexibility allows to manufacture

smaller product volumes, making the production of drug products for more rare pathologies less uneconomical (5).

- The quality is monitored and the process is controlled during manufacturing, allowing a real-time release of the finished products. Consequently, a faster release of high-quality end products is possible (15).
- In contrast to batch manufacturing, the process is capable to mitigate raw material and process variability by monitoring and controlling the process. Therefore, there is a smaller chance that the complete batch is at risk. In addition, non-conforming materials can selectively be removed through principles of traceability (7,16). Ultimately, this results in an improved product quality.
- A decreased environmental footprint is obtained because less material is used during process development, only a smaller part of a batch is discarded when productions are out-of-specification and the use of solvents during off-line analyses is reduced (2,17).
- A smaller floor space is required because the integrated line eliminates the need for storage of the intermediate product (4). In addition, a continuous manufacturing process set-up is far more compact compared to batch equipment. The smaller production facilities are ultimately more economical.
- Continuous manufacturing is less labour-intensive because manual interventions such as discharging, transfer or sampling for off-line analysis after each unit operation as for batch operations are not needed (2).
- A shorter processing time (18).

As a consequence, several new drug products are already continuously manufactured. In 2015, the first approved drug product was manufactured by Vertex for the treatment of cystic fibrosis: Orkambi®. The next year, a conversion from batch to continuous manufacturing for Prezista® tablets for the treatment of HIV was approved for Johnson & Johnson. Further, Symdeko® and its European counterpart Symkevi® and Trikafta® are manufactured by Vertex to treat cystic fibrosis, Verzenio® is manufactured by Eli Lilly for the treatment of advanced breast cancers, Daurismo® is manufactured by Pfizer to treat acute myeloid leukemia and Tramacet® is manufactured by Johnson and Johnson to treat pain (2,19).

### 1.3 CONTINUOUS PRODUCTION OF TABLETS

#### 1.3.1 TABLETS

The first existence of a dosage form resembling a tablet was found in the 10<sup>th</sup> century in the Arabic medical literature. At that time, a hammer was applied to compress drug particles between engraved ebony rods (20). Today, tablets are the most popular dosage form among all pharmaceuticals due to the many advantages (20). On the one hand, the accurate dosing, the ease of manufacturing, the long shelf life of tablets, the possibility to produce tablets at high speed, the low costs, the tamper-proofness in comparison to capsules and the ease of transportation makes this dosage form desirable for the pharmaceutical industry. While, on the other hand, the convenience of administration and the possibility to cover any unpleasant taste are very attractive for the patients (20,21).

#### 1.3.2 CONTINUOUS MANUFACTURING TECHNIQUES

Among the different techniques for continuous pharmaceutical manufacturing of solid-dosage forms, direct compression (DC) is the most desirable because it is a simple process which is the most cost-efficient (21–24). This processing route only involves a few intermediate process steps: continuous feeding and blending of the raw materials and tableting of the homogeneous powder blend (18). However, it is estimated that DC is only applicable for 20 % of the Active Pharmaceutical Ingredients (APIs) (21). Unfavourable raw material properties, such as a poor flowability and a poor compactibility due to insufficient binding potential and high electrostatics, can result in an inhomogeneous powder mixture and an inappropriate die filling during tableting. Consequently, this can lead to content uniformity issues and tablet mass variation, respectively (22). This can either occur for high-dose formulations as the API properties become more dominant or for low-dose formulations as it is very challenging to homogeneously disperse the poorly flowing API in the powder bed (22). Therefore, an intermediate granulation step may be required to overcome aforementioned issues (1).

##### 1.3.2.1 GRANULATION

Granulation is a size-enlargement process in which the primary powder particles are made to adhere to form large agglomerates called granules. In contrast to other pharmaceutical unit-operations such as extrusion and pelletization, the primary powder particles can still be



distinguished in the formed granules. Granulation is beneficial as it improves the drug-uniformity in the product, reduces segregation, increases the material density and reduces the formation of dust (25,26). Continuous dry, melt and wet granulation can be distinguished as granulation techniques.

### 1.3.2.2 DRY GRANULATION

Dry granulation makes use of roller compaction. In this process, ribbon-shaped compacts are formed by compacting the powder mixture between two counter-rotating rolls, as illustrated in Figure 1.3. Subsequently, these ribbons are milled to obtain granules suited for tableting. As this manufacturing technique does not involve the use of a liquid, it is attractive to granulate moisture and heat sensitive APIs. However, roller compaction is only suited for a powder mixture with excellent compactibility properties, as a loss in compactibility of the materials may occur after roller compaction, resulting in tablets with an inferior tablet hardness (1,7,27,28).

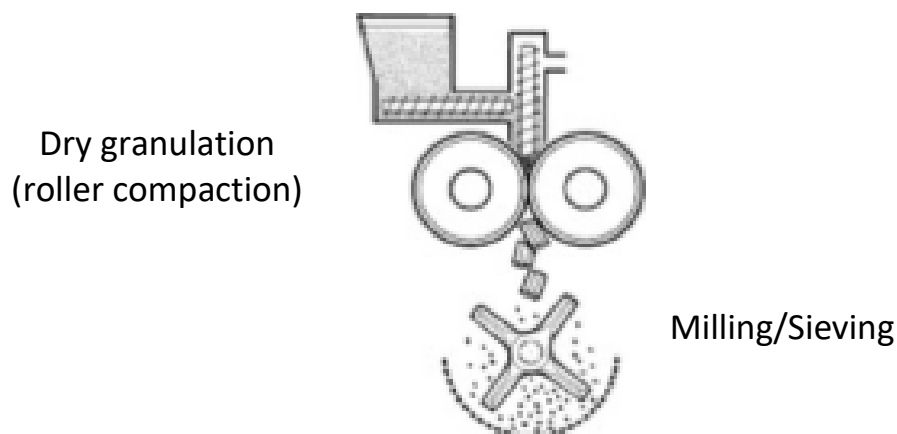


Figure 1.3: Schematic illustration of roller compaction (29).

### 1.3.2.3 MELT GRANULATION

Another alternative technique for moisture and heat sensitive APIs is melt granulation. Especially, for formulations consisting of poorly compactible powders (30). In this process, a molten binder enables the granulation process. Since no liquids are used, the process time and energy requirements are significantly reduced compared to wet granulation. In addition, melt granulation is also beneficial for the manufacturing of high-dose formulations with up to 90 % of API (31).

### 1.3.2.4 WET GRANULATION

Wet granulation implies the use of a wetting agent, such as water, to aid in the formation of granules instead of a compaction force like in dry granulation or a molten binder in melt granulation processes (26). Wet granulation consists of three mechanism that occur simultaneously and/or consecutively: (i) wetting and nucleation of the formulation ingredients, (ii) granule consolidation and coalescence (i.e., growth) and (iii) granule attrition and breakage (32). An overview of the different processes is shown in Figure 1.4.

Wetting is the primary stage of the wet granulation process where the first contact between the powder and the liquid occurs. It is a critical step to allow granule growth and consolidation, but also to ensure API distribution over the different granule size fractions (33). Wetting of primary particles gives rise to large, porous agglomerates called nuclei in a process named nucleation. Subsequently, shear stress is provided to the wetted powder. Therefore, nuclei can collide and form bigger agglomerates in a process called coalescence. In addition, the mechanical energy is also able to consolidate the nuclei, whereby the size and porosity decreases. This allows to squeeze out the entrapped air and liquid solvent towards the particle surface. On the one hand, ungranulated powder can stick to the wet granules in a process called layering. And, on the other hand, wet granules can further collide and form bigger granules. Both processes result in granule growth. Shear stress is also responsible for breakage of granules into smaller fragments or attrition of the granule edges. The extent in breakage and attrition depends on the initial granule properties such as granule strength (32,34). During the granulation process a portion of the solid material will dissolve into the wetting agent, these liquid bridges are transformed into stronger solid bridges once the liquid is evaporated and the dissolved particles are recrystallised (25).

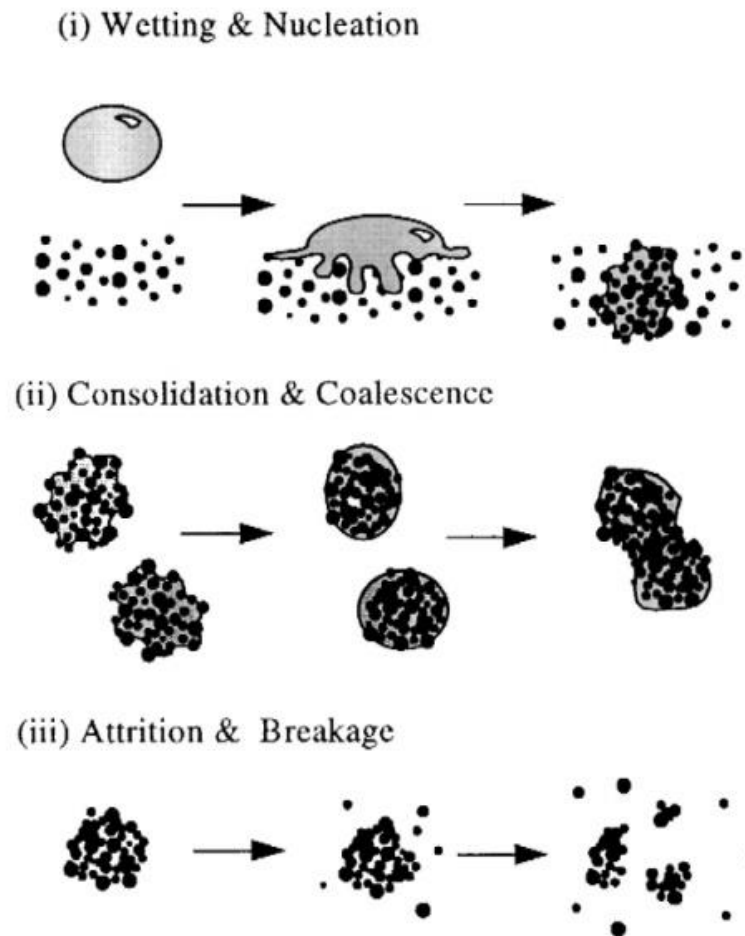


Figure 1.4: Schematic representation of the different steps involved in wet granulation (32).

Continuous wet granulation is preferred for the processing of low and high-dose formulations having a poor flow and poor compressibility (23). High-shear, low-shear (fluidized bed) and twin-screw wet granulation (TSG) can be differentiated among the different continuous wet granulations techniques (7). In this dissertation, there will be focussed on twin-screw wet granulation.

TSG is an inherent continuous granulation technique. During a TSG process, a powder mixture is fed by the feeder into the granulation module (Figure 1.5). The granulation module consists of a jacketed (to control the temperature) granulator barrel with co-rotating screws. The powder is transported by conveying elements towards the outlet. Before the powder reaches the outlet, granulation liquid is added in a section called the wetting zone. Subsequently, shear stress is provided to the wetted powder mass in several kneading zones with the formation of granules (35). The granule formation occurs spatially along the length of the granulation barrel

and the aforementioned key granulation mechanisms occur simultaneously and the different locations. Therefore, the material residence time is only limited to 4 – 20 seconds (36). The granule quality (e.g., size, strength, density, porosity,...) depends on the applied process parameters, such as screw speed, mass-feed-rate and the amount of liquid which was used. The latter is typically noted as the liquid-to-solid ratio (L/S ratio) (35).

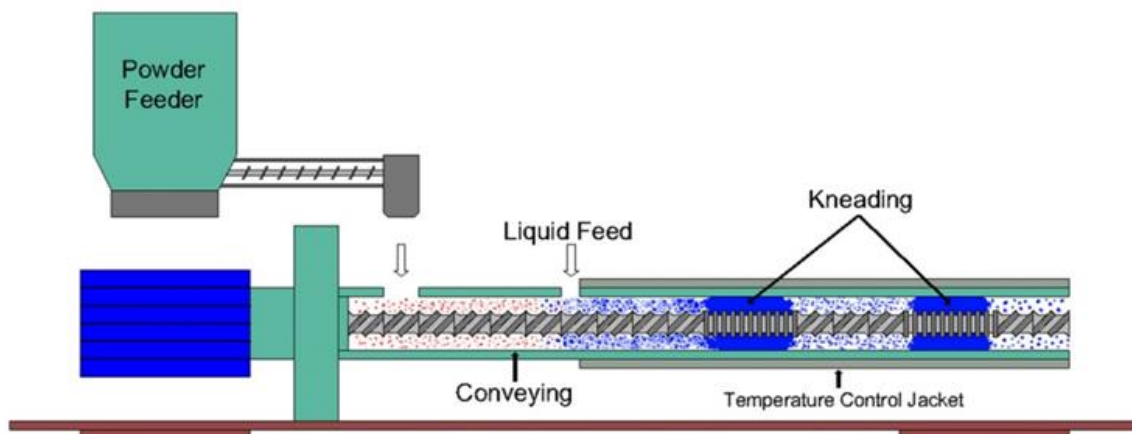


Figure 1.5: Schematic illustration of twin-screw wet granulator (35)

### 1.3.3 CONSIGMA™ CONTINUOUS MANUFACTURING LINE

The ConsiGma™-25 continuous manufacturing line commercialized by GEA Pharma systems was one of the first fully integrated from powder-to-tablet line based on twin-screw wet granulation (Figure 1.6). The different process units are discussed below:



Figure 1.6: ConsiGma™-25 continuous tableting line with (A) several loss-in-weight feeders, (B) a continuous powder blender, (C) a loss-in-weight feeder to dose the powder mixture, (D) a twin-screw wet granulation unit, (E) the six-segmented fluid bed dryer, (F) the granule conditioning unit with integrated mill, (G) loss-in-weight feeders and a blender to mix the external phase with the milled granules and (H) a Modul™P tablet press (Courtesy of GEA Pharma Systems).

**Loss-in-weight (LIW) feeders** (Figure 1.6 - A) consist of a load-cell (i.e., weighing platform), a hopper to store the powder, a feeding device to dispense the powder and a control system (37). The main goal of the LIW feeders is to achieve an accurate constant powder flow rate of the raw materials to attain a steady-state operation of the continuous line. Therefore, the difference in weight of the load cell over a time increment is measured to determine the actual feed rate (7,37). Subsequently, the control system compares the actual feed rate to the feed rate setpoint and the screw speed of the feeding device is adjusted to minimize their difference. Variations in feed rate due to the variation in powder bed density as the powder level in the hopper decreases, are therefore mitigated (37). **Continuous powder blenders** (Figure 1.6 - B) serve to make an homogeneous mixture of the different powders that are provided by the LIW feeders (7). In the **twin-screw wet granulation module** (Figure 1.6 - D), the granules are formed as discussed in section 1.3.2.4. These granules are thereafter transferred to the fluid bed dryer. The **six-segmented fluid bed dryer** (Figure 1.6 - E) cells are sequentially filled and discharged to ensure a continuous flow of granules through the line. As each cell contains a batch of granules, the drying system runs semi-continuously. Via a dry

transfer line, the dried granules are pneumatically transferred to the **conditioning unit** (Figure 1.6 - F). At this location, a co-mill is integrated to reduce the granules to the desired particle size. Thereafter, the milled granules are transferred to a continuous **blender** (Figure 1.6 - G) and mixed with an external phase (e.g., lubricant, disintegrant). The final blend is compressed to tablets in the **rotary tablet press** (Figure 1.6 - H): Modul™ P. First the final blend is stored and fed via a hopper which is located on top of the feed frame. Then the final blend flows into the feed frame, which consists of two chambers. The first chamber (i.e., the filling chamber) uses the rotating paddle to feed the powder into the empty dies, while the second chamber (i.e., dosing chamber) uses its paddle wheel to recover the powder which was left on the turret table after dosing. The filled dies and punches of this tablet press follow the rotation of a turret. After passing the filling station, the dies and punches sequentially pass the pre-compression roller to remove the interparticle air, the main-compression roller to form a solid compact and the ejection station to remove the tablet from the tablet press (Figure 1.7).

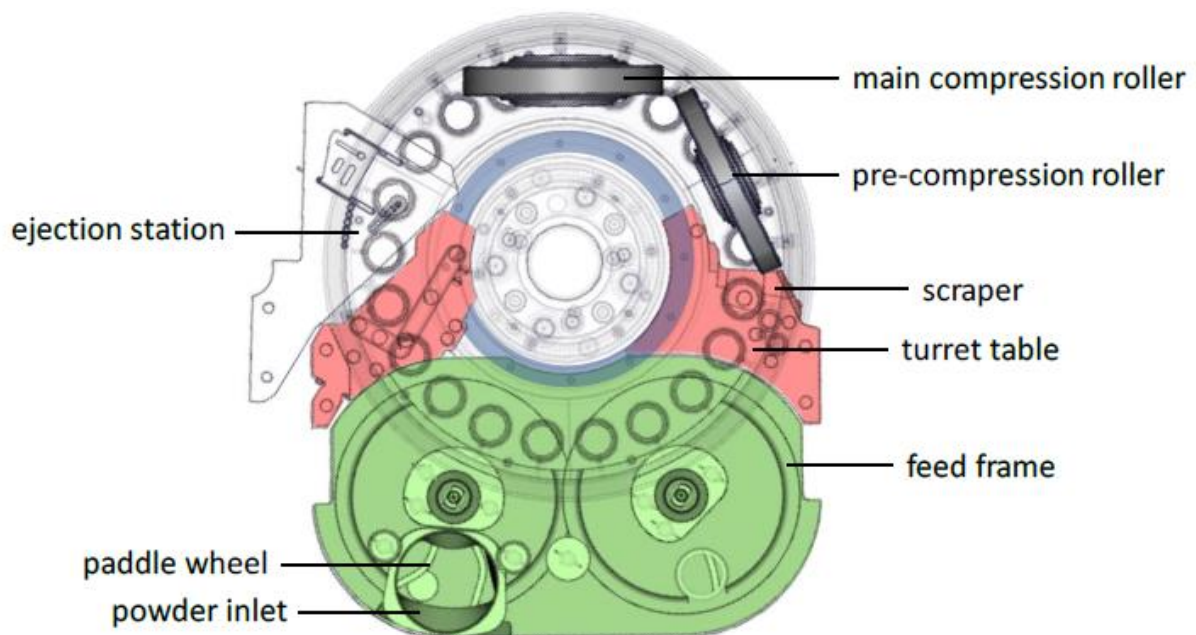


Figure 1.7: Illustration of the top-view of the turret table (Courtesy of GEA Process).

## 1.4 MULTIVARIATE DATA ANALYSIS

Multivariate data analysis (MVA) is needed when univariate data analysis is not sufficient. Univariate data analysis is applied when only one variable is measured and one variable is

predicted. A common example of univariate data analysis is the prediction of the concentration via UV-absorbance derived from Beer's law. Another example would be the prediction of the concentration by a single wavelength via Near Infrared (NIR) spectroscopy. However, different absorbers are present in a powder mixture, causing an overlap of the peaks in a spectrum (39). Therefore, it is usually not possible to predict the concentration by measuring the absorbance at a single wavelength. Hence, MVA is indispensable.

Generally, MVA facilitates the analysis of datasets consisting of multiple variables in order to understand their relationships. During pharmaceutical manufacturing, datasets can consist of multiple process and product variables or spectral information that is collected during production. Depending on the dataset and the purpose of the investigation, a different multivariate data analysis method might be required to reveal the information contained in the data. Three multivariate data analysis methods are discussed in more detail as these methods are used in this dissertation: Principal component analysis (PCA), Partial Least Squares (PLS) and T-shaped Partial Least Squares (TPLS).

#### 1.4.1.1 PRINCIPAL COMPONENT ANALYSIS

PCA is an exploratory data analysis method that tries to reveal hidden patterns in a dataset (40,41). Matrix  $X$  ( $N \times K$ ) in Equation 1.1 represents a dataset consisting of  $N$  observations with  $K$  variables. An univariate visualisation of the relationship between all the variables would require a minimum of  $\frac{K(K-1)}{2}$  plots. PCA tries to capture the variability in the multi-dimensional space by projecting it onto a lower number of variables, being a linear combination of the original variables, defined as the principal components.

$$X = \begin{bmatrix} x_{1,1} & \cdots & x_{1,K} \\ \vdots & \ddots & \vdots \\ x_{N,1} & \cdots & x_{N,K} \end{bmatrix} \quad [1.1]$$

#### 1.4.1.2 PARTIAL LEAST SQUARES

PLS, also known as projection to latent structures, is a regression analysis method (40). PLS is a technique that is applied to find relationships between two blocks of data, a dataset of regressors  $X$  and a set of response variables  $Y$ . In addition, it can also be used to predict a

response from a dataset. Similar to PCA, the multidimensional space is reduced by latent variables (similar to principal components) that attempt to explain the largest amount of variance in block X with the variance in block Y. It is often applied in spectroscopy, but it can also be used to correlate the behaviour of a pharmaceutical powder in a pharmaceutical application. For example, linking the feeding behaviour of a certain powder with its raw material properties.

1.4.1.3 T-SHAPED PARTIAL LEAST SQUARE

A major drawback of PLS is that it only investigates the correlation of one block of data with their corresponding responses. However, pharmaceutical powders are not only processed individually but typically a powder mixture is processed. In addition, process parameters can also be varied during processing of a powder mixture. Therefore, TPLS can be used to find relationships between the raw material properties (X), the proportions in which these raw materials are combined (R), process parameters that were applied during processing of the powder mixture (Z) and the corresponding results (Y). An overview of the four matrices that are related is shown in Figure 1.8.

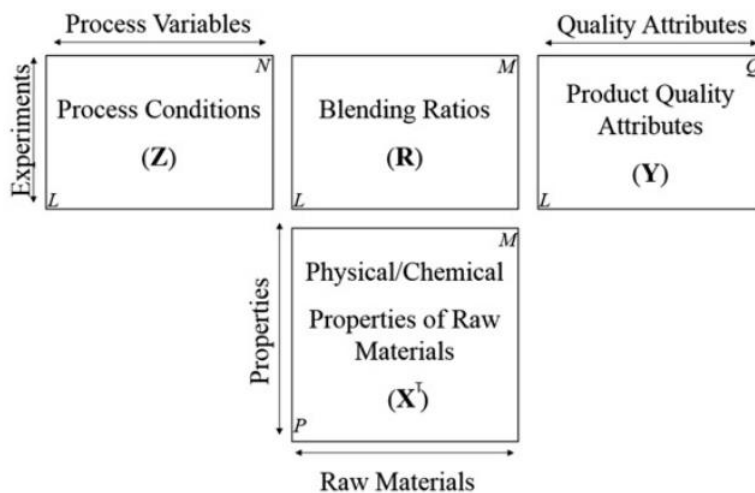


Figure 1.8: Schematic overview of the TPLS model consisting of 4 matrices to describe process conditions, raw material properties, ratios of usage and quality information (42).



## 1.5 REFERENCES

1. Vervaet C, Remon JP. Continuous granulation in the pharmaceutical industry. *Chem Eng Sci.* 2005;60(14):3949–57.
2. Vanhoorne V, Vervaet C. Recent progress in continuous manufacturing of oral solid dosage forms. *Int J Pharm [Internet].* 2020;579(December 2019):119194. Available from: <https://doi.org/10.1016/j.ijpharm.2020.119194>
3. Nicolai N, De Leersnyder F, Copot D, Stock M, Ionescu CM, Gernaey K V., et al. Liquid-to-solid ratio control as an advanced process control solution for continuous twin-screw wet granulation. *AIChE J.* 2018;64(7):2500–14.
4. Lee SL, O'Connor TF, Yang X, Cruz CN, Chatterjee S, Madurawe RD, et al. Modernizing Pharmaceutical Manufacturing: from Batch to Continuous Production. *J Pharm Innov.* 2015;10(3):191–9.
5. Plumb K. Continuous Processing in the Pharmaceutical Industry: Changing the Mind Set. *Chem Eng Res Des [Internet].* 2005 Jun 1 [cited 2018 May 6];83(6):730–8. Available from: <https://www.sciencedirect.com/science/article/pii/S0263876205727556>
6. Aksu B, De Beer T, Folestad S, Ketolainen J, Lindén H, Lopes JA, et al. Strategic funding priorities in the pharmaceutical sciences allied to Quality by Design (QbD) and Process Analytical Technology (PAT). *Eur J Pharm Sci [Internet].* 2012;47(2):402–5. Available from: <http://dx.doi.org/10.1016/j.ejps.2012.06.009>
7. Ierapetritou M, Muzzio F, Reklaitis G. Perspectives on the Continuous Manufacturing of Powder-Based Pharmaceutical Processes. *AIChE J.* 2016;62(6):1846–62.
8. Laske S, Paudel A, Scheibelhofer O, Sacher S, Hoermann T, Khinast J, et al. A Review of PAT Strategies in Secondary Solid Oral Dosage Manufacturing of Small Molecules. *J Pharm Sci.* 2017;106(3):667–712.
9. Ess SM, Schneeweiss S, Szucs TD. European Healthcare Policies for Controlling Drug Expenditure. *Pharmacoeconomics [Internet].* 2003;21(2):89–103. Available from: <https://doi.org/10.2165/00019053-200321020-00002>
10. Rios M. Continuous Processing - Finally. *Pharm Technol.* 2007;31:51–3.
11. Schaber SD, Gerogiorgis DI, Ramachandran R, Evans JMB, Barton PI, Trout BL. Economic analysis of integrated continuous and batch pharmaceutical manufacturing: A case study. *Ind Eng Chem Res.* 2011;50(17):10083–92.
12. FDA. Guidance for Industry PAT: A Framework for Innovative Pharmaceutical Development, Manufacturing, and Quality Assurance. *FDA Off Doc.* 2004;(September):16.
13. ICH. Pharmaceutical Development Q8. *ICH Harmon Tripart Guidel.* 2009;8(August):1–28.

14. Abboud L, Hensley S. Factory Shift: New Prescription For Drug Makers: Update the Plants; After Years of Neglect, Industry Focuses on Manufacturing; FDA Acts as a Catalyst; The Three-Story Blender. *The Wall Street Journal*. 2003 Sep 3;A.1.
15. Fonteyne M, Vercruyssen J, De Leersnyder F, Van Snick B, Vervaet C, Remon JP, et al. Process Analytical Technology for continuous manufacturing of solid-dosage forms. *TrAC - Trends Anal Chem* [Internet]. 2015;67:159–66. Available from: <http://dx.doi.org/10.1016/j.trac.2015.01.011>
16. Allison G, Cain YT, Cooney C, Garcia T, Bizjak TG, Holte O, et al. Regulatory and quality considerations for continuous manufacturing May 20-21, 2014 continuous manufacturing symposium. *J Pharm Sci* [Internet]. 2015;104(3):803–12. Available from: <http://dx.doi.org/10.1002/jps.24324>
17. De Soete W, Dewulf J, Cappuyns P, Van Der Vorst G, Heirman B, Aelterman W, et al. Exergetic sustainability assessment of batch versus continuous wet granulation based pharmaceutical tablet manufacturing: A cohesive analysis at three different levels. Vol. 15, *Green Chemistry*. 2013. p. 3039–48.
18. Byrn S, Futran M, Thomas H, Jayjock E, Maron N, Meyer RF, et al. Achieving Continuous Manufacturing for Final Dosage Formation: Challenges and How to Meet Them. May 20-21, 2014 Continuous Symposium. *J Pharm Sci* [Internet]. 2015;104(3):792–802. Available from: <http://dx.doi.org/10.1002/jps.24247>
19. Badman C, Cooney CL, Florence A, Konstantinov K, Krumme M, Mascia S, et al. Why We Need Continuous Pharmaceutical Manufacturing and How to Make It Happen. *J Pharm Sci* [Internet]. 2019;108(11):3521–3. Available from: <https://doi.org/10.1016/j.xphs.2019.07.016>
20. Armstrong N. *Encyclopedia of Pharmaceutical Technology: Tablet Testing*. In: Swarbrick J, editor. *Encycl Pharm Technol*. Pinehurst, North Carolina, USA; 2007. p. 3653–63.
21. Gohel MC, Jogani PD. A review of co-processed directly compressible excipients. *J Pharm Pharm Sci*. 2005;8(1):76–93.
22. Van Snick B, Holman J, Vanhoorne V, Kumar A, De Beer T, Remon JP, et al. Development of a continuous direct compression platform for low-dose drug products. *Int J Pharm* [Internet]. 2017;529(1–2):329–46. Available from: <http://dx.doi.org/10.1016/j.ijpharm.2017.07.003>
23. Leane M, Pitt K, Reynolds G, Anwar J, Charlton S, Crean A, et al. A proposal for a drug product Manufacturing Classification System (MCS) for oral solid dosage forms. Vol. 20, *Pharmaceutical Development and Technology*. 2015. p. 12–21.
24. Augsburger LL, Hoag SW. *Pharmaceutical Dosage Forms - Tablets*. Third Edit. Press C, editor. Boca Raton, Florida, USA; 2016. 1552 p.
25. Parikh D. *Handbook of Pharmaceutical Granulation Technology*. 3rd Editio. Press C, editor. Boca Raton, Florida, USA; 2016. 676 p.

26. Aulton M, Taylor K. Powders, granules and granulation. In: Livingstone C, editor. *Aulton's Pharmaceutics - The Design and Manufacture of Medicines*. 4th; 2013. p. 466–86.
27. Herting MG, Kleinebudde P. Studies on the reduction of tensile strength of tablets after roll compaction/dry granulation. *Eur J Pharm Biopharm*. 2008;70(1):372–9.
28. Kleinebudde P. Roll compaction/dry granulation: Pharmaceutical applications. *Eur J Pharm Biopharm*. 2004;58(2):317–26.
29. Hsu SH, Reklaitis G V., Venkatasubramanian V. Modeling and control of roller compaction for pharmaceutical manufacturing. Part I: Process dynamics and control framework. *J Pharm Innov*. 2010;5(1–2):14–23.
30. Psimadas D, Georgoulas P, Valotassiou V, Loudos G. Molecular Nanomedicine Towards Cancer : *J Pharm Sci*. 2012;101(7):2271–80.
31. Monteyne T, Adriaensens P, Brouckaert D, Remon JP, Vervaet C, De Beer T. Stearic acid and high molecular weight PEO as matrix for the highly water soluble metoprolol tartrate in continuous twin-screw melt granulation. *Int J Pharm*. 2016;512(1):158–67.
32. Iveson SM, Litster JD, Hapgood K, Ennis BJ. Nucleation, growth and breakage phenomena in agitated wet granulation processes: a review. *Powder Technol*. 2001;117(1):3–39.
33. Hapgood KP, Litster JD, Smith R. Nucleation regime map for liquid bound granules. *AIChE J*. 2003;49(2):350–61.
34. Burggraeve A, Monteyne T, Vervaet C, Remon JP, Beer T De. Process analytical tools for monitoring, understanding, and control of pharmaceutical fluidized bed granulation: A review. *Eur J Pharm Biopharm* [Internet]. 2013;83(1):2–15. Available from: <http://dx.doi.org/10.1016/j.ejpb.2012.09.008>
35. Seem TC, Rowson NA, Ingram A, Huang Z, Yu S, de Matas M, et al. Twin screw granulation - A literature review. *Powder Technol* [Internet]. 2015;276:89–102. Available from: <http://dx.doi.org/10.1016/j.powtec.2015.01.075>
36. Dhenge RM, Cartwright JJ, Hounslow MJ, Salman AD. Twin screw granulation: Steps in granule growth. *Int J Pharm*. 2012 Nov;438(1–2):20–32.
37. Bostijn N, Dhondt J, Ryckaert A, Szabó E, Dhondt W, Van Snick B, et al. A multivariate approach to predict the volumetric and gravimetric feeding behavior of a low feed rate feeder based on raw material properties. *Int J Pharm* [Internet]. 2019;557(December 2018):342–53. Available from: <https://doi.org/10.1016/j.ijpharm.2018.12.066>
38. Markl D, Warman M, Dumarey M, Bergman EL, Folestad S, Shi Z, et al. Review of real-time release testing of pharmaceutical tablets: State-of-the art, challenges and future perspective. *Int J Pharm* [Internet]. 2020;582(April):119353. Available from: <https://doi.org/10.1016/j.ijpharm.2020.119353>
39. Naes T, Isaksson T, Fear T, Davies T. *A user-friendly guide to multivariate Calibration and Classification*. First. Chichester, UK: NIR Publications; 1999. 345 p.

40. Swarbrick B. *Multivariate Data Analysis For Dummies®*, CAMO Software Special Edition [Internet]. Chichester, West Sussex: Wiley, John Wiley & Sons; 2012. 43 p. Available from: <https://downloads.deusm.com/pharmaevolution/CAMO-Multivariate-Data-Analysis.pdf>

41. Ferreira AP, Tobyn M. Multivariate analysis in the pharmaceutical industry : enabling process understanding and improvement in the PAT and QbD era. 2015;7450(5):513–27.

42. Garcia-Munoz S. Two novel methods to analyze the combined effect of multiple raw-materials and processing conditions on the product's final attributes: JRPLS and TPLS. *Chemom Intell Lab Syst.* 2014;133:49–62.

## **2 OBJECTIVES AND OUTLINE**

Continuous manufacturing (CM) offers many benefits compared to batch manufacturing such as a shorter time to market, less product variability, a decreased environmental footprint, a more flexible process and lower production costs. However, a comprehensive process understanding is needed to fully benefit from these advantages. In this dissertation, several unit-operations of a continuous pharmaceutical manufacturing process of tablets based on twin-screw wet (TSG) granulation are evaluated to acquire an enhanced process understanding.

In **chapter 3**, granule quality attributes along the length of the TSG barrel are evaluated together with heat transfers in order to achieve a more fundamental understanding of the granulation process. An experimental set-up is used allowing the collection of granules at the different TSG compartments (i.e., wetting, conveying and kneading compartments). In addition to the determination of typical granule attributes, mechanical energy, barrel and granule temperature (measured using an in-line implemented infra-red camera) are measured to evaluate heat transfer occurring at the different compartments and to relate them to granulation mechanisms.

The objective of **chapter 4** is to obtain a better physical understanding of the wetting stage in the TSG process. A modified granulator barrel is used allowing the collection of granules immediately after the wetting. The goal is to link wetting efficiency (i.e., fraction of powder being nucleated during the wetting stage) with in-line measurements of the granule temperature. Next, wetting efficiency is evaluated to be linked to final granule quality attributes (i.e., granule size distribution) at the outlet of the granulator.

**Chapter 5** aims to investigate the potential of torque as an in-process control to monitor the granule size in TSG. The experimental set-up of chapter 3 is used, allowing the collection of granules at four different locations (i.e., in the wetting zone, after the first and second kneading zone and at the end of the granulation barrel) of the granulator screws to determine the change in granule size along the length of the barrel and the contribution of each compartment to the overall torque.

In **chapter 6**, a TPLS model is developed to link raw material properties, the ratios in which these raw materials are combined and the applied process parameters for the TSG process with the granule quality attributes (size, friability and angle of repose). Next, the predictive

ability of the TPLS model is used to find a suitable combination of formulation composition and TSG process settings for a new API leading to desired granule quality attributes.

The goal of **chapter 7** is to investigate the breakage and attrition phenomena during transport of wet and dry granules, during filling of a drying cell and during fluid bed drying on the semi-continuous six-segmented fluid bed dryer of the ConsiGma™-25 system. Additionally, the influence of drying air temperature and drying time is assessed on granule quality attributes (i.e., granule size and residual moisture content per size fraction) for both the commercial-scale ConsiGma™-25 system and R&D-scale ConsiGma™-1 system.

**Chapter 8** evaluates the cell-to-cell variability in the six-segmented fluid bed dryer of the ConsiGma™-25 system. In this study, six different experiments (varying drying temperature and drying time) are performed to evaluate the granule quality (moisture content per sieve fraction, overall moisture content and granule size) obtained from the six different cells.

In **chapter 9**, in-line Near Infrared (NIR) measurements are obtained from a NIR spectrometer mounted in the filling chamber of the feed frame, in close proximity to the die filling station. The blend homogeneity was evaluated by a quantitative Partial Least Squares (PLS) regression model and a qualitative moving F-test. Three different case studies are performed to evaluate both techniques.

The broader international context, relevance of this research and the future perspectives are discussed in **chapter 10**. A final summary and the general conclusions are provided in **chapter 11**.

# 3 HEAT TRANSFER EVALUATION DURING TWIN- SCREW WET GRANULATION IN VIEW OF DETAILED PROCESS UNDERSTANDING

This chapter is published as:

Stauffer F.\*, Ryckaert A.\*, Van Hauwermeiren D., Funke A., Djuric D., Nopens .I, De Beer T., Heat Transfer Evaluation During Twin-Screw Wet Granulation in View of Detailed Process Understanding, AAPS PharmSciTech, 2019;20(7):1–13.

Shared first authorship



**ABSTRACT**

During the last decade, the pharmaceutical industry has shown a growing interest in continuous twin-screw granulation (TSG). Despite flourishing literature on TSG, limited studies focused on fundamental process understanding on its mechanisms. In current study, granule quality attributes along the length of the TSG barrel were evaluated together with heat transfer in order to achieve a more fundamental understanding of the granulation process. An experimental set-up was developed allowing the collection of granules at the different TSG compartments. In addition to the determination of typical granule attributes, mechanical energy, barrel and granule temperature (measured using an in-line implemented infra-red camera) were measured to evaluate heat transfer occurring at the different compartments and to relate them to granulation mechanisms. Collected data identified wetting enthalpy and friction forces as the main sources of heat along the granulator length. Wetting occurred in the wetting zone and generated temperature increase depending on liquid-to-solid ratio and powder wettability. In the kneading zones, granule temperature increase was proportional to mechanical energy. While it is usually admitted that granule consolidation and reshaping are the consequence of the high shear experienced by the granules, it was highlighted that most of the mechanical energy is converted into thermal energy with no correlation between mechanical energy and granule size distribution. Combined mass and energy balance of the granulation process are therefore necessary to capture the interaction between granule properties and physico-chemical and mechanical phenomena occurring in each compartment.

### 3.1 INTRODUCTION

The interest of the pharmaceutical industry for continuous manufacturing in general and for twin-screw granulation (TSG) in particular has grown constantly during the last decade. This growing interest in continuous manufacturing is driven by the cost reduction and flexibility opportunities (1–4). An additional advantage is the inherently amenable to quality by design characteristic of the technology, leading to improved process understanding obtained through science and risk-based approaches during development (5,6). Nevertheless, fundamental physical understanding of TSG is still limited. Most studies on TSG indeed investigated the influence of process (7,8) and formulation parameters (9,10) on the granule quality attributes at the end of the granulator barrel. While such models are useful from a process development point of view, they do not provide fundamental understanding of granulation mechanisms occurring during the granulation.

In recent years, population balance models (PBMs) have been developed describing TSG processes in a mechanistic way (11–13). Appropriate data collection is essential to be able to develop and validate proper PBMs. Since granulation occurs spatially along the length of the twin-screw granulator barrel, data collection of granules along the length of the barrel is needed (14). However, for TSG PBM calibration and validation, data is typically only collected at the granulator inlet and outlet (11,12). A few studies investigated the granule properties' evolution along the barrel length (15–17). The methodology described in these studies allows the collection of granules from the different screw compartments. Thanks to an extended granule analysis, a detailed understanding of the granulation mechanisms occurring in the different compartments could be achieved. As demonstrated by Van Hauwermeiren et al., improved understanding achieved by such data collection results in more reliable models based on more fundamental understanding (13).

Energetic aspects of the granulation process have nonetheless to date not been considered to assist in building such models. Kernel selection and description are based on hypotheses derived from experimental data. A combined mass and energy balance model would therefore allow quantifying more accurately physico-chemical and mechanical phenomena occurring along the length of the granulator barrel such as powder wetting or granule formation, breakage and densification. The only energetic term in process modelling attempts described

so far is the granulator torque (or specific mechanical energy derived from the torque) (18,19). TSG being a high-shear process, the granulator torque is often referred as an indicator of the shear experienced by the granules during the process (15,20). A formal demonstration of the link between granulation mechanisms and granulator mechanical energy is however still missing. Moreover, physico-chemical and mechanical phenomena occurring during the granulation and leading to the final granule quality attributes are expected to lead to heat exchanges which could be measured. Wetting is for instance an exothermic process which could be quantified by measuring granule temperature. As for the evaluation of granule quality attributes along the length of the granulator barrel, the main challenge in developing an energy balance model for TSG processes is the difficulty collecting local data at the intermediate compartments of the TSG barrel.

The purpose of this study was to analyse the TSG process, manufactured under different process settings such as liquid-to-solid (L/S) ratio, mass feed rate (MFR) and screw speed, in such way that the impact of the individual granulator barrel compartments (i.e. wetting, conveying and kneading compartments) upon granule formation and heat transfers can be linked and understood. The twin-screw granulator with extra liquid addition ports in the middle of the barrel as described by Verstraeten et al. (17) was used to collect granules representative for the different compartments of the granulator (i.e., wetting zone, kneading zones, end of the granulator screws). In addition to traditional off-line granule analysis (e.g., granule size distribution), an in-line thermo-camera was interfaced to the granulator to measure granule temperature at each compartment: information which is needed to develop corresponding energy balances. This methodology of data collection was performed to be able to link changes in granulation mechanisms (e.g., nucleation, consolidation, breakage) to physical phenomena occurring along the length of the granulator barrel (e.g., wetting, friction). Such results could ultimately be used to develop combined mass and energy balance models describing the physico-chemical and mechanical phenomena occurring during the granulation.

## 3.2 MATERIALS AND METHODS

### 3.2.1 MATERIALS

In current study, a low drug-load formulation was studied, the properties of the APIs are listed in Table 3.1. The formulation consisted of a poorly soluble API,  $\alpha$ -lactose (Pharmatose 200, DFE Pharma, Goch, Germany), microcrystalline cellulose (MCC, Avicel PH101, FMC biopolymer, Philadelphia, USA), hydroxypropyl methylcellulose (HPMC, Methocel E5, Dow, Midland, USA), croscarmellose sodium (Ac-Di-Sol, FMC, Philadelphia, USA) and sodium dodecyl sulfate (Kolliphor SLS, BASF, Ludwigshafen, Germany). Its granulation was performed with demineralized water. Formulation blends were prepared using a 20-L Inversina tumbling mixer blender (Bioengineering AG, Wald, Switzerland).

*Table 3.1: API properties*

API properties	
BCS class	Class II
Mean particle size	10 $\mu\text{m}$
Shape	Spherical
Contact angle in water	66°

### 3.2.2 METHODS

#### 3.2.2.1 EXPERIMENTAL SET-UP

Granules were produced using the twin-screw wet granulation unit of a ConsiGma™-25 system (GEA Pharma systems, Collette, Wommelgem, Belgium). Fonteyne et al. fully described the applied equipment in a previous study (21). The granulator consists of two 25-mm diameter co-rotating screws with a length-to-diameter (L/D) ratio of 20:1. The powder premix enters the granulator barrel using a gravimetric twin-screw loss-in-weight feeder (KT20, Coperion K-Tron, Niederlenz, Switzerland). Granulation liquid is gravimetrically dosed into the screw chamber using two peristaltic pumps (Watson Marlow, Cornwall, UK) out of phase and silicon tubes (internal and external diameter of 1.6 and 4.8 mm, respectively) connected to 1.6-mm nozzles.

## 3.2.2.2 DESIGN OF EXPERIMENTS

Design of experiments (DoE) was performed to study the influence of the granulation process parameters (i.e., MFR, screw speed (Scr) and L/S ratio) upon local and final granule size distribution (GSD) and granule temperature. Prior to the performance of the DoE, preliminary tests were carried out to determine suitable ranges for the DoE factors for both studied formulations. A screening D-optimal design was performed varying the MFR on five levels from 5 to 25 kg/h, the screw speed on three levels from 450 to 900 rpm and the L/S ratio on five levels from 18 to 27 % (Table 3.2). The DoE resulted in 14 experiments + 3 centre point experiments. The selected DoE had a resolution III. The resolution was sufficient for the scope of this study with no confounded effects.

*Table 3.2: Design of experiments*

<i>Experiment</i>	<i>MFR (kg/h)</i>	<i>Scr (rpm)</i>	<i>L/S ratio (%)</i>
1	5	450	18.0
2	5	450	27.0
3	5	675	22.5
4	5	900	18.0
5	5	900	27.0
6	10	675	27.0
7	15	450	20.3
8/9/10	15	675	22.5
11	15	900	24.8
12	20	675	18.0
13	25	450	18.0
14	25	450	27.0
15	25	675	22.5
16	25	900	18.0
17	25	900	27.0

The DoE was executed using a 2 × 6 screw configuration composed of two kneading zones of six kneading elements each at 60° stagger angle. For all experiments, the jacket of the granulator barrel was pre-heated to a temperature of 25 °C to ensure the same starting conditions for all experiments. The changes in jacket temperature were recorded to evaluate the heat transfer between the jacket and the granulation chamber. The granulator power requested to rotate the screws was recorded to evaluate the mechanical energy added to the system. The DoE was developed and analysed using MODDE 12.0 software (Umetrics, Umeå, Sweden). In a previous study, Verstraeten et al. described a modified granulation barrel

allowing to collect granules from different screw compartments along the length of the barrel (17). Screw compartments were defined as follows (Figure 3.1a):

- Compartment 1: before the first kneading compartment, where the granulation liquid is added (i.e., wetting zone)
- Compartment 2: first kneading compartment
- Compartment 3: after the first kneading compartment
- Compartment 4: second kneading compartment
- Compartment 5: after the second kneading compartment
- Compartment 6: after the narrow chopper section (i.e., granulator outlet)

An extra position for liquid addition was foreseen before the second kneading block. By using the second liquid addition port and using only conveying elements, granule samples collected at the end of the granulator barrel represent granules before the first kneading zone (compartment 1). By inserting a kneading zone after the second liquid port, samples collected represent granules after the first kneading zone (compartment 3). Samples after the second kneading zone (compartment 5) can be obtained at the outlet of the TSG barrel by using the first liquid addition port and by leaving out the chopper section (i.e., two narrow kneading elements) at the end of the barrel. Compartments 2 and 4 represent the kneading compartments, where no samples could be collected. The modified barrel allows producing large amounts of granules reflecting the state of intermediate granulator barrel compartments (i.e., compartments 1, 3 and 5). Moreover, as granules are collected at the end of the granulator barrel, process analytical technology (PAT) tools can easily be interfaced for in-line measurement of the granule quality attributes. For all experiments, granules were collected at compartments 1, 3, 5 and 6 and oven-dried (24 h, 40 °C, 25 % RH) for analysis (Figure 3.1a).

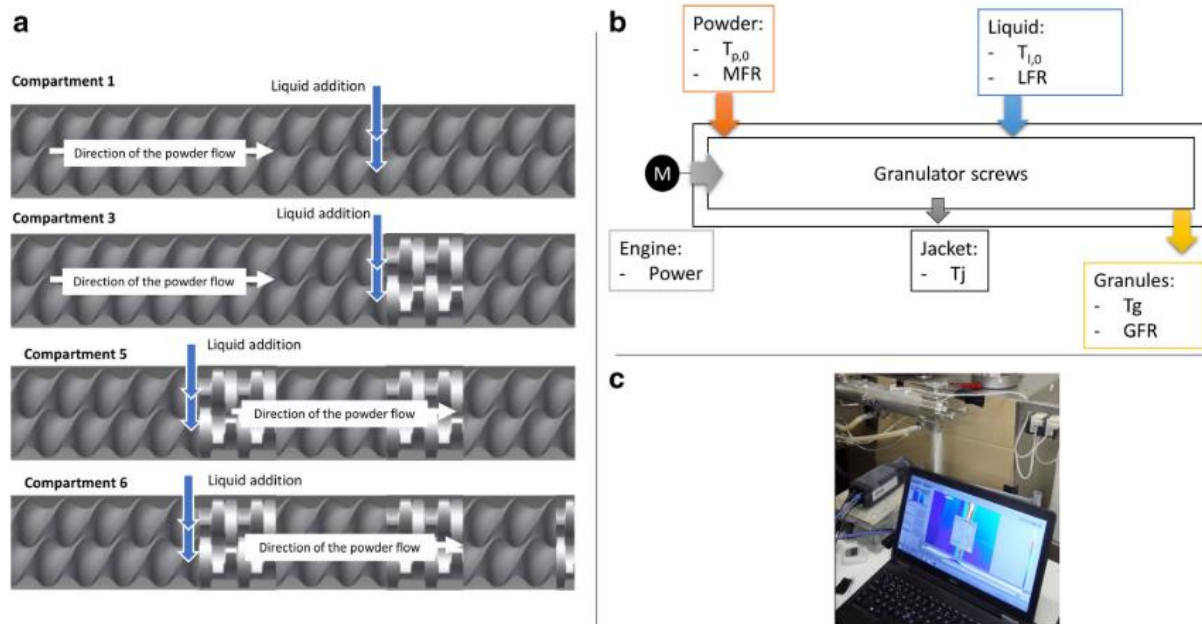


Figure 3.1: Experimental set-up. (a) Granulator set-up, (b) Monitored parameters: LFR: liquid feed rate, GFR: granule feed rate,  $T_{p,0}$ : dry powder temperature,  $T_{l,0}$ : liquid temperature,  $T_j$ : jacket temperature,  $T_g$ : granule temperature, (c) Granule temperature measurement set-up.

### 3.2.2.3 GRANULE TEMPERATURE

The temperature of the granules was continuously monitored during each experiment in each compartment (Figure 3.1b). Data collection was performed using a FLIR A655sc infrared camera (Thermal Focus, Ravels, Belgium) equipped with a 45° lens and an uncooled microbolometer as detector. As described in previous section, by having extra liquid addition ports in the TSG, it became possible to collect information of the individual granulator sections. The camera was therefore placed in front of the granulator outlet, measuring the granules falling. The camera was positioned at about 30 cm from the granulator outlet to ensure a proper focus on the granules (Figure 3.1c). Thermal images were recorded with an image size of 640 × 480 pixels. The thermal resolution of the camera was 30.10<sup>-3</sup> °C noise equivalent temperature difference. This set-up allowed measuring granule temperature for each barrel compartment. The granule temperature was measured for 1 min, recording thermal images every 2 s via the FLIR ResearchIR MAX software (Thermal Focus, Ravels, Belgium). Data processing was conducted using the same software. Granule mean temperature and standard deviation were recorded.

### 3.2.2.4 GRANULE SIZE DISTRIBUTION

Granules were oven-dried over night at 40 °C for characterization. The size distribution of the collected granule samples for each DoE experiment and in each compartment was measured via image analysis (QICPIC, Sympatec GmbH, Etten-Leur, the Netherlands) using a gravimetric feed tube to disperse the granules (Gradis 10-mm dispersion chamber). The amounts of fines, coarse granules and yield were defined as the fractions <150 µm, >1000 µm and 150 – 1000 µm, respectively. Ten grams of granules was dispersed in front of the measurement window using a vibratory feeder. Each sample was measured in triplicate.

## 3.3 RESULTS AND DISCUSSION

Thanks to the experimental set-up described in section 3.2, it was possible to collect and measure granules from compartments 1 (i.e., wetting zone), 3 (i.e., after first kneading zone), 5 (i.e., after second kneading zone) and 6 (i.e., end of the granulator barrel). The infrared camera described in section 3.2.2.3 allowed measuring the granule temperature in those corresponding compartments. Granulator power and barrel temperature were obtained for each compartment by deducing values from previous compartment to values for the studied compartment. It was therefore possible to analyse granule formation and heat transfers occurring in each compartment independently. Energy balances over the different compartments allowed identifying potential sources of heat transfer. A first energy input is the mechanical energy given by the motor of the granulator screws. The mechanical energy given by the motor ( $E_{motor}$ , in J) is used to move the screws at a certain speed and to transport the granules to the outlet of the granulator barrel ( $E_{screws}$ , in J) and to overcome friction work ( $F$ , in J).

$$F = E_{motor} - E_{screws} \quad [3.1]$$

As the aim was to study energy transfers occurring in each compartment, only the variation in friction work, mechanical energy and energy to move the screws between compartments were relevant for the analysis. Since  $E_{screws}$  is a constant term for given process conditions, whereas the increase in friction work was equal to the increase in mechanical energy ( $\Delta F = \Delta E_{motor}$ ). Wetting being an exothermic process, the enthalpy of wetting ( $H_{wetting}$ , in J) represents another source of heat generation within the system. Heat generated by friction forces and wetting is dissipated through thermal energy to the granules ( $E_{granules}$ , in J) and to



the granulator jacket ( $E_{jacket}$ , in J). The energy balance corresponding to the granules and granulator jacket is therefore given in Equation 3.2.

$$F + H_{wetting} = E_{granules} + E_{jacket} \quad [3.2]$$

Off-line granule analysis (i.e., GSD, shape, density, porosity) were performed to relate observed heat transfers to granule properties. Only the GSD and API repartition will be discussed in this section as other granule attributes were directly correlated to GSD for the studied formulations.

### 3.3.1 IMPACT OF PROCESS PARAMETERS ON GRANULE ATTRIBUTES

In a first step, the impact of the different process parameters on GSD and granule temperature was evaluated. As shown in Figure 3.2, the GSD was only impacted by the L/S ratio, as seen in many other studies on twin-screw granulation. On the other hand, granule temperature was impacted by both the L/S ratio and MFR. Screw speed presented no effect on any studied dependent parameter. This was most likely due to a minor impact of the screw speed on screw fill level in the studied range. In the following sections, only the effect of the L/S ratio and MFR upon granule temperature and granule size will consequently be discussed for each compartment.

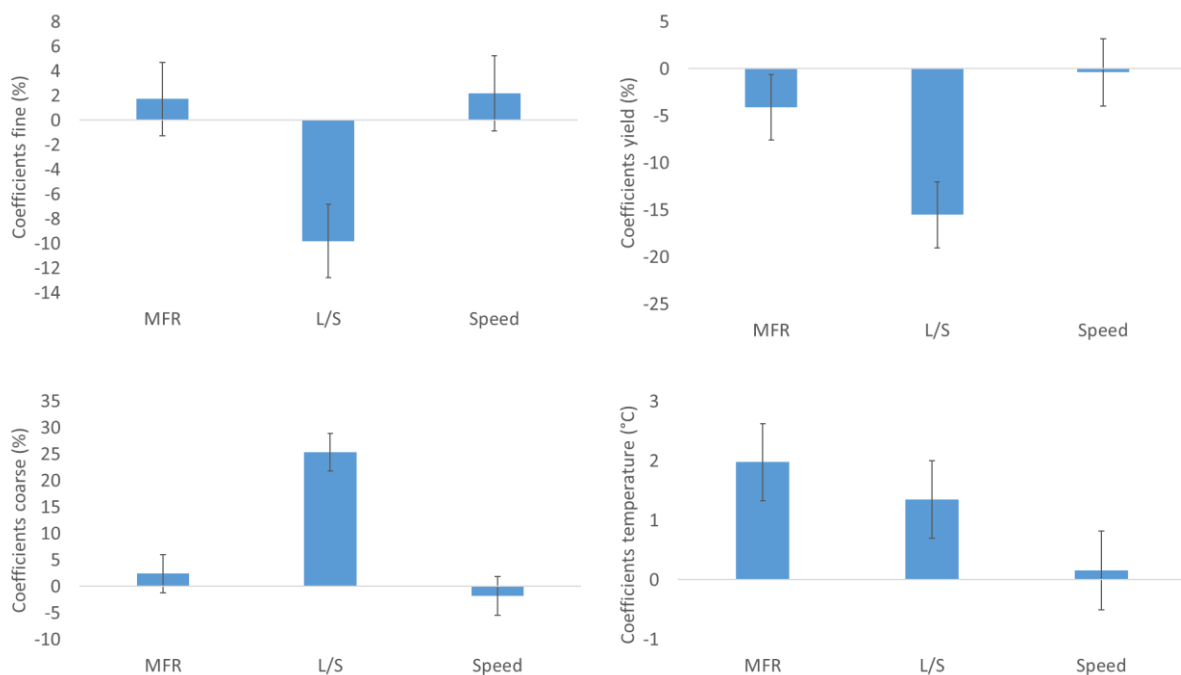


Figure 3.2: Impact of process parameters on granule attributes.

### 3.3.2 COMPARTMENT 1—WETTING ZONE

#### 3.3.2.1 GRANULE TEMPERATURE

Compartment 1 corresponds to the wetting zone where the granulation liquid is added to the moving powder bed. An increase in granule temperature was observed in the wetting zone (Figure 3.3) with no concomitant significant change in granulator power ( $\pm 5$  W). No jacket temperature increase was measured showing no significant heat exchange between the granules and the cooling jacket. As the mechanical energy did not increase significantly, it was concluded that only minor additional friction forces were induced by wet powder compared to dry powder conveying. Therefore, the observed increase in granule temperature was attributed to the enthalpy of wetting only in compartment 1. Since granule temperature elevation was limited to 2 °C (Figure 3.3), no heat transfers between granules and jacket were detected. The energy released during wetting ( $H_{wetting,1}$ , in J) led to granule energy increase ( $E_{granules,1}$ , in J Equation 3.3), and therefore into granule thermal energy increase (Equation 3.4). The thermal energy increase of the granules was calculated from  $m_g$  the mass of granules (g),  $c_{p,g}$  the granules specific heat capacity ( $J \cdot g^{-1} \cdot ^\circ C^{-1}$ ),  $T_1$  the granule temperature in compartment 1 and  $T_0$  the initial powder and liquid temperature (room temperature, in °C).

$$E_{granules,1} = H_{wetting,1} \quad [3.3]$$

$$m_g c_{p,g} (T_1 - T_0) = H_{wetting,1} \quad [3.4]$$

The granule temperature increased slightly from low to medium L/S ratio and then decreased for high L/S ratio (Figure 3.3). The enthalpy of wetting (Eq. 3.5) is expressed as the sum of the specific heat of wetting of the different components ( $h_i$ , in J/g) multiplied by the wetted mass of each component ( $m_{wetted,i}$  in g).

$$H_{wetting} = \sum_i m_{wetted,i} h_i \quad [3.5]$$

Granule temperature being proportional to the enthalpy of wetting, it is therefore expected that granule temperature would increase linearly until complete wetting is achieved. According to granule temperature profile in compartment 1 (Figure 3.3), complete wetting was achieved for L/S ratios around 22.5 %. For higher L/S ratios, additional granulation liquid resulted in temperature decrease due to cooling of the warmed granules with colder

granulation liquid (25 °C). GSD were used to verify that complete wetting was indeed achieved in the estimated ranges of L/S ratio (see next section).

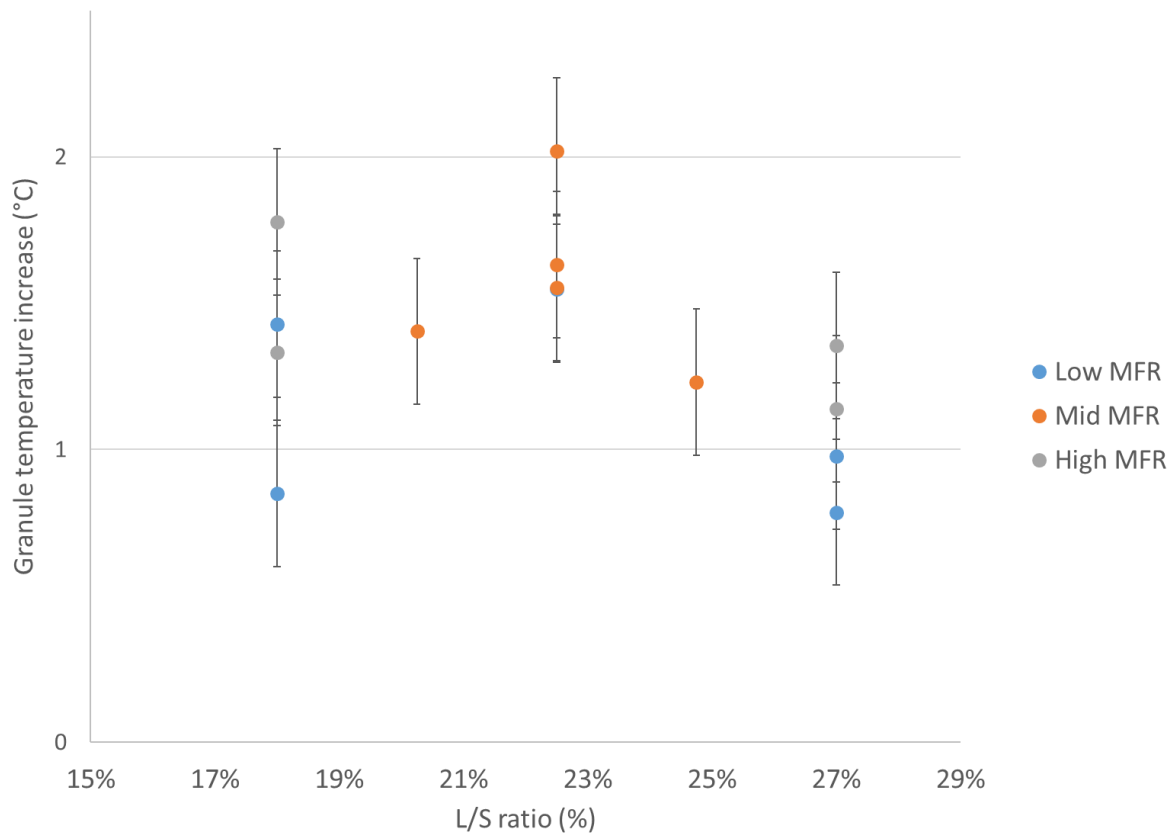


Figure 3.3: Influence of the L/S ratio and MFR on granule temperature increase in compartment 1. The error bars show the standard deviation around the mean value.

### 3.3.2.2 GRANULE SIZE DISTRIBUTION

A bimodal GSD was observed at all process conditions (Figure 3.4). As described in previous studies on GSD evolution along the screw length (15–17), the immersion type of nucleation inherent to the TSG process leads to a population of ungranulated powder (particle size below 150  $\mu\text{m}$ ) and a population of coarse loose nuclei having a size comparable to the size of the granulation liquid droplets (> 1000  $\mu\text{m}$ ). The peak of fine particles (< 150  $\mu\text{m}$ ) was reduced when L/S ratio increased from 18.0 (dotted line) to 24.8 % (long dashed line). No further reduction of the fines fraction was observed for higher L/S ratio. Maximum wetting would therefore be achieved for L/S ratios between 22.5 and 24.8 % in line with the temperature profile (Figure 3.3). The residual fraction of fine particles observed at highest L/S ratios could be due to incomplete wetting or breakage of the loose nuclei in the screws or during GSD

measurement. On the one hand, the fines fraction is characterized by a lower liquid content than the coarse fraction; thus, the residual fine fraction is more likely due to incomplete wetting. On the other hand, the decrease in granule temperature observed for highest L/S ratios (Figure 3.3) suggests that the maximum wetting was reached. These results therefore suggest that, for fixed equipment with a fixed formulation, there is a limit in liquid penetration preventing complete wetting to occur at nucleation step. Defining suitable equipment configuration (e.g., liquid addition method, screw dimension) to maximise nucleation efficiency might therefore improve further granulation process.

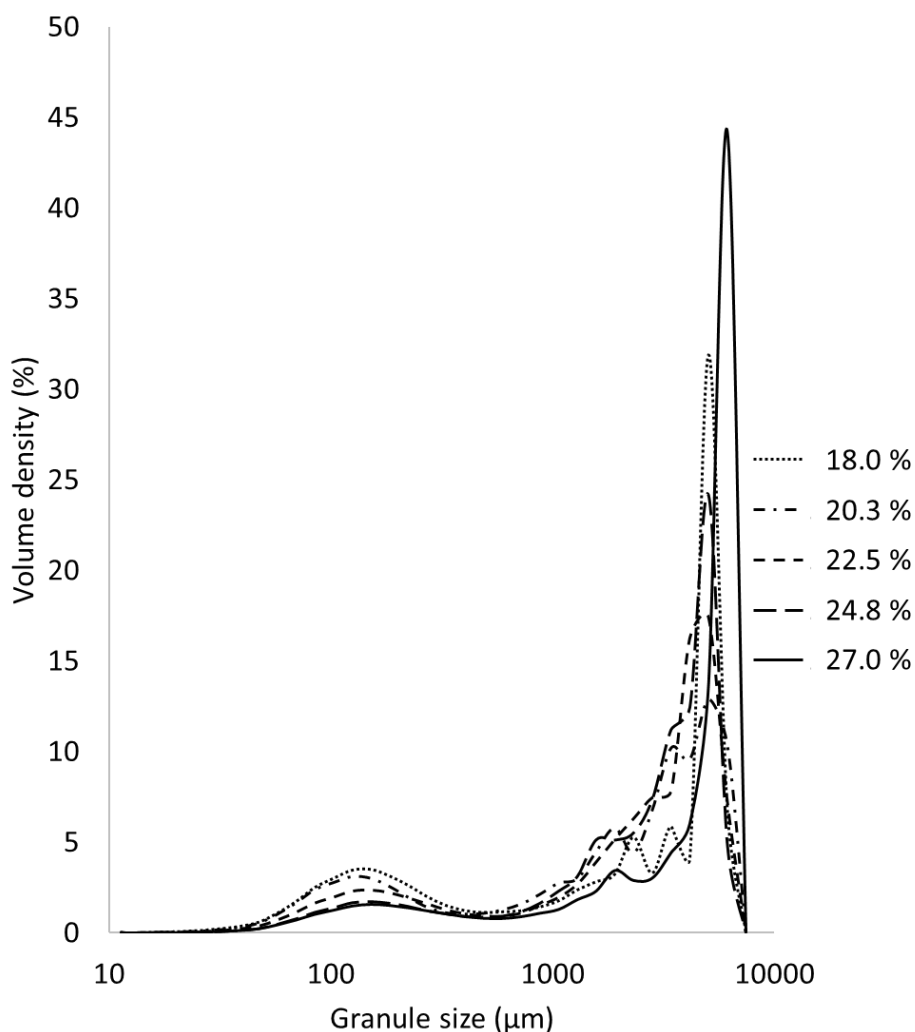


Figure 3.4: Influence of the L/S ratio on the granule size distribution in compartment 1.

The formulation tested in current study contained a poorly wettable API. Interestingly, the fraction of ungranulated particles was nonetheless rather small, even at low L/S ratio. This result seems to be in contradiction with the results described in a previous study from

Verstraeten et al. (17) in which a hydrophilic formulation and another hydrophobic formulation were studied. However, the formulation contained a high amount of lactose which likely compensated for the poor wettability of the API. Current formulation consequently behaved similarly to the hydrophilic formulation described in the previous study. Additionally, the minimum L/S ratio was higher than the maximum L/S ratio tested for previous hydrophilic formulation.

### 3.3.3 COMPARTMENTS 3 AND 5—KNEADING ZONES

Similar observations were made on compartments 3 and 5. They were therefore discussed together in detail in this section.

#### 3.3.3.1 GRANULE TEMPERATURE

An elevation in granule temperature was observed in compartments 3 and 5 at high L/S ratio but not at low L/S ratio (Figure 3.5). The granule temperature increased to the largest extent at high MFR and high L/S ratio.

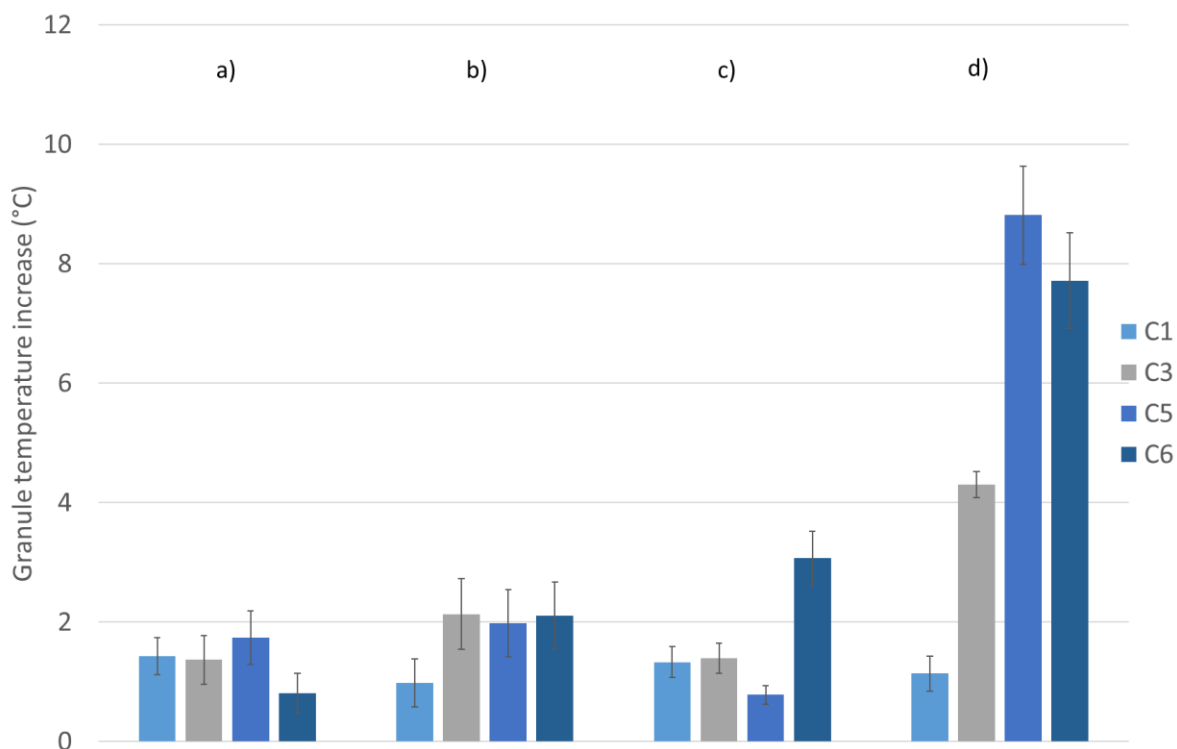


Figure 3.5: Temperature increase recorded for the granules in each compartment at different process settings: (a) Low MFR – Low L/S, (b) Low MFR – High L/S, (c) High MFR – Low L/S, (d) High MFR – High L/S.

For compartments 3 and 5, a linear trend was observed between granulator power (mechanical energy) increase and granule temperature increase for granulator power increase below 200 W (Figure 3.6 – dashed zone). For corresponding experiments, no jacket temperature increase was observed. For higher granulator power, granule temperature increase deviated from the linear trend observed at lower granulator power (Figure 3.6 – dotted zone). An elevation of the jacket temperature of 1–2 °C was observed for the corresponding experiments.

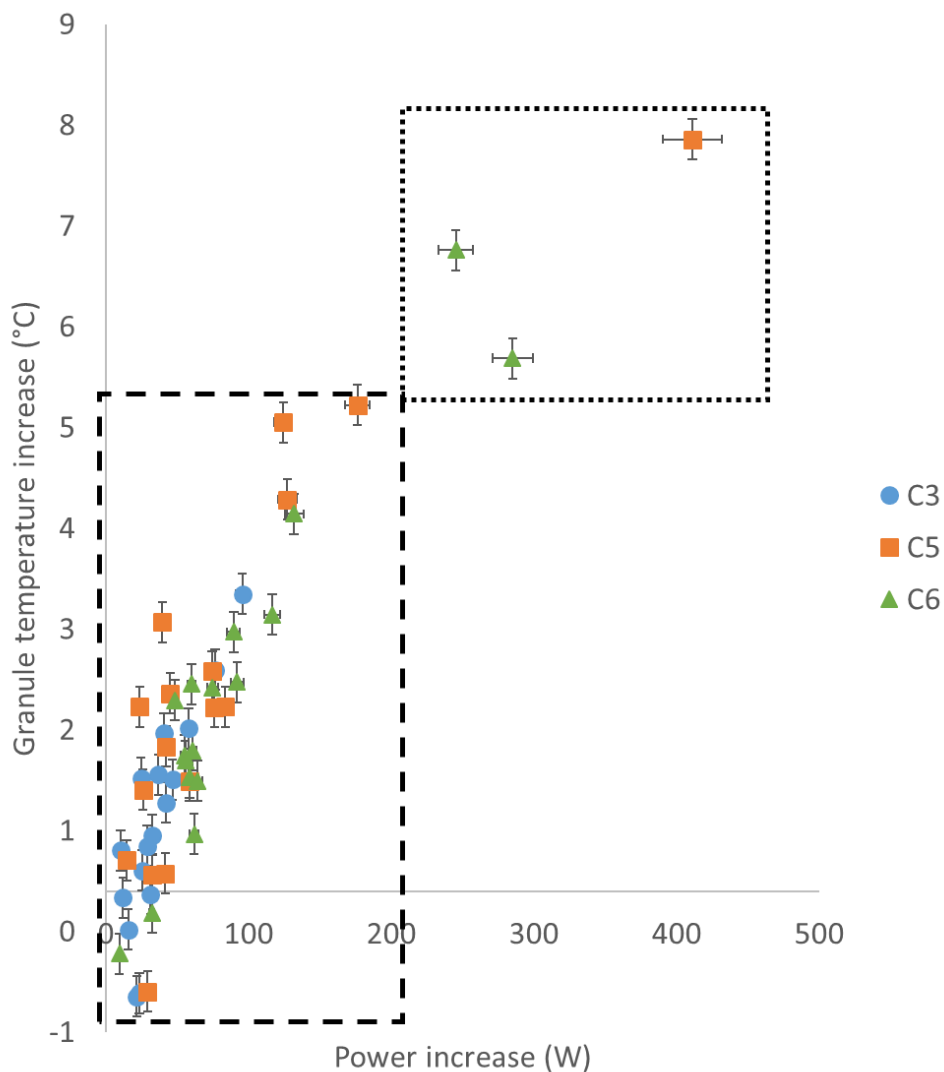


Figure 3.6: Correlation between the granulator power increase and granule heat increase in compartments 3, 5 and 6.

In the kneading zones, granules are forced between the flight tip of the kneading discs and the wall of the granulator barrel (25). As the largest available gap size is significantly smaller in kneading compartments (estimated at 5 mm) than in conveying compartments (estimated at 6.5 mm), granules are sheared and compacted. Friction forces therefore increase between the

granules and the screws and between the granules and the granulator barrel. To compensate the friction forces, the granulator motor needs to provide more power to achieve the same screw speed, explaining the granulator power increase observed in Figure 3.6. As friction forces increase in compartments 3 and 5 ( $F_{3/5}$ , in J), thermal energy generated by friction is mainly dissipated to the granules leading to granule temperature increase observed in Figure 3.5. Below a granule temperature of 30 °C (corresponding to a granule temperature increase of 5°C, Figure 3.6 – dashed zone, heat transfers between granules and granulator jacket are minor and could not be detected. When this granule temperature is exceeded (dotted zone in Figure 3.6), heat transfers between granules and granulator jacket become significant. Granule temperature increase is therefore limited by the dissipation of granule thermal energy ( $E_{granules,3/5}$ , in J) to the granulator jacket ( $E_{jacket,3/5}$ , in J). The influence of granulator jacket temperature on granule quality attributes is often investigated in the range 25 – 40 °C (7,26,27). Considering that granule temperature can increase up to 5 °C without significant heat exchange between the granules and the jacket, the ability of the granulator jacket to control the granulation process can be questioned. Part of the granule temperature increase could also be attributed to additional enthalpy of wetting ( $H_{wetting,3/5}$ , in J) due to liquid redistribution. The additional enthalpy of wetting is expected to be in line with observations made in the wetting zone. Its contribution to the granule temperature increase should therefore be below 0.5 °C, and therefore below the limit of significance. As a consequence, the contribution of the wetting to the final granule temperature increase is negligible compared to the contribution of the friction forces, and no deviation from the linear correlation between granulator power and granule temperature increase is observed in Figure 3.6. Based on these observations, the energy balance on compartments 3 and 5 can be expressed as Equation 3.6.

$$E_{granules,3/5} + E_{jacket,3/5} = F_{3/5} \quad [3.6]$$

### 3.3.3.2 GRANULE SIZE DISTRIBUTION

Figure 3.5 shows that granule temperature increase, and therefore friction forces, depends on the formulation and process parameters. The GSD evolution in the two kneading zones was used to understand the link between granule temperature increase and changes in GSD.

Figure 3.7 presents the GSD evolution between compartments 1, 3 and 5 at low and high L/S ratio.

Breakage of oversized granules was the main phenomenon observed in the first kneading zone at all process settings. The maximum granule size ( $d(99)$ ) was reduced from 6 to 4.5 mm between compartment 1 (Figure 3.7 – dotted line) and compartment 3 (Figure 3.7 – dashed line). The maximum granule size was not influenced by process parameters. As described in a recent study on granule breakage in TSG (28), the maximum granule size is only determined by the screw largest available gap size which differs between conveying elements (compartment 1, estimated to 6.5 mm) and kneading elements (compartments 3 and 5, estimated to 5 mm). At high L/S ratio (Figure 3.7b), breakage mainly occurred in compartment 3, and almost no breakage was observed in compartment 5 suggesting that the main source of breakage is the reduction of the largest available gap size. At low L/S ratio (Figure 3.7a), significant breakage was observed both, in compartments 3 and 5 suggesting another source of breakage that is affected by process and formulation parameters. The breakage rate for particles smaller than the largest available gap size can indeed occur for granules with an insufficient strength based on the probability and velocity of impacts between granules and between granules and screw elements or the barrel wall (29,30). Discrete element method simulations of the particle movement in each compartment could help quantifying impact probability and velocity in each compartment (31).

A reduction of the fines fraction (fraction below 150  $\mu\text{m}$ ) was also observed in all cases (Figure 3.7). This reduction was due to the layering of unwetted particles and granule coalescence. At low L/S ratio (Figure 3.7a), granule layering and coalescence were only observed in compartment 3 and were pronounced. At high L/S ratio (Figure 3.7b), granule layering and coalescence were observed in compartments 3 and 5. Similar results were described for a hydrophilic placebo and another hydrophobic formulation (17). As granules are compressed in the kneading elements, granulation liquid is redistributed allowing the formation of liquid bridges between particles (32). The amount of granulation liquid is therefore crucial to ensure the formation of strong liquid bridges between the powder particles (15) explaining the effect of the L/S ratio. Most layering and consolidation were observed in compartment 3 as the fines fraction is larger in compartment 1 than in compartment 3. Attempts were made to correlate GSD changes (e.g., decrease of fines or coarse fractions) along the length of the barrel to



measured mechanical energy or net energy (mechanical energy–thermal energy). However, no correlation could be found between any of the selected parameter. Granulator torque, and consequently granulator power, is sometimes described as an indicator of the shear and compaction forces experienced by materials inside the barrel (10,20) and therefore a potential in-process control for the granulation. The present study demonstrated that, while granulator torque or power can be used to estimate friction forces, it cannot be used to predict granulation efficiency. A potential explanation is that the granulator power or torque measures friction forces between the granules and the screws (see chapter 5). However, consolidation and breakage phenomena also depend on the wet granule quality attributes (e.g. porosity, strength, plasticity) and on granule probability of impact. A combined mass and energy balance including granule quality attributes and physico-chemical and mechanical phenomena is consequently necessary to better understand granule evolution in the kneading zones. It would therefore be hazardous to use granulator torque or power as single indicator for control of the granulation process.

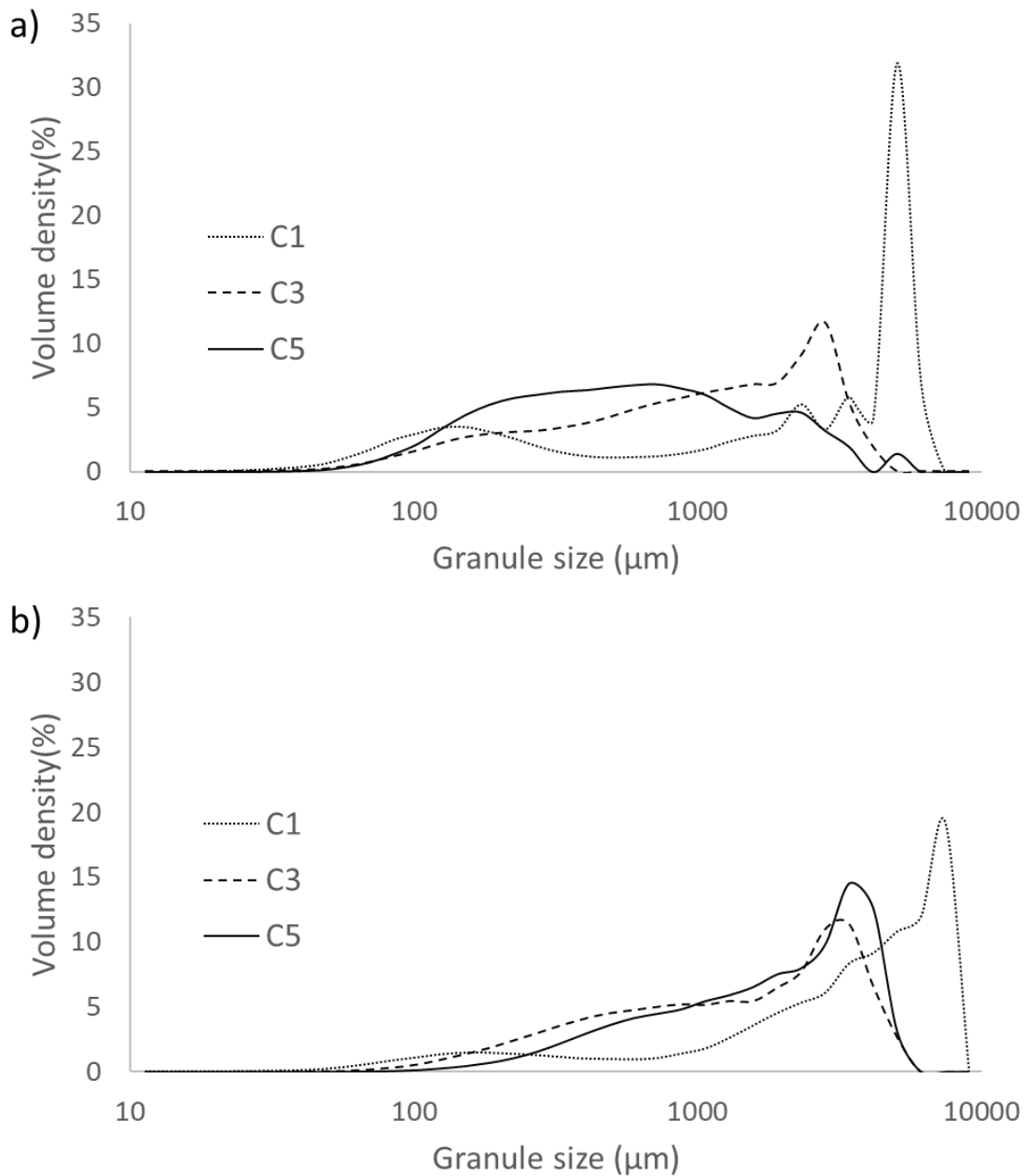


Figure 3.7: Granule size distribution in the wetting zone (C1, dotted line), first kneading zone (C3, dashed line) and second kneading zone (C5, solid line) at low (a) and high (b) L/S ratio.

### 3.3.4 COMPARTMENT 6—FINAL CHOPPING ZONE

The final compartment consisted of two narrow elements staggered at an angle of  $60^\circ$ . These elements are intended to break up oversized granules without affecting smaller granules.

#### 3.3.4.1 GRANULE TEMPERATURE

Only minor changes in granule temperature (Figure 3.5), granulator power ( $\pm 10$  W) and jacket temperature ( $\pm 0.5^\circ\text{C}$ ) were observed in compartment 6. As for compartments 3 and 5, the granule energy flow was proportional to the granulator power (Figure 3.6). The energy balance for compartment 6 was then similar to compartments 3 and 5 (Equation 3.6) except that no secondary wetting should occur in this compartment. The energy balance for compartment 6 (Equation 3.7) therefore included granule energy ( $E_{\text{granules},6}$ , in J), jacket energy ( $E_{\text{jacket},6}$ , in J) and friction forces ( $F_6$ , in J).

$$E_{\text{granules},6} + E_{\text{jacket},6} = F_6 \quad [3.7]$$

#### 3.3.4.2 GRANULE SIZE DISTRIBUTION

Figure 3.8 presents the GSD for in compartments 5 and 6. Significant breakage was observed at low L/S ratio (Figure 3.8a) and further granule growth was observed at high L/S ratio (Figure 3.8b). Previous findings on the evolution of GSD along the barrel length, however, showed no significant effect of compartment 6 on the GSD (17). The cutting elements behaved as an additional granulation zone where breakage occurred at low L/S ratio and consolidation occurred at high L/S ratio. Considering that the cutting elements are usually inserted to break remaining oversized granules, observing consolidation in this compartment is quite surprising. This tends to demonstrate that granule quality attributes obtained at high L/S ratio could be further improved by adding an extra kneading zone. Moreover, this result highlighted the need to also include the effect of the final cutting elements in PBM for certain type of formulations. Similar to compartments 3 and 5, no correlation could be established between the GSD evolution in compartment 6 and granulator power and/or granule temperature.

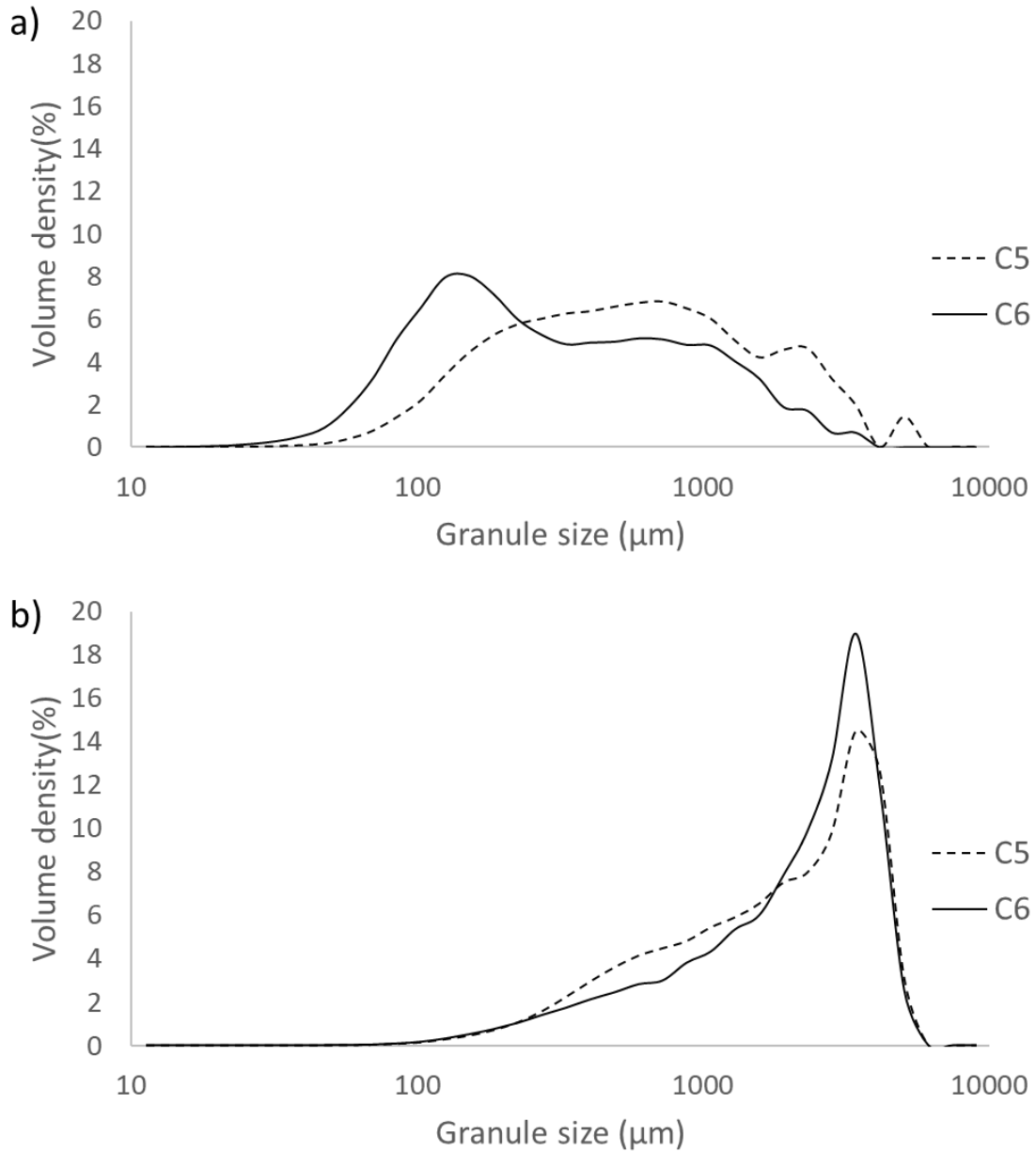


Figure 3.8. Granule size distribution in the second kneading zone (C5, dashed line) and at the end of the granulator (C6, solid line) at low (a) and high (b) L/S ratio.

### 3.4 CONCLUSION

In this study, heat transfer occurring during TSG was evaluated along the length of the granulator barrel. It was shown that the main sources of heat transfer were the enthalpy of wetting at the location of the liquid addition and friction forces in the kneading zones. In the wetting zone, granule temperature increase was directly linked to the fraction of ungranulated powder. It was therefore possible to estimate nucleation efficiency using granule temperature. In the kneading zones, granule temperature increase was proportional to

granulator power and therefore to the friction forces. Barrel jacket temperature is commonly used to control granule temperature and therefore granule quality attributes. Current study demonstrated that the limited heat transfer efficiency between the jacket and the granulator chamber allows for significant granule temperature increase. TSG process being followed by fluid-bed drying, this granule temperature increase might therefore affect mass and energy balances over the next unit operations and should be taken into account when modelling the subsequent drying process. Moreover, deviations in the jacket temperature could lead to mismatches and unstable granule quality attributes. As TSG process was derived from extrusion processes, it is usually admitted that mechanical energy measured by granulator torque or power could be used to predict GSD evolution. The absence of correlation between GSD and mechanical energy along the length questioned the use of this indicator to evaluate granulation efficiency. A detailed study on the validity of typical extrusion in-process control for TSG monitoring would be necessary to clarify this aspect. Combined mass and energy balance of the granulation process are therefore necessary to capture the interaction between local granule properties and physico-chemical and mechanical phenomena occurring in each compartment. Energy balance of the TSG process might advantageously complement population balance models (PBM) to support current hypothesis made on granulation mechanisms occurring in each compartment.

### 3.5 REFERENCES

1. Vervaet C, Vercruyssen J, Remon J, De Beer T. Continuous Processing of Pharmaceuticals. In: Francis & Taylor, editor. Encyclopedia of Pharmaceutical Science and Technology. Fourth Ed. 2013. p. 644–55.
2. Lee SL, O'Connor TF, Yang X, Cruz CN, Chatterjee S, Madurawe RD, et al. Modernizing Pharmaceutical Manufacturing: from Batch to Continuous Production. *J Pharm Innov*. 2015;10(3):191–9.
3. Leuenberger H. New trends in the production of pharmaceutical granules: batch versus continuous processing. *Eur J Pharm Biopharm* [Internet]. 2001 Nov 1 [cited 2018 May 6];52(3):289–96. Available from: <https://www.sciencedirect.com/science/article/abs/pii/S0939641101001990>
4. Srani JS, Badman C, Krumme M, Futran M, Johnston C. Future supply chains enabled by continuous processing-opportunities and challenges May 20-21, 2014 continuous manufacturing symposium. *J Pharm Sci* [Internet]. 2015;104(3):840–9. Available from: <http://dx.doi.org/10.1002/jps.24343>
5. Chatterjee S. FDA Perspective on Continuous Manufacturing [Internet]. Baltimore; 2012. Available from: <https://www.fda.gov/media/85366/download%0Ahttps://www.fda.gov/downloads/AboutFDA/CentersOffices/OfficeofMedicalProductsandTobacco/CDER/UCM341197.pdf>
6. Madurawe R. Continuous manufacturing: FDA perspective. E55/ASTM/FDA workshop. Silver Spring, MD, USA; p. 2016.
7. Vercruyssen J, Córdoba Díaz D, Peeters E, Fonteyne M, Delaet U, Van Assche I, et al. Continuous twin screw granulation: Influence of process variables on granule and tablet quality. *Eur J Pharm Biopharm* [Internet]. 2012;82(1):205–11. Available from: <http://dx.doi.org/10.1016/j.ejpb.2012.05.010>
8. Dhenge RM, Fyles RS, Cartwright JJ, Doughty DG, Hounslow MJ, Salman AD. Twin screw wet granulation: Granule properties. *Chem Eng J* [Internet]. 2010;164(2–3):322–9. Available from: <http://dx.doi.org/10.1016/j.cej.2010.05.023>
9. Fonteyne M, Wickström H, Peeters E, Vercruyssen J, Ehlers H, Peters BH, et al. Influence of raw material properties upon critical quality attributes of continuously produced granules and tablets. *Eur J Pharm Biopharm*. 2014;87(2):252–63.
10. Dhenge RM, Cartwright JJ, Hounslow MJ, Salman AD. Twin screw wet granulation: Effects of properties of granulation liquid. *Powder Technol* [Internet]. 2012;229:126–36. Available from: <http://dx.doi.org/10.1016/j.powtec.2012.06.019>
11. Barrasso D, El Hagrasy A, Litster JD, Ramachandran R. Multi-dimensional population balance model development and validation for a twin screw granulation process. *Powder Technol* [Internet]. 2015;270(PB):612–21. Available from: <http://dx.doi.org/10.1016/j.powtec.2014.06.035>

12. Shirazian S, Darwish S, Kuhs M, Croker DM, Walker GM. Regime-separated approach for population balance modelling of continuous wet granulation of pharmaceutical formulations. *Powder Technol.* 2018;325.
13. Van Hauwermeiren D, Verstraeten M, Doshi P, am Ende MT, Turnbull N, Lee K, et al. On the modelling of granule size distributions in twin-screw wet granulation: Calibration of a novel compartmental population balance model. *Powder Technol [Internet]*. 2019;341:116–25. Available from: <https://doi.org/10.1016/j.powtec.2018.05.025>
14. Kumar A, Gernaey K V., Beer T De, Nopens I. Model-based analysis of high shear wet granulation from batch to continuous processes in pharmaceutical production - A critical review. *Eur J Pharm Biopharm [Internet]*. 2013;85(3 PART B):814–32. Available from: <http://dx.doi.org/10.1016/j.ejpb.2013.09.013>
15. Kumar A, Vercruyssen J, Bellandi G, Gernaey K V., Vervaet C, Remon JP, et al. Experimental investigation of granule size and shape dynamics in twin-screw granulation. *Int J Pharm.* 2014 Nov;475(1–2):485–95.
16. Dhenge RM, Cartwright JJ, Hounslow MJ, Salman AD. Twin screw granulation: Steps in granule growth. *Int J Pharm.* 2012 Nov;438(1–2):20–32.
17. Verstraeten M, Van Hauwermeiren D, Lee K, Turnbull N, Wilsdon D, am Ende M, et al. In-depth experimental analysis of pharmaceutical twin-screw wet granulation in view of detailed process understanding. *Int J Pharm [Internet]*. 2017;529(1–2):678–93. Available from: <http://dx.doi.org/10.1016/j.ijpharm.2017.07.045>
18. Kumar A, Dhondt J, Vercruyssen J, De Leersnyder F, Vanhoorne V, Vervaet C, et al. Development of a process map: A step towards a regime map for steady-state high shear wet twin screw granulation. *Powder Technol [Internet]*. 2016;300:73–82. Available from: <http://dx.doi.org/10.1016/j.powtec.2015.11.067>
19. Tu W, Ingram A, Seville J. Regime map development for continuous twin screw granulation. *Chem Eng Sci [Internet]*. 2013;87:315–26. Available from: <http://dx.doi.org/10.1016/j.ces.2012.08.015>
20. Dhenge RM, Washino K, Cartwright JJ, Hounslow MJ, Salman AD. Twin screw granulation using conveying screws: Effects of viscosity of granulation liquids and flow of powders. *Powder Technol.* 2013;238:77–90.
21. Fonteyne M, Vercruyssen J, Díaz DC, Gildemyn D, Vervaet C, Remon JP, et al. Real-time assessment of critical quality attributes of a continuous granulation process. *Pharm Dev Technol.* 2013 Feb;18(1):85–97.
22. Buckton G, Beezer AE. The applications of microcalorimetry in the field of physical pharmacy. *Int J Pharm.* 1991;72(3):181–91.
23. El Hagrasy AS, Hennenkamp JR, Burke MD, Cartwright JJ, Litster JD. Twin screw wet granulation: Influence of formulation parameters on granule properties and growth

behavior. *Powder Technol* [Internet]. 2013;238:108–15. Available from: <http://dx.doi.org/10.1016/j.powtec.2012.04.035>

24. Kumar A, Alakarjula M, Vanhoorne V, Toiviainen M, De Leersnyder F, Vercruysse J, et al. Linking granulation performance with residence time and granulation liquid distributions in twin-screw granulation: An experimental investigation. *Eur J Pharm Sci* [Internet]. 2016 Jul 30 [cited 2018 May 7];90:25–37. Available from: <https://www.sciencedirect.com/science/article/pii/S0928098715300956>

25. Vercruysse J, Burggraeve A, Fonteyne M, Cappuyns P, Delaet U, Van Assche I, et al. Impact of screw configuration on the particle size distribution of granules produced by twin screw granulation. *Int J Pharm* [Internet]. 2015;479(1):171–80. Available from: <http://dx.doi.org/10.1016/j.ijpharm.2014.12.071>

26. Kim SH, Hwang KM, Cho CH, Nguyen TT, Seok SH, Hwang KM, et al. Application of continuous twin screw granulation for the metformin hydrochloride extended release formulation. *Int J Pharm* [Internet]. 2017;529(1–2):410–22. Available from: <http://dx.doi.org/10.1016/j.ijpharm.2017.07.019>

27. Fonteyne M, Correia A, Plecker D, Vercruysse J, Ili I, Zhou Q, et al. Impact of microcrystalline cellulose material attributes : A case study on continuous twin screw granulation. 2015;478:705–17.

28. Pradhan SU, Sen M, Li J, Litster JD, Wassgren CR. Granule breakage in twin screw granulation: Effect of material properties and screw element geometry. *Powder Technol* [Internet]. 2017;315:290–9. Available from: <http://dx.doi.org/10.1016/j.powtec.2017.04.011>

29. Iveson SM, Luster JD. Growth regime map for liquid-bound granules. *AIChE J*. 1998;44(7):1510–8.

30. Liu LX, Smith R, Litster JD. Wet granule breakage in a breakage only high-shear mixer: Effect of formulation properties on breakage behaviour. *Powder Technol* [Internet]. 2009;189(2):158–64. Available from: <http://dx.doi.org/10.1016/j.powtec.2008.04.029>

31. Barrasso D, Eppinger T, Pereira FE, Aglave R, Debus K, Bermingham SK, et al. A multi-scale, mechanistic model of a wet granulation process using a novel bi-directional PBM-DEM coupling algorithm. *Chem Eng Sci* [Internet]. 2015;123:500–13. Available from: <http://dx.doi.org/10.1016/j.ces.2014.11.011>

32. Vonk P, Guillaume CPF, Ramaker JS, Vromans H, Kossen NWF. Growth mechanisms of high-shear pelletisation. *Int J Pharm*. 1997;93–102.



# 4 IN-LINE TEMPERATURE MEASUREMENT TO IMPROVE THE UNDERSTANDING OF THE WETTING PHASE IN TWIN-SCREW WET GRANULATION AND ITS USE IN PROCESS DEVELOPMENT

This chapter is published as:

F. Stauffer, A. Ryckaert, V. Vanhoorne, D. Van Hauwermeiren, Adrian Funke, Dejan Djuric, C. Vervaet, I. Nopens, T. De Beer, In-line temperature measurement to improve the understanding of the wetting phase in twin-screw wet granulation and its use in process development, *International Journal of Pharmaceutics*, Volume 584, 2020, 119451, ISSN 0378-5173, <https://doi.org/10.1016/j.ijpharm.2020.119451>.

### **ABSTRACT**

Wetting is the initial stage of wet granulation processes during which the first contact between the powder and the liquid occurs. Wetting is a critical step to allow granule growth and consolidation, but also to ensure uniform active pharmaceutical ingredient (API) distribution over all granule size fractions. A physical understanding of the wetting stage is therefore crucial to design a robust granulation process. In twin-screw granulation, wetting is physically separated from granule consolidation, growth, breakage and attrition. The present study used this particularity to investigate the wetting step in such a way that the fundamental mechanisms governing the wetting can be linked and understood. A modified granulator barrel was used allowing the collection of granules immediately after the wetting. A low drug-loaded pharmaceutical formulation containing a poorly soluble and poorly wettable API was used for this investigation. Granules obtained after the wetting zone were analysed for granule size distribution, API distribution over the different size fractions and granule temperature. It was found that “wetting efficiency” (i.e., fraction of powder being nucleated during the wetting stage) could be predicted using an energy balance based on in-line measurement of the granule temperature. Wetting efficiency could moreover be linked to final granule quality attributes (i.e., granule size distribution) at the outlet of the granulator. It was further demonstrated that granule growth and consolidation could only be the dominant mechanism when complete wetting was achieved in the wetting zone of the granulator. This study suggested a methodology based on in-line temperature measurements to quickly determine wetting efficiency. The described methodology could therefore be used as a tool to gain more fundamental understanding of the wetting stage during twin-screw granulation as well as to define suitable formulation and process ranges for further granulation process development.

## 4.1 INTRODUCTION

According to the drug product Manufacturing Classification System, wet granulation is a preferred processing route for products sensitive to segregation and formulations existing of raw materials with poor flowability and poor compressibility (1). Developing a wet granulation process can nonetheless be challenging for poorly wettable active pharmaceutical ingredients (APIs). Three mechanisms have been described to govern wet granulation: (i) wetting and nucleation of the formulation ingredients, (ii) granule consolidation and growth, and (iii) granule attrition and breakage (2,3). Wetting is the primary stage of the wet granulation process where the first contact between the powder and the liquid occurs (3). It is a critical step to allow granule growth and consolidation, but also to ensure uniform API distribution over all granule size fractions. Preferential wetting of certain formulation ingredients due to inhomogeneous ingredient wettability (e.g., due to differences in surface roughness and hydrophilicity) can lead to multimodal granule size distributions, potentially resulting in segregation, or to uneven API distribution over different granule size fractions (4). A good understanding of the fundamental mechanisms governing the wetting step is therefore needed to design robust granulation processes.

Various methodologies have been described to characterize powder wettability. Capillary rise (5), contact angle on powder or tablet (6) and drop penetration time (7) are the most used ones. These methods measure the dynamics of liquid rise in a packed powder bed, static contact angles and the dynamic penetration of a liquid droplet in a static bed, respectively. The results obtained from the different methods however strongly depend on the preparation of the powder bed, and especially, on its degree of packing. Additionally, the interactions between the liquid and the static powder bed are not necessarily representative of what is occurring during a dynamic granulation process. Being able to characterize the wetting step during the actual granulation process would be more valuable and provide a better fundamental understanding of the wetting stage, and in the end allowing to design more robust granulation processes.

In continuous twin-screw granulation, the wetting stage is physically separated from the granule consolidation, growth, breakage and attrition stages (8,9). For most studies on twin-screw granulation, the granule quality attributes have been investigated - after passing the

complete screw configuration - at the outlet of the granulator. Consequently, the influence of individual granulation stages upon final granule quality attributes cannot be determined. A few studies investigated the evolution of the granule properties along the barrel length (8–12). The methodologies described in these studies allow to analyse granules from the different screw compartments (i.e., wetting zone, kneading zones and end of the granulator). Hence, a detailed understanding of the granulation mechanisms occurring in the different compartments can be achieved. These studies all showed that further granulation in the kneading zones was only possible when sufficient wetting efficiency was achieved. This suggests that gaining a more detailed understanding of the wetting step might allow designing more meaningful experiments for twin-screw wet granulation development. Previously cited studies focused mainly on granule size distribution as an indicator of granulation mechanisms. As demonstrated on other solid dosage forms processes, valuable information can nonetheless be derived from heat transfer evaluation (13–16). In a recent study, Stauffer et al. demonstrated that additional information could also be derived from heat transfer evaluation in the different screw compartments (17). This approach is even more applicable to wetting since wetting is an exothermic process (18). In-line monitoring of granule temperature after wetting could allow evaluating the wetting efficiency without extensive off-line analysis.

The objective of this study was to improve the understanding of the fundamental mechanisms governing the wetting step during twin-screw granulation of a pharmaceutical formulation in order to use this information for improved formulation and process development. Granules formed in the wetting zone were collected and analysed using the experimental set-up described by Verstraeten et al. (10). The API content in different size fractions of these granules was measured to investigate preferential wetting. Moreover, granule temperature was measured using an in-line thermo-camera. Monitored granule temperature was compared to granule quality attributes to link granule temperature in the wetting zone to wetting efficiency. In addition, granule characteristics in the wetting zone and at the outlet of the granulator were compared to link wetting efficiency to final granule quality attributes. This allows to determine the minimum fraction of wetted powder which is needed to obtain the desired final granule size.

## 4.2 MATERIAL AND METHODS

### 4.2.1 MATERIALS

A low drug-loaded formulation containing a poorly soluble and poorly wettable API (BCS class II), a large content of  $\alpha$ -lactose monohydrate (Pharmatose<sup>®</sup> 200, DFE Pharma, Goch, Germany), microcrystalline cellulose (MCC, Avicel<sup>®</sup> PH101, FMC biopolymer, Philadelphia, USA), hydroxypropyl methylcellulose (HPMC, Methocel<sup>®</sup> E5, Dow, Midland, USA), croscarmellose sodium (Ac-Di-Sol<sup>®</sup>, FMC, Philadelphia, USA) and sodium dodecyl sulphate (Kolliphor<sup>®</sup> SLS, BASF, Ludwigshafen, Germany) was used in this study. All ingredients were blended using a 20 L Inversina tumbling mixer blender (Bioengineering AG, Wald, Switzerland).

### 4.2.2 METHODS

#### 4.2.2.1 TWIN-SCREW GRANULATION EXPERIMENTAL SET UP

Granules were produced using the twin-screw wet granulation unit of the ConsiGma-25 system (GEA Pharma systems, Collette, Wommelgem, Belgium), described by Fonteyne et al. (19). The granulator consists of two 25 mm diameter co-rotating screws with a length-to-diameter ratio of 20:1. The powder premix is fed to the granulator barrel using a gravimetric twin-screw loss-in-weight feeder (KT20, Coperion K-Tron, Niederlenz, Switzerland). Granulation liquid is gravimetrically dosed into the screw chamber using two out-of-phase peristaltic pumps (Watson Marlow, Cornwall, UK) via silicon tubing (internal and external diameter of 1.6 and 4.8 mm, respectively) connected to 1.6 mm nozzles. In current study, demineralized water was used as granulation liquid.

The DoE was executed using a 2x6 screw configuration composed of two kneading zones of six kneading elements, each at 60° stagger angle (20). For all experiments, the jacket of the granulator barrel was pre-heated to a temperature of 25 °C to ensure the same starting conditions for all experiments. The changes in jacket temperature were recorded to evaluate heat transfers between the jacket and the granulation chamber. The granulator power requested to rotate the screws at a constant speed was recorded to evaluate the mechanical energy added to the system.

In a previous study, Verstraeten et al. described a modified granulation barrel allowing to collect granules from different screw compartments along the length of the barrel (10). Screw compartments were defined as follow (Figure 4.1):

- Compartment 1: Wetting zone: before the first kneading compartment, where the granulation liquid is added
- Compartment 2: First kneading compartment
- Compartment 3: After the first kneading compartment
- Compartment 4: Second kneading compartment
- Compartment 5: After the second kneading compartment
- Compartment 6: After the narrow chopper section (i.e., granulator outlet)

An extra position for liquid addition was foreseen before the second kneading block. By using the second liquid addition port and using only conveying elements, granule samples collected at the end of the granulator barrel represent granules before the first kneading zone, i.e., after wetting (compartment 1 – wetting zone). By inserting a kneading zone after the second liquid port, samples collected represent granules after the first kneading zone (compartment 3). Samples after the second kneading zone (compartment 5) can be obtained at the outlet of the granulator barrel by using the first liquid addition port and by leaving out the chopper section (i.e., two narrow kneading elements) at the end of the barrel. Compartments 2 and 4 represent the kneading compartments, where no samples could be collected.

The barrel with 2 extra liquid addition ports hence allows producing large amounts of granules reflecting the state of intermediate granulator barrel compartments (i.e., compartment 1, 3 and 5). Moreover, as granules are collected at the end of the granulator barrel, process analytical technology tools can easily be interfaced for in-line measurement of the granule quality attributes (see section 4.2.2.3 in materials and methods).

### 4.2.2.2 DESIGN OF EXPERIMENTS (DOE)

A DoE was performed to study the influence of two granulation process parameters: the mass feed rate (MFR) and the liquid-to-solid ratio (L/S ratio) upon granule properties (i.e., API repartition in size fractions, granule size distribution and granule temperature increase) after the wetting zone and at the outlet of the granulator. MFR was varied at three levels from 5 to 25 kg/h covering the broadest processible range on the equipment for the studied

formulation. Furthermore, as all previous studies on twin-screw granulation reported the dominating effect of the L/S ratio upon granule quality attributes, this factor was varied at seven levels to have a detailed description of its influence. The lowest L/S ratio (12 %) corresponded to the minimum amount of liquid that could be added by the peristaltic pump, while the highest L/S ratio (27 %) corresponded with the maximum amount of liquid that did not result in the formation of a paste inside the granulator. The screw speed was fixed at 675 rpm for all experiments. The resulting DoE was composed of 11 runs (Table 4.1). For all experiments, granules were collected at compartment 1 (wetting zone) and 6 (end of the granulator) and oven dried (24 h, 40 °C, 25 % RH) for off-line analysis (Figure 4.1a).

*Table 4.1: Design of experiments. Investigating the effect of varying MFR and L/S ratio on the fraction in fines and coarse granules and the temperature increase in the wetting zone.*

Experiment	MFR (kg/h)	L/S ratio (%)	Wetting: fines (%)	Wetting: coarse (%)	Wetting: $\Delta T$ (°C)
1	5	12	23.5	37.5	0.60
2	5	18	13.6	55.1	1.32
3	5	23	8.2	62.0	1.72
4	5	27	6.0	65.9	1.06
5	15	15	23.6	44.8	1.18
6	15	20	15.0	60.2	1.76
7	15	25	8.0	70.7	1.11
8	25	12	29.1	33.7	1.01
9	25	18	19.6	50.2	0.91
10	25	23	7.6	80.3	1.68
11	25	27	7.1	77.8	1.21

#### 4.2.2.3 API CONTENT UNIFORMITY IN GRANULE SIZE FRACTIONS

Granules collected in the wetting zone were oven dried and sieved using a Retsch VE 1000 sieve shaker (Haan, Germany) using a series of sieves (150, 500, 1400, 2000 and 3150  $\mu\text{m}$ ). An UV/VIS spectroscopy method was established to determine the API content in the different granule size fractions. First, 250 mg of the sieve fraction was mixed with acetonitrile to 50 mL and centrifugated for 15 minutes at 4000 rpm (Heraeus Multifuge 3 S-R, Thermo scientific, USA). Then, the supernatant was removed and 1/100 diluted with acetonitrile before the API concentration was measured with UV absorbance at 251 nm.

### 4.2.2.4 SCANNING ELECTRON MICROSCOPY

Scanning electron microscopy (SEM) was used to visualize the presence of particle-particle interactions in the formulation blend. Samples were sputter-coated with gold under vacuum in an argon atmosphere for 160 s using an Emitech SC7620 (Quorum technologies, East Grinstead, UK). They were then examined in a SEM FEI Quanta™ 200F (FEI, Hillsboro, USA) using secondary electron imaging at a distance of 20 mm.

### 4.2.2.5 GRANULE TEMPERATURE

The temperature of the wetted granules was continuously monitored during each DoE experiment. Data collection was performed using a FLIR A655sc infra-red camera (Thermal Focus, Ravels, Belgium) equipped with a 45° lens and an uncooled micro-bolometer as detector. The camera was placed in front of the granulator outlet to measure the granules leaving the granulator. The camera was positioned at about 30 cm from the granulator outlet to ensure a proper focus on the granules (Figure 4.1b). The emissivity was adjusted to the correct value by comparing thermal images with thermocouple data as a reference. Thermal images were recorded with an image size of 640 x 480 pixels. The thermal resolution of the camera was  $30 \cdot 10^{-3}$  °C noise equivalent temperature difference. The granule temperature was measured for 1 min, recording thermal images every two seconds via the FLIR ResearchIR MAX software (Thermal Focus, Ravels, Belgium). Data processing was conducted using the same software. Granule mean temperature and standard deviation were calculated. Furthermore, dry powder and liquid temperature were measured to determine the corresponding baseline temperature for each experiment. For each experiment, granule temperature increase was calculated as follow:

$$\Delta T = T_g - T_{p,0} \quad [4.1]$$

Where  $\Delta T$  is the temperature increase (in °C),  $T_g$  is the granule temperature (in °C) and  $T_{p,0}$  is the temperature of the dry powder (in °C).



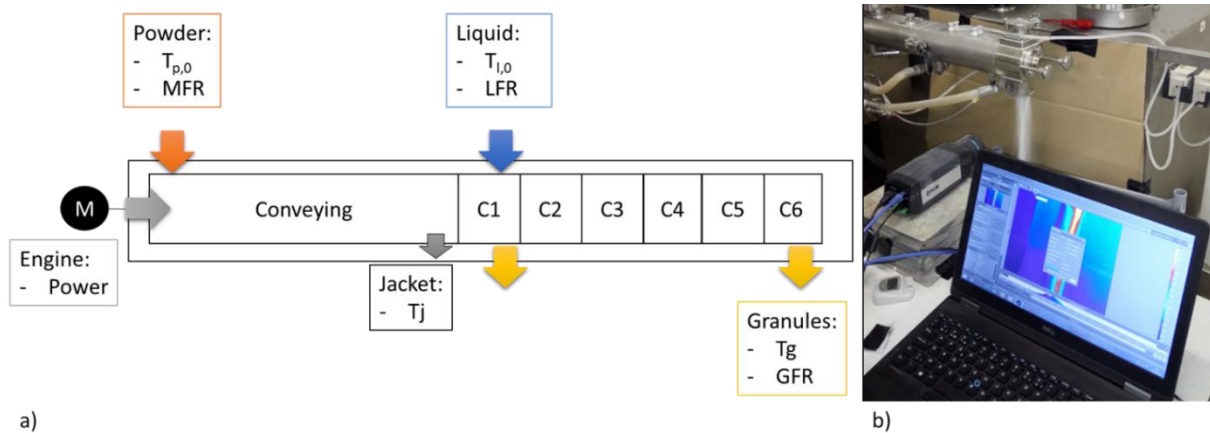


Figure 4.1: Experimental set-up. a) Monitored parameters and different compartments.  $T_{p,0}$ : dry powder temperature,  $T_{l,0}$ : liquid temperature,  $T_j$ : jacket temperature,  $T_g$ : granule temperature, LFR: liquid feed rate, GFR: granule feed rate. b) Granule temperature measurement set-up.

#### 4.2.2.6 GRANULE SIZE DISTRIBUTION

The size distribution of the oven-dried granule samples collected at both compartments was measured via image analysis (QICPIC, Sympatec, Etten-Leur, The Netherlands) using a gravimetric feed tube to disperse the granules (Gradis 10 mm dispersion chamber). 10 g of granules were dispersed in front of the measurement window using a vibratory feeder. Each sample was measured in triplicate. The fraction ungranulated material was defined as the fines fraction, it corresponded with the size fraction smaller than  $150\ \mu\text{m}$ . In addition, the fraction of coarse granules was equal to the size fraction larger than  $1000\ \mu\text{m}$ .

### 4.3 RESULTS AND DISCUSSION

The objective of this study was to unravel the wetting step during twin-screw granulation of a pharmaceutical formulation. In a first step, the API repartition in the different granule size fractions after the wetting zone was determined. Secondly, in-line monitored granule temperature was compared to off-line determined granule properties to link granule temperature in the wetting zone to wetting efficiency. Thirdly, granule characteristics obtained after the wetting zone and at the outlet of the granulator were compared to correlate wetting efficiency with the final granule quality attributes.

#### 4.3.1 API CONTENT IN GRANULE SIZE FRACTIONS

The formulation under investigation was predominantly composed of a hydrophilic component: lactose (freely soluble, contact angle  $19^\circ$ ) and two hydrophobic components:

MCC (insoluble, contact angle 45 °) and API (poorly soluble, contact angle 66 °). In multi-component formulations, hydrophilic compounds are expected to be preferentially wetted (21). For current formulation, it was therefore anticipated that lactose would be preferentially wetted, then MCC and then API. As a consequence, API was expected to be more present in the ungranulated fraction (i.e., size fraction < 150 µm). When analysing the API distribution in the different granule size fraction though, it was observed that the API was preferentially present in granule fractions above 500 µm (Figure 4.2). Moreover, API distribution was not influenced by process conditions, as similar API repartition was observed at the most extreme process conditions of the DoE (Figure 4.2).

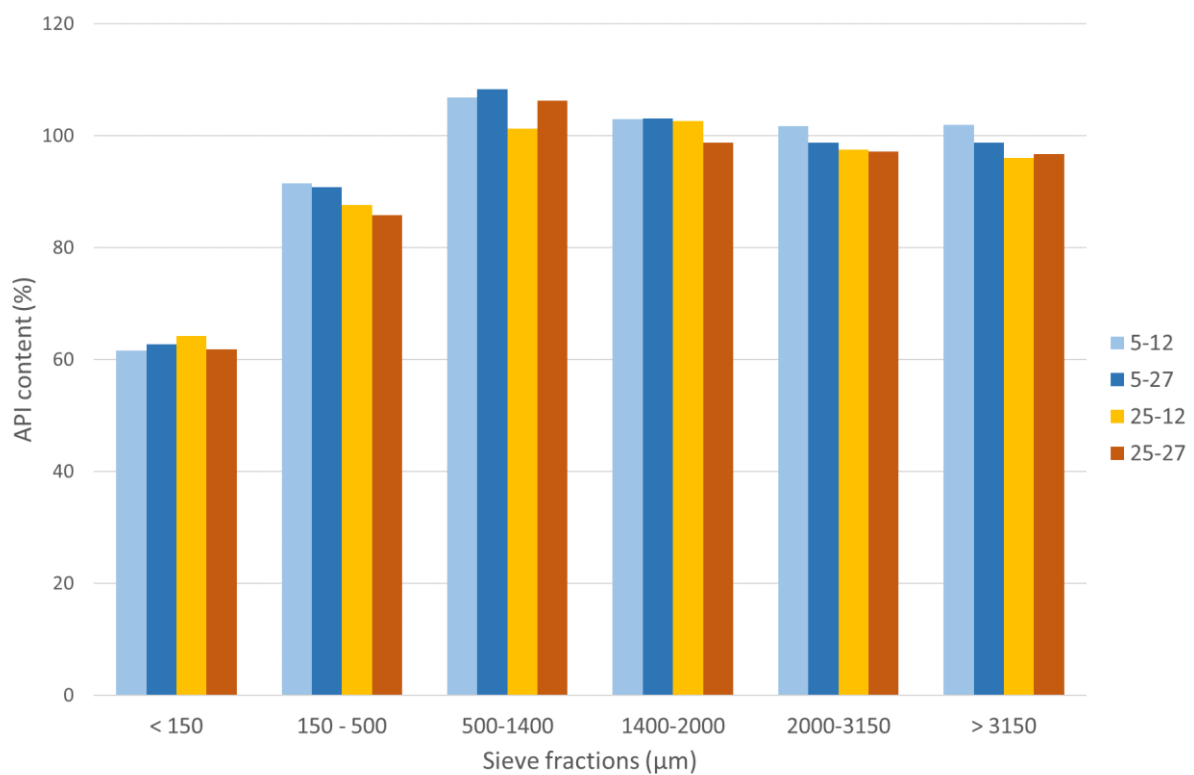


Figure 4.2: API recovery per size fraction (% w/w) at low MFR-low L/S (DoE experiment 1), low MFR-high L/S (DoE experiment 4), high MFR-Low L/S (DoE experiment 8) and high MFR/high L/S (DoE experiment 11) in the wetting zone.

The assumption that the ingredient repartition within the size fractions is led by ingredient wettability relies on the fact that the different ingredients in the formulation are not interacting with each other. Adhesion forces between the API and excipients might nonetheless impact the API repartition in the granule size fractions. Therefore, in order to elucidate the cause of the unexpected API repartition, the dry formulation blend was analysed by SEM prior to granulation (Figure 4.3). It was seen that the hydrophobic API particles (small

spherical particles) tend to spread on excipients' surfaces due to adhesion forces. It could therefore be assumed that, API particles spread on excipients' surfaces are wetted together with the respective excipient and are consequently agglomerated with those. Lactose being the principal ingredient in the formulation, the API particles are more likely to adhere on lactose surface than on other excipients. Moreover, lactose being a hydrophilic ingredient in the formulation, the observed API repartition could be explained by the fact that, not only the lactose particles, but also the API particles spread on lactose particles surface are preferentially wetted. The ungranulated particles would consequently be constituted of the less hydrophilic excipients (MCC in particular) and the API layered on their surface. These assumptions could not be tested due to the absence of a detection method for individual excipients.

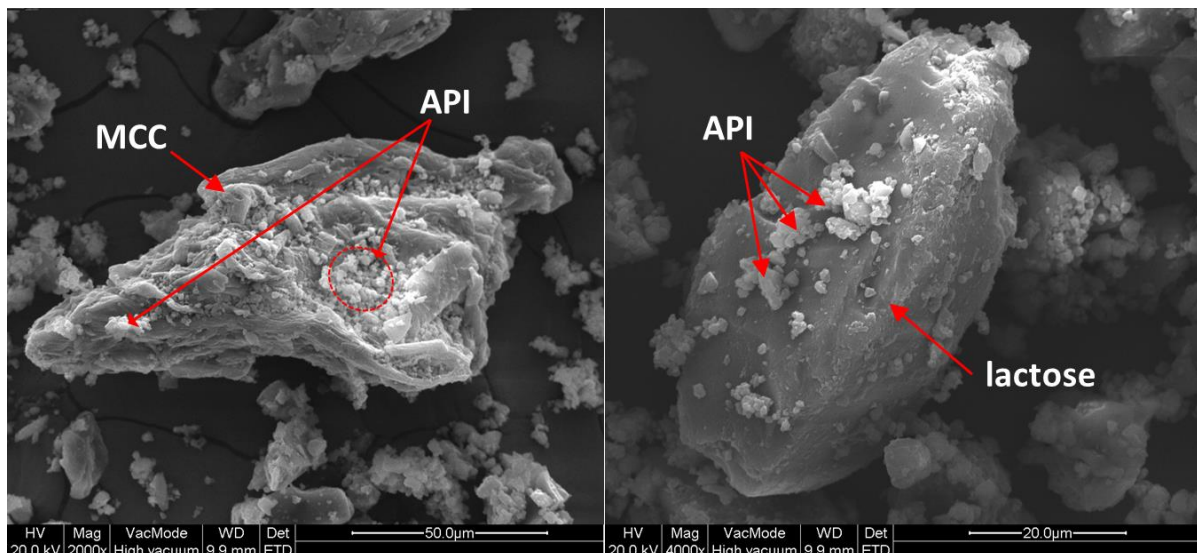


Figure 4.3: SEM pictures of MCC (left) and lactose (right) particles layered by API crystals (small particles).

### 4.3.2 DETERMINATION OF WETTING EFFICIENCY

#### 4.3.2.1 GRANULE TEMPERATURE AFTER THE WETTING ZONE

Figure 4.4 presents the evolution of the granule temperature increase as a function of L/S ratio and MFR.

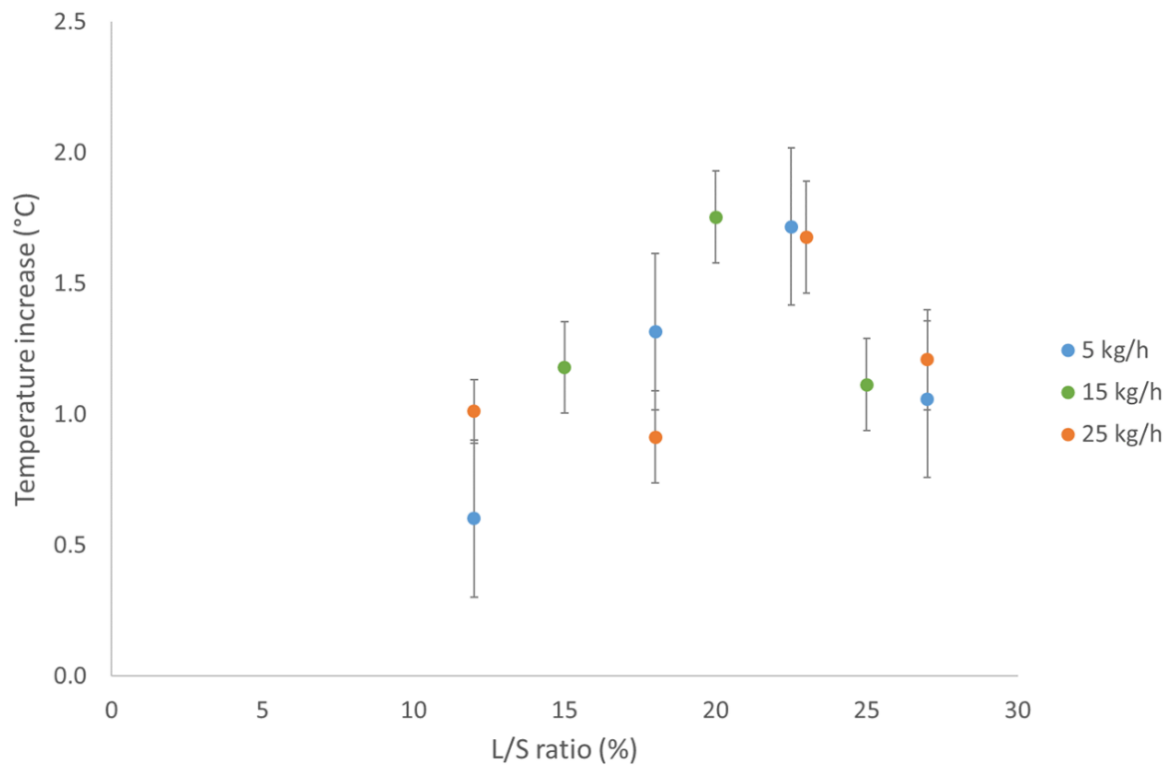


Figure 4.4: Evolution of the product temperature in function of the L/S ratio and MFR.

An increase in granule temperature after wetting from 0.5 to 2.0 °C was observed. All raw materials (i.e., blend ingredients and water) had the same initial ( $T_0$  in °C, temperature of the blend and liquid before liquid addition) and final temperature ( $T_g$ , in °C, temperature of the wet granules just after liquid addition). The temperature increase of each raw material (i.e., powder and liquid) ( $j$ ) depended on its specific heat capacity ( $c_{p,j}$ , in  $J \cdot g^{-1} \cdot ^\circ C^{-1}$ ) and mass ( $m_j$ , in g). Granule temperature increase reflected the increase of thermal energy of the formulation ( $\Delta E_{granules}$ , in J in equation 4.2).

$$\Delta E_{granules} = \sum_j m_j c_{p,j} (T_g - T_0) \quad [4.2]$$

A potential source of temperature increase is friction forces. As powder / granules move through the granulator barrel, the friction forces resulting from their motion could result in temperature increase, warming up the granules. The granulator power was used to evaluate friction forces. In the wetting zone, no concomitant significant change in granulator power ( $\pm 5$  W) was observed, and therefore friction forces were comparable between wet granules in the wetting zone and dry powder conveying. Another potential source of temperature change is the heat transfer through the granulator jacket. Jacket temperature and corresponding

control variables were recorded to evaluate heat transfer between the granules and the jacket. No jacket temperature increase was detected, indicating no significant heat exchange between the granules and the cooling jacket. The measured increase in granule temperature was consequently attributed exclusively to the enthalpy of wetting ( $H_{wetting}$ , in J in equation 4.3).

$$\Delta E_{granules} = H_{wetting} \quad [4.3]$$

For a multi-component blend, the enthalpy of wetting (Equation 4.4) is the sum of the specific heat of wetting of the different blend materials ( $h_i$ , in J/g) multiplied by the wetted mass of each blend material ( $m_{wetted,i}$  in g).

$$H_{wetting} = \sum_j m_{wetted,i} h_i \quad [4.4]$$

Equation 4.2, 4.3 and 4.4 could be combined to express the temperature increase of the different raw materials in function of the mass of wetted powders (Equation 4.5).

$$\sum_i m_{wetted,i} h_i = \sum_j m_j c_{p,j} (T_f - T_{0,j}) \quad [4.5]$$

Finally, Equation 4.6 gives the granule temperature increase in function of process conditions. The wetted mass ( $m_{wetted}$ ) being a combination of formula composition, MFR and L/S ratio and the blend mass ( $m$ ) being a combination of formula composition and MFR and L/S ratio.

$$(T_f - T_0) = \frac{\sum_i m_{wetted,i} h_i}{\sum_j m_j c_{p,j}} \quad [4.6]$$

The powder bed is characterized by a porosity which depends on the formula composition and powder densification. During wetting, the intergranular and intragranular pores are filled by the granulation liquid. The proportion of pores occupied by the granulation liquid is called the pore saturation. A dry powder bed has a pore saturation of 0 %. In the theoretical case where all pores are occupied by the granulation liquid, the pore saturation is 100 %. In reality, the pore saturation of a given formulation wetted under given conditions cannot exceed a maximum limit which is called the maximum pore saturation. Two cases can be distinguished according to the pore saturation of the powder bed. Below the maximum pore saturation (i.e., incomplete wetting), the wetted mass ( $m_{wetted}$ ) increases with the amount of liquid. The total mass ( $\sum_j m_j$ ) also increases as liquid is added to the granules. As every single drop is used to

wet the powder bed, the energy generated by the wetting ( $\sum_i m_{wetted,i} h_i$ ) is larger than the dilution induced by the liquid addition ( $\sum_j m_j$ ). Based on Equation 4.6, for incomplete wetting, granule temperature should hence increase linearly with the L/S ratio until maximum pore saturation is achieved. There indeed seems to be a linear increase of the granule temperature with the L/S ratio between 12 and 23 % (Figure 4.4). It could thus be estimated that complete wetting or a maximal wetting efficiency was achieved at an L/S ratio around 23 %.

Adsorption of the liquid on dry powder surface has been described as being the first and most exothermic phase of the wetting process (22). Beyond pore saturation, the dry powder surface is completely wetted by the granulation liquid. Extra liquid therefore bounds on a wetted surface. Further liquid addition is hence less exothermic and the corresponding energy increase ( $\sum_i m_{wetted,i} h_i$ ) is minor. On the other hand, the total mass of compounds ( $\sum_j m_j$ ) still increases as more liquid is added to the granules. Therefore Equation 4.6 predicts a decrease of the product temperature by increasing the L/S ratio above the maximum pore saturation. A granule temperature decrease with the L/S ratio was indeed observed above 23 % L/S ratio (Figure 4.4).

No significant effect of the MFR, and therefore of the screw fill level, was observed in the studied range (Figure 4.4). Based on Equation 4.6, increasing the MFR results in an increase of wetted mass ( $m_{wetted}$ ) proportional to the increase of total mass ( $m_j$ ) explaining the absence of effect of this parameter on granule temperature. Based on granule temperature evolution, it was estimated that maximum pore saturation and therefore maximum wetting was achieved for a L/S ratio around 23 %. Granule size distribution of the corresponding granules were measured to evaluate whether granule temperature increase can be used as indicator of the wetting efficiency.

#### 4.3.2.2 GRANULE SIZE DISTRIBUTION AFTER THE WETTING ZONE

Wetting does not only result in granule temperature change, but more importantly in nuclei formation. Assuming granule temperature changes are only related to wetting, the wetting efficiency determined by temperature profiles should be related to changes in granule size. Below the maximum pore saturation (i.e., incomplete wetting), increasing the L/S ratio should result in more nuclei formation as more pores are occupied by the granulation liquid. Above maximum pore saturation, no additional nuclei are formed when more granulation liquid is

added. Granule size distribution was measured to evaluate the nuclei formation for all experiments (Figure 4.5) and to compare these observations to the wetting efficiency determined by the granule temperature profile.

A bimodal distribution was obtained for all tested conditions (Figure 4.5). A first population was observed around 150  $\mu\text{m}$  (i.e., fines fraction). This population corresponded to the ungranulated particles. A second population was observed between 2000 and 9000  $\mu\text{m}$  (i.e., coarse fraction). This population corresponded to nuclei and their mean diameter was impacted by process conditions. The fraction of fine and coarse particles for each experiment are shown in Table 4.1. For all studied MFRs, a reduction of the proportion of ungranulated particles was observed when increasing L/S ratio from 12 to 23 % (Figure 4.5). For L/S ratios higher or equal to 23 %, no significant reduction of the fines fraction was detected. As increasing the L/S ratio from 23 to 27 % did not reduce further the residual fines fraction, it could be concluded that the maximum wetting efficiency was achieved for a L/S ratio around 23 %. This observation confirmed the maximum wetting efficiency derived from the granule temperature profile. It was therefore concluded that in-line granule temperature measurements could be used to determine the maximum wetting efficiency of a formulation.

Fine particles were nevertheless still observed even at maximum L/S ratio (6 % at low MFR and 7 % at high MFR). This result suggested that the residual amount of fine particles after wetting and therefore the maximum wetting efficiency is hampered due to formula characteristics such as porosity and hydrophilicity and / or equipment set-up. The experimental set-up allowed to illustrate the status immediately after nucleation, so that it was possible to differentiate between granulated (i.e., nuclei) and ungranulated material. Nevertheless, breakage of the porous nuclei in the short conveying zone after wetting (due to the experimental set-up) or during the granule size distribution measurements itself could also enlarge the fines fraction. Therefore, possibly overestimating the fines fraction. The impact of the residual fraction of fine particles among final granule properties should be evaluated to determine their criticality. If found to be critical, changes of formulation and or equipment set-up should be considered to allow complete wetting to occur (e.g., multiple wetting zones).

No significant effect of the MFR, and therefore screw fill level, upon the fraction of ungranulated material was observed (Figure 4.5). MFR nonetheless impacted the size of the nuclei as a higher MFR resulted in larger nuclei. A higher screw fill level induced by higher MFR could indeed result in larger granules as more powder is available for each liquid droplet. The size of the nuclei also depended on the L/S ratio (Figure 4.5). The wetting stage in twin-screw granulation is characterized by an immersion type of nucleation for which the nuclei size is comparable to the size of the granulation liquid droplets [19]. Increasing the liquid flow rate by increasing the MFR and / or L/S ratio results in a larger droplet size and therefore into larger nuclei. The effect of MFR on nuclei size was not translated into a difference in granule temperature. It was therefore highlighted that the proposed in-line granule temperature analysis after the wetting zone could be used to quickly determine the optimal L/S ratio needed to achieve maximum wetting efficiency but not to anticipate nuclei size.



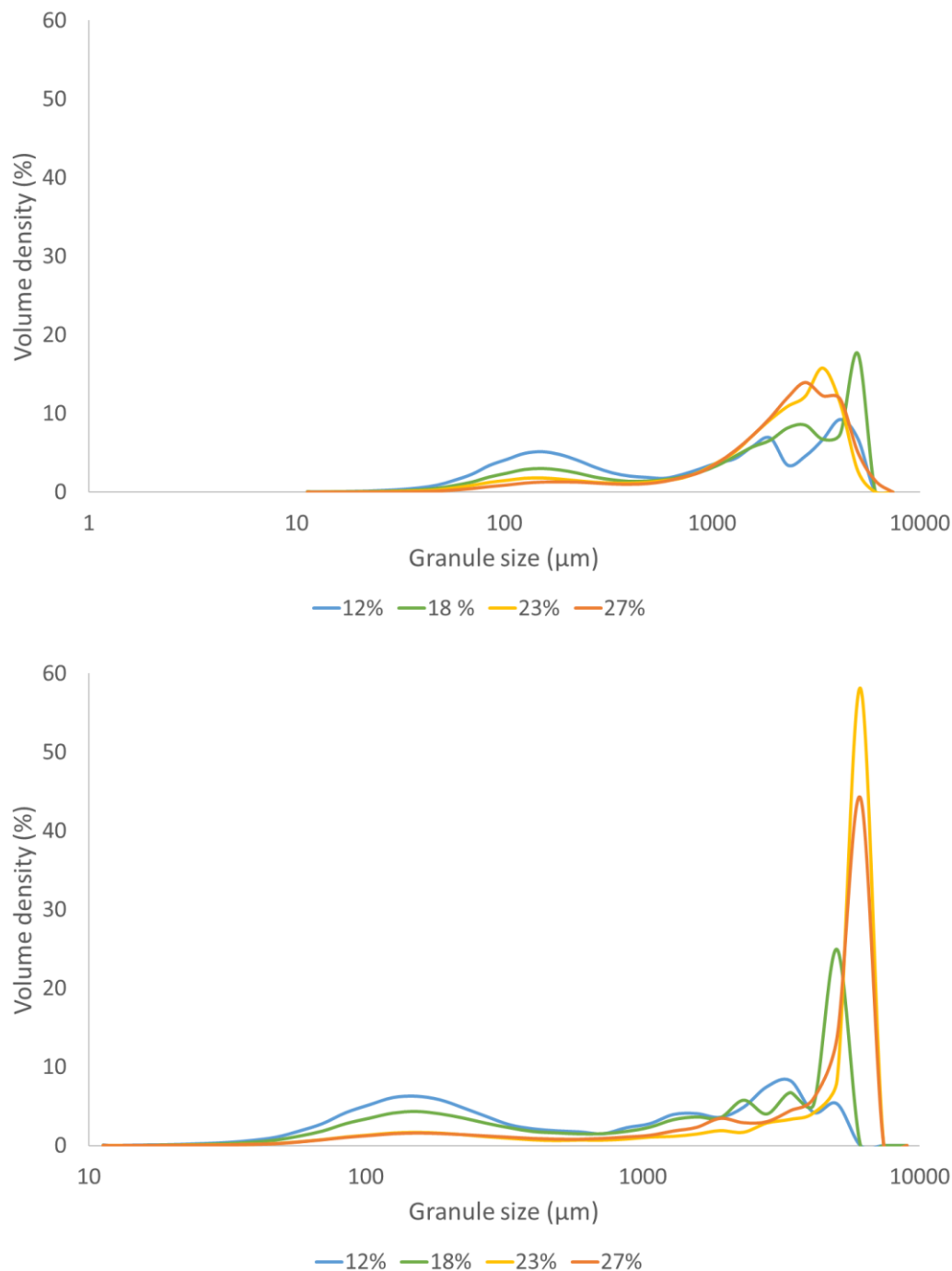


Figure 4.5: Evolution of the granule size distribution according to the L/S ratio.  
Top: 5 kg/h. Bottom: 25 kg/h.

#### 4.3.3 LINKING WETTING EFFICIENCY TO FINAL GRANULE CQAS

The last step of this study consisted in comparing wetting efficiency to final granule quality attributes (i.e., granules in compartment 6). To allow this comparison, the size distribution of granules collected in compartment 1 (wetting zone) was compared to the size distribution of granules collected after the narrow chopper section at the end of the screws (compartment

6). Figure 4.6 presents the results of granule size distribution at different L/S ratios for low and high MFR in both compartments.

Breakage of the nuclei was the only phenomenon observed for granules produced with L/S ratios between 12 and 18 % (Figure 4.6 A/B). The amount of available liquid was limited for these experiments, hence only weak nuclei with few liquid bridges were formed. These nuclei were easily broken in the kneading zones and by the chopper section at the end of the screw configuration. Consequently, the amount fraction of fines in the final granules increased. An increase in fines fraction from 24 to 32 % for DoE experiment 1 (Figure 4.6A), 14 to 19 % for DoE experiment 2 (Figure 4.6A), 16 to 29 % for DoE experiment 8 (Figure 4.6B) and 13 to 20 % for DoE experiment 9 (Figure 4.6B).

At 23 % L/S ratio (Figure 4.6C), although breakage was still observed, a significant fraction of coarse particles (above 1000  $\mu\text{m}$ ) still remained after granulation. The amount of oversized granules decreased from 62 to 22 % for DoE experiment 3 (low MFR) and from 80 to 30 % for experiment 10 (high MFR) (Figure 4.6C). In addition, the fraction of fine particles (fraction below 150  $\mu\text{m}$ ) was reduced from 8 to 5 % for DoE experiment 3 and from 8 to 7 % for DoE experiment 10 demonstrating that granule growth and consolidation occurred in the kneading zones. At 27 % L/S ratio (Figure 4.6D), breakage was minimal as only the largest size fraction (above 5000  $\mu\text{m}$ ) was affected. Simultaneously, granule growth and consolidation occurred at this L/S ratio, as the fines fraction decreased from 6 to 0.5 % for DoE experiment 4 (low MFR) and from 7 to 1 for DoE experiment 11 (high MFR) (Figure 4.6D). In addition, a more monomodal size distribution was observed for the final granules at high L/S ratio. At higher L/S ratios (at least 23 %), an excess in liquid that initially bounded to the nuclei in the wetting zone could be distributed in the kneading zones, allowing further granule growth and consolidation. Moreover, the liquid bounds were strong enough to mitigate granule breakage.

Interestingly, the limit of L/S ratio allowing to achieve granule growth and consolidation and to limit breakage seemed to correspond to the L/S ratio leading to maximum wetting (23 %). In order to design granules with acceptable size and hardness, the maximum wetting efficiency should be achieved in the wetting zone. As wetting efficiency could be determined by in-line analysis of the granule temperature in the wetting zone, it would be possible to

rapidly and efficiently determine operational ranges for further process development using the experimental setup described in current study.

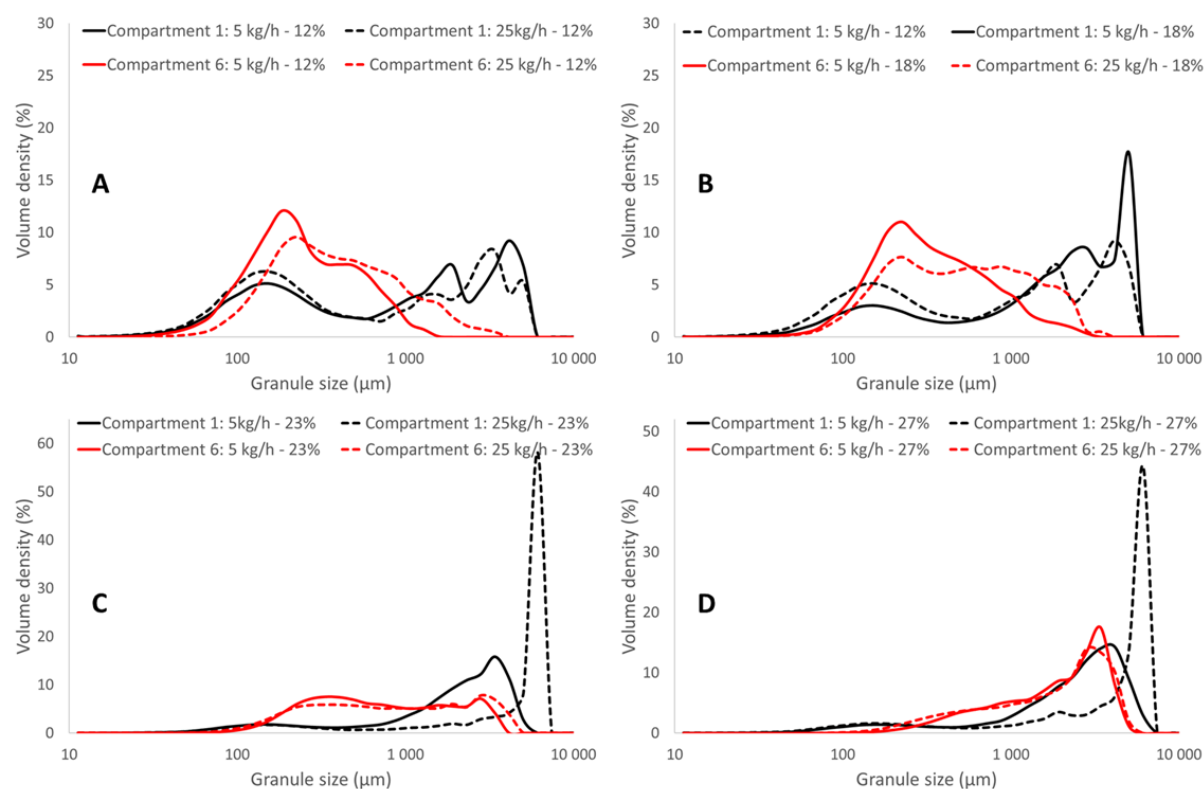


Figure 4.6: GSD in the wetting zone and at the granulator outlet for low and high MFR: (A) 12 % (experiment 1 and 8), (B) 18 % (experiment 2 and 9), (C) 23 % (experiment 3 and 10) and (D) 27 % L/S ratio (experiment 4 and 11).

## 4.4 CONCLUSIONS

This study allowed to gain more fundamental understanding of the wetting step during twin-screw granulation. Using the experimental setup described in current study, the energy balance of the wetting stage could be derived from in-line measurement of granule temperature in the wetting zone. The energy balance was in good agreement with the wetting efficiency determined by off-line granule size distribution analysis. Wetting efficiency was moreover linked to final wet granule quality attributes at the outlet of the granulator. It was demonstrated that granule growth and consolidation could only be achieved when complete wetting was obtained in the wetting zone of the granulator.

The implementation of in-line thermal imaging was shown to be a fast and efficient way for studying the wetting stage. By allowing to quickly investigate wetting efficiency, this method could be used as a complementary tool to gain more fundamental understanding of the

wetting stage during twin-screw granulation as well as to define suitable ranges for further granulation development. Finally, in this study, the use of in-line thermal imaging to determine wetting efficiency has been tested on a single formulation as a proof of concept. Extension of current study on several formulations having different properties would be of interest to further refine the scope and limitations of this methodology. This would also be an opportunity to explore potential material characterization techniques to predict wetting behaviour using twin-screw granulation.

## 4.5 REFERENCES

1. Leane M, Pitt K, Reynolds G, Anwar J, Charlton S, Crean A, et al. A proposal for a drug product Manufacturing Classification System (MCS) for oral solid dosage forms. Vol. 20, *Pharmaceutical Development and Technology*. 2015. p. 12–21.
2. Parikh D. *Handbook of Pharmaceutical Granulation Technology*. 3rd Editio. Press C, editor. Boca Raton, Florida, USA; 2016. 676 p.
3. Hapgood KP, Litster JD, Smith R. Nucleation regime map for liquid bound granules. *AIChE J*. 2003;49(2):350–61.
4. Oka S, Emady H, Kašpar O, Tokárová V, Muzzio F, Štěpánek F, et al. The effects of improper mixing and preferential wetting of active and excipient ingredients on content uniformity in high shear wet granulation. *Powder Technol*.
5. Washburn EW. The Dynamics of Capillary Flow. *Phys Rev*. 1921 Mar;17(3):273–83.
6. Van Oss CJ, Ju L, Chaudhury MK, Good RJ. Estimation of the polar parameters of the surface tension of liquids by contact angle measurements on gels. *J Colloid Interface Sci*. 1989 Mar;128(2):313–9.
7. Hapgood KP, Litster JD, Biggs SR, Howes T. Drop Penetration into Porous Powder Beds. *J Colloid Interface Sci*. 2002 Sep;253(2):353–66.
8. Dhenge RM, Cartwright JJ, Hounslow MJ, Salman AD. Twin screw granulation: Steps in granule growth. *Int J Pharm*. 2012 Nov;438(1–2):20–32.
9. Kumar A, Vercruyssen J, Bellandi G, Gernaey K V., Vervaet C, Remon JP, et al. Experimental investigation of granule size and shape dynamics in twin-screw granulation. *Int J Pharm*. 2014 Nov;475(1–2):485–95.
10. Verstraeten M, Van Hauwermeiren D, Lee K, Turnbull N, Wilsdon D, am Ende M, et al. In-depth experimental analysis of pharmaceutical twin-screw wet granulation in view of detailed process understanding. *Int J Pharm [Internet]*. 2017;529(1–2):678–93. Available from: <http://dx.doi.org/10.1016/j.ijpharm.2017.07.045>
11. Mundozah AL, Yang J, Tridon CC, Cartwright JJ, Omar CS, Salman AD. Assessing Particle Segregation Using Near-Infrared Chemical Imaging in Twin Screw Granulation. *Int J Pharm [Internet]*. 2019;568(February):118541. Available from: <https://doi.org/10.1016/j.ijpharm.2019.118541>
12. Mundozah AL, Cartwright JJ, Tridon CC, Hounslow MJ, Salman AD. Hydrophobic/hydrophilic powders: Practical implications of screw element type on the reduction of fines in twin screw granulation. *Powder Technol [Internet]*. 2019;341:94–103. Available from: <https://doi.org/10.1016/j.powtec.2018.03.018>
13. Krok A, Mirtic A, Reynolds GK, Schiano S, Roberts R, Wu CY. An experimental investigation of temperature rise during compaction of pharmaceutical powders. *Int J Pharm*

[Internet]. 2016;513(1–2):97–108. Available from:  
<http://dx.doi.org/10.1016/j.ijpharm.2016.09.012>

14. Krok A, Wu CY. Evolutions of temperature and density during roll compaction of a pharmaceutical excipient. *Int J Pharm* [Internet]. 2019;572(September):118822. Available from: <https://doi.org/10.1016/j.ijpharm.2019.118822>

15. Holm P, Schaefer T, Kristensen HG. Granulation in high-speed mixers Part V. Power consumption and temperature changes during granulation. *Powder Technol*. 1984;43:213–23.

16. Ibarra-Castanedo C, Tarpani JR, Maldague XPV. Nondestructive testing with thermography. *Eur J Phys*. 2013;34(6):2020.

17. Stauffer F, Ryckaert A, Van Hauwermeiren D, Funke A, Djuric D, Nopens I, et al. Heat Transfer Evaluation During Twin-Screw Wet Granulation in View of Detailed Process Understanding. *AAPS PharmSciTech*. 2019;20(7):1–13.

18. Buckton G. Applications of isothermal microcalorimetry in the pharmaceutical sciences. *Thermochim Acta*. 1995 Jan;248(Supplement C):117–29.

19. Fonteyne M, Vercruyse J, Díaz DC, Gildemyn D, Vervaet C, Remon JP, et al. Real-time assessment of critical quality attributes of a continuous granulation process. *Pharm Dev Technol*. 2013 Feb;18(1):85–97.

20. Vercruyse J, Córdoba Díaz D, Peeters E, Fonteyne M, Delaet U, Van Assche I, et al. Continuous twin screw granulation: Influence of process variables on granule and tablet quality. *Eur J Pharm Biopharm* [Internet]. 2012;82(1):205–11. Available from: <http://dx.doi.org/10.1016/j.ejpb.2012.05.010>

21. Charles-williams H, Wengeler R, Flore K, Feise H, Hounslow MJ, Salman AD. Granulation behaviour of increasingly hydrophobic mixtures. *Powder Technol* [Internet]. 2013;238:64–76. Available from: <http://dx.doi.org/10.1016/j.powtec.2012.06.009>

22. Gary Hollenbeck R, Peck GE, Kildsig DO. Application of Immersional Calorimetry to Investigation of Solid–Liquid Interactions: Microcrystalline Cellulose–Water System. *J Pharm Sci*. 1978 Nov;67(11):1599–606.

**5 EVALUATION OF TORQUE  
AS AN IN-PROCESS CONTROL  
FOR GRANULE SIZE DURING  
TWIN-SCREW WET  
GRANULATION**

**ABSTRACT**

In this study, the potential of torque as an in-process control (IPC) to monitor the granule size in twin-screw wet granulation (TSG) was investigated. An experimental set-up allowing the collection of granules at four different locations (i.e., in the wetting zone, after the first and second kneading zone and at the end of the granulation barrel) of the granulator screws was used to determine the change in granule size along the length of the barrel and the contribution of each compartment to the overall torque. A D-optimal Design of Experiments (DoE) was performed to evaluate the influence of screw speed (Scr) (450 – 900 rpm), mass feed rate (MFR) (5 – 25 kg/h) and liquid-to-solid (L/S) ratio (18 – 27 %) upon those responses. Herewith, the correlation between granule size change (expressed as the fine fraction < 150  $\mu\text{m}$  and the oversized fraction > 2000  $\mu\text{m}$ ) and the increase in torque was investigated at each location. No correlation was observed between changes in the granule size and torque in the wetting zone, after the second kneading zone and at the end of the granulator. The only observed correlation was between the granule size and torque increase after the first kneading zone ( $R^2 = 0.74$ ). In the wetting zone, the granule size was mainly due to nucleation which is a shear-independent mechanism. In the first kneading zone, the torque increase was an indication of the degree in granule growth which was consistently observed with all applied granulation process parameters. In the second kneading zone and at the end of the granulator, changes of torque were accompanied to granule breakage and / or growth depending on applied process conditions. Moreover, a higher torque increase in these locations was correlated to a higher granule temperature, suggesting that the energy put into the granulator by the applied process settings was partly used to heat up the material being processed and explains additionally why no correlation between granule size and torque was established. As no direct correlation could be observed between final wet granule size and torque, this study showed that torque could not be used as an IPC to monitor and control the wet granule size in a TSG process.



## 5.1 INTRODUCTION

The pharmaceutical industry aims at manufacturing high-quality end-products (1). Since a pharmaceutical manufacturing process typically consists of multiple sequential unit operations before obtaining the final drug product, the quality attributes of the intermediate products need to be guaranteed as well. Hence, the impact of raw material variables and manufacturing variables on all (intermediate) processes should be well understood. In addition, these variables need to be in a state of control during production (2,3). In 2004, the pharmaceutical industry was therefore encouraged by the US Food and Drug Administration (FDA) to implement the concept of Process Analytical Technology (PAT) (3). This initiative aims at improving the process understanding for an optimal manufacturing control, leading to proper quality assurance (3). This makes it is also indispensable in the current switch from traditional batch manufacturing towards continuous manufacturing. According to the PAT principle, all critical quality attributes (CQAs) for each (intermediate) process need to be identified and controlled by timely measurements (i.e., in-process controls (IPCs)) to assure the final drug product quality (3,4,5). If needed, adjustments of critical process parameters (CPPs), i.e., process parameters affecting CQAs, are needed to keep CQAs within the predefined specifications (2,5,6). These timely measurements during manufacturing allow the replacement of traditional and labour-intensive end-testing of the final product and thus potentially achieving real-time drug product release (2,3,6).

Drive motor torque is commonly monitored in granulation and extrusion processes (7–9). The torque is derived from the power required to transport and/or mix the material being processed and to rotate screws or paddles (8,10,11). A common assumption states that torque represents the energy which is absorbed by the material due to shear and compaction forces, and this energy is assumed to determine the product properties (12). The use of torque as an IPC during a batch high shear wet granulation process was investigated by Leuenberger et al. (7). By monitoring torque during the granulation process, the end-point of the granulation process was determined, yielding granules with desired properties. Hence, over-wetting of granules was avoided and narrow granule size distributions were obtained. However, the determination of the granulation end-point was only valid for the tested formulation in the tested range. A linear correlation between torque and pellet size was observed by Kristensen et al. (8) for a pelletization process in a rotary processor. In this case, the torque increase was

correlated to the amount of liquid added to the formulation, which was the most important process parameter impacting the pellet size. In that study, the use of torque for process control and end-point determination of liquid addition was therefore suggested (8). It was nonetheless observed that the correlation was only valid when the rotation speed of the friction plate and the batch size were kept constant, although the torque is also affected by these variables. In an additional study, Kristensen et al. (9) showed that controlling pellet size with the aid of torque was suitable for formulations with varying concentrations of microcrystalline cellulose.

Similar to the aforementioned batch processes, torque has also often been monitored during twin-screw wet granulation (TSG) (10,11,13–21). In several studies the influence of process parameters on torque (10,11,13,18–21) was studied to gain process understanding. In others, it has also been timely monitored to observe the stability of the granulation process, especially to determine the end of the start-up phase of a TSG process (10,16,17,20). Typically, initial layering of the granulator screws and the screw chamber walls occurs during this period, leading to torque fluctuation before a more stable value is reached. However, no study to date has investigated the potential use of torque as an IPC for the TSG process. The use of torque as an IPC could facilitate the production of granules with a predefined quality. Since the TSG process is typically part of a continuous manufacturing line, a fast and reliable control of the granule quality would be a major advantage as it could possibly eliminate the need for other PAT tool implementation after the granulator.

In current study, the potential use of torque as an IPC for granule size in the TSG process was investigated by evaluating the correlation between the granule size and torque. Process settings such as screw speed (Scr), mass feed rate (MFR) and liquid-to-solid (L/S) ratio were varied, since changing these parameters might cause a change in the granule size and/or the torque value (10,13,19,22–24). The twin-screw granulator with extra liquid addition ports in the middle of the barrel as described by Verstraeten et al. (23) was used to enable the collection of granules representative for the different compartments of the granulator (i.e., after the wetting zone, after each of the kneading zones and at the outlet of the granulation barrel). The change in granule size along the length of the barrel was compared with the corresponding local torque increase. The experimental set-up also allowed to observe the contribution of each compartment to the overall torque. In addition, the overall torque (in-

line monitored by the torque gauge) was compared with the final granule size. Since torque is related to friction forces, and therefore to heat generation, also granule temperature was measured along the length of the granulator (14). This allows discriminating between friction forces used for the granulation process and friction forces which heat the granules.

## 5.2 MATERIALS AND METHODS

### 5.2.1 MATERIALS

A low drug-loaded formulation containing a poorly soluble API (BCS class II),  $\alpha$ -lactose monohydrate (Pharmatose<sup>®</sup> 200M, DFE Pharma, Goch, Germany), microcrystalline cellulose (MCC, Avicel<sup>®</sup> PH101, FMC biopolymer, Philadelphia, USA), hydroxypropyl methylcellulose (HPMC, Methocel<sup>®</sup> E5, Dow, Midland, USA), croscarmellose sodium (Ac-Di-Sol<sup>®</sup>, FMC, Philadelphia, USA) and sodium dodecyl sulphate (Kolliphor<sup>®</sup> SLS, BASF, Ludwigshafen, Germany) was used in this study.

### 5.2.2 METHODS

#### 5.2.2.1 GRANULATION EXPERIMENTS

Granulation experiments were performed using the granulation module of the ConsiGma<sup>™</sup>-25 unit (GEA Pharma Systems, Collette, Wommelgem, Belgium). First, all raw materials were preblended in a tumbling mixer (Inversina Bioengineering, Wald, Switzerland) for 15 minutes at 25 rpm. Thereafter, this pre-blend was gravimetrically fed to the granulation module by a K-Tron KT20 loss-in-weight feeder (Coperion K-Tron, Niederlenz, Switzerland). The granulator had a length-to-diameter ratio of 20:1, consisting of two 25 mm diameter co-rotating screws. Furthermore, a twin-peristaltic pump (Watson Marlow, Cornwall, UK) was used for the addition of demineralized water as granulation liquid. The twin-peristaltic pump was positioned out-of-phase and connected to silicon tubing with an internal and external diameter of 1.6 mm and 4.8 mm, respectively. The silicon tubes were connected to nozzles with an orifice of 1.6 mm. The barrel jacket was kept constant at 25 °C during granulation experiments.

### 5.2.2.2 COMPARTMENTAL GRANULE COLLECTION

The experimental set-up introduced by Verstraeten et al. (23) was used to collect granules along the length of the barrel. The set-up allowed to investigate the relationship between local granule size, local granule temperature increase and local torque increase. The screw configuration was divided into the following six compartments (Figure 5.1):

- Compartment 1: The zone before the first kneading compartment is defined as the wetting zone, because the liquid is added there.
- Compartment 2: The first kneading zone.
- Compartment 3: After the first kneading zone, before the second kneading zone.
- Compartment 4: The second kneading zone.
- Compartment 5: After the second kneading zone, before the two narrow chopper elements.
- Compartments 6: At the end of the screw configuration, after the two narrow chopper elements.

As it was not possible to collect granules in the kneading zones themselves (i.e., compartment 2 and 4), granules were therefore collected at the four remaining locations (i.e., compartment 1, 3, 5 and 6) along the granulation barrel. For these four compartments, the collection occurred at the outlet of the granulator. This was possible by changing the screw configuration and by using a modified granulation barrel with a second liquid port located close to the granulator outlet (Figure 5.1). Hence, the collection of granules occurred as if granules were taken in a certain compartment. For compartment 1, the screw configuration consisted of only conveying elements and the second liquid addition port was used. The second liquid addition port was also used to collect granules in compartment 3, while the screw configuration consisted of conveying elements and 6 kneading elements which were located just after the second liquid addition port. The first liquid addition port was used to collect granules at compartment 5 and 6. For compartment 5, a full screw configuration (i.e., conveying elements with 2 kneading zones of 6 kneading elements) without the chopper elements was configured. The granules in compartment 6 were collected at the granulator outlet by using a full screw configuration (i.e., conveying elements with 2 kneading zones of 6 kneading elements and two small narrow chopper elements at the end). The kneading elements were always arranged at

a stagger angle of  $60^\circ$ . For all experiments, the collected granules were oven dried (24 h,  $40^\circ\text{C}$ , 25 % RH) before further characterization.

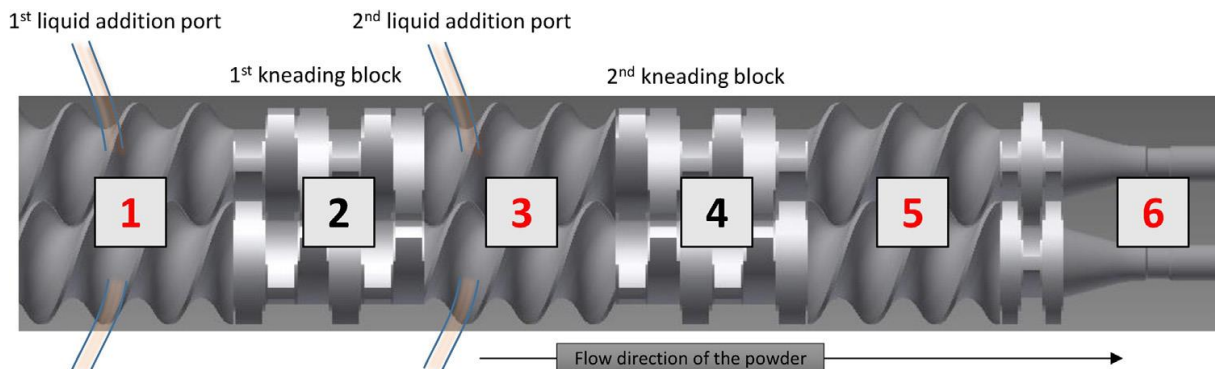


Figure 5.1: Granule collection at different compartments along the length of the barrel: compartment 1 (wetting zone), compartment 3 (after the first kneading zone), compartment 5 (after the second kneading zone) and compartment 6 (at the outlet of the granulator)(23).

### 5.2.2.3 DESIGN OF EXPERIMENTS

For each compartment, a D-optimal Design of Experiments (DoE) with 14 experiments and 3 centre point experiments was performed (Table 5.1). The DoE was used to study the influence of L/S ratio, MFR and screw speed upon granule size, local torque increase and granule temperature increase. Pre-tests showed that MFR and L/S ratio were the most influencing process parameters. Therefore, MFR and L/S ratio were varied at five levels, while screw speed was only varied at three levels. MFR was varied from 5 to 25 kg/h, corresponding to the minimal and maximal capacity of the granulation equipment. Based on preliminary trials the L/S ratio was varied between 18 and 27 % as these L/S ratios resulted in very fine and coarse granules, respectively. The screw speed was varied from 450 to 900 rpm, corresponding with the maximal filling degree and the maximal screw speed, respectively.

Table 5.1: Design of Experiments and overall results for each compartment. Fines: fraction of fines; Oversized: fraction of oversized granules;  $\Delta$ Torque: increase in torque;  $\Delta$ Tem: increase in temperature.

Experiment		1	2	3	4	5	6	7	8	9	10	11	12	13	14	15	16	17
Process parameters	L/S (%)	18	18	18	18	18	20.25	22.5	22.5	24.75	27	27	27	27	27	22.5	22.5	22.5
	Scr (rpm)	450	900	675	450	900	450	675	675	900	450	900	675	450	900	675	675	675
	MFR (kg/h)	5	5	20	25	25	15	5	25	15	5	5	10	25	25	15	15	15
C1	$\Delta$ Tem ( $^{\circ}$ C)	1.4	0.8	0.7	1.8	1.3	1.4	1.6	0.7	0.2	1	0.8	1.1	1.4	1.1	1.6	1.6	2
	$\Delta$ Torque (Nm)	0	0.1	0.1	0.2	0.1	0.1	0.1	0	0	0	0	0	0.2	0.1	0	0	0
	Oversized (%)	66	55	65	60	61	60	62	80	71	69	63	84	778	75	68	77	74
	Fines (%)	11	12	14	17	17	15	8	8	8	6	4	4	7	6	11	8	8
C3	$\Delta$ Tem ( $^{\circ}$ C)	1.4	1.4	1.9	1.4	1.3	1.8	2	2.3	2.1	2.1	1.9	3.3	4.3	2.8	1.8	0.6	1
	$\Delta$ Torque (Nm)	0.2	0.3	0.4	0.5	0.4	0.3	0.5	0.6	0.5	0.7	0.4	1.1	2.3	0.6	0.4	0.4	0.3
	Oversized (%)	24	28	31	35	35	31	39	36	51	54	51	51	77	46	41	34	31
	Fines (%)	11	10	12	11	9	9	5	8	3	1	3	2	0	4	5	4	7
C5	$\Delta$ Tem ( $^{\circ}$ C)	1.7	2.3	3.4	0.8	1.5	3.2	1.7	4.6	5.9	2	1.9	2.9	8.8	6	3.4	3.8	4
	$\Delta$ Torque (Nm)	0.2	0.4	0.6	0.8	0.5	0.6	0.6	1.8	1.3	0.5	0.5	1.1	8.1	1.9	1.2	1.1	0.7
	Oversized (%)	14	22	17	20	16	29	41	46	50	59	59	62	71	55	39	37	35
	Fines (%)	14	16	14	10	13	8	3	4	3	1	2	1	0	1	5	5	6
C6	Overall torque (Nm)	0.5	0.7	1.1	1.4	1.2	1.6	1.4	1.2	1.8	1	1.6	2	8	3.4	1.7	1.3	1.7
	$\Delta$ Tem ( $^{\circ}$ C)	0.8	0.6	2.6	3.1	3.4	2.8	2.1	2.7	5	2.1	1.9	3.9	7.7	6.4	4.1	3	4.1
	$\Delta$ Torque (Nm)	0.1	0.3	0.7	1.1	0.9	1.3	1	0.9	1.4	0.7	1.2	1.7	7.7	3	1.3	0.9	1.3
	Oversized (%)	8	8	10	14	5	26	35	35	47	53	50	64	74	64	39	33	34
	Fines (%)	22	22	20	17	35	12	6	5	4	1	2	1	0	1	7	9	8

#### 5.2.2.4 GRANULE SIZE

The granule size distribution (GSD) was measured by image analysis (QICPIC system equipped with WINDOX 5.4.1.0 software, Sympatec, Clausthal-Zellerfeld, Germany). The GSD was expressed by the fraction of fines and oversized granules. Fines were defined as the size fraction smaller than 150  $\mu\text{m}$ , which corresponded with ungranulated raw materials. Particles larger than 2000  $\mu\text{m}$  were classified as oversized. The fraction in oversized granules indicated the shift in GSD towards smaller or larger granules. Each sample was measured in triplicate.

#### 5.2.2.5 GRANULE TEMPERATURE

During each experiment, a FLIR A655sc infra-red camera (Thermal Focus, Ravels, Belgium) was positioned in front of the granulator outlet to measure the granule temperature. A distance of 30 cm between outlet and camera allowed a proper focus. The camera was equipped with a 45° lens, an uncooled micro-bolometer as detector and had a thermal resolution of 30 mK noise equivalent. The emissivity was adjusted to the correct value by comparing thermal images with thermocouple data as a reference. Thermal images were recorded with an image size of 640  $\times$  480 pixels. The thermal resolution of the camera was 30  $\cdot$  10<sup>-3</sup> °C noise equivalent temperature difference. For each DOE experiment, thermal images were recorded with the FLIR ResearchIR MAX software (Thermal Focus, Ravels, Belgium). Then, the granule temperature and corresponding standard deviation were calculated from each thermal image. Furthermore, for each experiment, the granule temperature was also measured for a dry powder experiment (i.e., no liquid addition) to determine the corresponding (i.e., identical screw speed and MFR) baseline temperature. This was needed to distinguish the temperature increase caused by granulation from the smaller temperature increase due to transport of dry powder. The granule temperature increase was calculated according to Equation 5.1 for each experiment, allowing to observe the change in granule temperature along the length of the barrel.

$$\Delta Temperature (^{\circ}C) = Temperature_{DoE\ experiment} - Temperature_{Dry\ powder} \quad [5.1]$$

#### 5.2.2.6 TORQUE

The ConsiGma™-25 unit has an in-built torque gauge to record the torque every second. Once steady state was reached, the mean torque and the corresponding standard deviation was

calculated for each DoE experiment at each barrel location. The compartmental approach allowed to determine the contribution of each compartment to the overall torque. The local torque was also measured for a dry powder experiment (i.e., no liquid addition) to determine the corresponding baseline torque for each experiment (i.e., identical screw speed and MFR). Torque increase is defined in Equation 5.2:

$$\Delta Torque (Nm) = Torque_{DoE\ experiment} - Torque_{Dry\ powder} \quad [5.2]$$

#### 5.2.2.7 DATA ANALYSIS

The effect of the process settings on the torque increase and the granule size was evaluated with MODDE 12.0 software (Umetrics, Umeå, Sweden). Multiple linear regression (MLR) was performed to build effect plots. Effects were calculated as twice the coefficient of MLR-model.

### 5.3 RESULTS AND DISCUSSION

The goal of this study was to investigate the potential of torque as an IPC for granule size during TSG. Hence, the correlation between torque increase (Equation 5.2) and granule size (expressed as fines and oversized granules) was examined. In general, it is challenging to describe a size distribution by a single value. And, especially the traditional d-values (d10, d50 and d90) have difficulties to describe multimodal, irregular size distributions such as a granule size distribution according to Van Hauwermeiren et al. (25). Therefore, the fines and oversized fraction were chosen as indicators of the granule size distribution because the combination of these values better reflects the changes (i.e., granule growth or granule breakage) in a granule size distribution. In addition, full PSDs of two extremely opposite formulations were also visually inspected.

The torque value recorded during a TSG process is an overall value for the complete granulator. Nevertheless, the amount of work effectively used for granulation might be spatially different along the length of the barrel, because the screw configuration consists of kneading zones that are spatially distributed over the screws. In these different zones, the shear stress, the compaction forces, the interparticle friction and friction between particles and the barrel wall may be different than in the conveying zones (23). In addition, as it is possible that not all generated friction forces are used for the granulation process, the granule temperature increase (Equation 5.1) was also monitored along the length of the granulator to



discriminate between the friction forces that contribute to granule formation and granule heating. The applied experimental compartmental approach was therefore indispensable to determine the individual local contribution to torque increase and the local temperature increase along the length of the barrel. In addition, the compartmental approach also helped to have an enhanced process understanding.

### 5.3.1 LOCAL GRANULE SIZE DISTRIBUTION AND LOCAL TORQUE INCREASE

The stepwise formation of granules along the length of the granulation barrel (i.e., change in GSD) was compared to the local torque increase along the granulation barrel for the two most opposite DoE experiments (i.e., experiments 2 and 13 in Table 5.1). The changes in GSD and the local torque increase for DoE experiment 2 (i.e., the experiment with the lowest filling degree (i.e., lowest MFR (5 kg/h) combined with the highest screw speed (900 rpm) and the lowest L/S-ratio (18 %)) are depicted in Figure 5.2A and 5.2B, respectively. Figure 5.2C and 5.2D represent the change in GSD and local torque increase, respectively, for granulation experiment 13 in which the highest filling degree (i.e., MFR (25 kg/h) combined with the lowest screw speed (450 rpm)) and the highest L/S-ratio (27 %) were applied. It has to be emphasized that the change in granule size and torque increase along the length of the granulation barrel of these two experiments are shown as an example. The other DoE experiments were analysed in a similar way, resulting in the DoE responses presented in Table 5.1. Figure 5.2 will now be discussed in detail in following sections.

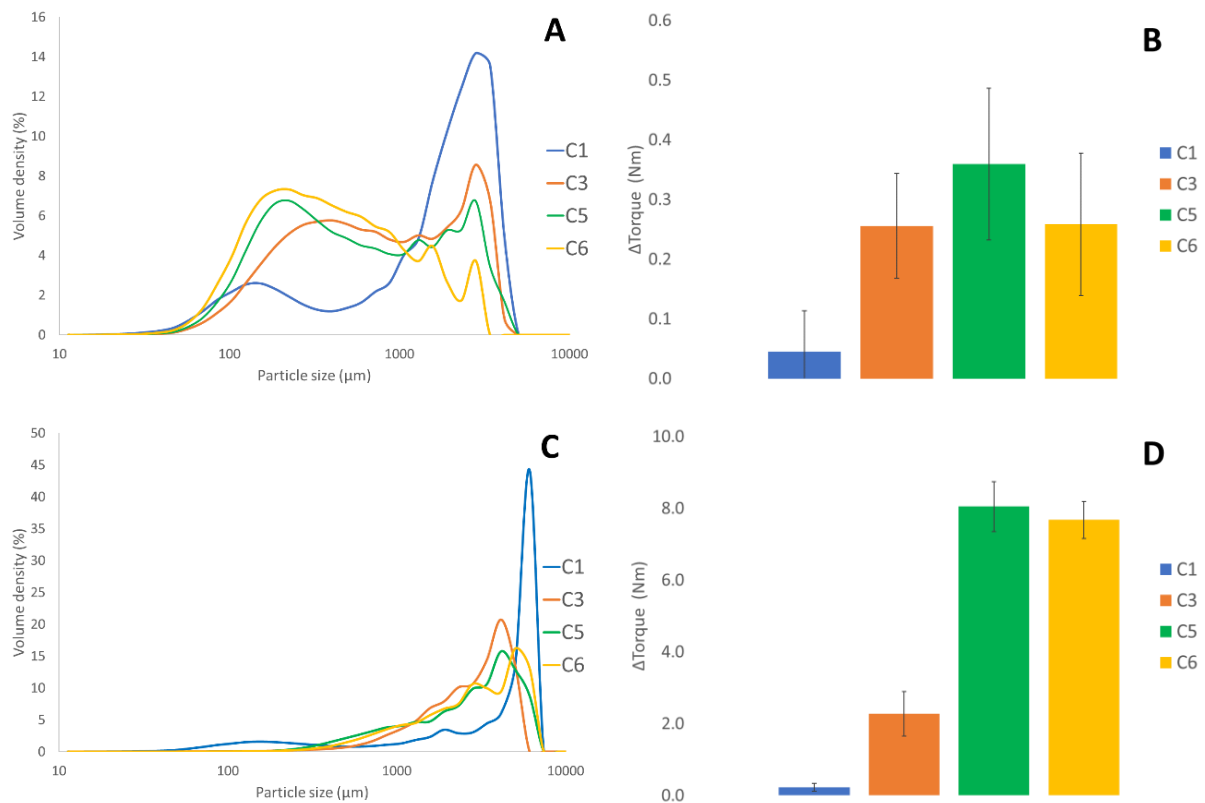


Figure 5.2: Granule size distributions (A&C) and corresponding  $\Delta$ Torque (local torque increases) (B&D) at different locations along the length of the barrel (compartment 1 (blue), compartment 3 (orange), compartment 5 (green) and compartment 6 (yellow)) for experiments 2 (MFR: 5 kg/h – L/S: 18% – Scr: 900 rpm) (A&B) and 13 (MFR: 25 kg/h – L/S: 27% – Scr: 450 rpm) (C&D). Error bars represent the standard error of the mean torque increase.

### 5.3.2 COMPARTMENT 1: THE WETTING ZONE

For all granulation experiments a large fraction of oversized granules and a smaller fraction of ungranulated powder was observed in compartment 1 (Table 5.1). This can be explained by the formation of big, wet, loose agglomerates (i.e., nuclei) when liquid enters the granulation barrel in the first compartment (i.e., wetting zone) in a process called nucleation (15,26). It has been demonstrated that the size of the nuclei depends on the size of the granulation liquid droplets (23). Therefore, the nuclei formed for the DoE experiment with the highest L/S ratio were clearly larger (Figure 5.2C; blue) compared to the lower L/S ratio experiment (Figure 5.2A; blue). In addition, a more pronounced bimodal GSD was seen for the experiment where less liquid was added due to an incomplete wetting (Figure 5.2A; blue).

The wetting zone (Compartment 1, Figure 5.1) corresponds to the conveying zone where shear forces are limited (15,23). This was clearly observed for experiment 2 (i.e., lowest L/S ratio, lowest filling degree), as no significant increase in local torque was observed in this first compartment (Figure 5.2B). However, in contrast, a small increase in torque ( $0.2 \pm 0.1$  Nm) was observed in compartment 1 when the dense, wetted mass of experiment 13 (i.e., highest L/S ratio, highest filling degree) had to be transported towards the first kneading zone, even though the conveying section of the wetting zone is very small.

The fractions of oversized nuclei and of the remaining ungranulated powder (i.e., fines) in the first compartment are plotted as a function of the torque increase for all DoE experiments in Figures 5.3A and 5.3B, respectively. During most experiments, no significant torque increase was observed, while the fines or oversized fractions were strongly affected by the process parameters (Table 5.1). A significant torque increase was observed for a few experiments (i.e., experiments 4, 6, 13, 14) which were performed at a high filling degree. However, this significant increase in torque did not unambiguously affect the GSD in a specific way (Figure 5.3). Therefore, it was concluded that the fines ( $R^2=0.11$ ) and oversized ( $R^2=0.0037$ ) fractions in compartment 1 were not correlated to the torque increase.

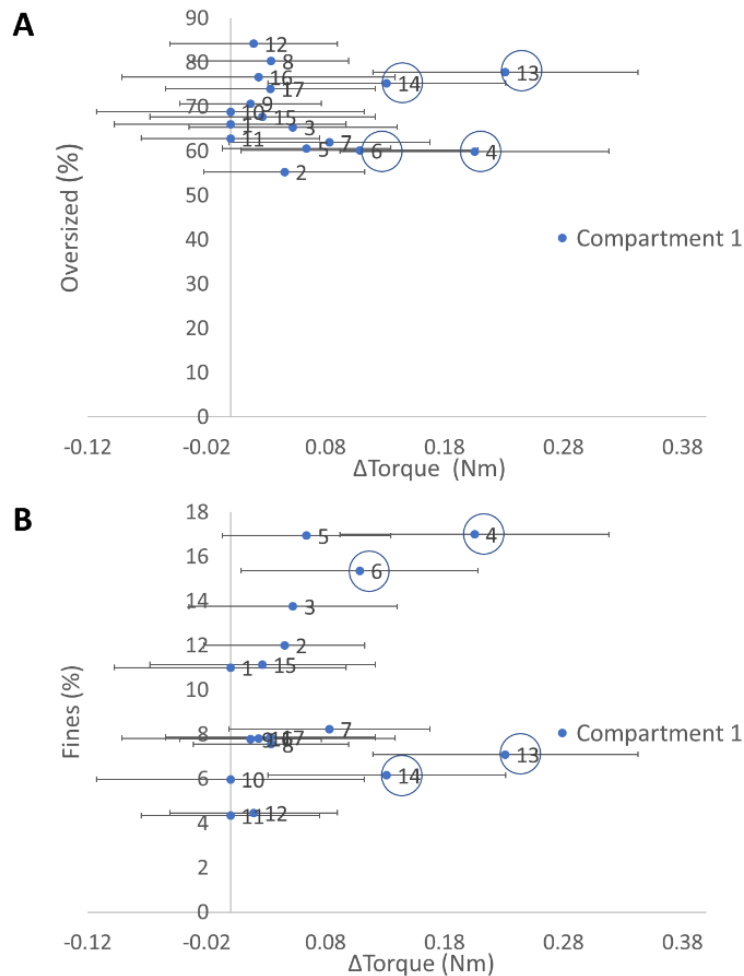


Figure 5.3: Fraction of oversized granules (A) and fines (B) as a function of  $\Delta$ Torque (torque increase) in the wetting zone. Horizontal error bars represent the standard error of the mean torque increase.

The effect plots in Figure 5.4A show the main effects of the process parameters upon torque increase and granule size (i.e., amount of fines and oversized granules) in the wetting zone. Each bar in the plot represents the average change in response when the corresponding process parameter is changed from its lowest to its highest value, while the remaining process parameters are kept at their intermediate level. The error bars represent 95 % confidence intervals. An effect is significantly different from zero when the error bars do not intersect with the zero baseline. In the wetting zone, torque increase was significantly affected by MFR, but it has to be noted that the small increase is not physically relevant as the torque increase was limited to 0.1 Nm. Furthermore, in this compartment, the granule size was highly affected by L/S ratio. In addition, the fines fraction was also slightly affected by MFR. Increasing the MFR resulted in slightly more fines (+ 3 %), suggesting that the liquid penetration is impeded by a denser powder bed. Moreover, increasing MFR also results in more oversized nuclei

because larger liquid drops are added as a higher liquid flow rate is needed at high MFR. In addition, coalescence of smaller nuclei is also favoured at a higher filling degree. The fact that granule size and torque are not influenced by the same process parameters supports the lack of a correlation between torque and granule size (Figure 5.3).

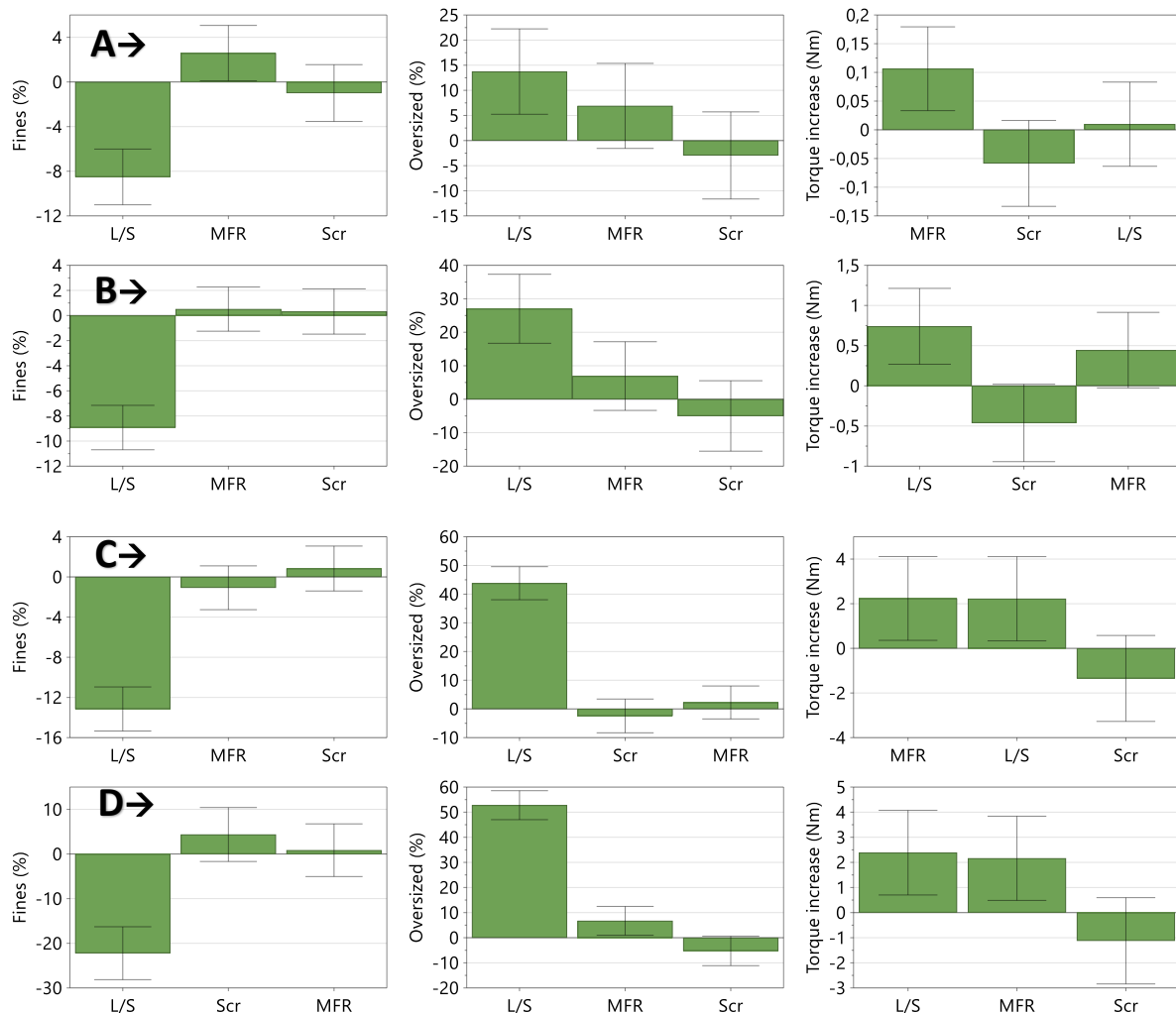


Figure 5.4: Effect plots showing the influence of process parameters on fines, oversized granules and torque increase in the first compartment (wetting zone) (A), the third compartment (after the first kneading zone) (B), the fifth compartment (after the second kneading zone) (C) and the sixth compartment (at the outlet) (D). L/S: liquid-to-solid; MFR: mass feed rate; Scr: screw speed.

### 5.3.2.1 COMPARTMENT 3: AFTER THE FIRST KNEADING ZONE

In the first kneading zone, the nuclei are forced between the barrel wall of the granulator and the flight tip of the kneading elements in compartment 2. According to Pradhan et al. this results in breakage of the nuclei and ultimately in an effective liquid redistribution (27). According to Verstraeten et al., the breakage of the oversized nuclei occurs simultaneously

with consolidation and the further agglomeration of ungranulated powder due to the process of layering (23). Since consolidation and layering are favoured at higher L/S ratio (23,28), a more narrow GSD was obtained at higher L/S ratio (Figure 5.2C), compared to lower L/S ratio (Figure 5.2A), confirming the findings of Verstraeten et al. (23). The change in GSD was concomitant with a significant increase in torque for both experiments (Figure 5.2B, 5.2D; orange). The torque increase was more pronounced at a high filling degree and high L/S ratio. In general, the torque increases at higher L/S ratio until a critical L/S ratio is reached with the formation of over-wetted plastic particles, resulting in a lower torque (20). In this study, this critical point is not reached and torque only increased at higher L/S ratio. At high MFR and high L/S ratio, a heavy wetted powder mass was created, enhancing the level of shear mixing with high friction forces and resulting in a sluggish flow of the wetted mass with a longer residence time. Therefore, more energy is required to convey the mass and higher torque values are recorded (Figure 5.2D) (21,28).

Figure 5.5 shows the amount of fines (Figure 5.5B) and oversized (Figure 5.5A) granules in the wetting zone (blue) and after the first kneading zone (orange) as a function of the torque increase, the torque increase of compartment 3 being the combined increase in torque caused by compartments 1 to 3 compared to the baseline torque. A significant increase in torque provoked by kneading in the first kneading zone is observed for each experiment (Figure 5.5A and B, orange). Lower L/S ratios (i.e., lower than the intermediate level: experiments 1-6) resulted in a limited torque increase, more fines and less oversized granules, while the opposite was observed for experiments processed at a higher L/S ratio (i.e., higher than the intermediate level: experiments 10-14) (Table 5.1). The highest increase in torque combined with the largest oversized and lowest fines fraction was observed for DoE experiment 13 (25 kg/h – 450 rpm – 27% L/S ratio). The combination of the high MFR and low screw speed results in a high filling degree and high residence time inside the granulator, favouring extensive granule growth and ultimately resulting in a higher resistance to convey the dense mass of granules and thus an extensive increase in torque is observed (13). Regardless of the applied process parameters, a similar granulation mechanism occurs in the first kneading zone, yielding a more monomodal GSD with less ungranulated particles and less oversized granules compared to the wetting zone (Figure 5.2A and 5.2C, Table 5.1). A linear correlation ( $R^2=0.74$ ) between the oversized fraction and the torque increase caused by the first to third

compartment was seen. A weak linear correlation ( $R^2=0.35$ ) was observed for the fines fraction. As observed in Figure 5.5B, the amount of fines is reduced to zero and reaches an asymptote for torque values superior to 1.0 Nm as all particles are granulated. The correlation was close to an exponential with negative power ( $R^2=0.70$ ).

The observed correlations can also be explained by a complete DoE analysis after the first kneading zone. As already mentioned in this section, nuclei are broken and liquid is redistributed in the first kneading zone. More liquid promotes an enhanced consolidation accompanied with layering and coalescence, resulting in granule growth. This is clearly shown in the effect plot (Figure 5.4B) with a large significant effect of L/S ratio, reducing the fines and increasing the oversized granules. A large significant effect of L/S ratio was seen on torque increase. Moreover, it has to be noted that the interplay between a high MFR and low screw speed is also seen in the effect plot for torque increase, although it is not significant. The same trend was also observed for the effect on oversized granule, indicating granule growth, but the effect was even less significant. As both granule formation and torque increase are largely dominated by the L/S ratio, this suggest that at this stage of the granulation process, torque might have some potential as an IPC for granule size during a TSG process.

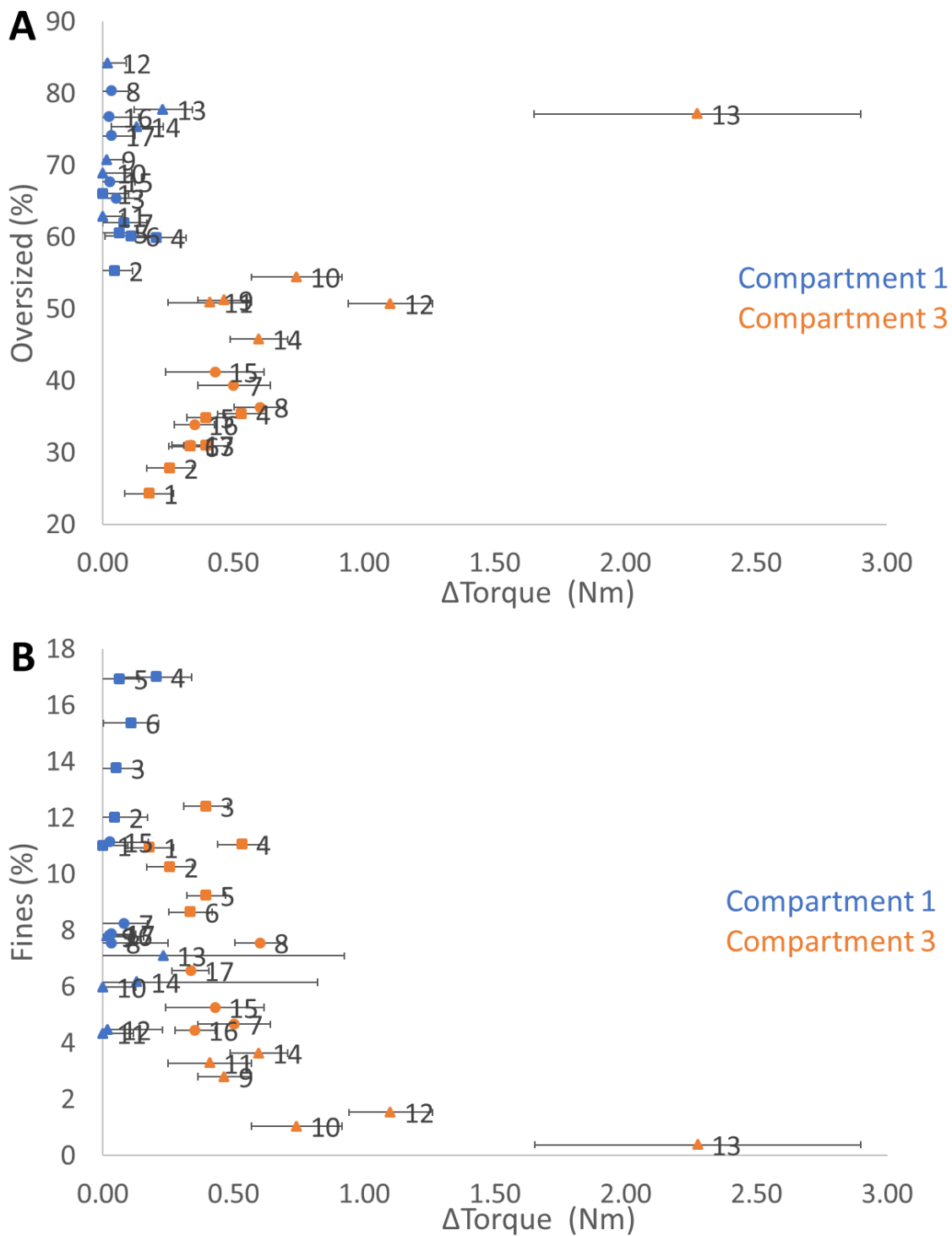


Figure 5.5: Fraction of oversized granules (A) and fines (B) as a function of  $\Delta$ Torque (torque increase) caused by compartment 1 (blue) and compartment 1 to 3 (orange). Horizontal error bars represent the standard error of the mean torque increase. Experiments with a L/S ratio lower than the intermediate level are plotted as  $\square$ , while experiments with a L/S ratio higher than the intermediate level are plotted as  $\Delta$ .



## 5.3.2.2 COMPARTMENT 5: AFTER THE SECOND KNEADING ZONE

A different change in GSD was observed after the second kneading zone (i.e., compartment 5) as the GSD change depended on the available amount of granulation liquid. This is illustrated by experiments 2 (low L/S) and 13 (high L/S) in Figure 5.2. At low L/S ratio, weaker liquid bonds between the powder particles were formed in compartment 3 (23,28). Therefore, more brittle granules were formed in the first kneading zone and breakage of those brittle granules occurred when passing through the second kneading zone. Hence, the amount of fines increased, while the amount of oversized granules decreased (Figure 5.2A; green). Breakage of brittle granules (produced with lower L/S) occurred without significant torque increase (Figure 5.2B; green). Verstraeten et al. observed a comparable change in GSD after compartment 5 for a hydrophilic and hydrophobic formulation studied at lower L/S ratio (23). In contrast, a different mechanism was observed when higher amounts of granulation liquid were added (i.e., at high L/S). An excess of granulation liquid was squeezed towards the surface in the first kneading compartment, leading to even more coalescence of colliding granules in the second kneading compartment (23,26). Consequently, the amount of fines decreased, while the amount of oversized granules increased (Figure 5.2C, green). As large, plastic granules were further densified, consolidated and transported in the second kneading zone, additional compaction and shear forces were generated which caused a significant increase in torque (Figure 5.2D; green). Verstraeten et al. only observed a similar change in GSD caused by the second kneading zone when granulating a hydrophilic formulation at high L/S ratio, while this did not occur for the hydrophobic formulation (23) showing the impact of the formulation properties on granulation behaviour as well.

In Figure 5.6, the torque increase in the second kneading zone could be determined by comparing the torque increase caused by the compartment 1 to 3 (orange) and the torque increase caused by compartments 1 to 5 (green). It has to be noted that the x-axis was interrupted for scaling reasons on Figure 5.6 due to the enormous torque increase of experiment number 13. Generally, an indication of the change in GSD can be observed by comparing the amount in fines and oversized granules at zone 3 and 5. The change caused by the second kneading zone depended on the L/S ratio for all experiments. A decrease in the amount of oversized granules in combination with an increase in the amount of fines was observed at compartment 5 at lower L/S ratios (i.e., experiments 1, 2, 3, 4, 5 and 6), indicating

that the second kneading zone mainly caused breakage of the brittle granules. In contrast, a clear increase in the oversized fraction and a concomitant drop in fines was observed at the highest L/S ratio at compartment 5 (i.e., experiments 10, 11, 12, 13 and 14). For all experiments a higher absolute value in torque increase was provoked by the second kneading zone in comparison to the first kneading zone (Figure 5.6A and 5.6B). However, the torque increase was minimal for experiments 1, 2, 5, 7, 10, 11 and 12 (Figure 5.6). As these experiments were not only processed at low L/S ratio but also at an intermediate and high level, the small increase in torque was attributed to their lower filling degree. Nevertheless, this minimal torque increase in the second kneading zone was either related to breakage (i.e., experiment 1, 2 and 5) or further consolidation (i.e., experiments 7, 10, 11 and 12). Since limited energy was needed to break or to further agglomerate the granules coming from the first kneading zone when the filling level in granulator was lower, it explains the observed minimal torque increase. At higher filling levels combined with low (i.e., experiments 3, 4 and 6), intermediate (i.e., experiments 8, 15, 16 and 17) or high L/S (i.e., experiments 13 and 14), the conveying, shearing and compaction of the denser mass caused a significant increase in torque (Figure 5.6). As aforementioned, the results at low filling degree showed that limited energy was needed to break or further consolidate granules. This implies that not all energy that is put into the granulator is used for granulation but that it is rather absorbed by the powder at high filling degree, especially experiment 13 showed an immense increase in torque (Figure 5.6).

In summary, a plateau for the amount in oversized granules was observed around 75 % (Figure 5.6A). This can be due to some energy which was absorbed and therefore not used for the granulation process. Consequently, the linear correlation between the torque increase and the fraction in fines ( $R^2=0.18$ ) and oversized ( $R^2=0.30$ ) granules was poor after compartment 5 (Figure 5.6).

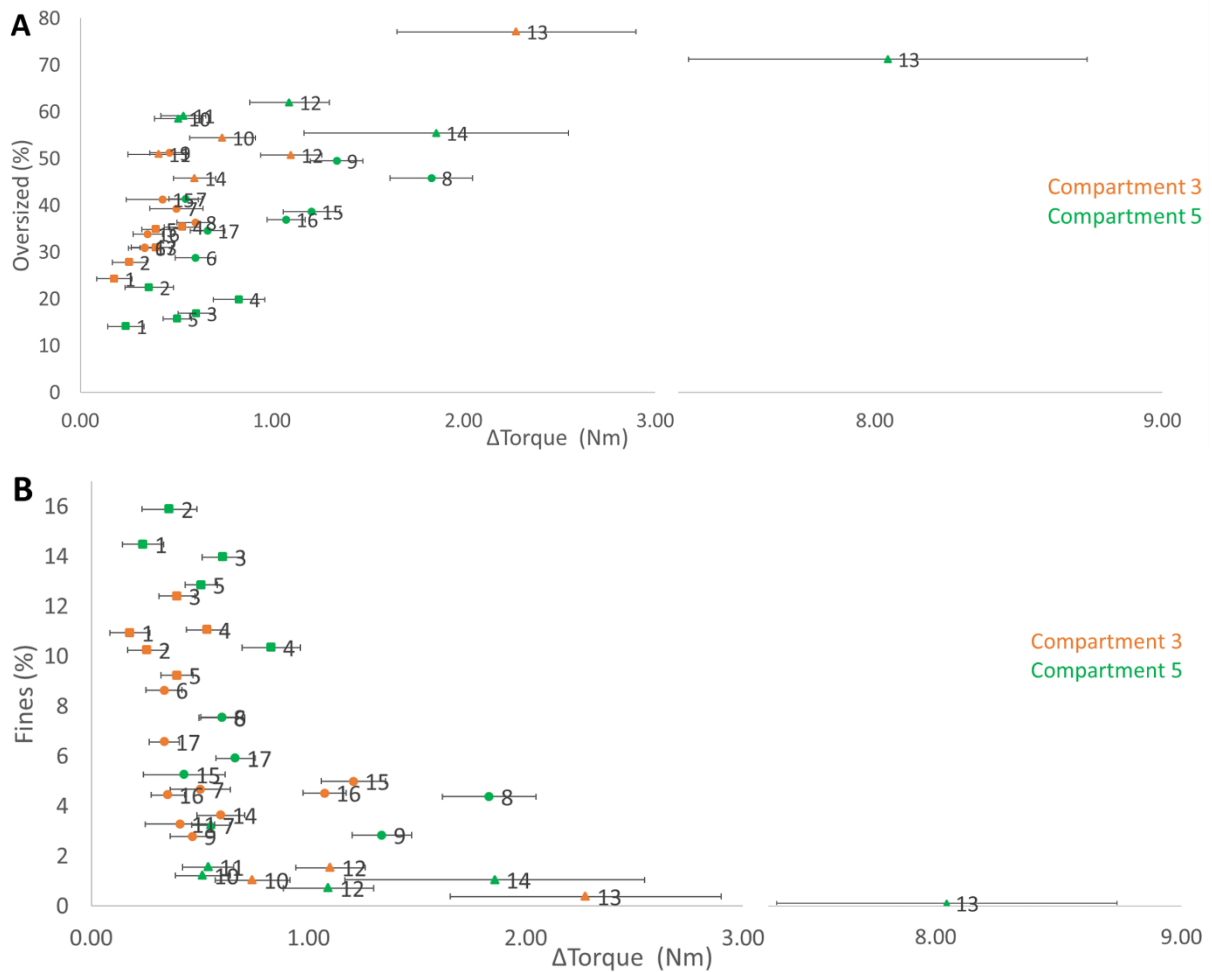


Figure 5.6: Fraction of oversized granules (A) and fines (B) as a function of  $\Delta$ Torque (torque increase) caused by compartment 1 to 3 (orange) and compartment 1 to 5 (green). Horizontal error bars represent the standard error of the mean torque increase. Experiments with a L/S ratio lower than the intermediate level are plotted as  $\square$ , while experiments at the highest L/S are plotted as  $\Delta$ .

The effect plots for compartment 5 (Figure 5.4C) show the dominating effect of L/S ratio on the amount of fines and oversized granules. The torque increase is now significantly affected by MFR and L/S ratio. The influence of these process parameters is equally important for the torque increase. Since torque increase and granules size responses are not significantly affected by the same process parameters, it proves in addition to what has been discussed previously in this section why a correlation between amount in fines and oversize granules and torque increase is missing after the second kneading zone.

## 5.3.2.3 COMPARTMENT 6: AT THE OUTLET

The effect of the two small chopper elements at the end of the screw configuration also depended on the applied granulation settings as illustrated for experiments 2 and 13. The aforementioned brittle granules of experiment 2 (i.e., lowest L/S ratio, lowest filling degree) were further broken by the chopper elements (Figure 5.2A; yellow), whereas the change in GSD for experiment 13 (i.e., highest L/S ratio, highest filling degree) was completely different (Figure 5.2C; yellow). Surprisingly, the amount of oversized granules even increased for this experiment, while the amount of smaller granules decreased, implying that further agglomeration of the granules occurred. It appeared that the plastic granules were slightly more affected by shear and compressive forces in the small region at the end of the screw configuration (Figure 5.2C; yellow). However, despite the change in GSD, the torque increase due to two additional kneading elements was not significantly different from the previous compartment (Figure 5.2B and 5.2D; yellow).

Figure 5.7 shows the change in the fraction of fines and oversized granules caused by the two small chopper elements as a function of the change in torque increase. Similar to Figure 5.6, the x-axis was interrupted for scaling reasons. An increase in the fraction of oversized agglomerates from compartment 5 to 6 was observed for experiment 12, 13 and 14. These three experiments were granulated with the highest L/S ratio and a high filling degree, creating an extrusion effect between the free volume of chopper elements. The amount of fines remained unchanged for these experiments, indicating the lack of breakage. Breakage of the granules was clearly seen for all other experiments, since the amount of oversized granules decreased and the amount of fines increased from compartment 5 to 6. This effect was more pronounced for the experiments performed at a lower L/S ratio (i.e., experiments 1, 2, 3, 4, 5 and 6), as these brittle granules were more susceptible to breakage (23,28). Furthermore, it has to be noted that a clear increase in torque was not observed for any of these experiments. Thus, although a change in GSD was caused by the small chopping elements, it was not accompanied with a clear change in torque.

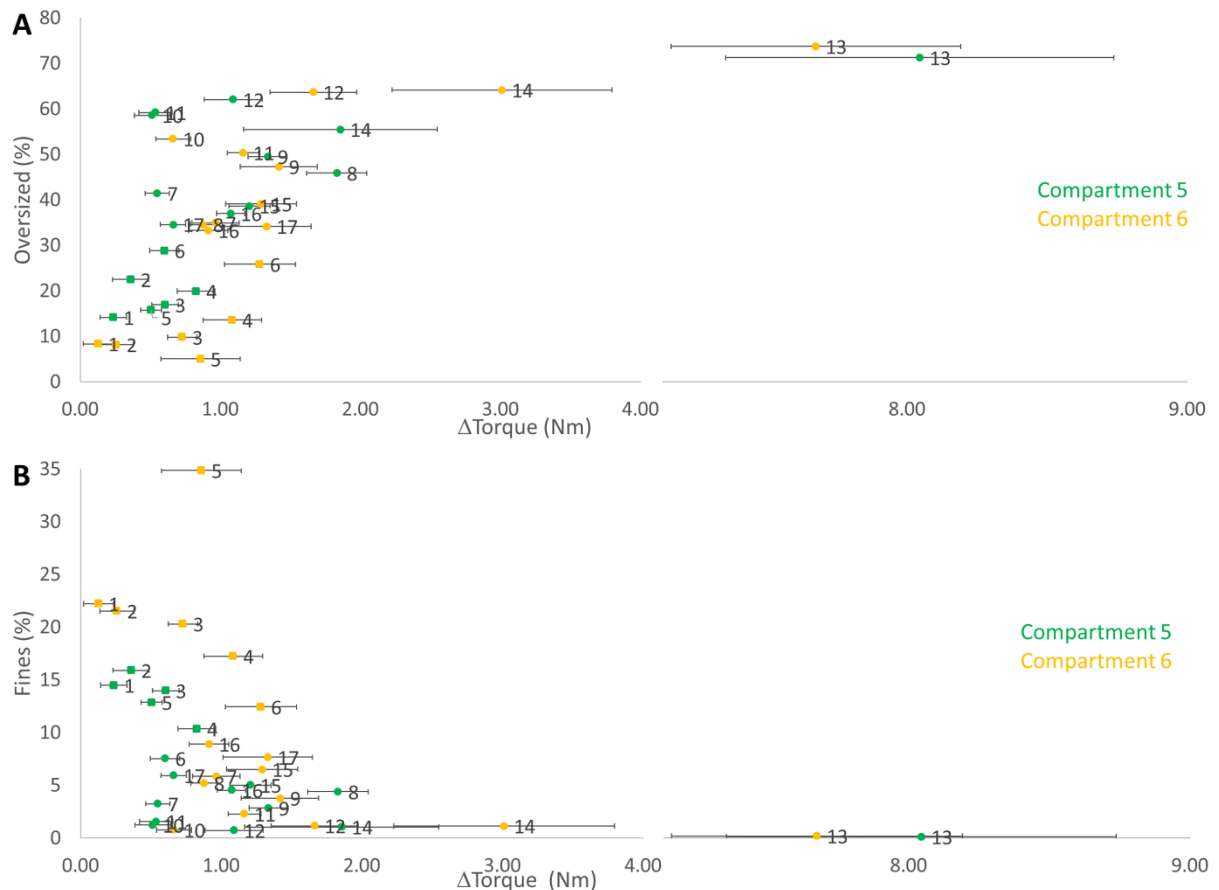


Figure 5.7: Fraction of oversized granules (A) and fines (B) as a function of  $\Delta$ Torque (torque increase) caused by compartment 1 to 5 (green) and the full configuration (yellow). Horizontal error bars represent the standard error of the mean torque increase. Experiments with a L/S ratio lower than the intermediate level are plotted as  $\square$ .

The effect plots (Figure 5.4D) for the complete configuration show that the effect of L/S ratio on granule size is even more pronounced than after the second kneading zone. After the small chopper elements at the end of the screws, the application of low L/S or higher L/S – low filling degree caused breakage while high L/S – high filling degree led to further agglomeration. Therefore, the fraction of oversized granules was also significantly affected by MFR. The influence of MFR and L/S ratio was not equally important as for their effect on torque increase.

Finally, the correlation between the overall torque and the final granule size after granulation was also plotted in Figure 5.8, because the overall torque is the torque that is monitored during granulation and it is this torque value that would be used as an IPC. A correlation was clearly missing (fines ( $R^2=0.18$ ) and oversized ( $R^2=0.40$ )) and, therefore, it is not possible to monitor the granule size by the use of torque as an IPC during a TSG process.

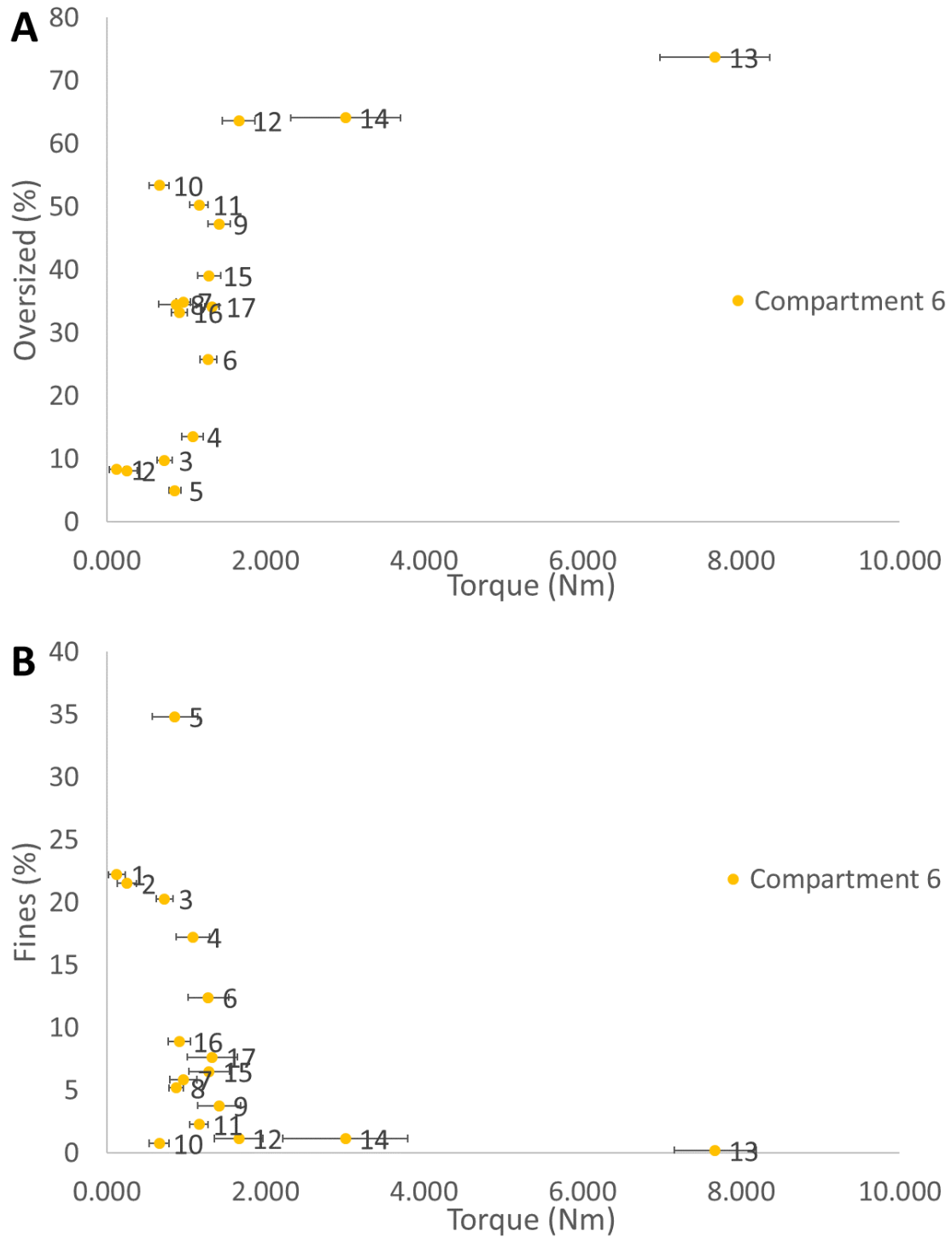


Figure 5.8: Fraction of oversized granules (A) and fines (B) as a function of overall torque caused by the full configuration (yellow). Horizontal error bars represent the standard error of the mean torque.

### 5.3.3 CORRELATION BETWEEN TORQUE INCREASE AND GRANULE TEMPERATURE INCREASE

The previous section has demonstrated that the increase in torque could not be related to the change in GSD, as torque increase was affected by both MFR and L/S ratio, while granule size was mainly affected by L/S ratio rather than MFR.

As torque is also resulting from shear and friction forces, and as it is known that friction forces are related to the generation of heat (14), the temperature of the granules along the length of the granulator was monitored. The increase in granule temperature as a function of the increase in torque for each DoE experiment at each location along the length of the barrel is shown in Figure 5.9. An increase of up to 2 °C in granule temperature occurred for the nuclei in the wetting zone, although a limited amount of friction forces was present in this compartment. The temperature increase in this first compartment is explained by the adsorption of water on dry powder during the wetting of the powder, which was demonstrated by Stauffer et al. to be an exothermic reaction (chapter 4) (29). At the following granulator compartments, a higher increase in torque resulted in a higher increase in granule temperature (linear correlation,  $R^2 = 0.70$ ). The increase in granule temperature along the length of the granulator is now explained for experiment 13. This experiment is highlighted for each location on Figure 5.9. As the highest amount of L/S ratio was used for this granulation experiment, only 7 % of the powder bed remained ungranulated in the wetting zone (Figure 5.2C). Hence, a high increase in granule temperature (1.36 °C) was observed at the first compartment due to complete wetting (29). In section 5.3.1.2, it was already demonstrated that these nuclei were broken and that the remaining ungranulated powder was granulated in the first kneading zone (Figure 5.2), while a significant change in torque increase (2.3 Nm) was noticed (Figure 5.2B). Figure 5.9 shows that the processing of the material through the first kneading zone resulted in a high granule temperature increase (4.3 °C). This suggests that part of the friction forces that were generated in the first kneading compartment, were used to heat up the granules and indicates that the energy which was introduced into the granulator system, was partly absorbed by the materials. An increase in the material temperature before the second kneading zone was also observed by Meier et al. (30). In that study, the material temperature was measured on top of the screws and it was concluded that a higher filling degree resulted in higher increase of temperature. This is in accordance with the results from this study as shown in Figure 5.6 (experiment 13 corresponded with the

highest filling degree). Further, torque increased (8.1 Nm) in the second kneading zone and an even higher granule temperature increase (8.8 °C) was measured at location 5. Finally, a non-significant change in torque was seen when using the small kneading elements at the end of the screw configuration, together with a non-significant change in granule temperature. Thus, a part of the energy was not involved in the granulation process, but used to heat the processed granules. Consequently, these results further explain the missing correlation between the torque increase and the granule size.

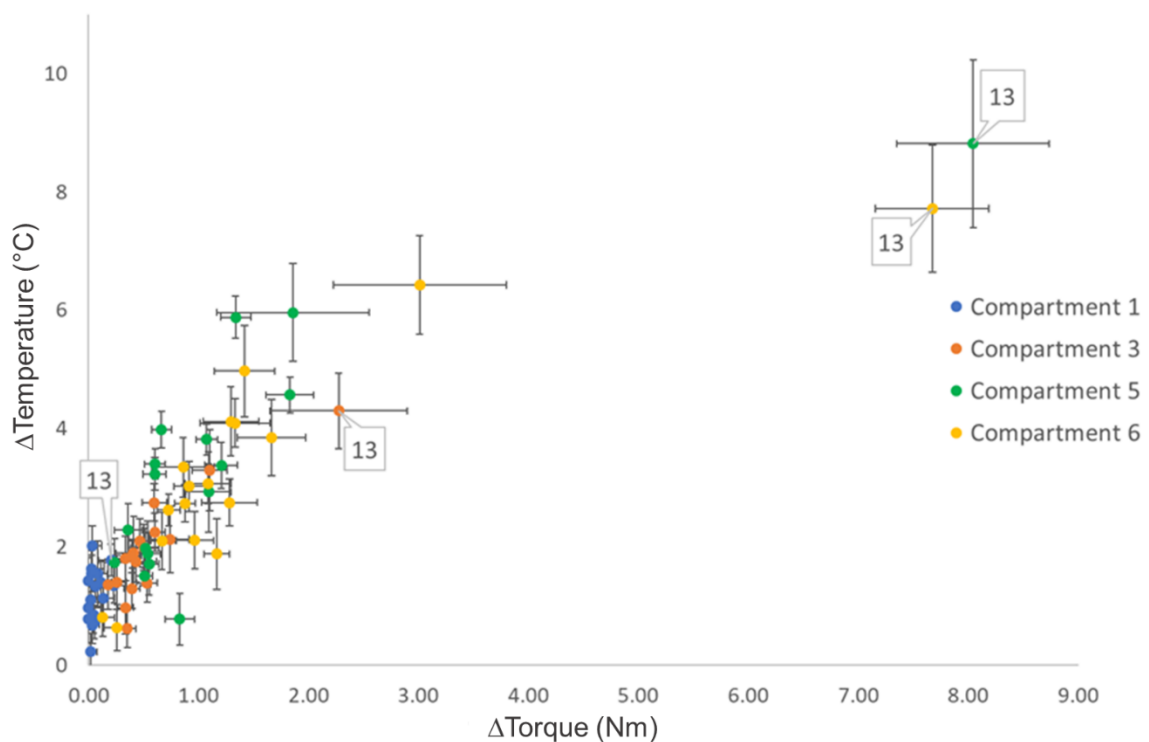


Figure 5.9: Correlation plot for each DoE experiment at each location (compartment 1 (blue), compartment 3 (orange), compartment 5 (green), compartment 6 (yellow)) between  $\Delta$ Temperature (temperature increase) and  $\Delta$ Torque (torque increase). Horizontal error bars represent the standard error of the mean torque increase, while the vertical error bars represent the standard error of the mean temperature increase.

## 5.4 CONCLUSIONS

In this study, the potential use of torque as an IPC during a TSG process was investigated. A compartmented granulator was used to determine the local granule size, the local torque increase and the local granule temperature increase along the length of the barrel. The only observed correlation was between the granule size and torque increase after the first



kneading zone ( $R^2 = 0.74$ ). In this kneading zone, breakage of the oversized nuclei occurred simultaneously with consolidation and further agglomeration of ungranulated powder. Generally, a higher torque increase promoted granule growth. In the second kneading zone, the torque was significantly higher when applying a higher fill-level of the granulator. However, the effect on GSD could either be dominated by breakage or granule growth. Therefore, a poor correlation was found between the granule size and the torque increase. Furthermore, it was seen that the small kneading elements at the end of the screw configuration did not significantly change the torque, although GSD was affected. The absence of correlation could be explained as well by the fact that a higher granule temperature was measured along the length of the granulator when a higher increase in torque was recorded. This suggests that a part of the energy introduced into the system is absorbed by the materials to heat them up, rather than for granule growth. Therefore it was concluded that torque could not be used as an IPC to monitor the final wet granule size in a TSG process.

## 5.5 REFERENCES

1. Ferreira AP, Menezes JC, Tobyn M. MULTIVARIATE ANALYSIS IN THE PHARMACEUTICAL INDUSTRY. Elsevier; 2018. 434 p.
2. Yu LX, Amidon G, Khan MA, Hoag SW, Polli J, Raju GK, et al. Understanding Pharmaceutical Quality by Design. *AAPS J*, 2014;16(4):771–83. Available from: <http://link.springer.com/10.1208/s12248-014-9598-3>
3. FDA. Guidance for Industry PAT: A Framework for Innovative Pharmaceutical Development, Manufacturing, and Quality Assurance. FDA Off Doc. 2004;(September):16.
4. Vargas JM, Nielsen S, Cárdenas V, Gonzalez A, Aymat EY, Almodovar E, et al. Process analytical technology in continuous manufacturing of a commercial pharmaceutical product. *Int J Pharm*, 2018;538(1–2):167–78. Available from: <https://doi.org/10.1016/j.ijpharm.2018.01.003>
5. Glassey J, Gernaey K V, Clemens C, Schulz TW, Oliveira R, Striedner G. Process analytical technology ( PAT ) for biopharmaceuticals. 2011;369–77.
6. ICH. Pharmaceutical Development Q8. ICH Harmon Tripart Guidel. 2009;8(August):1–28.
7. Leuenberger H, Puchkov M, Krausbauer E, Betz G. Manufacturing pharmaceutical granules: Is the granulation end-point a myth? *Powder Technol*, 2009;189(2):141–8. Available from: <http://dx.doi.org/10.1016/j.powtec.2008.04.005>
8. Kristensen J, Schæfer T, Kleinebudde P. Direct Pelletization in a Rotary Processor Controlled by Torque Measurements. I. Influence of Process Variables. *Pharm Dev Technol*. 2000;5(2):247–56.
9. Kristensen J, Schæfer T, Kleinebudde P. Direct pelletization in a rotary processor controlled by torque measurements. II. Effects of Changes in the Content of Microcrystalline Cellulose. *Pharm Dev Technol*. 2000;2(3):45–42.
10. Kumar A, Dhondt J, Vercruyssen J, De Leersnyder F, Vanhoorne V, Vervaet C, et al. Development of a process map: A step towards a regime map for steady-state high shear wet twin screw granulation. *Powder Technol*, 2016;300:73–82. Available from: <http://dx.doi.org/10.1016/j.powtec.2015.11.067>
11. Kumar A, Alakarjula M, Vanhoorne V, Toiviainen M, De Leersnyder F, Vercruyssen J, et al. Linking granulation performance with residence time and granulation liquid distributions in twin-screw granulation: An experimental investigation. *Eur J Pharm Sci*, 2016 Jul 30;90:25–37. Available from: <https://www.sciencedirect.com/science/article/pii/S0928098715300956>
12. Dhenge RM, Washino K, Cartwright JJ, Hounslow MJ, Salman AD. Twin screw granulation using conveying screws: Effects of viscosity of granulation liquids and flow of powders. *Powder Technol*. 2013;238:77–90.

13. Dhenge RM, Fyles RS, Cartwright JJ, Doughty DG, Hounslow MJ, Salman AD. Twin screw wet granulation: Granule properties. *Chem Eng J*, 2010;164(2–3):322–9. Available from: <http://dx.doi.org/10.1016/j.cej.2010.05.023>
14. Vercruysse J, Córdoba Díaz D, Peeters E, Fonteyne M, Delaet U, Van Assche I, et al. Continuous twin screw granulation: Influence of process variables on granule and tablet quality. *Eur J Pharm Biopharm*, 2012;82(1):205–11. Available from: <http://dx.doi.org/10.1016/j.ejpb.2012.05.010>
15. Vercruysse J, Burggraeve A, Fonteyne M, Cappuyns P, Delaet U, Van Assche I, et al. Impact of screw configuration on the particle size distribution of granules produced by twin screw granulation. *Int J Pharm*, 2015;479(1):171–80. Available from: <http://dx.doi.org/10.1016/j.ijpharm.2014.12.071>
16. Vercruysse J, Peeters E, Fonteyne M, Cappuyns P, Delaet U, Van Assche I, et al. Use of a continuous twin screw granulation and drying system during formulation development and process optimization. *Eur J Pharm Biopharm*, 2015;89:239–47. Available from: <http://dx.doi.org/10.1016/j.ejpb.2014.12.017>
17. Vercruysse J, Delaet U, Van Assche I, Cappuyns P, Arata F, Caporicci G, et al. Stability and repeatability of a continuous twin screw granulation and drying system. *Eur J Pharm Biopharm*, 2013;85(3 PART B):1031–8. Available from: <http://dx.doi.org/10.1016/j.ejpb.2013.05.002>
18. Vanhoorne V, Bekaert B, Peeters E, De Beer T, Remon J-P, Vervaet C. Improved tableability after a polymorphic transition of delta-mannitol during twin screw granulation. *Int J Pharm*, 2016 Jun 15;506(1–2):13–24.
19. Vanhoorne V, Vanbillemont B, Vercruysse J, De Leersnyder F, Gomes P, De Beer T, et al. Development of a controlled release formulation by continuous twin screw granulation: Influence of process and formulation parameters. *Int J Pharm*, 2016;505(1–2):61–8. Available from: <http://dx.doi.org/10.1016/j.ijpharm.2016.03.058>
20. Vanhoorne V, Janssens L, Vercruysse J, De Beer T, Remon JP, Vervaet C. Continuous twin screw granulation of controlled release formulations with various HPMC grades. *Int J Pharm*, 2016;511(2):1048–57. Available from: <http://dx.doi.org/10.1016/j.ijpharm.2016.08.020>
21. Dhenge RM, Cartwright JJ, Hounslow MJ, Salman AD. Twin screw wet granulation: Effects of properties of granulation liquid. *Powder Technol*, 2012;229:126–36. Available from: <http://dx.doi.org/10.1016/j.powtec.2012.06.019>
22. Tu W, Ingram A, Seville J. Regime map development for continuous twin screw granulation. *Chem Eng Sci*, 2013;87:315–26. Available from: <http://dx.doi.org/10.1016/j.ces.2012.08.015>
23. Verstraeten M, Van Hauwermeiren D, Lee K, Turnbull N, Wilsdon D, am Ende M, et al. In-depth experimental analysis of pharmaceutical twin-screw wet granulation in view of detailed process understanding. *Int J Pharm*, 2017;529(1–2):678–93. Available from: <http://dx.doi.org/10.1016/j.ijpharm.2017.07.045>

24. Fonteyne M, Correia A, Plecker D, Vercruysse J, Ili I, Zhou Q, et al. Impact of microcrystalline cellulose material attributes : A case study on continuous twin screw granulation. 2015;478:705–17.
25. Van Hauwermeiren D. On the Simulation of Particle Size Distributions in Pharmaceutical Twin-Screw Wet Granulation, Ghent University; 2020. Available from: <https://biblio.ugent.be/publication/8667346>
26. Dhenge RM, Cartwright JJ, Hounslow MJ, Salman AD. Twin screw granulation: Steps in granule growth. *Int J Pharm.* 2012 Nov;438(1–2):20–32.
27. Pradhan SU, Sen M, Li J, Litster JD, Wassgren CR. Granule breakage in twin screw granulation: Effect of material properties and screw element geometry. *Powder Technol* 2017;315:290–9. Available from: <http://dx.doi.org/10.1016/j.powtec.2017.04.011>
28. Kumar A, Vercruysse J, Bellandi G, Gernaey K V., Vervaet C, Remon JP, et al. Experimental investigation of granule size and shape dynamics in twin-screw granulation. *Int J Pharm.* 2014;475(1–2):485–95.
29. Stauffer F, Ryckaert A, Vanhoorne V, Van Hauwermeiren D, Funke A, Djuric D, et al. In-line temperature measurement to improve the understanding of the wetting phase in twin-screw wet granulation and its use in process development. *Int J Pharm.* 2020;584.
30. Meier R, Moll KP, Krumme M, Kleinebudde P. Impact of fill-level in twin-screw granulation on critical quality attributes of granules and tablets. *Eur J Pharm Biopharm* 2017;115:102–12. Available from: <http://dx.doi.org/10.1016/j.ejpb.2017.02.010>

**6 TPLS AS PREDICTIVE  
PLATFORM FOR TWIN-  
SCREW WET GRANULATION  
PROCESS AND  
FORMULATION  
DEVELOPMENT**

**ABSTRACT**

In recent years, the interest in continuous manufacturing techniques, such as twin-screw wet granulation, has increased. However, the understanding of the influence of the combination of raw material properties and process settings upon the granule quality attributes is still limited. In this study, a TPLS model was developed to link raw material properties, the ratios in which these raw materials were combined and the applied process parameters for the twin-screw wet granulation process with the granule quality attributes. A raw material property database including dry (size, flow, etc.) and wet (solubility, contact angle, etc.) properties was first established for Active Pharmaceutical Ingredients (APIs) and excipients. Hereafter 10 different formulations consisting of an API, a filler and a binder were selected, and the API content was varied at three levels (10, 40 and 70 %) for each formulation. A total of 30 powder mixtures were subsequently granulated under different twin-screw granulation process settings. Finally, granule quality attributes (i.e., friability, fines and oversized size fraction and angle of repose) were determined for all granules after oven-drying. TPLS highlighted L/S ratio as the most influencing process setting and dissolution rate, solubility, compressibility, density and water binding capacity as the most influencing raw material properties upon granule quality. In addition, the predictive ability of the TPLS model was used to find a suitable combination of formulation composition and twin-screw granulation process settings for a new API leading to desired granule quality attributes. In a next step, these predicted granule quality attributes were compared to the experimental values. Although the predictions were not optimal over the entire examined twin-screw granulation process settings space, it was possible to predict a suitable combination of process settings and formulation properties for the new API which resulted in the desired granule quality attributes. As TPLS is a self-learning, data-driven platform, the inclusion of more data would improve the predictive ability. Overall, this study helped to better understand the link between raw material properties, formulation composition and process settings on granule quality attributes. In addition, as TPLS can provide a reasonable starting point for formulation and process development for new APIs, it can reduce the experimental development efforts and consequently the consumption of expensive (and often limited available) new API.

## 6.1 INTRODUCTION

Twin-screw wet granulation is the most studied continuous wet granulation technique (1). Generally, the granules' critical quality attributes (CQAs) depend on the properties of the selected raw materials, the ratio in which these raw materials are combined and the applied process settings during granulation. Understanding how the combination of these three aspects affects granule quality is not only an advantage during manufacturing, it is extremely beneficial during the formulation and continuous twin-screw wet granulation process design for a new API (2). Especially when limited amounts of expensive API are available during the early drug product development stages (3,4).

Multiple studies have investigated the effect of twin-screw granulation process parameters – such as liquid-to-solid (L/S) ratio, mass feed rate (MFR) and screw speed – upon granule quality (5–11). Generally, L/S ratio was the most influencing process parameter. However, contradictory results were often seen for the effect of MFR and screw speed upon the granules' CQAs, due to the different formulations under study. Others have investigated the effect of raw materials properties on granule quality (5,12). However, these investigations were only limited to one ingredient at a time, because different compositions of studied formulations require different process settings, resulting in a complicated data analysis (13).

Willecke et al. (14,15) were able to study more divergent formulations by investigating the impact of excipient characteristics in a two-part study. In the first part, an extensive raw material characterization was performed on the excipients (fillers and binders) prior to Principal Component Analysis (PCA). Subsequently, the large number of the material properties of the excipients were reduced by identifying representative overarching properties from the PCA (14). In the second part, different excipients were selected representing these overarching properties. Then, after granulation and tableting experiments, the influence of the overarching properties of binder and filler upon granule and tablet quality was studied (15). The impact of API properties on granule quality was however not investigated. More recently, Portier et al. (10) investigated the impact of granulation process settings and screw configuration on granulation behaviour of different formulations. These formulations varied in API content, API type and filler type (i.e., lactose or lactose/microcrystalline cellulose (MCC) (1:1)). The study showed that lactose in combination

with MCC resulted in improved process robustness. For both the study of Willecke et al. and Portier et al., a one-on-one comparison of the granules' CQAs of different formulations was unfortunately still impeded due to different L/S ratios. This shortcoming of aforementioned studies can be overcome using T-shaped partial least squares (TPLS), a method developed by Munoz et al. (2). TPLS allows to investigate the individual and combined effect of formulation and process parameters on granule quality. In a case study, the author was able to determine the most influencing process parameters and raw material properties upon dissolution time after encapsulation of granules. By understanding the lot-to-lot variability of the different ingredients, it was possible to selectively combine certain lots of the different ingredients to minimize the variability in final product quality.

TPLS, being a regression method, has also the ability to predict the product quality attributes for given raw material properties, blend ratio's and process settings. Hence, the prediction of the optimal combination of formulation composition and twin-screw process parameters for a new API based on its critical material properties leading to desired granule quality attributes is possible. This is very beneficial as it could reduce the experimental effort, the consumption of the expensive API and the development time during early drug product development.

The goal of current study was to better understand the link between raw material properties, formulation composition and process settings on granule quality attributes, and to develop a TPLS model allowing the fast formulation and twin-screw granulation process development for new APIs (with limited experimental efforts). The study consisted of three major parts. In the first part, a TPLS model was established for twin-screw granulation. First, an extensive raw material database was developed by determining multiple raw material characteristics of excipients and APIs. Next, APIs and excipients with varying raw material properties were selected based on PCA. Subsequently, these selected APIs (10, 40 or 70 % API content) and excipients were combined to obtain very divergent powder mixtures for granulation experiments. Then, each powder mixture was granulated under different twin-screw granulation process settings followed by oven-drying. Finally, granule size, granule strength and granule flow were determined for all the different produced granules. In the second part of the study, a TPLS model was developed to understand the effect of the raw material properties and process parameters on granule quality attributes. In the third part of the study, the TPLS model was used to predict an optimal formulation composition and twin-screw



granulation process settings for a new API based on its determined critical material properties. In this case-study, suitable formulation compositions and corresponding optimal process settings for three different API contents were selected in order to obtain granules with desired quality attributes. This approach could be very beneficial during the formulation and process development of new APIs as the availability of the API is then limited. A stepwise overview of the approach to develop the TPLS model is shown in Figure 6.1.

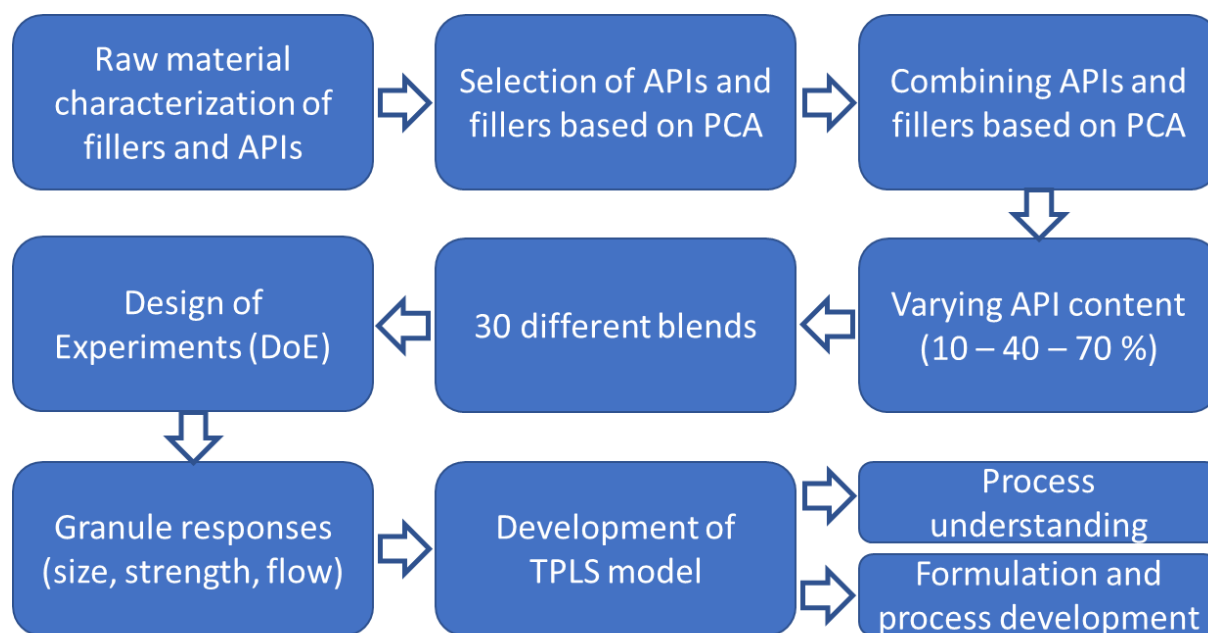


Figure 6.1: Stepwise overview of the systematic approach to develop the TPLS model and its use for process understanding and process and formulation development.

## 6.2 MATERIALS

15 different APIs, 9 fillers and 3 binders (Table 6.1) that are intended for immediate release formulations were used in this study. The materials were purchased from Granules India (Hyderabad, India), BASF (Ludwigshafen, Germany), Siegfried PharmaChemikalien (Minden, Germany), Utag (Almere, The Netherlands), Polydrug Laboratories (Ambernath, India), FARMHISPANIA (Barcelona, Spain), Mallinckrodt (Dublin, Ireland), The Dow Chemical Company (Midland, US), Ashland (Covington, US), Meggle (Wasserburg, Germany), DFE Pharma (Veghel, The Netherlands), FMC BioPolymer (Cork, Ireland), Cargill (Minneapolis, US), Roquette (Lestrem, France) and Cargill (Minneapolis, US). An overview of the materials is shown in Table 6.1.

Table 6.1: Overview of the used powders

Type	Material	Brand name	ID	Manufacturer
API	Metformin regular Theophylline Anh. Powder	/	M_r	Granules India
API	200M	/	T_A_200M	BASF
API	Theophylline Anh. Powder 200	/	T_A_200	Siegfried
API	Theophylline Micronized	/	T_μ	BASF
API	Caffeine powder	/	C_p	Siegfried
API	Hydrochlorothiazide	/	HCT	UTAG
API	Metoprolol Tartrate	/	MPT_μ	Polydrug Laboratories
API	Celecoxib	/	Cel	Utag
API	Metformin fine	/	M_f	FARMHISPANIA
API	Ibuprofen	/	Ibu	BASF
API	Naproxen	/	Nap	Utag
API	Paracetamol semi fine	/	P_sf	Mallinckrodt
API	Paracetamol micronized	/	P_μ	Mallinckrodt
API	Paracetamol dense powder	/	P_dp	Mallinckrodt
API	API X	/	X	Bayer AG
Binder	Hydroxypropyl methylcellulose (HPMC)	Methocel E5	E5	Dow Chemical Company
Binder	Hydroxypropyl cellulose (HPC)	Klucel EF	KEF	Ashland
Binder	Polyvinylpyrrolidone (PVP)	Kollidon 30	K30	BASF
Filler	Lactose	Tabletose T80	T80	Meggle
Filler	Lactose	Pharmatose 200M	200M	DFE Pharma
Filler	Lactose	Subertab 11SD	11SD	DFE pharma
Filler	Microcrystalline cellulose	Avicel PH301	PH301	FMC BioPolymer
Filler	Microcrystalline cellulose	Avicel PH105	PH105	FMC BioPolymer
Filler	Microcrystalline cellulose	Avicel PH101	PH101	FMC BioPolymer
Filler	Mannitol	Pearlitol 160C	160C	Roquette
Filler	Mannitol	Pearlitol 100SD	100SD	Roquette
Filler	Unmodified maize starch	C*PharmGel	Pgel	Cargill

## 6.3 METHODS

### 6.3.1 RAW MATERIAL PROPERTY DATABASE

The raw material property database consists of two parts. One part contains 39 physicochemical and solid state properties of the APIs and fillers, while the other part holds 9 properties of the 3 binders used in this study.

## 6.3.1.1 APIS AND FILLERS

## 6.3.1.1.1 Laser diffraction

Laser diffraction (Mastersizer 2000, Malvern Instruments, Worcestershire, UK) was used via a dry dispersion method to measure a volume-based particle size distribution. Powder was fed towards a 550 RF lens at a rate of 3.0 G, using a standard jet pressure of 2.0 bar. Each powder was measured in triplicate and analysed by the Mastersizer 2000 software. The 10 %, 50 % and 90 % cumulative undersize fraction of the size distribution were reported by d10, d50 and d90, respectively.

## 6.3.1.1.2 Bulk and tapped density

A known mass ( $[m] = \text{g}$ ) of each powder was poured into a 250 mL graduated cylinder to record the bulk volume ( $[V_b] = \text{ml}$ ). Consequently, the graduated cylinder was tapped 1250 times using a tapping machine (J. Engelsman, Ludwigshafen, Germany) to record the tapped volume ( $[V_t] = \text{mL}$ ). Bulk ( $[\rho_b] = \text{g/mL}$ ) and tapped ( $[\rho_t] = \text{g/mL}$ ) density were calculated by Equation 6.1 and 6.2, respectively.

$$\rho_b = \frac{m}{V_b} \quad [6.1]$$

$$\rho_t = \frac{m}{V_t} \quad [6.2]$$

## 6.3.1.1.3 True density and porosity

An AccuPyc 1330 helium pycnometer (Micromeritics, Norcross, GA, USA) was used to measure true density ( $[\rho_{\text{true}}] = \text{g/ml}$ ) of each powder. The equilibration rate was set at 0.0050 psig/min and 10 purges were performed for each test. Each powder was measured in duplicate. Powder bed porosity ( $\epsilon$ , dimensionless) was calculated using equation 6.3.

$$\epsilon = 1 - \frac{\rho_b}{\rho_{\text{true}}} \quad [6.3]$$

## 6.3.1.1.4 Ring shear test

Each powder was analysed in triplicate in a ring shear tester (RST-XS, Dietmar Schulze Schüttgutmesstechnik, Wolfenbüttel, Germany) to measure powder flowability and cohesivity. First, a pre-shear step was performed by applying a normal load of 1000 Pa on the

sample. Next, three consolidation stresses of 400, 600 and 800 Pa were used to provide shear stress on the powder. Powder flowability is characterized as the ratio of the unconfined yield strength ( $[\sigma_c] = \text{Pa}$ ) to the major principal stress ( $[\sigma_1] = \text{Pa}$ ), defined as the dimensionless flow function coefficient (ffc) (Equation 6.4). Powder flowability under influence of gravity was characterized by the bulk (ffp) (Equation 6.5) and consolidated (ffrho) density-weighted flow (Equation 6.6). In the latter equation, density under consolidation (1000 Pa) is represented by  $\rho_{Consolidation}$ , whereas  $\rho_w$  represents the density of water. Furthermore, powder cohesivity ( $\tau_c$ ) was described as the intercept of the yield locus with the shear stress axis. For further details on analysis and interpretation of ring shear test data, the reader is referred to Schulze et al. (16).

$$ffc = \frac{\sigma_1}{\sigma_c} \quad [6.4]$$

$$ff_\rho = ffc \times \frac{\rho_{bulk}}{\rho_w} \quad [6.5]$$

$$ff_{rho} = ffc \times \frac{\rho_{Consolidation}}{\rho_w} \quad [6.6]$$

#### 6.3.1.1.5 Powder elasticity and plasticity

A fully instrumented compaction simulator (Styl'one evolution, Medelpharm, France) was used to determine the elasticity and plasticity of each raw material powder. Compacts were prepared using 10 mm flat faced Euro B-tooling (Natoli Engineering Company, Saint Charles, MO, USA) with approximately 15 kPa of pressure and 18 mm fill depth. A compaction speed of 10 mm/s was applied. Prior to manual powder filling, the die was manually lubricated with magnesium stearate. For each studied material, 5 compacts were prepared. After compaction, a force-displacement curve (Figure 6.2) (17) was established by the ANALIS software. Work of compression (in J) was calculated as area ABC, elastic energy (in J) was calculated as area DBC and work of compaction as ABD. Elastic recovery ( $[\text{Elas}] = \%$ ) was calculated as per Equation 6.7. Specific work of compaction ( $[\text{WoC}] = \text{J/g}$ ) was calculated using the recorded masses ( $[m] = \text{g}$ ) of compacts produced (Equation 6.8).

$$\frac{\text{Elastic energy}}{\text{Work of compression}} = \text{Elastic recovery} \quad [6.7]$$

$$\frac{\text{Work of compaction}}{\text{mass of compact}} = \text{Specific work of compaction} \quad [6.8]$$

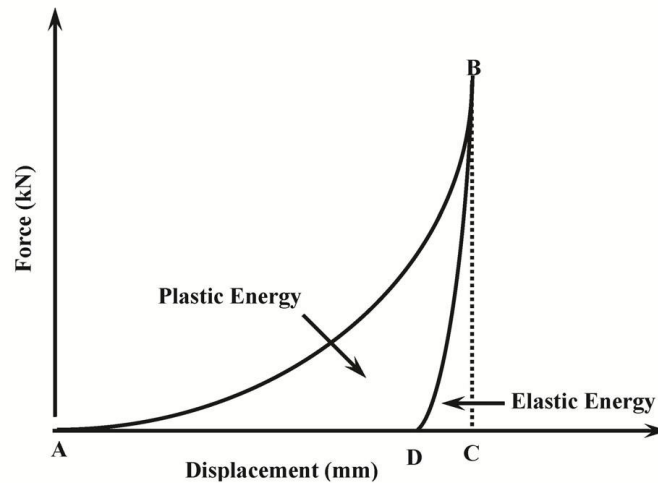


Figure 6.2: Typical force-displacement curve of a powder (17).

#### 6.3.1.1.6 Powder rheology

As powder flow depends on multiple physical properties such as particle size, cohesivity, shape, texture, particle stiffness and density, it is difficult to describe it by a single value. Therefore, a FT4 powder rheometer (Freeman Technology, Tewkesbury, UK) was used to measure several powder flow characteristics. Compressibility, aeration and variable flow rate tests were performed on the FT4 equipment. For each of the following test, the powder bed was first preconditioned. A preconditioning step is needed to start with a standardized packing of the powder particles. All powder rheology tests were performed in triplicate.

#### *Stability and variable flow rate*

The resistance (i.e., required energy in mJ) of a powder is measured by a moving blade up and down through the powder bed. First, seven consecutive test cycles at 100 mm/s were executed to obtain a stable flow energy. Consequently, the flow energy value was measured while gradually reducing the blade tip speed (100, 70, 40, 10 mm/s). The Basic Flow Energy ([BFE] = mJ) is the flow energy at 7<sup>th</sup> test, while the Flow Rate Index ([FRI] = dimensionless) is the ratio of the flow energy at 10 mm/s and 100 mm/s.

### *Compressibility*

The powder was compressed under increasing normal stress (0.5, 1, 2, 4, 6, 8, 10, 12 and 15 kPa) using a vented piston. Compressibility ( $[Com] = \%$ ) is defined as the relative change in volume at the end of the test.

### *Aeration*

An air flow was provided from the bottom of the vessel. The air velocity was gradually increased (0, 0.5, 1, 2, 4, 6, 8, 10, 15, 20, 30 and 40 mm/s) during the test. At each air velocity, the corresponding flow energy was measured. The flow energy (in mJ) at 40 mm/s was reported as AE40 ( $[AE40] = \text{mJ}$ ). The ratio of the flow energy at 0 mm/s and at 40 mm/s was reported as AR40 ( $[AR40] = \text{dimensionless}$ ).

#### 6.3.1.1.7 Charge density

Charge density was measured in triplicate using an electric charge analyser (GranuGcharge, Granutools, Awans, Belgium). A vibrating feeder was used to feed 30 mL powder into two stainless steel tubes arranged in a V-shape to induce an electrostatic charge of the powder. Thereafter, the charged powder was collected in a Faraday cup connected to an electrometer. Charge density ( $[CD] = \text{C/kg}$ ) was calculated as the ratio of net charge to the mass of the powder bed. The absolute value of the charge density was taken, as the net charge could be either negative or positive. All samples were measured in triplicate.

#### 6.3.1.1.8 Specific surface area

Before specific surface area ( $[SSA] = \text{m}^2/\text{g}$ ) measurements were executed, the samples were degassed in vacuum (VacPrep Micrometrics, Norcross, USA) for 24 h at 60 °C and purged with nitrogen for 1 h to remove impurities. Afterwards, the adsorption isotherm was determined by nitrogen adsorption (TriStar 3000 V6.08A, Micrometrics, Norcross, USA) and SSA was derived using the Brunauer-Emmett-Teller theory.

#### 6.3.1.1.9 Water binding capacity

Water binding capacity ( $[WBC] = \%$ ) is the tendency of a powder to bind and to hold water. 5.00 g of each material was transferred into centrifuge tubes and suspended in 20 mL of demineralized water. These tubes were centrifuged (Heraeus Multifuge 3 S-R, Thermo

scientific, USA) at 4000 rpm for 25 minutes. The supernatant was discarded and the sample weight ( $[m] = g$ ) was recorded. WBC was calculated as per Equation 6.9. Any negative values that results from the powder dissolving during the experiment were considered as zero.

$$WBC\% = \frac{m(\text{wet powder}) - m(\text{dry powder})}{m(\text{dry powder})} \quad [6.9]$$

#### 6.3.1.1.10 Solubility

The maximal solubility ( $[S_{\text{true}}] = g/100\text{mL}$ ) of each powder was empirically determined by gradually adding powder to 100 g of demineralized water. The temperature of the mixture was kept constant at 23 °C. A petri dish was used to protect the mixture from evaporation and a stirring bar was added to obtain optimal wetting of the powder. More water was added when the maximal solubility was exceeded or additional powder was added when maximal solubility was not yet reached. The maximal solubility was calculated by Equation 6.10.

$$S_{\text{true}} = \frac{m_{\text{powder}} [g]}{\left( \frac{m_{\text{powder}} [g]}{\rho_{\text{powder}} \left[ \frac{g}{\text{mL}} \right]} \right) + \left( \frac{m_{\text{water}} [g]}{\rho_{\text{water}} \left[ \frac{g}{\text{mL}} \right]} \right) + V_{\text{water}} [mL]} * 100 \quad [6.10]$$

Where  $m_{\text{powder}}$  is the amount of powder,  $\rho_{\text{powder}}$  is the true density of the powder,  $m_{\text{water}}$  is the initial amount of water,  $\rho_{\text{water}}$  is the density of water at 23 °C and  $V_{\text{water}}$  is the additional volume of water. As maize starch and the different grades of microcrystalline cellulose are insoluble, their solubility value was set at  $1 \times 10^{-8} g/100\text{mL}$ .

#### 6.3.1.1.11 Dissolution rate

A customized closed configuration system of the USP4 Flow-Through Dissolution Systems (Figure 6.3) (Sotax, Allschwil, Switzerland) was used to determine dissolution rate. The configuration consisted of 4 parts: (i) a piston pump (Sotax Cp 7-35, Sotax, Allschwil, Switzerland) to transport the dissolution medium through the system, (ii) a flow cell (Sotax CE 7 smart, Sotax, Allschwil, Switzerland) containing a membrane (Float-A-Lyzer G2 Dialysis Device, Spectrum Laboratories, Rancho Dominguez CA, VS) of 1 mL. 200 mg sample was added to the membrane. (iii) A media reservoir filled with 250 mL demineralized water. (iv) An autosampler (Agilent 8000 Dissolution Sampling Station, Agilent Technologies, Santa Clara,

U.S.) coupled to the media reservoir to collect 5 mL samples after 1, 3, 5, 10, 20, 30 and 60 min.

The collected samples were analysed by UV-VIS spectrophotometry (UV-1650 PC, Shimadzu, Suzhou New District, China). A calibration model was first established to determine the concentration for each powder, except for maize starch, microcrystalline cellulose, lactose and mannitol. Maize starch and microcrystalline cellulose were not measured due to their insolubility. As lactose and mannitol do not absorb UV, indirect measurements were needed for both materials. Lactose (Enzym Bio-analysis Lactose/D-glucose, R-biopharm AG, Darmstadt, Germany) and mannitol (D-mannitol assay kit, Megazyme, Wicklow, Ireland) concentrations were determined by an enzymatic detection kit. Both methods indirectly measured the sample concentration by detection of nicotinamide-adenine dinucleotide hydrogenate after enzymatic reactions. For all measured powders, the fraction powder dissolved after 1, 3, 5, 10, 20, 30 and 60 min were expressed as DR1, DR3, DR5, DR10, DR20, DR30 and DR60, respectively.

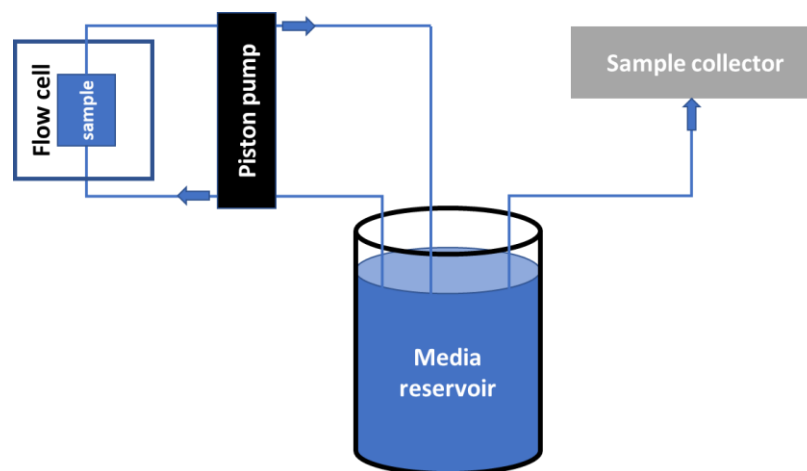


Figure 6.3: Schematic overview of the closed configuration system of the USP4 Flow-Through Dissolution Systems.

#### 6.3.1.1.12 Sorption properties

Hygroscopicity or water sorption behaviour of the studied materials was determined with dynamic vapour sorption (DVS) (DVS intrinsic, Surface Measurement Systems, London, U.K). First, approximately 15 mg powder sample was dried at 25 °C under a dry nitrogen stream. Then, the relative humidity (RH) was gradually increased from 0 to 80 % in steps of 20 % to calculate sorption values (percentage of moisture uptake). Finally, the RH was again gradually



decreased in steps of 20 % to measure desorption (percentage of moisture reduction). Sorption and desorption values at 40, 60 and 80 % RH were noted as S40, S60, S80, D40, D60 and D80, respectively. At 40 and 60 % RH, sorption values were subtracted from desorption values to calculate hysteresis values (i.e., H40 and H60).

#### 6.3.1.1.13 Contact angle

Powder wettability was determined through contact angle measurements applying a drop shape analyzer (DSA30, Krüss, Hamburg, Germany). Before contact angle measurements, pure raw material was tableted under high force using a single station tablet press (Korsch EKO, Korsch, Berlin, Germany). The tablet porosity did not exceed 10 % and draining of the liquid drop via interparticle and intraparticle pores was therefore limited. The sessile drop method was used for these measurements. A water drop of 5  $\mu\text{L}$  was applied on a tablet and the contact angle was measured after 1 (CA1), 30 (CA30) and 60 (CA60) s. The contact angle ([CA] =  $^\circ$ ) was calculated from the Young-Laplace equation (Equation 6.11).

$$\Delta p = \sigma \times \left( \frac{1}{r_1} + \frac{1}{r_2} \right) \quad (6.11)$$

Where  $\Delta p$  (in Pa) is the pressure across the fluid interface,  $\sigma$  (in  $\text{J}/\text{m}^2$ ) is the surface tension and  $r_1$  and  $r_2$  (in m) are the radii of curvature.

#### 6.3.1.2 BINDER-SPECIFIC PROPERTIES

Binder-specific properties were partly taken from a study of Vandevivere et al. (18).

##### 6.3.1.2.1 Dissolution rate

Binders (10 % w/w) were added to demineralized water and mixed for 30, 60 or 90 s. Subsequently, the mixture was filtered using a cellulose-based filter (Grade 2, Whatman, USA). The fraction of dissolved binder was measured via the refractive index. For each binder, a calibration curve was established. Tests were performed in triplicate and the fraction binder dissolved after 30, 60 and 90 s was expressed as BDR30, BDR60 and BDR90, respectively.

##### 6.3.1.2.2 Surface tension

A Drop Shape Analyzer (DSA 30, KRÜSS, Hamburg, Germany) was used to determine the surface tension (ST) of an aqueous binder dispersion (8 % w/w) via the pendant drop method

in air. For each binder, the curvature of a droplet was used to calculate the surface tension. Experiments were performed in triplicate.

#### 6.3.1.2.3 Viscosity

The dynamic viscosity of an aqueous binder dispersion (8 % w/w) was measured using a rotational rheometer (HAAKE MARS® III, Thermo Scientific, Massachusetts, USA) with the plate-plate technique. A gap size between 0.9 and 1.1 mm was applied, while temperature was set at 25 °C. 5 mL of the binder dispersion was transferred between the two plates. The viscosity values (mPa·s) were derived from a total of 20 data points when the shear rate varied from 0.1 to 1000 s<sup>-1</sup>.

#### 6.3.1.2.4 Contact angle

Similar to 6.3.1.13, powder wettability was determined through contact angle measurements using a drop shape analyzer (DSA30, Krüss, Hamburg, Germany). Two set of experiments were performed. For the first set the contact angle of demineralized water on a pure binder tablet was determined (see 3.1.1.13). For the second part, the contact angle of an aqueous binder dispersion (8 % w/w) on a hydrophobic polytetrafluoroethylene surface was determined. Experiments were performed in triplicate. The contact angle calculation was calculated using aforementioned Equation 6.11. The hydrophilic contact angle for binders after 1, 30 and 60 seconds was reported as CAb1, CAb30, CAb60. The hydrophobic contact angle was reported as CA<sub>h</sub>.

#### 6.3.1.3 OVERVIEW

An overview of the characterization techniques, the corresponding descriptor and the abbreviation of the descriptor are shown in Table 6.2.

Table 6.2: Overview of the characterization techniques with their obtained corresponding descriptors (properties) and abbreviation. The upper part of the table shows the properties of fillers and APIs, whereas the lower part of the tables shows binder-related properties. Descriptors shown in bold were used for the TPLS model development.

Characterization technique	Descriptor	Abbreviation
Laser diffraction	10, 50 and 90 % cumulative undersize fraction of volumetric particle size distribution	d10, <b>d50</b> and d90
Powder density and porosity	Bulk, tapped and true density	<b><math>\rho_b</math></b> , <b><math>\rho_t</math></b> and <b><math>\rho_{true}</math></b>
	Porosity	<b><math>\epsilon</math></b>
Ring shear test	Flow function coefficient	<b>ffc</b>
	Bulk and consolidated density weighted flow	<b><math>ff_\rho</math></b> and <b><math>ff_{rho}</math></b>
	Powder cohesivity	<b><math>\tau c</math></b>
Powder elasticity and plasticity	Elastic recovery	<b>Elas</b>
	Work of compaction	<b>WoC</b>
Powder rheometer: Stability and variable flow rate	Basic flow energy	<b>BFE</b>
	Flow rate index	FRI
Powder rheometer: compressibility	Compressibility at 15 kPa	<b>Com</b>
Powder rheometer: aeration	Flow rate energy at 40 mm/s	AE40
	Ratio of flow energy at 40 and 0 mm/s	<b>AR40</b>
Charge density	Charge-to-mass ratio	<b>CD</b>
Specific surface area	Specific surface area	<b>SSA</b>
Water binding capacity	Water binding capacity	<b>WBC</b>
Solubility	Maximal powder solubility	<b>S<sub>true</sub></b>

<b>Dissolution rate</b>	Fraction powder dissolved after 1, 3, 5, 10, 20, 30 and 60 min	DR1, DR3, DR5, DR10, DR20, DR30 and <b>DR60</b>
<b>Dynamic vapour sorption</b>	Moisture content in sorption and desorption mode at 40, 60 and 80 % RH	<b>S40</b> , S60, S80, D80, D60 and D40
	Hysteresis values 40 and 60 % RH	H40 and H60
<b>Contact angle</b>	Hydrophilic contact angle after 1, 30 and 60 s	<b>CA1</b> , CA30 and CA60
<b>Dissolution rate</b>	Fraction binder dissolved after 30, 60 and 90 s	DR30, DR60 and <b>DR90</b>
<b>Contact angle</b>	Contact angle of the aqueous binder dispersion on a hydrophobic surface	<b>CAbh</b>
	Hydrophilic contact angle after 1, 30 and 60 s	<b>CAb1</b> , CAb30 and CAb60
<b>Viscosity</b>	Dynamic viscosity	<b>Vis</b>
<b>Surface tension</b>	Surface tension	<b>ST</b>

### 6.3.2 BLEND RATIOS

Ten different formulations were selected for granulation experiments. The selection of APIs and fillers was based on PCA of the API material characterization data and filler material characterization data individually (see 6.4.1.1.1 and 6.4.1.1.2). Next, the complete dataset of API and filler material properties was subjected to PCA to link an API with a filler (see 6.4.1.1.3). For one formulation, a mixture of two fillers was used (Formulation 6). For each selected formulation the API content was 10, 40 or 70 %, resulting in a total of 30 different blends. Binders were added dry in a concentration of 2 or 5 %. Binders were added dry because the binder solubility in aqueous dispersions is limited and the pumpability and control of a constant liquid flow for highly concentrated binder dispersions is limited. The allocation of a binder to a API/filler combination was done at random. Table 6.2 gives an overview of the 30 different formulation blends.

Table 6.2: Overview of the formulation blend compositions.

Code	API		Filler		Binder	
	Name	Content (%)	Name	Content (%)	Name	Content (%)
F1B1	ibu	10	200M	85	E5	5
F1B2	ibu	40	200M	55	E5	5
F1B3	ibu	70	200M	25	E5	5
F2B1	P_sf	10	160C	85	K30	5
F2B2	P_sf	40	160C	55	K30	5
F2B3	P_sf	70	160C	25	K30	5
F3B1	T_A_200	10	PH101	85	KEF	5
F3B2	T_A_200	40	PH101	55	KEF	5
F3B3	T_A_200	70	PH101	25	KEF	5
F4B1	M_f	10	T80	85	E5	5
F4B2	M_f	40	T80	55	E5	5
F4B3	M_f	70	T80	25	E5	5
F5B1	Nap	10	PH105	85	K30	5
F5B2	Nap	40	PH105	55	K30	5
F5B3	Nap	70	PH105	25	K30	5
F6B1	HCT	10	200M/PH105	44/44	KEF	2
F6B2	HCT	40	200M/PH105	29/29	KEF	2
F6B3	HCT	70	200M/PH105	14/14	KEF	2
F7B1	Mpt_μ	10	PH101	88	E5	2
F7B2	Mpt_μ	40	PH101	58	E5	2
F7B3	Mpt_μ	70	PH101	28	E5	2
F8B1	P_dp	10	11SD	88	KEF	2
F8B2	P_dp	40	11SD	58	KEF	2
F8B3	P_dp	70	11SD	28	KEF	2
F9B1	M_f	10	T80	88	E5	2
F9B2	M_f	40	T80	58	E5	2
F9B3	M_f	70	T80	28	E5	2
F10B1	Cel	10	SD100	88	KEF	2
F10B2	Cel	40	SD100	58	KEF	2
F10B3	Cel	70	SD100	28	KEF	2

### 6.3.3 PROCESS CONDITIONS

#### 6.3.3.1 GRANULATION EXPERIMENTS

All raw materials from each formulation blend were preblended in a tumbling mixer (Inversina Bioengineering, Wald, Switzerland) for 15 minutes at 25 rpm. Granulation experiments were performed using the granulation module of the ConsiGma™-25 unit (GEA Pharma Systems, Collette, Wommelgem, Belgium). This granulation module consists of two 25 mm diameter co-rotating screws with a length-to-diameter (L/D) ratio of 20:1. The preblend was gravimetrically fed to the granulation module by a K-tron KT20 loss-in-weight feeder (Coperion K-tron, Niederlenz, Switzerland). Granulation liquid (i.e., demineralized water) was added before the first kneading zone. Therefore, a twin-peristaltic pump was positioned out-of-phase and connected to silicon tubing with an internal and external diameter of 1.6 and 2.4 mm, 1.6 and 3.2 mm, 1.6 and 4.8 mm or 1.6 and 6.4 mm, respectively. The silicon tubes were connected to nozzles with an orifice of 0.8, 1.6, 2.4 or 3.2 mm. The selection of tubes and nozzles depended on the liquid flow rate. After wetting, the wetted mass is sheared and compressed in a first kneading zone, this zone consists of 6 kneading elements ( $L=D/4$  for each kneading element) arranged at an angle of 60 degrees. After passing a small conveying zone ( $L=1.5D$ ), granules were further processed in another kneading zone arranged identically to the first kneading zone. The granules were then transported by conveying elements ( $L=1.5D$ ) towards the end of the granulator. At the end of the screws, two small kneading discs ( $L=D/6$  for each kneading element) were positioned to limit the fraction of oversized granules. Before sample collection, a stabilisation period was needed to reach steady-state conditions. All collected granules were oven dried (24 h, 40 °C, 25 % RH) prior to further granule characterization.

#### 6.3.3.2 DESIGN OF EXPERIMENTS

A 2-level full factorial Design of Experiments (DoE) was performed on each formulation blend to investigate the influence of the granulation process parameters MFR and L/S ratio on the granule quality attributes. Each DoE resulted in 4 experiments and 3 centerpoint experiments. MFR was varied from 10 to 20 kg/h, while the applicable L/S ratio ranges were experimentally determined for each formulation blend. L/S ranges were chosen so that both very small

granules and oversized granules were obtained. Operating outside these L/S ranges would either result in ungranulated powder or in the formation of paste.

### 6.3.4 PRODUCT QUALITY ATTRIBUTES

#### 6.3.4.1 GRANULE SIZE

An image analysis system (QICPIC particle size analyzer, Sympatec, Clausthal-Zellerfeld, Germany) was used to measure the granule size distribution based on the equivalent projected circle. Samples of 15 g were measured in triplicate. The fraction of ungranulated raw material was defined as fines, it corresponds to the size fraction smaller than 200  $\mu\text{m}$ . Particles larger than 2000  $\mu\text{m}$  were defined as oversized granules.

#### 6.3.4.2 FRIABILITY

Granule friability was measured to determine granule strength using a friabilator (Pharmatest PTF E, Hainburg, Germany). Before each measurement granules were pre-sieved at 250  $\mu\text{m}$ . Consequently, 10 g (initial weight ([Iw] = g)) of the fraction larger than 250  $\mu\text{m}$  was combined with 200 glass beads (diameter 5 mm) and subjected to 250 rotation in 10 min. Then, the fraction smaller than 250  $\mu\text{m}$  was removed and the remaining mass (final weight ([Fw] = g)) was weighted. Friability was calculated using Equation 6.12. Experiments were performed in duplicate.

$$Friability (\%) = 100 * \frac{(Iw - Fw)}{Iw} \quad (6.12)$$

#### 6.3.4.3 GRANULE FLOW

Granule flow was measured using the GranuHeap instrument (GranuTools, Awans, Belgium). After manually filling the initialization tube with 60 mL of granules, the tube was lifted at a constant speed of 5 mm/s. Hereafter, granules formed a heap on the support. The support rotated subsequently around its axis to take 17 pictures of the shape of the granule heap. The pictures were used to calculate the angle of repose ([AoR] = $^{\circ}$ ) as an indication for granule flow. Excellent (25-30 $^{\circ}$ ), good (31-35 $^{\circ}$ ), fair (36-40 $^{\circ}$ ), passable (41-45 $^{\circ}$ ), poor (46-55 $^{\circ}$ ) and very poor flow (56-65 $^{\circ}$ ) can be defined based on the measured AoR.

### 6.3.5 TPLS MODELING

Figure 6.4 illustrates a schematic overview of the structure of the developed TPLS model in this study. Munoz et al. (2) already showed that the TPLS model involves 4 different matrices, whereby the applied process conditions (matrix Z), the raw material properties (matrix X) and ratios in which these raw materials are combined (matrix R) determine the quality attributes (matrix Y). The mathematics behind TPLS modelling are extensively described by Munoz et al. (2). Prediction of the granule quality (Y) for a given X, R and Z can be performed by TPLS. First, the predictive power was tested by performing a cross-validation for all experiments of F1B1. The predicted values were then compared to the experimental values to investigate the goodness of the predictions. The predictive ability of the TPLS model was also evaluated for a case study where a suitable formulation with suitable process setting was defined for a new API (at 3 content levels) based on its determined properties. The following steps were therefore performed for this new API. First, powder characterization was performed for the new API to determine all raw material properties. Then, these API properties were added to the database of API and filler material properties to perform a new PCA. The score plot of the PCA was then created to determine the closest neighbours (i.e., powders having similar properties) of the API. Subsequently, the weighted (depending of the distance between the neighbouring powders and the new API) scores of the neighbouring powders were assigned to the new API. This is needed to add the new API to the initially developed TPLS model. In a next step, constraints were set on the composition of the new formulation, the desired granule quality and the desired process settings (see section 6.4.3.2.2.). Next, the granule quality attributes of 25,000,000 different scenarios were predicted. The prediction of a scenario is defined as the prediction of the granule quality of a certain formulation while applying certain process parameters, and while keeping the constraints into account. After each prediction, the predicted quality is compared to the desired quality. Based on these predictions, suitable excipients and 3 appropriate blend ratios were selected to obtain granules with 3 different API contents. Additional predictions were then performed for the selected formulation to establish contour plot for each of response. Finally, verification experiments were performed to compare predicted values with the experimental outcome.



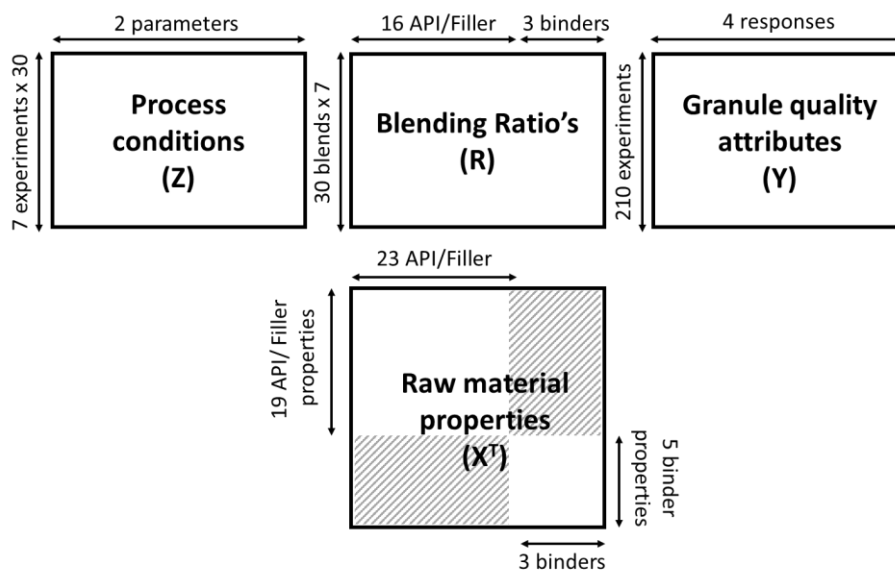


Figure 6.4: Structure of the established TPLS model.

### 6.3.6 DATA ANALYSIS

SIMCA 16.0 software (Umetrics, MKS, Umea, Sweden) was used to construct PCA models. MODDE Pro 12.0 (Umetrics, Sartorius Stedim Biotech, Malmö, Sweden) was used to analyse each DoE. TPLS analysis was performed by a user-developed MATLAB (R2016b, MathWorks, Natick, MA, USA) 220 toolbox (Phi\_1.8).

## 6.4 RESULTS AND DISCUSSION

### 6.4.1 RAW MATERIAL DATABASE (X)

Binders behave differently once in contact with the granulation liquid and their relevant physical properties are different compared to those from the APIs and fillers. As suggested by Munoz et al. (2), the raw material database (X-matrix) consisted therefore of a sub-data matrix containing 39 raw material properties of 23 APIs and fillers and a sub-data matrix containing 9 binder-specific properties (Figure 6.4).

For the complete dataset only 15 of the 987 descriptors were missing (i.e., 1.51%). These missing data were due to failure of a few characterization techniques for certain materials. For example, contact angle descriptors were missing for theophylline micronized and metformin fine. For these APIs, it was not possible to make tablets with a porosity lower than 10 %, due to their poor compaction properties. This very low fraction of missing data does not further impact multivariate data analysis according to Nelson et al. (19).

Before multivariate data analysis (PCA) and TPLS modelling were performed, data was pre-processed. First, unit variance scaling and mean-centering were performed. Unit variance was performed by dividing each value by the standard deviation of that descriptor, whereas the mean was subtracted from the data of each variable to mean-center. Therefore, the different numerical ranges of the descriptors were normalized and a repositioning of the coordinate system was obtained which improved the interpretability of the model. In a second step, non-normally distributed descriptors (d10, d50, d90, ffc, ffp, ffrho,  $\tau_c$ , CA1, CA30, CA60, AE40, AR40) were log-scaled to approach a normal distribution. In addition, the numerical overweight of some descriptors was overcome by excluding descriptors representing similar raw material properties. The exclusion of similar descriptors was based on their goodness of prediction ( $Q^2X$ ). The  $Q^2X$  of a variable is the cumulative predicted fraction of the variation of X using cross-validation (leaving a variable out of the dataset and predicting that variable based on the remaining variables in the dataset). Hence, an unbalanced model was avoided and all remaining descriptors were equally important. Thus, the 39 API- and filler-descriptors were reduced to 19 descriptors (**d50**,  $\rho_b$ ,  $\rho_t$ ,  $\rho_{true}$ ,  $\epsilon$ , ffc,  $\tau_c$ , S40, Strue, DR60, CA1, WBC, Com, SSA, CD, Elas, WoC, BFE and AR40) and the 9 binder-specific descriptors were reduced to 5 (DR90, ST, CAb1, CABh and Vis). These descriptors are shown in bold in Table 6.2. For each PCA, the goodness of fit of the model ( $R^2X$ ) and goodness of prediction ( $Q^2X$ ) was calculated.  $R^2X$  relates to the amount of variability that is captured by the model. A two-principal component model was developed for each (sub)dataset, as this facilitates the interpretation and was sufficient to differentiate the powders according to their properties.

#### 6.4.1.1 BLEND SELECTION

##### 6.4.1.1.1 API selection

PCA ( $R^2X = 0.596$  and  $Q^2Y = 0.204$ ) was applied on the refined (only including 19 descriptors) API subset of the database as a helpful tool to differentiate between the 14 APIs based on their raw material properties. The resulting loadings and score plots are shown in Figure 6.5. For a more in depth interpretation of the loadings and score plots, the reader is referred to (3,14). The first principal component (PC) describes the greatest amount of variance in this sub-dataset. Density-related descriptors such as  $\rho_b$  and  $\epsilon$  have high loadings for this first principal component, whereas negative loadings were observed for the anti-correlated descriptors such as porosity and compressibility (Figure 6.5 – top). The second PC was

identified to explain the variability in solubility, dissolution rate and sorption. APIs were selected with the aim to cover a broad range in API properties, so that future APIs for which predictions are needed would most probably fall within these ranges. Therefore, APIs located at the borders of the scores plot such as Cel, HCT, P\_dp, MPT\_μ and M\_f (Figure 6.5 – bottom) were selected. In addition, less extreme APIs that are located closer to the origin were also selected because these powders differ from powders located at the borders (i.e., P\_sf and T\_A\_200).

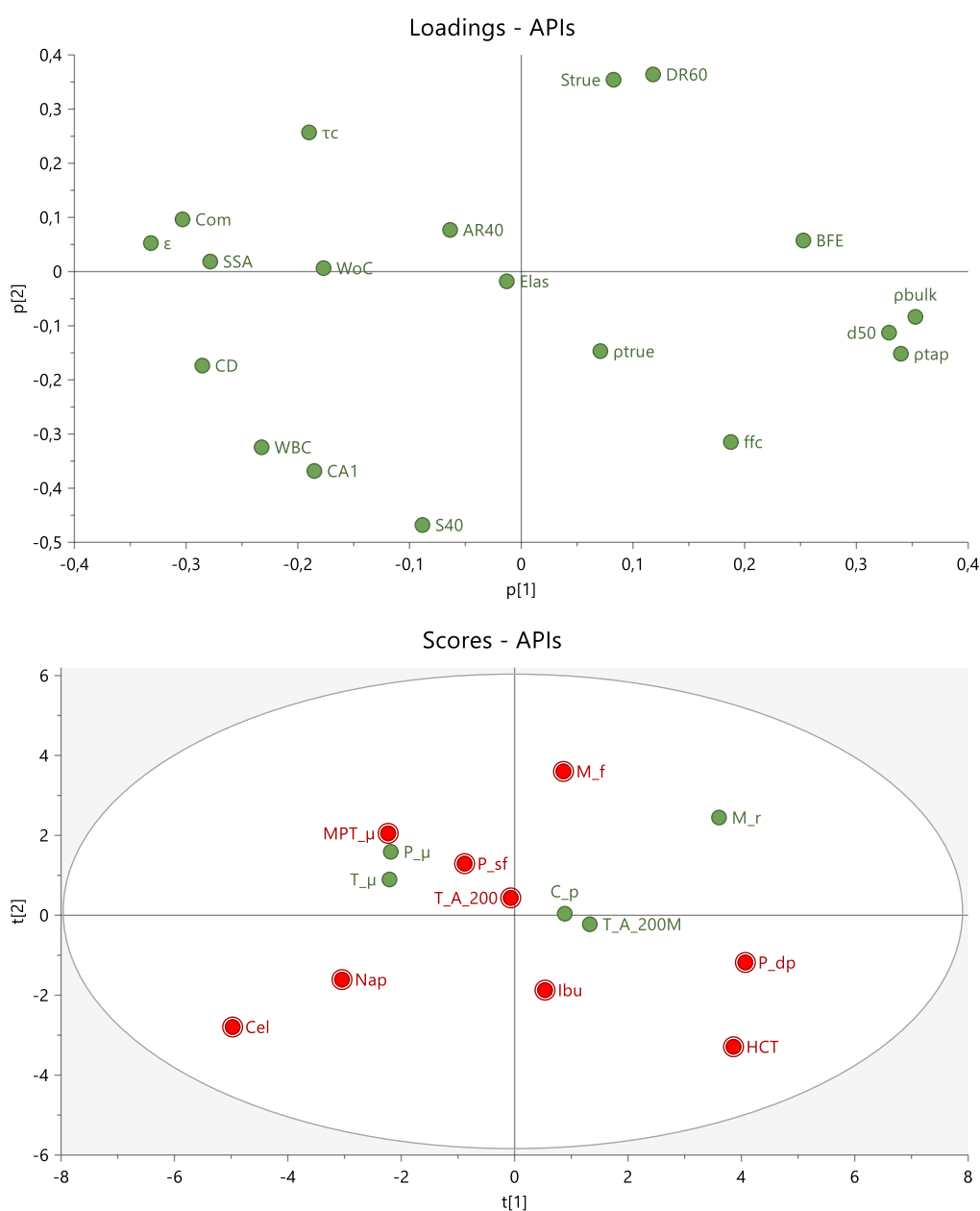


Figure 6.5: Loadings- (top) and score (bottom) plot for API sub-dataset. The selected APIs are shown in red.

6.4.1.1.2 Filler Selection

An identical approach as in 6.4.1.1.1 was used to select the fillers ( $R^2X = 0.701$  and  $Q^2Y = 0.216$ ). The loadings plot (Figure 6.6 – top) shows that the first principal component of the sub-dataset for fillers distinguished the fillers in solubility, dissolution rate and water binding capacity. The second PC captured mainly variance of flow-related descriptors. High positive PC2 loadings were observed for ffc, BFE and d50, and those descriptors were anti-correlated with cohesivity. Fillers were selected in order to cover the most variability in filler properties (Figure 6.6 – bottom).

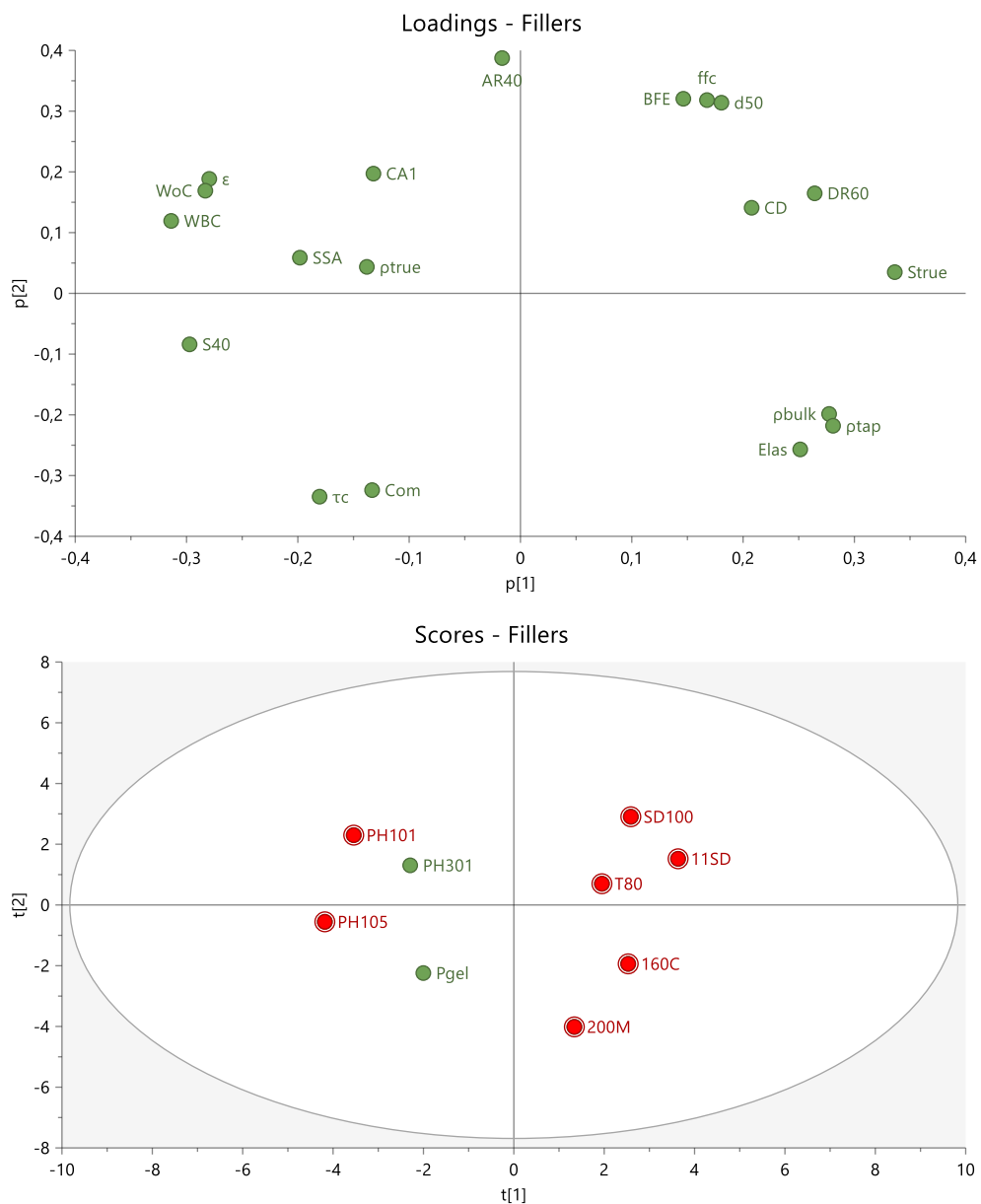


Figure 6.6: Loadings- (top) and score (bottom) plot for filler sub-dataset. The selected fillers are shown in red.

#### 6.4.1.1.3 Combining APIs with fillers

PCA ( $R^2X = 0.554$  and  $Q^2Y = 0.306$ ) was also performed on the complete data set containing all 9 fillers and 14 APIs and all their properties. The scores plot (Figure 6.7 – top) clearly shows clusters of APIs (blue) and fillers (green) indicating fillers and APIs with similar raw material properties. Fillers are mostly located in the upper right quadrant of the scores plot indicating good flow properties as suggested by the loadings plot (Figure 6.7 – bottom). APIs from different quadrants in the scores plot were linked to fillers located in the same or in different quadrants in order to increase the variability in formulation composition because each quadrant is correlated to different raw material properties. For example, APIs from the upper left quadrant of the scores plot were combined with fillers from the upper right quadrant (Cel – SD100, Mpt\_μ – PH101) and fillers from the upper left quadrant (Nap – PH105). The differences in directions and distance of the arrow between API and filler from one quadrant to another quadrant even further increase variability. For example, the arrow between Cel and SD100 is from the left-to-right and, in addition, longer than the arrow between MPT\_μ and PH101 which is rather from bottom-to-top. Consequently, the formulation properties of Cel-SD100 and MPT\_μ-PH101 are very different. This approach results in a large variability in formulation composition. Ultimately, this was even further increased by varying the API content at 3 levels (10, 40 and 70 %) for each selected formulation (Table 6.2).

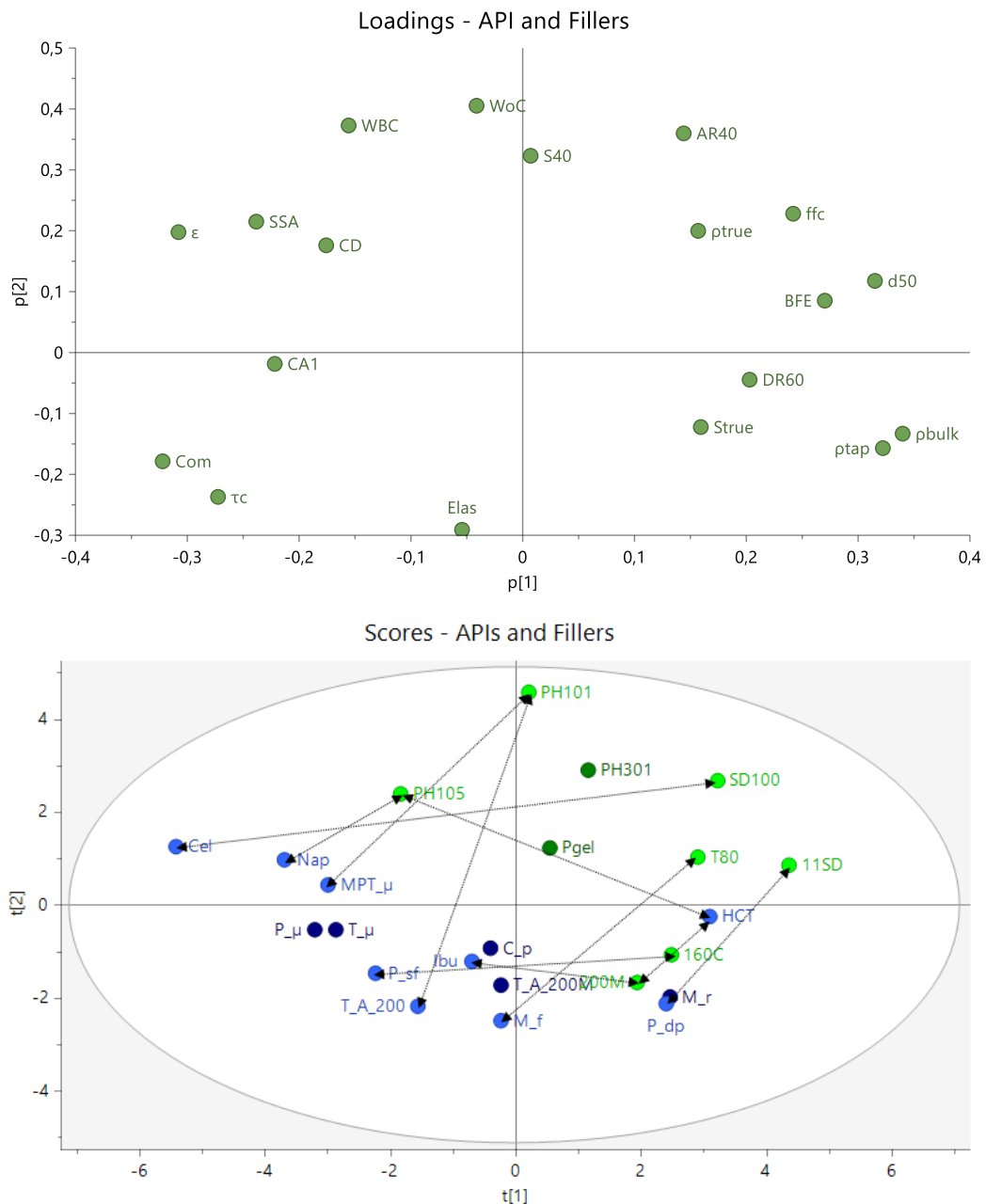


Figure 6.7: Loadings- (top) and score (bottom) plot for the API-Filler-dataset. Light blue dots correspond to the selected APIs, dark blue dots correspond to the remaining APIs, light green dots correspond to the selected fillers and dark green dots to the remaining fillers. Arrows indicate the link between an API and a filler.

#### 6.4.1.2 GRANULATION EXPERIMENTS AND GRANULE QUALITY ATTRIBUTES

The study resulted in a total of 210 experiments (10 formulations x 3 API levels x 7 DoE experiments) whereof 13 experiments could not be accomplished. This was observed for the blends consisting of 70 % of a low dense API: naproxen of F5B3 ( $\rho_b = 0.25 \text{ g/mL}$ ,  $\rho_t = 0.35 \text{ g/mL}$ )

and celecoxib of F10 ( $\rho_b = 0.16$  g/mL,  $\rho_t = 0.27$  g/mL). It was possible to gravimetrically feed these blends at 20 kg/h, but their volume exceeded the free volume in the granulator.

The L/S ratio ranges for each formulation and each blend were varied to obtain differences in granule quality. Since the variability in blend composition is very large, different L/S ratio ranges were required. An overview of the applied process settings per experiment is shown in Appendix A. For example, a L/S ratio of 84 % was used to produce coarser granules for F5B1 (i.e., 10% nap – 85% PH101 – 5% HPMC), as this formulation lacks a soluble API or filler, hence requiring a high quantity of granulation liquid.

## 6.4.2 TPLS MODELLING

### 6.4.2.1 TPLS MODEL DEVELOPMENT AND INTERPRETATION

A two-latent variable (LV) TPLS model was fit to the data as  $R^2$  only slightly increased when a third LV was added. Moreover, the addition of a third LV complicated the physical interpretation of the results. The Variable Importance for the Projection (VIP) plot was developed to highlight the most influencing raw material properties in the TPLS model (Figure 6.8). Generally, the variability in raw material properties with the highest importance explains the variability in granule quality attributes the most. DR60, Com, WoC, S40, WBC,  $\rho_t$ ,  $S_{true}$  were the seven most influencing raw material properties upon granule quality attributes. Flow-related properties (ffc, BFE, AR40), SSA and CD appeared to be less influential for the granule quality attributes. In addition, binder-specific properties were less important. This can be explained by the variability within a binder-specific property. This variability is generally lower because the binders are less different, as all three binders are all typically used for immediate release. In addition, as the binder content was only varied from 2 to 5 %, it is possible that these powders were less dominant than API/filler properties.

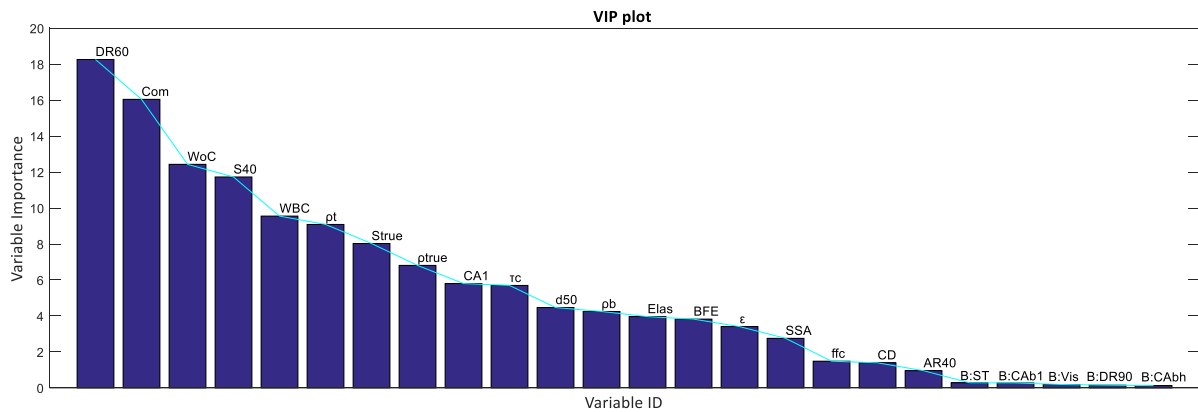


Figure 6.8: VIP plot for the TPLS model.

The effect of the raw material properties upon the different granule quality attributes was studied in more detail by interpreting their loadings for each LV. The first LV mainly captured the variability in AoR and fines fraction (Figure 6.9 – top). Fines fraction was correlated to the AoR, fewer ungranulated material (i.e, lower fines fraction) resulted in a better flow (lower AoR values). Furthermore, a higher DR60,  $S_{true}$ , BFE and  $\rho_b$  tended to result in a better flow, while a higher  $\epsilon$ , SSA, CD, WBC, WoC and S40 tended towards poorer flow (Figure 6.9). For the wet powder properties (i.e.,  $S_{true}$ , DR60, WBC), a higher  $S_{true}$  and DR60 resulted in more or faster powder dissolution, respectively, consequently resulting in more granulated material and a smaller fines fraction as more liquid bridges are made. As less liquid is available for the granulation process, a higher WBC resulted in more ungranulated material.

For the dry powder properties (i.e., BFE,  $\rho_b$ ,  $\epsilon$ , SSA and CD), it is suggested that their effect on AoR can be explained by the flow properties of the ungranulated powder. On the one hand, porous ( $\epsilon$ ) and electrically charged (CD) properties impair powder flowability, resulting in a higher granule AoR. On the other hand, a higher bulk density and BFE value typically corresponds to denser and larger powder particles with a better flow, thereby resulting in a negative correlation with AoR. It is not possible to give a good physical interpretation for each raw material property even though it has a high loading value. For example, it was observed that WoC and S40 negatively affected granule flow, but an explanation related to the granulation process cannot be given. Therefore, the deviation from the mean for each powder of the API/filler dataset was shown for WoC, WBC and S40 (Figure 6.10). All MCC grades had high values for these properties. A correlation (clustering) between these three descriptors was also seen on the scores plot for APIs and filler (Figure 6.7 – top), but this was not seen in



the scores plot (Figure 6.5 – top) of the API subset. This highlights the unique properties of MCC. As a consequence, the effect of WoC and S40 on the granule quality attributes was probably due to a mathematical coincidence.

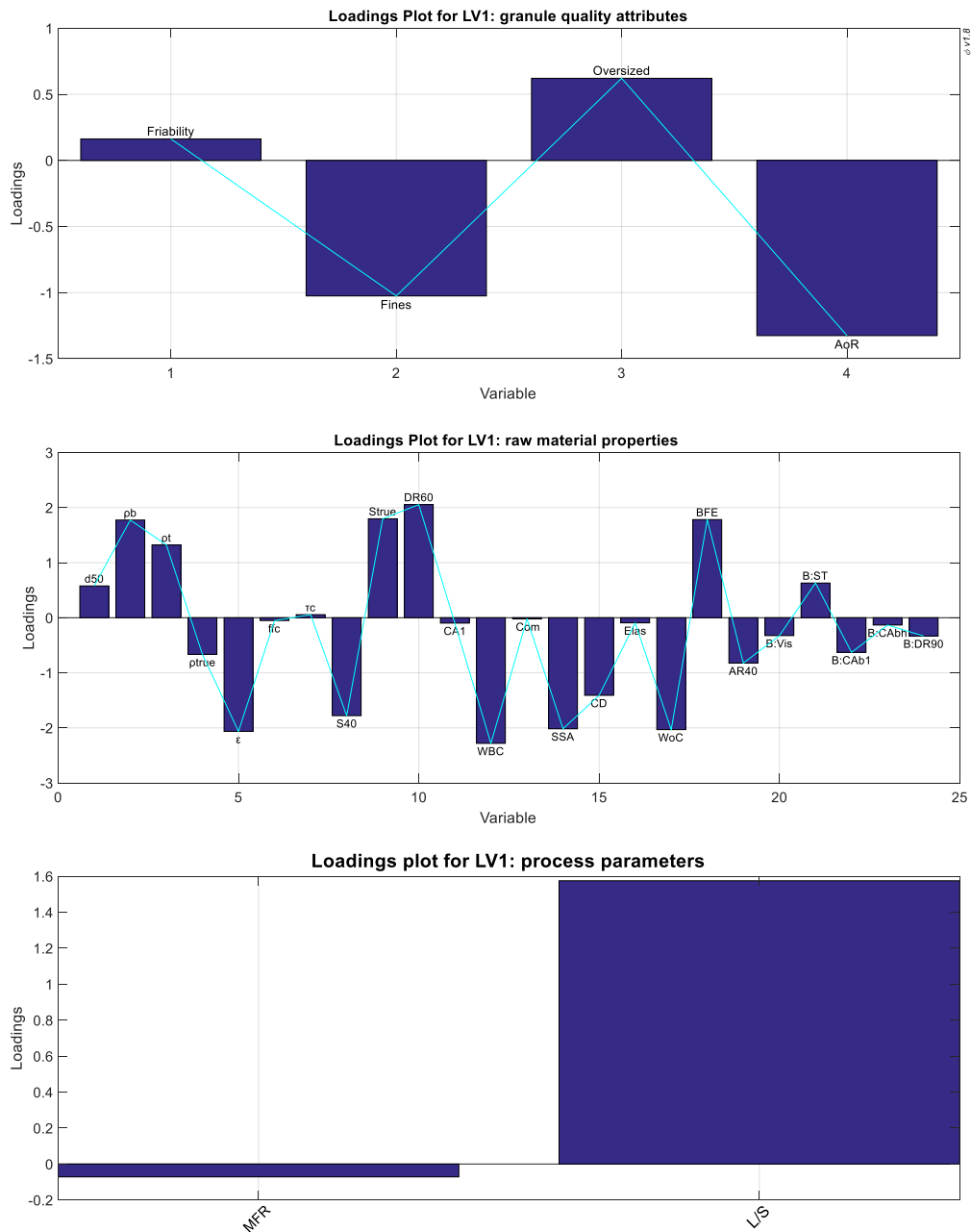


Figure 6.9: Loadings plot for granule quality attributes (top), loadings plot for the raw material properties (middle) and loadings plot for the process parameters (bottom) for LV1.

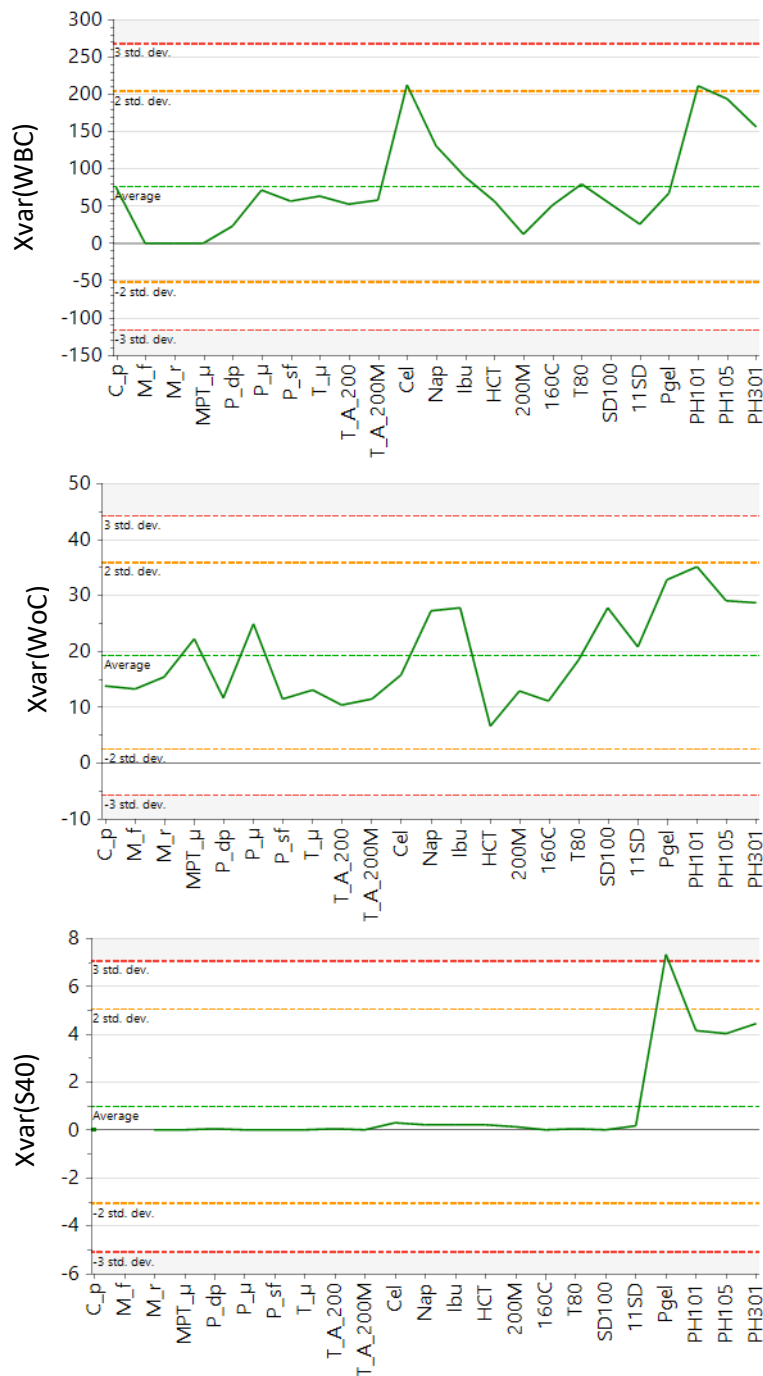


Figure 6.10: The deviation for each powder of the API/filler dataset from the average value within a dataset for WBC (top), WoC (middle) and S40 (bottom).

The second LV captured the variability in granule size and friability (Figure 6.11 – top). Larger granules were typically stronger. A higher DR60 and Com tended to result in larger and stronger granules, while higher WBC, S40, WoC,  $\rho_b$  and  $\rho_{true}$  were linked to more fines and weaker granules. The previously mentioned mechanism (i.e., the creation of more liquid bridges) is also valid for the effect of DR60 and WBC on granule size and friability. Again, the effect of WoC and S40 was explained by their mathematical coincidence. A lower powder bed

density, lower particle density and higher compressibility tended to result in larger and stronger granules. This suggested that a higher available void volume (i.e., inter- and intra-particulate voids) of the powder bed in the granulator is beneficial for the granulation process. It is possible that the wetting and (re)distribution of liquid is enhanced for those powders. First, the penetration of the liquid into the inner core of the powder bed could be enhanced and secondly the redistribution of the liquid in the kneading zones could occur more easily because the powder volume can be reduced. This is in contrast to a denser powder bed where the liquid penetration or liquid distribution is more hampered due to the more efficient packing of the denser particles.

The effect of the process parameters upon the different granule quality attributes was also studied by interpreting their loadings for each LV. From these figures (Figure 6.9 – bottom and Figure 6.11 – bottom), it is clear that granules with a smaller fines fraction, a larger oversized fraction, a lower friability and a lower AoR were obtained when a higher MFR and L/S ratio were applied. For both LVs, a higher loading was observed for L/S ratio, indicating its dominant influence on granule quality attributes. This result was expected as this has already been reported by multiple studies (5–11). Overall, the raw material properties were more influencing the granule quality attributes than the process settings because the loadings for most raw material properties were higher for both LVs (Y-axes on Figure 6.9 and 6.11 (middle and bottom)).

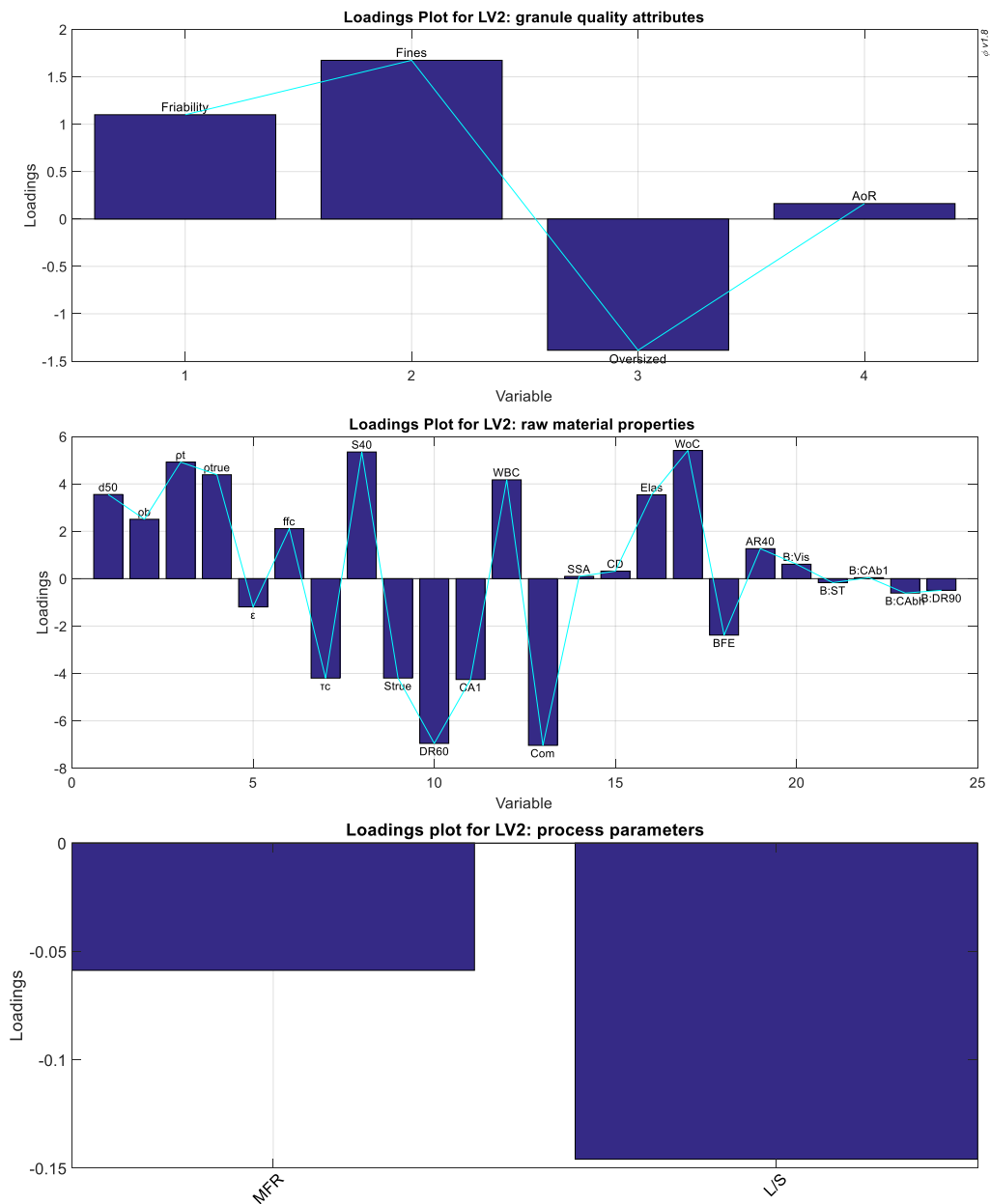


Figure 6.11: Loadings plot for granule quality attributes (top), loadings plot for the raw material properties (middle) and loadings plot for process parameters (bottom) for LV2.

### 6.4.3 PREDICTIONS USING DEVELOPED TPLS MODEL

Using the developed TPLS model, it is possible to predict granule quality attributes (Y) for a given X, R and Z. In this section, the predictive performance is first evaluated by cross-validation of one of the blends. As a final model verification exercise, a suitable formulation and corresponding process settings were predicted for a new API which was not used for the model development.

## 6.4.3.1 CROSS-VALIDATION

The predictive quality of the developed TPLS model was first evaluated for the F1B1 formulation. The 5 experiments covering the completely performed DoE of F1B1 (10 % ibu, 85 % 200M and 5 % E5) were tested for this leave-one-out cross-validation exercise. The predicted granule quality attributes based on the material properties and process settings (used as input in the model for granule quality attribute prediction) were compared to the experimental values for friability, AoR and fines fraction and oversized granules (Figure 6.12). Predicted values were (very) different from the experimental values for experiments at low MFR – low L/S, low MFR – high L/S and high MFR – low L/S. Good predictions were seen at intermediate process settings and at high MFR – high L/S. At these process setting, the predicted values were very close to the experimental values demonstrating some predictive quality of TPLS model, however not over the entire design space.

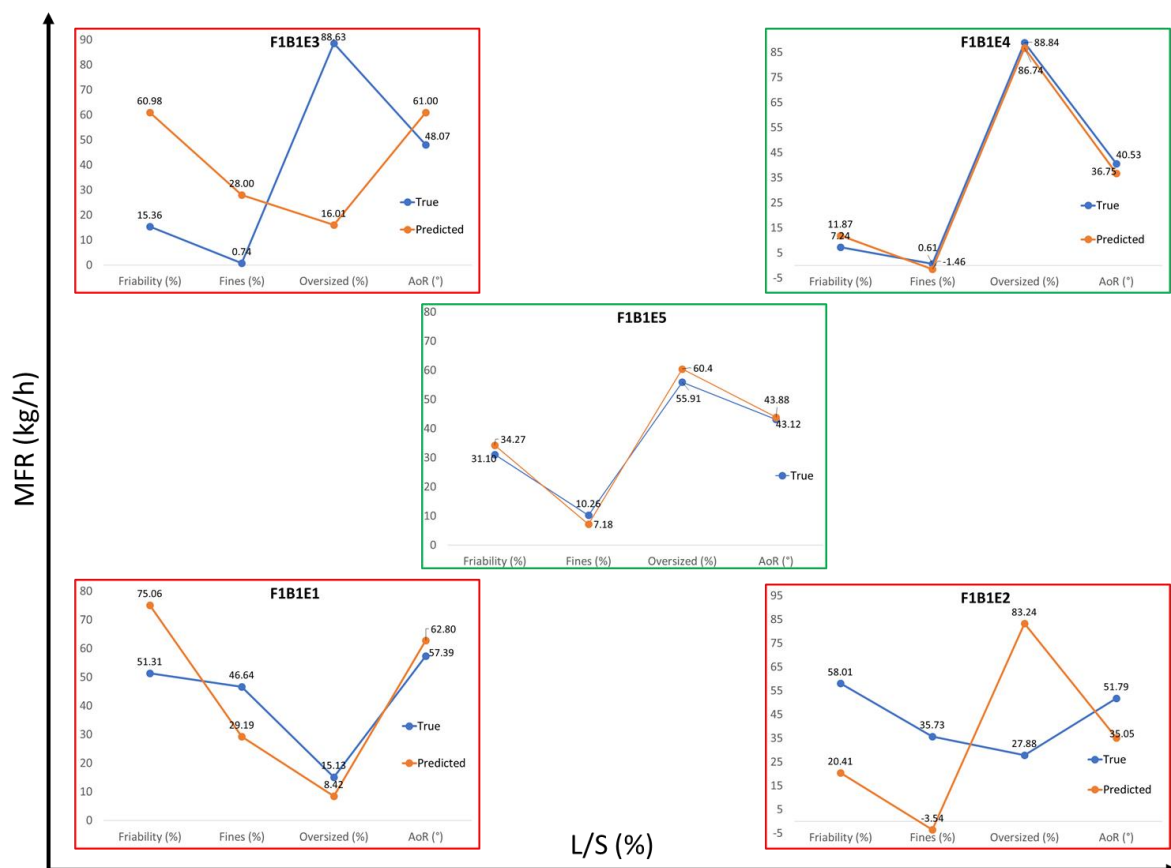


Figure 6.12: Cross-validation of F1B1. True values were compared with predicted values at different process setting covering the design space. Experiments shown in red resulted in poor predictions and in green in good predictions.

## 6.4.3.2 TPLS MODEL USE FOR FORMULATION DEVELOPMENT

The ability to predict granule quality for given combination of X, R and Z could be helpful in formulation development. In this section, API X was considered as a new API. After performing a full raw material characterization for this API X, appropriate excipients and processable ranges were predicted using the TPLS model to result in granules with the desired quality attributes (see section 6.4.3.2.2). A stepwise overview to obtain suggestions for the selection of a formulation and the process settings resulting in the desired granule quality for new APIs is schematically shown in Figure 6.13 and intensively discussed in following sections.

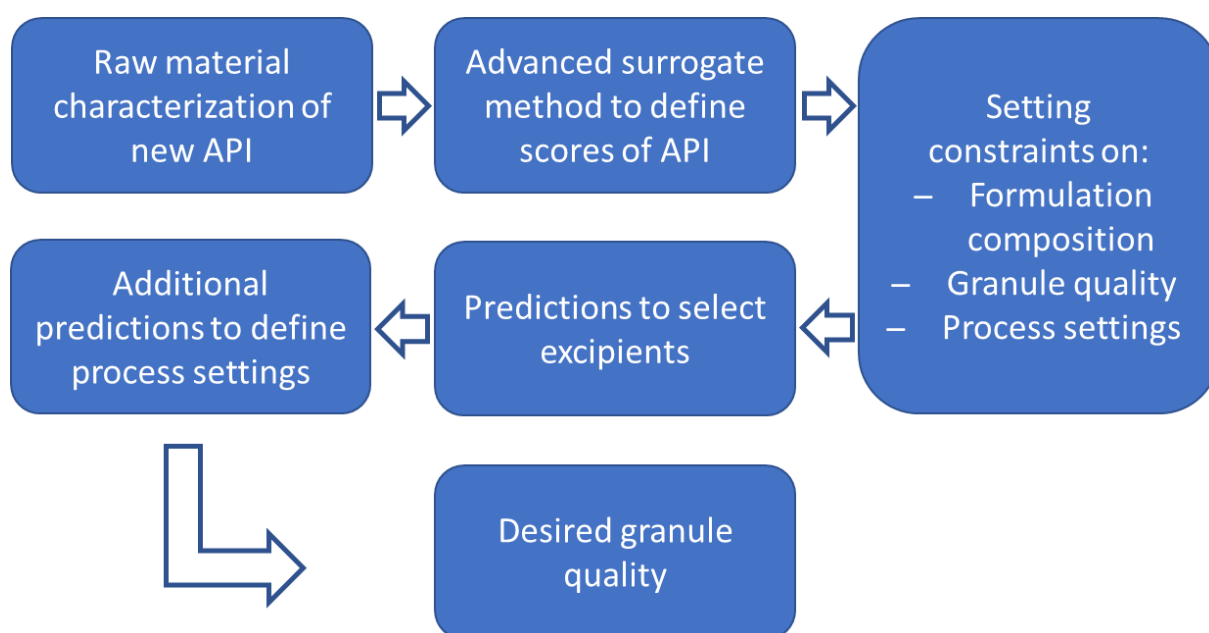


Figure 6.13: Stepwise overview of the systematic approach to select a formulation and the corresponding process settings for a new API.

## 6.4.3.2.1 Advanced surrogate method

As API X was not used in the granulation experiments, the scores of API X could not be determined by the TPLS model. Hence, its location in the regressor space cannot be found. To overcome this issue, an advanced surrogate method was used. First, PCA was used to create a score plot including API X, the 9 APIs and the 7 excipients that were used during the granulation experiments (Figure 6.14). Subsequently, the closest neighbours of API X were determined according to a k-nearest neighbours algorithm (20). Including too many materials may result in uninvestigated interactions, including too few materials may result in properties not being captured well. Hence, the weights of following 5 powders were used to describe the

properties of API X: 59.3 % 'Ibu', 20.4 % 'Nap', 8.7% 'T\_A\_200', 7.5% 'P\_SF' and 4.1% 'Cel'. These weights are the inverse distance of API X to its neighbours.

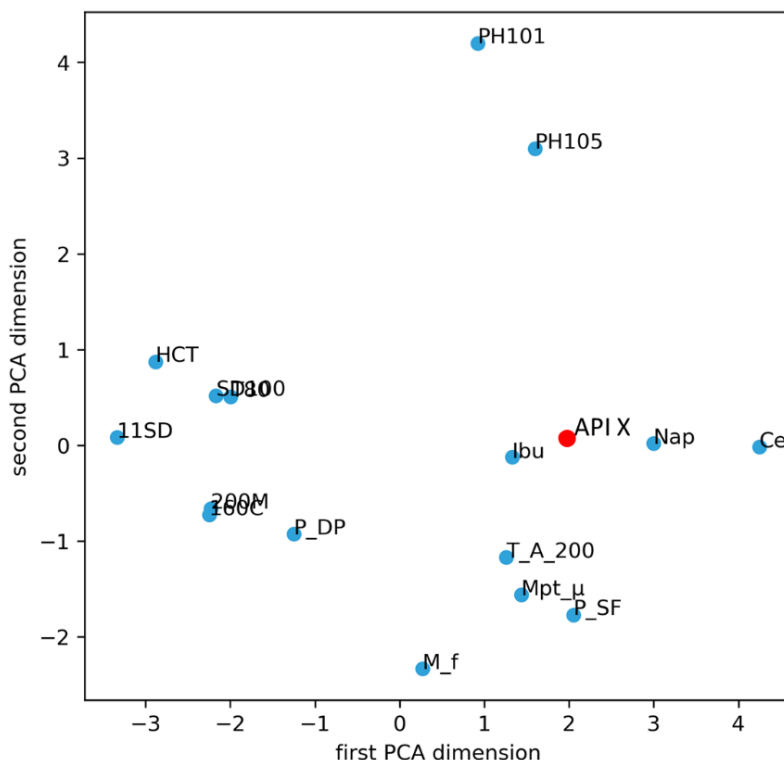


Figure 6.14: PC1 versus PC2 scores plot for the API and excipient dataset.

#### 6.4.3.2.2 Setting constraints

##### *Desired formulation*

As multiple formulations can lead to the desired granule quality, constraints were given to define the formulation by TPLS. The content of API X was allowed to vary between 2 and 25 % (w/w), so that three formulations with a different API content (i.e., 3, 12 and 24 %) could ultimately be selected using the same excipients. The new formulation also had to include MCC due to its added value for granulation robustness (21). The content of the most suitable grade of MCC (i.e., filler 1) should be between 10 and 20 % (w/w). A binder was needed in a fraction between 2 and 5 % (w/w), as the model was trained for this range of binder content. Finally, one soluble filler (i.e., filler 2) was required to complete the formulation to minimize the amount of granulation liquid.

*Desired granule quality*

As TSG is an intermediate process step, a specific granule quality is demanded for further downstream processing. In this study, the fines fraction was limited to 10 % to avoid filter clogging in the drying cells during the drying process. Friability could not exceed 20 % to yield granules which resist the impact of the wet and dry transfer line and the drying phase. In addition, the angle of repose had to be below 45° to guarantee a passable flow. No constraints were set on the oversized fraction because a small fraction in oversized granules is typically correlated with a larger fraction in fines (see constraint on fines) and an excess in oversized granules can be milled in the conditioning unit of the ConsiGma™-25 system. It has to be emphasized that the desired granule quality is chosen based on the experience of the authors. However, the desired granule responses can be easily modified before the start of the predictions.

*Process settings*

Constraints were also set on the process settings. MFR was only allowed to vary between 10 and 20 kg/h, as those ranges were also used to calibrate the TPLS model. L/S could not exceed 20 % to avoid a too long drying time. Similar to the constraints on the desired granule quality, the maximal allowed L/S ratio can also be modified.

## 6.4.3.2.3 Selection of optimal excipients and process settings

In this section, different scenarios were predicted. The prediction of a scenario is defined as the prediction of the granule quality attributes for a certain formulation, whereof the formulation properties are dependent of the properties of the selected raw materials (X) and the ratios in which these raw materials are combined (R), processed at specific process parameters (Z), herewith taking all of the aforementioned constraints (section 6.4.3.2.2) into account. The different scenarios could differ in filler 1 (PH101 or PH105), filler 2 (200M, 11SD, 160C, T80 or 100SD), binder (E5, K30 or KEF), API content and excipient content (resulting in different blend ratios) and in process settings. Clearly, an infinite number of combinations are possible. As a consequence, an infinite amount of scenarios could be predicted. Therefore, a total of 25,000,000 different scenarios were predicted. Subsequently, after each prediction, the predicted granule quality was compared to the desired quality set at constraints. An example of a scenario can be found in Table 6.3.



Table 6.3: Example of a possible scenario: a random combination of the different excipients and process setting, taking all constraints into account.

<b>Formulation composition</b>	
<b><i>Raw material</i></b>	<b><i>Fraction (%)</i></b>
API X	18.4
Filler 1: PH101	19.1
Filler 2: 160C	59.3
Binder: K30	3.2
<b>Process settings</b>	
MFR (kg/h)	12.4
L/S ratio (%)	7.2

Table 6.4 shows the fraction in successful predictions for each excipient. This is the fraction of predictions (only predictions at which the certain excipient was involved), that resulted in the desired granule quality (see 6.4.3.2.2: desired granule quality). As the fraction of successful predictions was slightly higher with PH101, it was chosen as filler 1. Although Lactose 200M did not have the highest fraction of successful predictions, it was selected as filler 2 in the formulation. The higher dissolution rate of 11SD and 160C explained the higher fraction of successful predictions as a higher dissolution rate was related to a lower fraction of fines, a lower friability and a lower AoR (Figure 6.9 and 6.11). However, the higher dissolution rate also reduces the process robustness, since small deviations in liquid flow rate or mass feed rate during manufacturing could strongly affect the granule quality. Therefore, the selection of 200M was justified. HPMC E5 and PVP K30 clearly had a higher probability to result in the desired granule quality compared to HPC KEF. HPMC E5 was selected as it resulted in the highest success rate.

Table 6.4: Overview of the fraction of successful predictions for each filler 1 (MCC filler), filler 2 (soluble filler) and binder.

Excipient	Raw material	Fraction of successful predictions (%)
Filler 1	<b>MCC PH101</b>	43.41
Filler 1	MCC PH105	42.70
Filler 2	<b>Lactose 200M</b>	41.02
Filler 2	Lactose T80	41.00
Filler 2	Mannitol SD100	37.52
Filler 2	Lactose 11SD	49.02
Filler 2	Mannitol 160C	46.68
Binder	<b>HPMC E5</b>	45.10
Binder	PVP K30	44.35
Binder	HPC KEF	39.72

In a next step, only the successful predictions with the formulation consisting of API X, lactose 200M, MCC PH101 and HPMC E5 were taken into account to create Figure 6.15. This figure plots the fraction of successful predictions for each content of each raw material which results in a granule quality within specifications. This allowed to identify the content of a certain raw material in the formulation that has a higher probability to result in granule quality within the set specifications. Multiple combinations of raw materials could result in the desired granule quality. In general, a lower binder content resulted in more successful predictions, as the highest peak was observed around 2 % (Figure 6.15 – yellow peak). This result is in contrast to the findings of Keleb et al. and Dhenge et al. (22,23). Granule growth was favoured in these studies at higher binder concentration. However, a wet binder addition was used in these studies in contrast to our study. It is possible that for our study a higher content of filler 2 (i.e., lactose 200M) at the expense of the binder results in more granule growth. This was confirmed when the 4 centerpoint experiments of the DoE of F4B2 (i.e., 40 % M<sub>f</sub>, 55 % T80 and 5 % E5) and F9B2 (i.e., 40 % M<sub>f</sub>, 58 % T80 and 2 % E5) were one-on-one compared, as both formulations applied identical process settings. The latter blend contained 3 % less binder in favour of lactose T80. Figure 6.16 demonstrated that, except for the experiment at low MFR and low L/S ratio, stronger granules (i.e., lower friability), less fines, more oversized granules and better flowing granules (i.e., lower AoR) were obtained at the lower binder content. Granule growth was hence clearly promoted at lower binder content for this formulation. As

the residence time in a twin-screw granulation process is rather short (i.e., 4-20 seconds (9)), it is suggested that the high dissolution rate of the hydrophilic filler is more effective for granule growth due to the formation of strong liquid bonds than a larger fraction of dry binder that still needs to be activated during the short residence time in the granulator. Lower MCC concentrations also yielded the desired granule quality more often (Figure 6.15 – red peak). According to the constraints (see 6.4.3.2.2), the L/S ratio was not allowed to exceed 20 % but higher L/S ratios are generally needed at higher MCC content due to their high WBC (21), explaining the lower probability to result in successful predictions. Less successful predictions were also observed when the API content increased, this is probably due to its hydrophobic characteristics (Figure 6.14). More successful predictions were observed using a higher 200M content as this hydrophilic filler is advantageous for granule growth. The decrease observed at a 200M content above 78 % was due to the lower number of predictions executed at a high lactose content, as in that scenario the binder, API and MCC content all had to be lower in order not to exceed the total of 100 %.

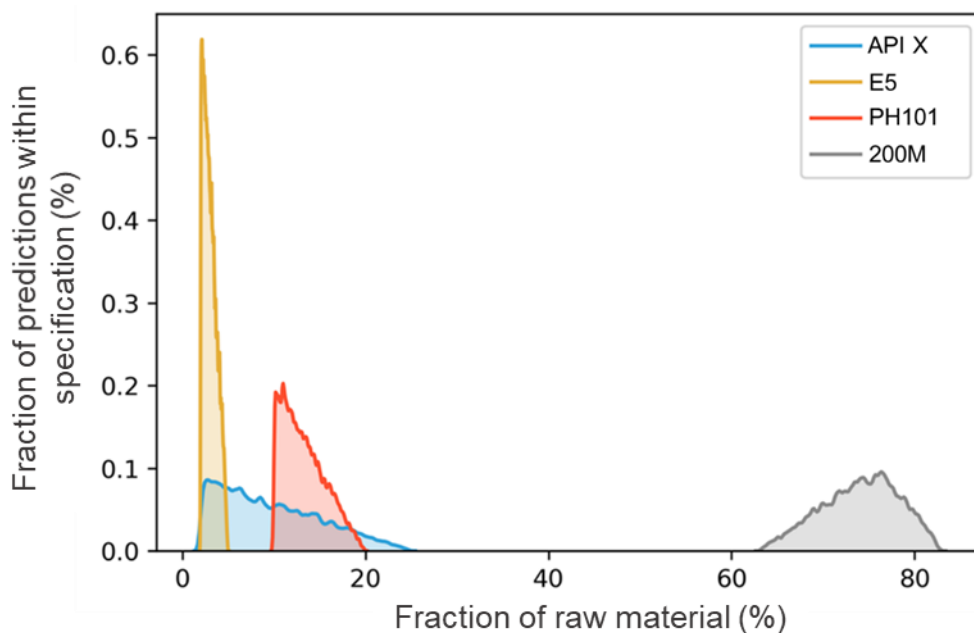


Figure 6.15: Fraction of successful predictions for each fraction of the different raw materials.

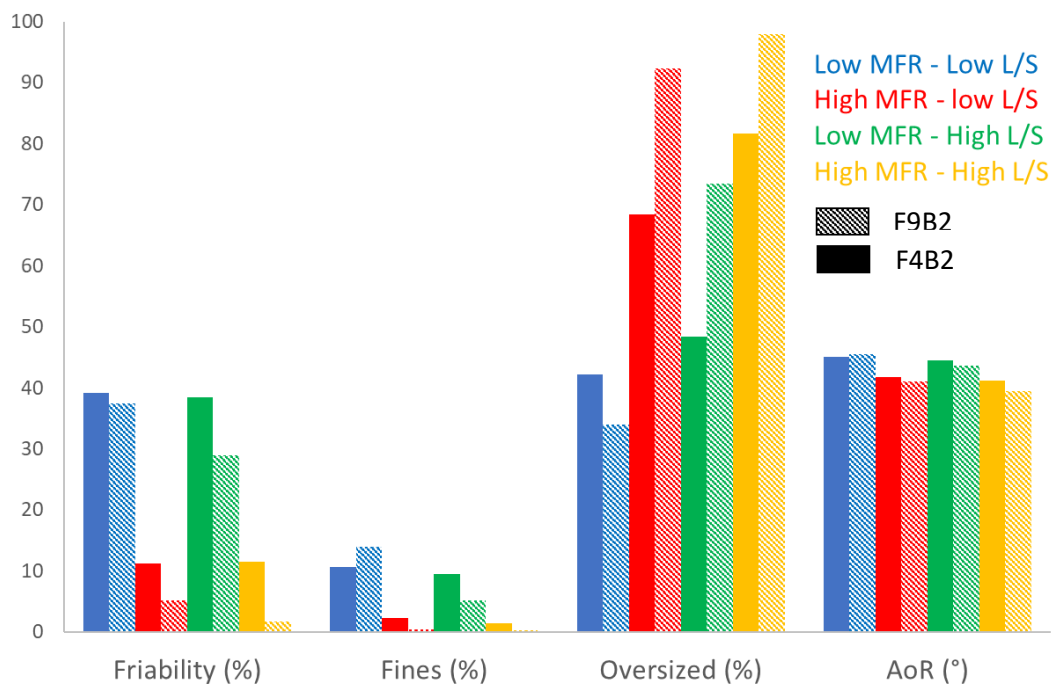


Figure 6.16: Comparison of friability, fines, oversized granules and AoR results of F4B2 (solid bars) and F9B2 (striped bars) for the 4 DoE experiments: low MFR – low L/S (blue), high MFR – low L/S (red), low MFR – high L/S (green) and high MFR – high L/S (orange).

In this case study, the API content was varied at three levels, yielding granules with a different potency. The blend composition for these 3 API concentrations which are predicted to provide the desired granule quality attributes are shown in Table 6.5. In a next step, additional predictions, during which the process settings for each of these 3 formulations were varied, were performed. This allowed to establish contour plots for friability, fines and AoR for each blend (Figure 6.17). Only the area (i.e., combination of MFR and L/S ratio) which yielded the desired granule quality, according to the prediction by the TPLS model, was coloured in the plots. The colour gradient in Figure 6.17 corresponds to the predicted change in fines, friability or AoR at different combinations of MFR and L/S ratio. It can be seen that the area of successful predictions was very similar for all three formulations. Although formulation 3 contained more hydrophobic API at the expense of the hydrophilic filler lactose, a similar granule quality was predicted for the combination of MRF and L/S values. This can be explained by other properties of API X, having a favourable effect on granule growth. In contrast to 200M, API X has a lower density and a higher compressibility which have previously been identified having a positive effect on granule growth. It is suggested that a better liquid distribution could be obtained for formulation 3. This is also confirmed by the results in Figure 6.18, showing the comparison of the experimentally determined granule quality attributes for

the three different blends using three different process settings. It was demonstrated that the granule quality attributes were similar for the three blends at these process settings.

Table 6.5: Overview of the composition of the three formulation with varying content of API X.

Raw material	Formulation 1	Formulation 2	Formulation 3
API X	3 %	12 %	24 %
200M	82 %	73 %	61 %
PH101	10 %	10 %	10 %
E5	5 %	5 %	5 %

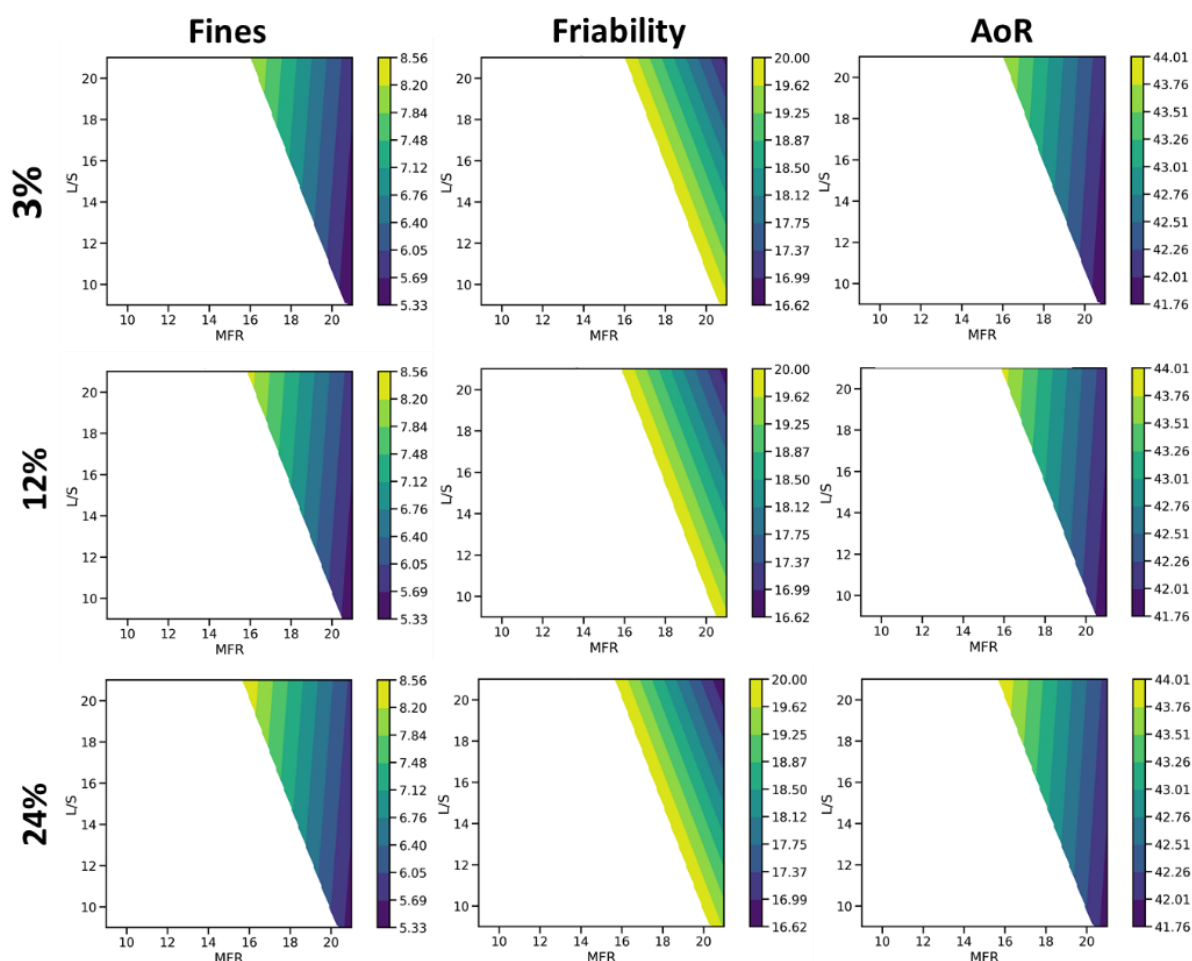


Figure 6.17: Contour plots for the formulation with 3 (top), 12 (middle) and 24 % of API for the fines fraction, friability and angle of repose. The quantitatively predicted responses are indicated by the coloured gradient axes for a certain combination of process settings. The area in the parameter space where the granule quality targets were not met are masked out (white).

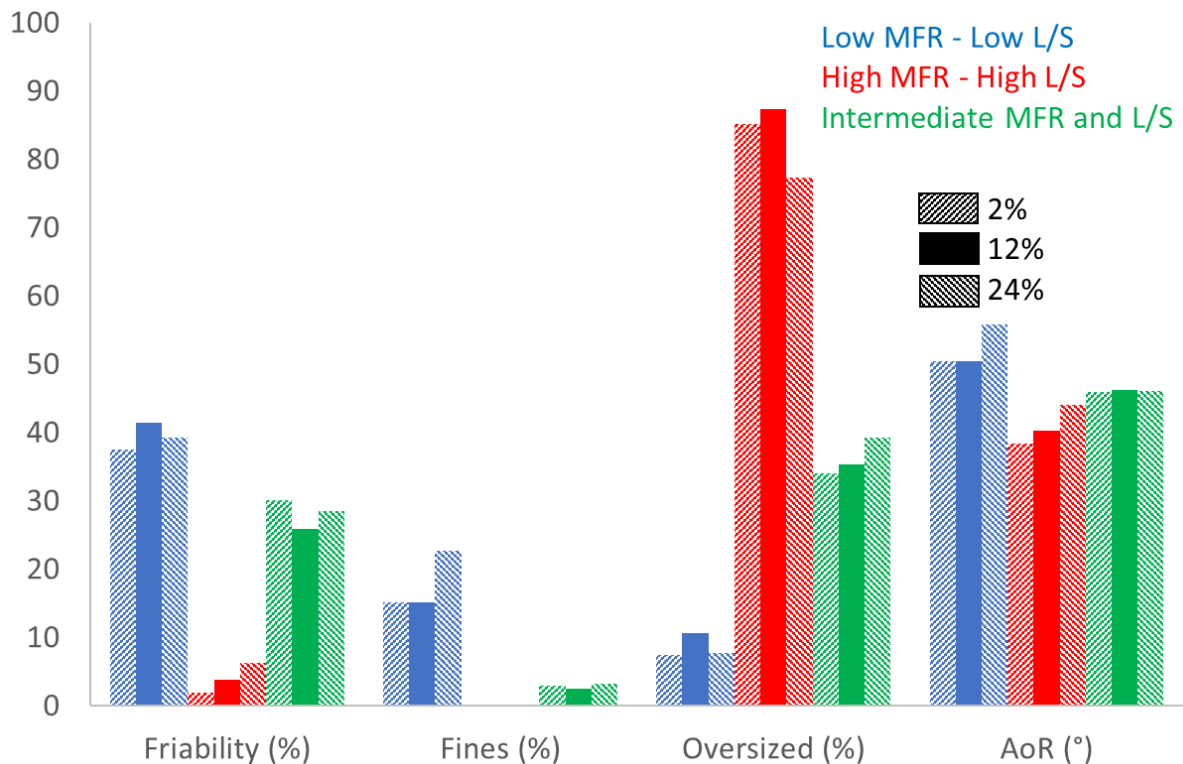


Figure 6.18: Granule quality (friability, fines and oversized fraction and angle of repose) for the formulations consisting of 3, 12 and 24 % API processed at three different process settings: low MFR: 10 kg/h – low L/S: 10 % (blue), high MFR: 20 kg/h – high L/S: 20 % (red) and intermediate MFR/ 15 kg/h and L/S: 15 % (green).

Finally, the predicted granule quality attributes for each of the three blends were compared to the experimentally determined granule quality attributes. The four edges of the contour plot (Figure 6.17) and a centre point were verified. The comparison of the experimentally determined granule quality attributes with the predicted granule quality was shown for the blend containing 12 % API in Figure 6.19. A similar comparison was also seen for the blends with 2 and 24 % API. Similar to the cross-validation results (Figure 6.11), the best predictions were observed for the intermediate and high MFR – high L/S process settings. At these process settings the predicted values were, except for the oversized fraction, close to the experimental values, indicating some predictive quality of the TPLS model. It is possible that the fraction of oversized granules is harder to predict as it is a cut-off value (i.e., >2000  $\mu\text{m}$ ) of the granule size distribution to indicate the granule size. The validation experiments showed that large oversized fraction and a fines fraction of almost zero was observed at high L/S and high MFR, indicating that a paste would be formed at higher L/S ratio. However, an actual cut-off for the

formation of a paste cannot be predicted by the model. Possible reasons of the TPLS model prediction challenges are discussed in the next section.

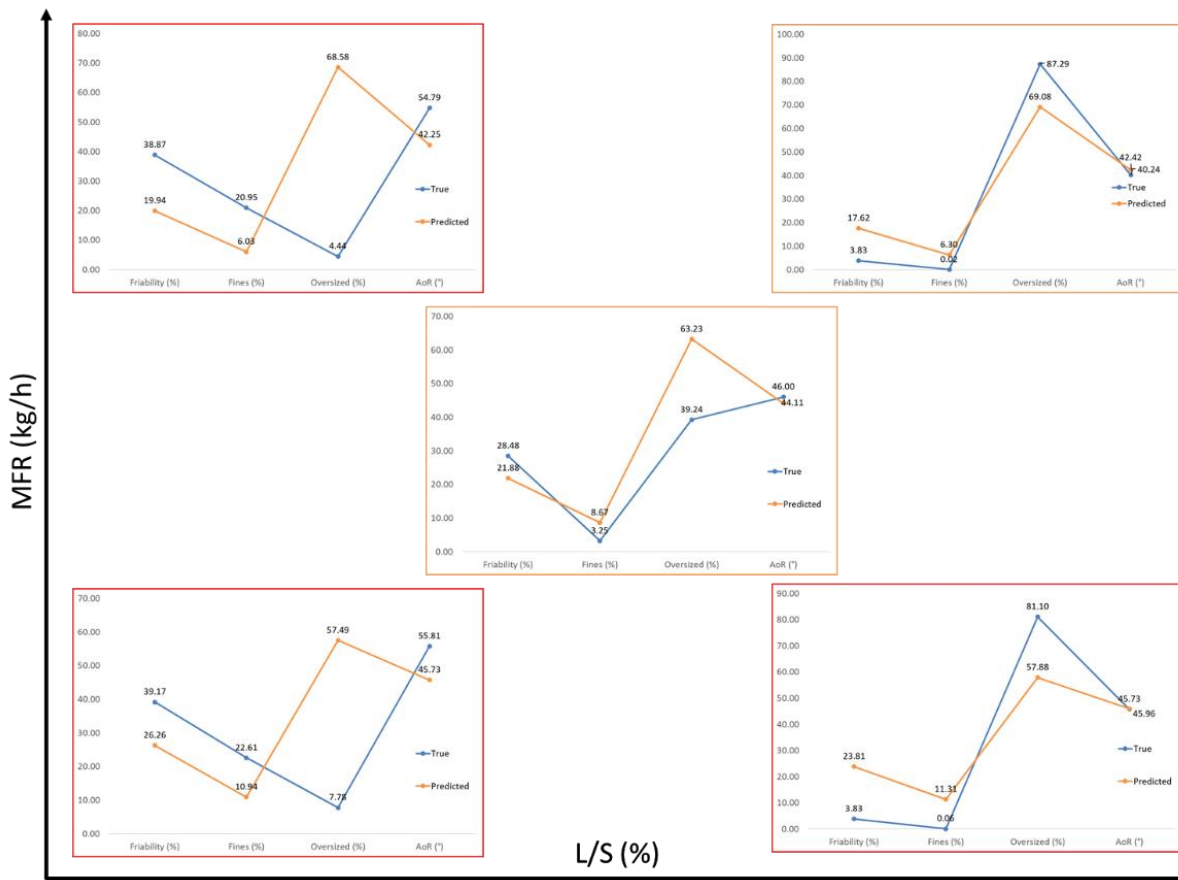


Figure 6.19: Comparison of predicted versus experimentally determined granule quality attributes at different process setting for the blend consisting of 12 % API. The L/S ratio for these validation experiments was varied from 10 to 20 %, whereas the MFR was varied from 10 to 20 kg/h.

#### 6.4.4 LIMITATIONS, CHALLENGES AND FUTURE PERSPECTIVES

In general, the predictions of current TPLS model are only valid for the studied experimental space and for fixed conditions such as the screw configuration and screw speed because both have an impact on the granule quality (8,24,25). Further, only dry binders were added to the powder mixture.

The predictions, either for the cross-validation (Figure 6.11) and the new formulation (Figure 6.19), were not reliable for all process setting (lower MFR and lower L/S ratio). As TPLS is a linear regression technique, it allows a straightforward interpretation which gives an enhanced process understanding. However, this method has a lower predictive ability compared to non-linear techniques (35).

Multiple studies have already shown interactions (i.e., non-linear correlations) between different process settings (MFR, screw speed and/or L/S ratio) (6,22–26). Most likely interactions between the process settings or between raw material properties and process settings occurred, resulting in a non-linear correlation with the granule quality. In addition, extreme formulations (e.g., formulation 5 which lacked soluble components and which was processed with L/S ratios up to 84 %) were selected for the granulation experiments. This is beneficial for process understanding as the inclusion of more divergent formulations allows to highlight the most influencing raw material properties. In addition, a more divergent dataset also increases the probability that a future API will fall within the already investigated ranges (i.e., the regressor space). However, the very divergent formulations processed with different process settings resulted in diverse granule quality attributes. This enlarges the regressor space, making it more complicated to find the correct real values in that space. In general, the addition of granulation experiments, performed with new APIs or excipients, will also increase the predictive ability of the TPLS model because it is a data-driven model. The large database can also be used for other predictions such as non-linear PLS. As these techniques make non-linear correlations, their predictions may be closer to the real values.

## 6.5 CONCLUSIONS

In this study, a TPLS model was developed to link raw material properties, the ratios in which these raw materials were combined and the applied process parameters for a twin-screw wet granulation process. Very divergent APIs and excipients were combined for granulation experiments under different process settings. This allowed to enhance the process understanding of the granulation process. First, the effect of the different raw material properties on granule quality was studied. The variability in dissolution rate, compressibility, water binding capacity, powder density and solubility affected the variability in granule quality the most. Overall, the raw material properties were more influencing the granule quality attributes than the process parameters. Further, the predictive ability of the TPLS model was used to select a suitable formulation for a new API. A first run of predictions suggested to use lactose 200M, microcrystalline cellulose PH101 and HPMC E5 as suitable excipients in combination with different API contents. However, the comparison of the experimental granule quality with the predicted granule quality at different process settings indicated that the predictive ability of TPLS was only valid at specific process settings. However, despite the



current pitfalls, the TPLS model has the potential to predict a reasonable starting point for formulation and process parameters for new APIs. This approach can reduce the experimental effort, the consumption of the expensive API and the development time to select a suitable formulation and to find optimal process parameters during product development. In a next step, other modelling techniques such as non-linear PLS can be used to increase the predictive power.

## 6.6 ACKNOWLEDGMENTS

The authors would like to thank Salvador García-Muñoz for the lectures on the use of multivariate data in pharmaceutical development and providing access to the Phi\_1.8 toolbox.

## 6.7 REFERENCES

1. Vervaet C, Remon JP. Continuous granulation in the pharmaceutical industry. *Chem Eng Sci.* 2005;60(14):3949–57.
2. Garcia-Munoz S. Two novel methods to analyze the combined effect of multiple raw-materials and processing conditions on the product's final attributes: JRPLS and TPLS. *Chemom Intell Lab Syst.* 2014;133:49–62.
3. Van Snick B, Dhondt J, Pandelaere K, Bertels J, Mertens R, Klingeleers D, et al. A multivariate raw material property database to facilitate drug product development and enable in-silico design of pharmaceutical dry powder processes. *Int J Pharm [Internet].* 2018;549(1–2):415–35. Available from: <https://doi.org/10.1016/j.ijpharm.2018.08.014>
4. Lee SL, O'Connor TF, Yang X, Cruz CN, Chatterjee S, Madurawe RD, et al. Modernizing Pharmaceutical Manufacturing: from Batch to Continuous Production. *J Pharm Innov.* 2015;10(3):191–9.
5. Fonteyne M, Correia A, Plecker D, Vercruyssen J, Ili I, Zhou Q, et al. Impact of microcrystalline cellulose material attributes : A case study on continuous twin screw granulation. 2015;478:705–17.
6. Meier R, Moll KP, Krumme M, Kleinebudde P. Impact of fill-level in twin-screw granulation on critical quality attributes of granules and tablets. *Eur J Pharm Biopharm [Internet].* 2017;115:102–12. Available from: <http://dx.doi.org/10.1016/j.ejpb.2017.02.010>
7. Vanhoorne V, Janssens L, Vercruyssen J, De Beer T, Remon JP, Vervaet C. Continuous twin screw granulation of controlled release formulations with various HPMC grades. *Int J Pharm [Internet].* 2016;511(2):1048–57. Available from: <http://dx.doi.org/10.1016/j.ijpharm.2016.08.020>
8. Vercruyssen J, Burggraeve A, Fonteyne M, Cappuyns P, Delaet U, Van Assche I, et al. Impact of screw configuration on the particle size distribution of granules produced by twin screw granulation. *Int J Pharm [Internet].* 2015;479(1):171–80. Available from: <http://dx.doi.org/10.1016/j.ijpharm.2014.12.071>
9. Vercruyssen J, Córdoba Díaz D, Peeters E, Fonteyne M, Delaet U, Van Assche I, et al. Continuous twin screw granulation: Influence of process variables on granule and tablet quality. *Eur J Pharm Biopharm [Internet].* 2012;82(1):205–11. Available from: <http://dx.doi.org/10.1016/j.ejpb.2012.05.010>
10. Portier C, Pandelaere K, Delaet U, Vigh T, Di Pretoro G, De Beer T, et al. Continuous twin screw granulation: A complex interplay between formulation properties, process settings and screw design. *Int J Pharm [Internet].* 2020;576(December 2019):119004. Available from: <https://doi.org/10.1016/j.ijpharm.2019.119004>
11. Verstraeten M, Van Hauwermeiren D, Lee K, Turnbull N, Wilsdon D, am Ende M, et al. In-depth experimental analysis of pharmaceutical twin-screw wet granulation in view of

- detailed process understanding. *Int J Pharm* [Internet]. 2017;529(1–2):678–93. Available from: <http://dx.doi.org/10.1016/j.ijpharm.2017.07.045>
12. Fonteyne M, Wickström H, Peeters E, Vercruyse J, Ehlers H, Peters BH, et al. Influence of raw material properties upon critical quality attributes of continuously produced granules and tablets. *Eur J Pharm Biopharm* [Internet]. 2014;87(2):252–63. Available from: <http://dx.doi.org/10.1016/j.ejpb.2014.02.011>
13. Thompson MR. Twin screw granulation-review of current progress. *Drug Dev Ind Pharm*. 2015;41(8):1223–31.
14. Willecke N, Szepes A, Wunderlich M, Remon JP, Vervaet C, Beer T De. Identifying overarching excipient properties towards an in-depth understanding of process and product performance for continuous twin-screw wet granulation. *Int J Pharm* [Internet]. 2017;522(1–2):234–47. Available from: <http://dx.doi.org/10.1016/j.ijpharm.2017.02.028>
15. Willecke N, Szepes A, Wunderlich M, Remon JP, Vervaet C, Beer T De. A novel approach to support formulation design on twin screw wet granulation technology : Understanding the impact of overarching excipient properties on drug product quality attributes. *Int J Pharm* [Internet]. 2018;545(1–2):128–43. Available from: <https://doi.org/10.1016/j.ijpharm.2018.04.017>
16. Schulze D. Practical determination of flow properties. In: *Powders and Bulk Solids: Behavior, Characterization, Storage and Flow* [Internet]. Berlin, Heidelberg: Springer Berlin Heidelberg; 2008. p. 75–111. Available from: [https://doi.org/10.1007/978-3-540-73768-1\\_4](https://doi.org/10.1007/978-3-540-73768-1_4)
17. Patel S, Kaushal AM, Bansal AKB. The effect of starch paste and sodium starch glycolate on the compaction behavior of wet granulated acetaminophen formulations. *J Excipients Food Chem*. 2011;
18. Vandevivere L, Denduyver P, Portier C, Häusler O, Beer T De, Vervaet C. Influence of binder attributes on binder effectiveness in a continuous twin screw wet granulation process via wet and dry binder addition. *Int J Pharm* [Internet]. 2020;585(February):119466. Available from: <https://doi.org/10.1016/j.ijpharm.2020.119466>
19. Nelson PRC, Taylor PA, MacGregor JF. Missing data methods in PCA and PLS: Score calculations with incomplete observations. *Chemom Intell Lab Syst*. 1996;35(1):45–65.
20. Triguero I, Maillo J, Luengo J, Garcia S, Herrera F. From Big Data to Smart Data with the K-Nearest Neighbours Algorithm. *Proc - 2016 IEEE Int Conf Internet Things; IEEE Green Comput Commun IEEE Cyber, Phys Soc Comput IEEE Smart Data, iThings-GreenCom-CPSCoM-Smart Data 2016*. 2017;859–64.
21. Portier C, De Vriendt C, Vigh T, Di Pretoro G, De Beer T, Vervaet C, et al. Continuous twin screw granulation: Robustness of lactose/MCC-based formulations. *Int J Pharm* [Internet]. 2020;588(June):119756. Available from: <https://doi.org/10.1016/j.ijpharm.2020.119756>
22. Keleb EI, Vermeire A, Vervaet C, Remon JP. Twin screw granulation as a simple and efficient tool for continuous wet granulation. *Int J Pharm*. 2004;273(1–2):183–94.

23. Dhenge RM, Cartwright JJ, Hounslow MJ, Salman AD. Twin screw wet granulation: Effects of properties of granulation liquid. *Powder Technol* [Internet]. 2012;229:126–36. Available from: <http://dx.doi.org/10.1016/j.powtec.2012.06.019>

24. Portier C, Pandelaere K, Delaet U, Vigh T, Kumar A, Di Pretoro G, et al. Continuous twin screw granulation: Influence of process and formulation variables on granule quality attributes of model formulations. *Int J Pharm* [Internet]. 2020;576(December 2019):118981. Available from: <https://doi.org/10.1016/j.ijpharm.2019.118981>

25. Thompson MR, Sun J. Wet Granulation in a Twin-Screw Extruder: Implications of Screw Design. *J Pharm Sci* [Internet]. 2010 Apr 1 [cited 2019 Jan 23];99(4):2090–103. Available from: <https://www.sciencedirect.com/science/article/pii/S0022354916304920>

## 6.8 APPENDIX

Appendix A: Overview of applied process setting for all experiments. Experiments that were not able to be processed are depicted in red.

1	MFR	L/S	2	MFR	L/S	3	MFR	L/S	4	MFR	L/S
F1B1E1	10	6	F2B1E1	10	6	F3B1E1	10	18	F4B1E1	10	6
F1B1E2	20	6	F2B1E2	20	6	F3B1E2	20	18	F4B1E2	20	6
F1B1E3	10	12	F2B1E3	10	12	F3B1E3	10	79	F4B1E3	10	10
F1B1E4	20	12	F2B1E4	20	12	F3B1E4	20	78	F4B1E4	20	10
F1B1E5	15	9	F2B1E5	15	9	F3B1E5	15	48.5	F4B1E5	15	8
F1B1E6	15	9	F2B1E6	15	9	F3B1E6	15	48.5	F4B1E6	15	8
F1B1E7	15	9	F2B1E7	15	9	F3B1E7	15	48.5	F4B1E7	15	8
F1B2E1	10	8	F2B2E1	10	6	F3B2E1	10	24	F4B2E1	10	6
F1B2E2	20	8	F2B2E2	20	6	F3B2E2	20	24	F4B2E2	20	6
F1B2E3	10	14	F2B2E3	10	14	F3B2E3	10	78	F4B2E3	10	9.0
F1B2E4	20	14	F2B2E4	20	14	F3B2E4	20	78	F4B2E4	20	9.0
F1B2E5	15	11	F2B2E5	15	10	F3B2E5	15	51	F4B2E5	15	7.5
F1B2E6	15	11	F2B2E6	15	10	F3B2E6	15	51	F4B2E6	15	7.5
F1B2E7	15	11	F2B2E7	15	10	F3B2E7	15	51	F4B2E7	15	7.5
F1B3E1	10	8	F2B3E1	10	9	F3B3E1	10	24	F4B3E1	10	6
F1B3E2	20	8	F2B3E2	20	9	F3B3E2	20	24	F4B3E2	20	6
F1B3E3	10	16	F2B3E3	10	15	F3B3E3	10	42	F4B3E3	10	8
F1B3E4	20	16	F2B3E4	20	15	F3B3E4	20	42	F4B3E4	20	8
F1B3E5	15	12	F2B3E5	15	12	F3B3E5	15	33	F4B3E5	15	7
F1B3E6	15	12	F2B3E6	15	12	F3B3E6	15	33	F4B3E6	15	7
F1B3E7	15	12	F2B3E7	15	12	F3B3E7	15	33	F4B3E7	15	7

5	MFR	L/S	6	MFR	L/S	7	MFR	L/S
F5B1E1	10	36	F6B1E1	10	24	F7B1E1	10	30
F5B1E2	20	36	F6B1E2	20	24	F7B1E2	20	30
F5B1E3	10	84	F6B1E3	10	45	F7B1E3	10	60
F5B1E4	20	85	F6B1E4	20	45	F7B1E4	20	60
F5B1E5	15	59	F6B1E5	15	34.5	F7B1E5	15	45
F5B1E6	15	59	F6B1E6	15	34.5	F7B1E6	15	45
F5B1E7	15	59	F6B1E7	15	34.5	F7B1E7	15	45
F5B2E1	10	36	F6B2E1	10	13	F7B2E1	10	15.5
F5B2E2	20	36	F6B2E2	20	13	F7B2E2	20	15.5
F5B2E3	10	58	F6B2E3	10	39	F7B2E3	10	21
F5B2E4	20	58	F6B2E4	20	39	F7B2E4	20	21
F5B2E5	15	47	F6B2E5	15	26	F7B2E5	15	18.25
F5B2E6	15	47	F6B2E6	15	26	F7B2E6	15	18.25
F5B2E7	15	47	F6B2E7	15	26	F7B2E7	15	18.25
F5B3E1	10	24	F6B3E1	10	11	F7B3E1	10	6
F5B3E2			F6B3E2	20	11	F7B3E2	20	6
F5B3E3	10	48	F6B3E3	10	35	F7B3E3	10	8
F5B3E4			F6B3E4	20	35	F7B3E4	20	8
F5B3E5			F6B3E5	15	23	F7B3E5	15	7
F5B3E6			F6B3E6	15	23	F7B3E6	15	7
F5B3E7			F6B3E7	15	23	F7B3E7	15	7

8	MFR	L/S	9	MFR	L/S	10	MFR	L/S
F8B1E1	10	6	F9B1E1	10	7	F10B1E1	10	15
F8B1E2	20	6	F9B1E2	20	7	F10B1E2	20	15
F8B1E3	10	11	F9B1E3	10	10	F10B1E3	10	27
F8B1E4	20	11	F9B1E4	20	10	F10B1E4	20	27
F8B1E5	15	8.5	F9B1E5	15	8.5	F10B1E5	15	21
F8B1E6	15	8.5	F9B1E6	15	8.5	F10B1E6	15	21
F8B1E7	15	8.5	F9B1E7	15	8.5	F10B1E7	15	21
F8B2E1	10	6	F9B2E1	10	6	F10B2E1	10	27
F8B2E2	20	6	F9B2E2	20	6	F10B2E2		
F8B2E3	10	14	F9B2E3	10	9	F10B2E3	10	36
F8B2E4	20	14	F9B2E4	20	9	F10B2E4		
F8B2E5	15	10	F9B2E5	15	7.5	F10B2E5	15	32
F8B2E6	15	10	F9B2E6	15	7.5	F10B2E6	15	32
F8B2E7	15	10	F9B2E7	15	7.5	F10B2E7	15	32
F8B3E1	10	9	F9B3E1	10	6	F10B3E1	10	39
F8B3E2	20	9	F9B3E2	20	6	F10B3E2		
F8B3E3	10	15	F9B3E3	10	9	F10B3E3		
F8B3E4	20	15	F9B3E4	20	9	F10B3E4		
F8B3E5	15	12	F9B3E5	15	7.5	F10B3E5		
F8B3E6	15	12	F9B3E6	15	7.5	F10B3E6		
F8B3E7	15	12	F9B3E7	15	7.5	F10B3E7		

**7 THE INFLUENCE OF  
EQUIPMENT DESIGN AND  
PROCESS PARAMETERS ON  
GRANULE BREAKAGE IN A  
SEMI-CONTINUOUS FLUID  
BED DRYER AFTER  
CONTINUOUS TWIN-SCREW  
WET GRANULATION**

**ABSTRACT**

The semi-continuous drying unit of a continuous from-powder-to-tablet manufacturing line (ConsiGma™ 25, GEA Pharma Systems) is a crucial intermediate process step to achieve the desired tablet quality. The understanding of the size reduction of pharmaceutical granules during the semi-continuous six-segmented fluid bed drying process is however still lacking. The major goal of this study was to investigate these breakage and attrition phenomena during transport of wet and dry granules (i.e., before and after semi-continuous drying), during filling of a drying cell and during fluid bed drying on a ConsiGma™-25 system (C25). Therefore, the granule size distribution (GSD) was determined at 8 different locations of the continuous manufacturing line. Additionally, the influence of drying air temperature and drying time was assessed. For this purpose, granule size and residual moisture content per size fraction were characterised for granules processed with a commercial-scale ConsiGma™-25 system as well as those produced with the R&D-scale ConsiGma™-1 (C1) system.

Pneumatic transport of the wet granules after twin-screw granulation towards the semi-continuous dryer via the wet transfer line induced extensive breakage. Hereafter, the turbulent filling phase of the fluid bed drying cells caused further moderate breakage and attrition, while additional breakage during drying was limited. Subsequently, the dry transfer line connecting the semi-continuous dryer with the conditioning unit, was responsible for additional extensive breakage and attrition. Generally, a faster drying rate was observed for granules dried with the C25 system in comparison to granules dried with the C1 system, presumably because of heat being transferred by convection and conduction from the surrounding empty cells. Furthermore, for C25, the final GSD was governed by the moisture content of the granules. Both, higher (> 3 %) and very low moisture content (< 1 %) resulted in more breakage and attrition in the dry transfer line. As the final GSD after drying for granules processed with C1 differed significantly from those processed on C25, it is challenging during process and formulation development to produce granules with the C1 that results in a representative GSD for the C25 process.



## 7.1 INTRODUCTION

Among the different techniques for continuous pharmaceutical manufacturing of solid-dosage forms, continuous direct compression (CDC) is the most preferred technique if the involved material and formulation properties allow CDC (1–3). As CDC only involves continuous feeding and blending of the raw materials, followed by tableting of the homogeneous powder blend, the number of intermediate process steps is limited (4). However, CDC is not always applicable due to unfavourable material properties of the Active Product Ingredient (API), such as poor flowability and compatibility and high electrostatics. Obviously, this is even more pronounced for high-loaded formulations (1,3). In addition, low-dose formulations are also often impacted by poorly flowing APIs making it extremely challenging to homogeneously disperse such API in the formulation powder blend. Consequently, tablet content uniformity might be impaired (1). An intermediate granulation step such as roller compaction or twin-screw granulation (TSG) may be required to overcome aforementioned issues (5).

In the last fifteen years, continuous twin-screw wet granulation has gained an increased interest within the pharmaceutical industry (6,7). Many investigations have already been performed on continuous twin-screw wet granulation as unit operation. Some studies have been focussing on the influence of process parameters (6,8–10) and formulation properties (11–18) upon granule quality attributes. Other studies targeted a more fundamental understanding of the twin-screw granulation mechanism (7,8,19–23). Many of these studies used the granulation module of a continuous from-powder-to-tablet line: the ConsiGma™ system (GEA Pharma systems, Wommelgem, Belgium) (7–9,11–14,19). The six-segmented fluid bed drying following the granulation unit of the ConsiGma™ system has been investigated to a lesser extent, although the drying process is crucial to guarantee a good final product.

The stability and repeatability during a long production run of 5 hours was evaluated using 1 formulation for the twin-screw granulation and six-segmented drying unit by Vercruyssen et al. (24). The study showed that the residual moisture content after drying remained stable during the complete run, indicating a reliable drying process for the formulation under study. Additionally, Vercruyssen et al. (25) evaluated whether the product quality (i.e., residual moisture content, particle size distribution, bulk and tapped density, and friability) obtained

by using only a single cell of the segmented dryer unit of the ConsiGma™-25 system (C25) was comparable to the granule quality of granules collected during full-scale manufacturing when all drying cells were filled. As the granule quality was indeed similar, the use of a single cell could therefore be favourable during formulation and process development. However, the study did not investigate potential effects of varying drying parameters. In addition, the granule quality for an identical drying experiment (i.e., identical drying parameters) performed with a mobile ConsiGma™-1 system (designed for R&D studies) was compared to the quality obtained during full-scale manufacturing with the ConsiGma™-25 system. A deviating granule quality was observed, indicating that the ConsiGma™-1 (C1) system was not predictive for the granule quality at steady state phase during full-scale manufacturing.

Other studies aimed at determining the granule moisture content by in-line NIR measurements in the ConsiGma™-25 dryer (26,27). In a recent study, Stauffer et al. (28) highlighted the influence of wet granule properties on drying stability (i.e., air flow deviations). Their study emphasized the importance of granule properties prior to drying as an excess of fine particles accumulating on the surface of the drying filter resulted in an unstable drying process. Moreover, an extensive investigation on the influence of drying process parameters on granule quality attributes and breakage behaviour was performed by De Leersnyder et al. (29). Both a horizontal and vertical set-up of the ConsiGma™-25 was used in this study. The granulator is positioned next to the dryer in the horizontal set-up with a pneumatic granule transfer via a wet transfer line, whereas the granulator is positioned above the dryer with a gravimetric transfer of wet granules to the dryer in a vertical set-up. However, none of these aforementioned studies explored the evolution of the granule size between the granulator outlet and the conditioning unit. In addition, a one-on-one comparison of the drying behaviour and granule quality between ConsiGma™-1 and ConsiGma™-25 had also never been performed at varying drying settings. However, it would facilitate the transfer from R&D equipment (ConsiGma™-1) to clinical and commercial manufacturing (ConsiGma™-25).

In the present study, granules were collected after the granulation module, after the wet transfer line connecting the granulator and dryer, in each of the drying cells (i.e., at different drying times) and after the dry transfer line connecting the dryer with the mill. This allowed to evaluate the granule size distribution at each location throughout the process, whereby the degree of breakage and attrition could be attributed to each individual unit of a horizontal

ConsiGma™-25 line. Hence, this study is designed to fundamentally understand the impact of each process part on granule size. Moreover, these experimental results are essential in the development of a general flowsheet model as well as for a general drying model for the drying-unit of the ConsiGma™-25 line. In addition, the current study also focussed on a more in-depth comparison between the ConsiGma™-1 and ConsiGma™-25. Therefore, the effect of different drying parameters on final granule size, moisture content per size fraction and overall moisture content was investigated. First, this allows to evaluate whether the drying behaviour and resulting granule quality obtained with ConsiGma™-1 is predictive for the ConsiGma™-25. Secondly, the effect of drying settings on granule size could also be determined, allowing to indicate the suboptimal settings that are responsible for excessive breakage of granules whereby the generation of a large amount of fine particles could negatively impact tableting (due to segregation or poor flowability).

## 7.2 MATERIALS AND METHODS

### 7.2.1 MATERIALS

The formulation under study consisted of a low drug-loaded, poorly soluble and poorly wettable API (BCS class II), a large content of  $\alpha$ -lactose monohydrate (Pharmatose® 200, DFE Pharma, Goch, Germany), microcrystalline cellulose (MCC, Avicel® PH101, FMC biopolymer, Philadelphia, USA), hydroxypropyl methylcellulose (HPMC, Methocel® E5, Dow, Midland, USA), croscarmellose sodium (Ac-Di-Sol®, FMC, Philadelphia, USA) and sodium dodecyl sulphate (Kolliphor® SLS, BASF, Ludwigshafen, Germany).

### 7.2.2 METHODS

#### 7.2.2.1 EQUIPMENT

In this study, a horizontal ConsiGma™-25 system (C25) (GEA Pharma Systems, Wommelgem, Belgium) and a ConsiGma™-1 system (C1) (GEA Pharma Systems, Wommelgem, Belgium) were used. The former is a continuous manufacturing line consisting of a twin-screw wet granulation module, a six segmented fluid bed dryer, a granule conditioning unit with a mill (Figure 7.1-A), as previously discussed in detail by several authors (24,29,31) and in section 1.3.3. This ConsiGma™-25 line can also be connected to a tablet press. The ConsiGma™-1, on the other hand, is a mobile laboratory unit consisting of a twin-screw wet granulation module

(identical to the granulation module of C25) and a single fluid bed dryer (Figure 7.1-B). The drying module of the C1 has the same design as one drying segment of the six-segmented dryer of the C25 system.

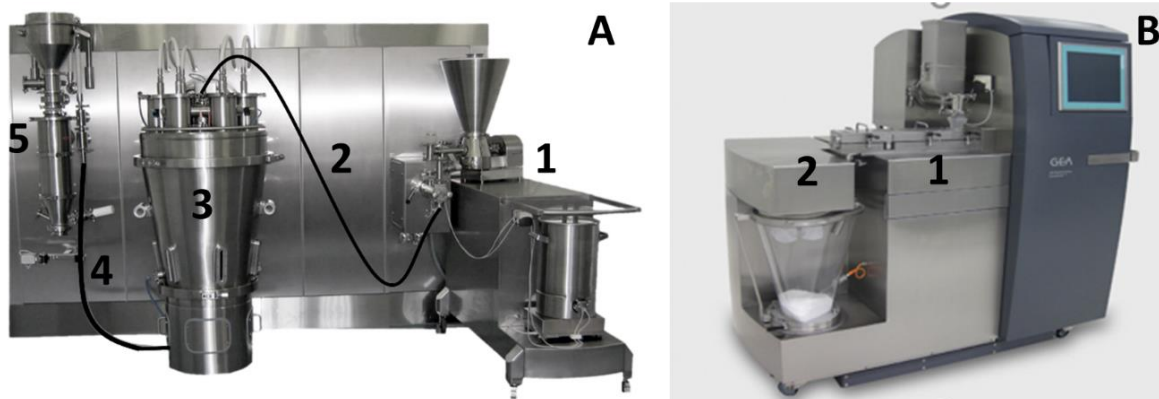


Figure 7.1: ConsiGma™-25 line (A): twin-screw wet granulation module (1), wet transfer line (2), six-segmented fluid bed dryer (3), dry transfer line (4) and conditioning unit with mill (5). Laboratory ConsiGma™-1 unit (B): twin-screw wet granulation module (1) and one-segmented fluid bed dryer (2).

#### 7.2.2.2 GRANULATION MODULE

First, a 20 L tumbling blender (Inversina-Bioengineering, Wald, Switzerland) was used during 15 minutes at 25 rpm to prepare the formulation pre-blend. Subsequently, the pre-blend was transferred to the gravimetric loss-in-weight feeder of the C25 (KT20, K-Tron Soder, Niederlenz, Switzerland) or the C1 (Brabender DDSR20, Duisburg, Germany). Thereafter, the powder mixture was fed into the granulator. For both systems, the granulator was identical and consisted of two 25 mm diameter co-rotating screws with a length-to-diameter (L/D) ratio of 20:1. Demineralized water was used as granulation liquid and was gravimetrically dosed into the granulator using two out-of-phase peristaltic pumps (Watson Marlow, Cornwall, UK). Silicon tubing with an internal and external diameter of 1.6 and 4.0 mm, respectively, was connected to 1.6 mm nozzles. The screw configuration was composed of two kneading zones of six kneading elements ( $L/D = 1/4$ ) and two small chopper elements ( $L/D = 1/6$ ), inserted at the end of the screws. All elements were positioned in a forward stagger angle of  $60^\circ$  and separated by conveying elements. The jacket of the granulator barrel was pre-heated and furthermore maintained at a temperature of  $25^\circ\text{C}$ .

Process settings were kept constant during all experiments. A mass feed rate (MFR) of 10 kg/h, a screw speed of 675 rpm and a liquid-to-solid (L/S) ratio of 23 % were applied. These settings

were chosen based on previous trials (see chapter 3, 4 and 5) as this resulted in granules with a friability (indication for granule strength) of 22 %, a fines fraction of 1.6 % and an oversized fraction of 77.1 %. From previous experience, the authors know that processing granules having a friability of 22 % allows to observe breakage in the system, yet without the creation of an excessive amount of fines. The latter could result in clogging of the drying filters.

### 7.2.2.3 FLUID BED DRYER

For the C25, wet granules were pneumatically transferred from the granulator outlet to the six-segmented fluid bed dryer via the wet transfer line. The cells were consecutively filled and emptied in the same order. While one cell was filled for a set filling time, another was drying, discharging or remained empty, as schematically shown in Figure 7.2. After completing a drying cycle in a cell, the rotating discharge valve allowed to pneumatically transport the granules to the granule conditioning unit. To avoid an effect of the start-up phase of the drying process, samples were only collected when the number of operational cells (i.e., number of cells that are simultaneously being filled or dried) was constant. The number of operational cells may vary as this depends on the set drying time. The drying cell of the C1 was gravimetrically filled since the granulator outlet is located on top of the drying cell inlet. Granules were manually collected after the drying process. For all experiments, an identical filling time of 120 s was applied in both equipment, resulting in a nominal cell load of  $\pm 333$  g. The drying air flow was set at 300 m<sup>3</sup>/h or 50 m<sup>3</sup>/h for the C25 and C1, respectively, as this resulted in an adequate fluidisation in both systems. For all experiments the drying air temperature was preheated to the desired temperature of 40 or 60 °C before the start of an experiment.

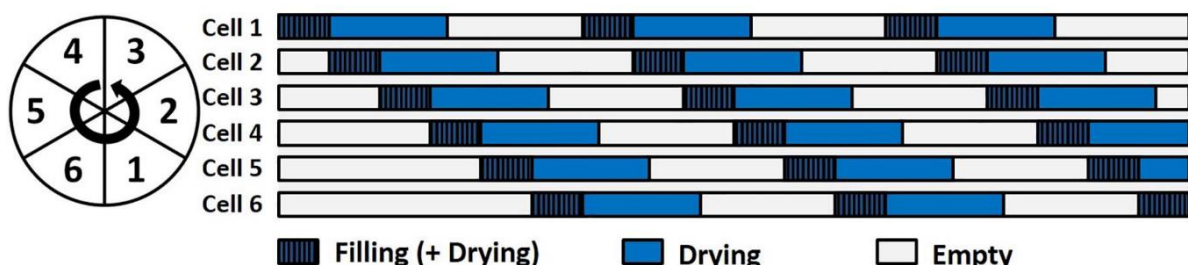


Figure 7.2: Schematic overview of the different phases during drying in the six-segmented fluid bed dryer of a ConsiGma™-25 line (29).

### 7.2.2.4 INVESTIGATING THE PARTICLE SIZE EVOLUTION ALONG THE CONSIGMA™-25 LINE

The evolution of the granule size along the C25 line was evaluated, i.e., between the granulator outlet and the condition unit. For this experiment, an overall drying time of 600 s (including the filling time of 120 s) was applied, while the drying air temperature was set at 40 °C. Granules were collected at 8 different locations to evaluate the granule size (Figure 7.3 – A):

- Location 1: After the granulation module. Only the granulation module was used and granules were subsequently collected at the end of the granulation barrel.
- Location 2: After the wet transfer line connecting the granulator outlet and dryer inlet. A plastic bag was installed in one cell (Figure 7.3 – B/C) in order to gently collect the granules coming out of the wet transfer line. Once the filling phase was completed, the drying process was stopped and granules were manually removed from the bag.
- Location 3-7: In the drying cells 1-5: After completing a full drying cycle (i.e., filling, drying and emptying of cell 1-6), the process was stopped during the second cycle just before the emptying of cell 1 (Figure 7.3 – D). Consequently, cells 1, 2, 3 and 4 corresponded with a drying time of 600, 480, 360 and 240 s, respectively. Cell 5 (120 s) thus corresponded to a complete filling phase only.
- Location 8: After the conditioning unit (no mill was installed). Granules subjected to a complete drying process were transferred via the dry transfer line and collected after the conditioning unit.

For all samples, the overall moisture content was evaluated using part of the produced samples. The remainder of each sample served for granule size characterisation (Section 7.2.2.6), for which it was oven-dried (40 °C, 25 % RH) until a moisture content of 1.5-2.5 % was obtained.

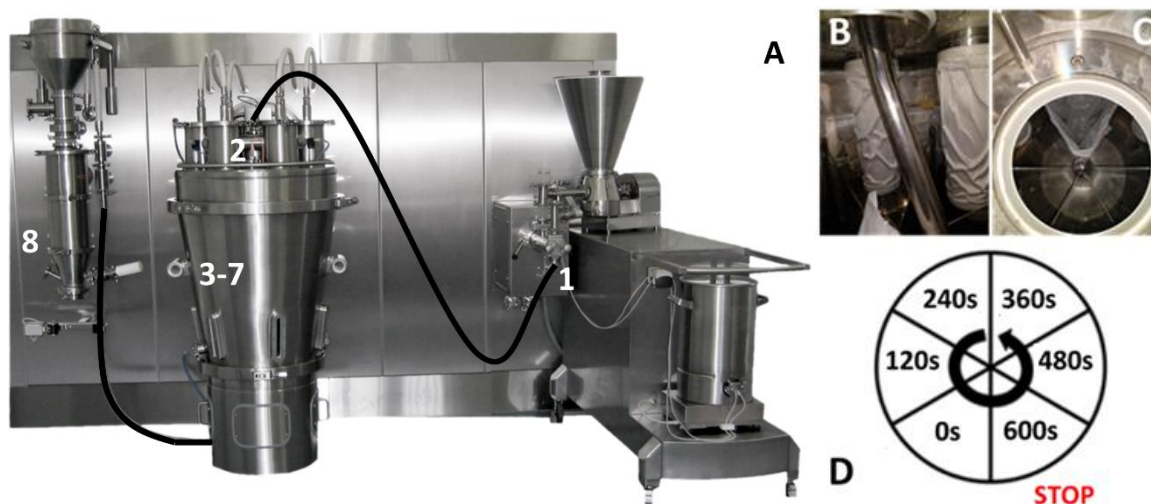


Figure 7.3: Overview of sample collection at different locations along the ConsiGma™-25 line (A): after the granulation module (1), after the wet transfer line (2), at different time points during drying (3-7) and after the conditioning unit (8). Tube (B) dividing the granules over the different cells transfers granules directly in a bag (C). Schematic overview of drying time corresponding to each cell when process was stopped (D).

#### 7.2.2.5 INVESTIGATING THE INFLUENCE OF DRYER SETTINGS ON GRANULES' CQAS FOR C1 AND C25

Drying time and drying air temperature were varied to establish a drying profile for different granule size fractions. In addition, the influence of the drying time and drying air temperature on granule size was investigated. For both systems, drying time was varied at 4 levels, whereas two levels of the drying air temperature (40 or 60 °C) were studied. A total of 8 experiments was performed per equipment (Table 7.1).

Additionally, granules were also produced using only the granulation module. These granules were collected at the outlet and intensively oven-dried at 70°C. Samples were removed from the oven in function of time and, subsequently, their overall moisture content was determined. These granules were then subjected to a friability test to investigate the influence of moisture content on breakage behaviour.

*Table 7.1: Overview of the applied drying parameters.*

Experiment number	Drying time (s) C1	Drying time (s) C25	Drying temperature (°C)
1	240	200	40
2	300	300	40
3	450	450	40
4	600	600	40
5	240	200	60
6	300	300	60
7	450	450	60
8	600	600	60

#### 7.2.2.6 GRANULE CHARACTERISATION

##### 7.2.2.6.1 Granule size distribution

Dynamic image analysis (QICPIC, Sympatec, Etten-Leur, The Netherlands) was performed to evaluate the granule size distribution (GSD) of the dried granules. A representative sample of 80 g of granules was fed by a vibratory feeder towards a gravimetric feed tube where the granules were dispersed in front of the measurement window. Volume size distributions were calculated by the WINDOX 5 software (Sympatec, Etten-Leur, the Netherlands). Measurements were performed in duplicate. The size fraction smaller than 150  $\mu\text{m}$  was defined as the fines fraction. On the other hand, the fraction larger than 1000  $\mu\text{m}$  corresponded to oversized granules.

##### 7.2.2.6.2 Residual moisture content

The overall residual moisture content and the residual moisture content per sieved granule fraction (i.e., > 2000, 1000–2000, 850–500, 150–500 and < 150  $\mu\text{m}$ ) was determined via loss-on-drying (LOD) using a Mettler LP16 moisture analyser (Mettler-Toledo, Zaventem, Belgium). A sample of approximately 3 g was dried at 105°C until its weight was constant for 30 s. At this point, the % LOD was recorded. Measurements were performed in triplicate.

##### 7.2.2.6.3 Friability

Granule friability was measured to determine granule strength using a friabilator (Pharmatest PTF E, Hainburg, Germany). Before each measurement, granules were pre-sieved at 250  $\mu\text{m}$ .



Subsequently, 10 g ( $Iw$ ) of the fraction larger than 250  $\mu\text{m}$  was combined with 200 glass beads (4 mm diameter) and subjected to 250 rotations for 10 min. Then, the fraction smaller than 250  $\mu\text{m}$  was again removed and the remaining mass ( $Fw$ ) was weighted. Friability was calculated using Equation 7.1. Experiments were performed in duplicate.

$$\text{Friability (\%)} = 100 * \frac{(Iw - Fw)}{Iw} \quad [7.1]$$

Where  $Iw$  is the initial weight (in g) and  $Fw$  is the final weight (in g).

## 7.3 RESULTS AND DISCUSSION

### 7.3.1 GRANULE SIZE EVOLUTION ALONG THE LENGTH OF THE CONSIGMA™-25

The aim of this first part of the study was to evaluate the breakage and attrition phenomena at different locations along the length of the ConsiGma™-25 to have an enhanced process understanding. Granule size distributions obtained at the different locations and their corresponding fractions of fines (< 150  $\mu\text{m}$ ) and oversized granules (> 1000  $\mu\text{m}$ ) are shown in Figure 7.4. Figure 7.4-A illustrates that the wet transfer line caused breakage and attrition to the wet granules. Since crystallisation of solubilised powder did not take place before and during this transfer, solids bonds were not yet formed, making granules prone to breakage and attrition. Hence, the fraction of oversized granules decreased from 77.11 to 63.02 %, while the amount of fines increased from 1.56 to 4.40 %. De Leersnyder et al. (29) also reported breakage caused by the wet transfer while comparing a horizontal and vertical set-up of the ConsiGma™-25, albeit to a greater extent. In their study, a decrease in oversized granules of 40 – 60 % and an increase in fines from 4 to 8 % was observed. The variation in the extent of breakage is possibly due to differences in binder potency, raw material properties such as solubility and granulation process parameters such as the L/S ratio. Although it is not straightforward to compare different formulations manufactured under different process settings, weaker granules were presumably obtained as a lower L/S ratio was used to granulate a more hydrophobic formulation consisting of two insoluble fillers (maize starch and powdered cellulose). This indicates that formulation and process optimization could minimize breakage in the wet transfer line.

The impact of the filling phase (120 s drying time) as well as the fluid bed drying process (600 s) on the granule size is illustrated in Figure 7.4-B. During the filling phase the granules entered the cell at high velocity, thereby colliding with the bottom or wall. The first granules were subjected to a turbulent flow due to the limited cell load, enhancing particle-particle and particle-cell wall collisions. As more granules have entered the dryer cell, the wetted mass became heavier and the entering granule flow was more stable. Therefore, only a very small shift in GSD and a small change in fines from 4.4 to 5.4 % and oversized granules from 63.0 to 60.8 % was observed after the filling phase. Furthermore, granule breakage and attrition inside the drying cell was limited during drying. The change in GSD inside the cell after 120 s and 600 s drying was small (Figure 7.4-B). Once the cells were filled, the decrease in oversized granules (60.8 to 58.8 %) and the increase in fines fraction after 600 s of drying (5.4 to 7.0 %) was very moderate. In contrast, the impact of the dry transfer line connecting the dryer cell outlet with the conditioning unit was severe (Figure 7.4-C). Even though the granules were sufficiently dried (LOD of 1-3%) and solid bonds were formed, the powerful vacuum transport and the accompanying blowbacks to completely empty the cell had a large impact on the granule size: the oversized fraction decreased (58.8 to 47.7%), the fines fraction increased (7.00 to 18.7) and a bimodal distribution was obtained (Figure 7.4-C).

The applied methodology could determine the initial size distribution of granules entering the cell as well as the change in GSD during drying. As particle size has a great influence on the drying rate (29), the obtained results are important in the development of a generic drying model. Moreover, the results are needed for the development of a general flowsheet model focussing on granule size. A flowsheet model combines several unit operation models to ultimately simulate the final granule size distribution. Van Hauwermeiren et al. (23) presented a first step towards a generalised mechanistic Population Balance Model (PBM) for the prediction of granule size obtained via the twin-screw granulation unit. This study supports this approach as it improves our understanding of the dynamic behaviour of the granule size along the other units of the manufacturing line.

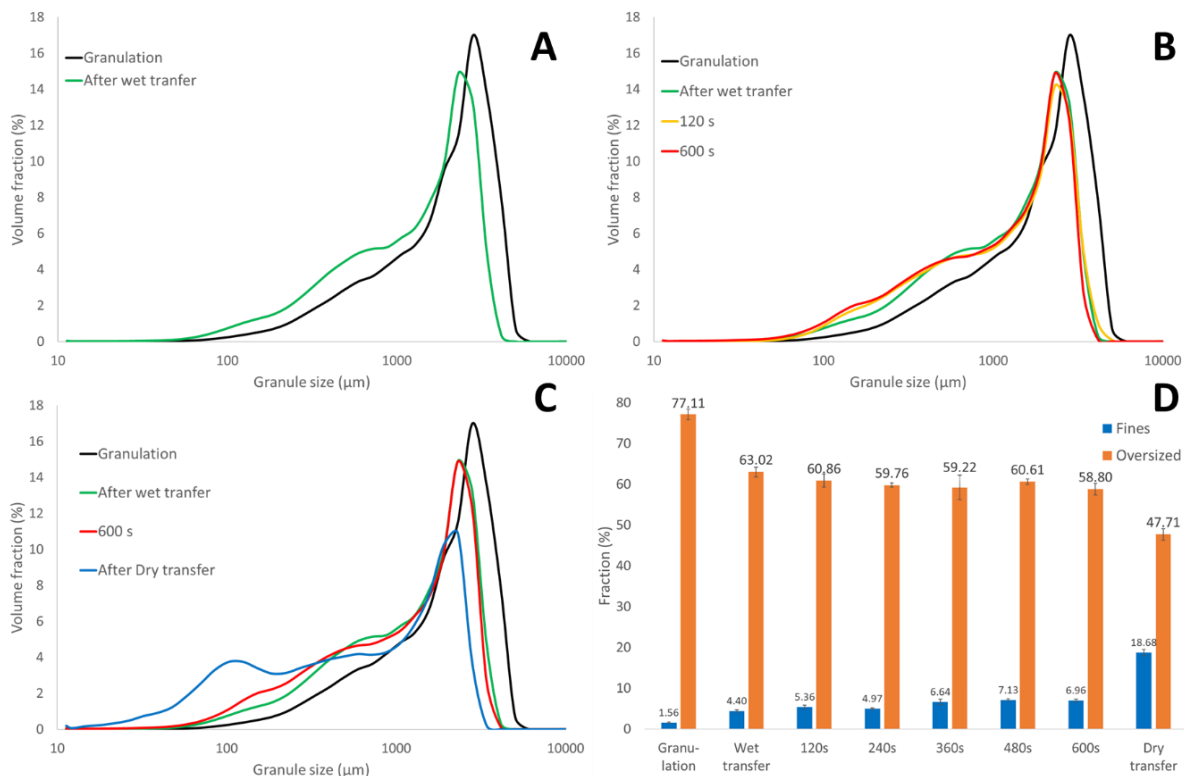


Figure 7.4: Granule size distributions to study the effect of the transfer via the wet transfer line (A), the drying process (B) and the transfer of the dried granules via the dry transfer line (C). The fraction in fines and oversized granules is shown at different drying times and along the length of the C25 (D).

### 7.3.2 INFLUENCE OF DRYER PARAMETERS ON GRANULE CQAS PER EQUIPMENT

#### 7.3.2.1 MOISTURE CONTENT

In this section, the impact of drying air temperature and drying time on moisture content was evaluated and compared for granules processed with C1 and C25 (Table 7.1). The granule drying profiles per granule size fraction at 40 and 60°C are illustrated in Figure 7.5. During the complete filling phase, granules with an overall moisture content of 18.7 % were introduced into the cells, based on the powder and liquid feeding rate. Generally, a fast water evaporation occurs at the surface of the granules in the first drying phase, resulting in a fast decline of moisture content. Hereafter, intra-granular liquid evaporation starts during the second drying phase and the produced vapour is transferred through the granule pores towards the surface. Hence, the second drying phase is slower and finally ends when a similar and targeted residual moisture content (1.0 – 2.5 %) was reached for all size fractions. This 2-phase drying trajectory indicates that a sufficient drying time needs to be applied to reach a uniform drying of the

particles. At that moment all particles – independent of granule size – are in equilibrium with the drying medium (32).

Larger granules dried slower than smaller size fractions due to three reasons. First, as in accordance with the results of De Leersnyder et al. (29), the surface-to-volume ratio is lower for larger granules. Secondly, larger granules contain more liquid since heterogeneous powder-granulation liquid mixing is realized during twin-screw granulation (7) and hence, more time is needed to remove the liquid. And, further, intra-granular vapour has to traverse a larger length as the distance between granule core and surface is larger. Figure 7.5 also shows that a high drying temperature strongly affects the drying trajectory, whereby a fast initial decline in moisture content was obtained at a high temperature. But even at 60 °C, the moisture content even further slightly decreased from 450 to 600 s, showing that the equilibrium is reached slowly.

In this study, a fixed filling time of 120 s was used. Therefore, the number of operational cells while applying a drying time of 300, 450 and 600 s was 3, 4 and 5 on the C25, respectively. Since the resistance to the air flow is higher in filled cells, the drying air is expected to preferentially pass through empty cells (28). Consequently, a more efficient drying was expected on C1 because the equipment consisted only of a single cell. However, the second drying phase was delayed for granules processed on the C1, as a plateau phase only started after 450 and 600 s for a drying temperature of 60 and 40 °C, respectively, whereas this was already seen after 300 and 450 s when drying in the C25. The lower moisture content in the C25 compared to the C1 can be explained by the transfer of heat by convection and conduction from the surrounding empty cells to the cells filled with granules. A similar phenomenon is impossible on the C1 and a higher moisture content is therefore obtained. Similar results were observed by Stauffer et al. and Vercruyse et al. (25,28). In addition, it is possible that the pneumatic transport on the C25 can provide additional evaporation of the liquid on the granule surface. As previously mentioned, this study could help in the development of a generic drying model. Ghijs et al. (33) already modelled the drying behaviour, at a constant material flow rate and filling time and with respect to granule size, in the drying-unit of the vertical ConsiGma™-25 line. Since the moisture content per size fraction was determined in this study, this study could also serve to improve the calibration of the mechanistic drying model.

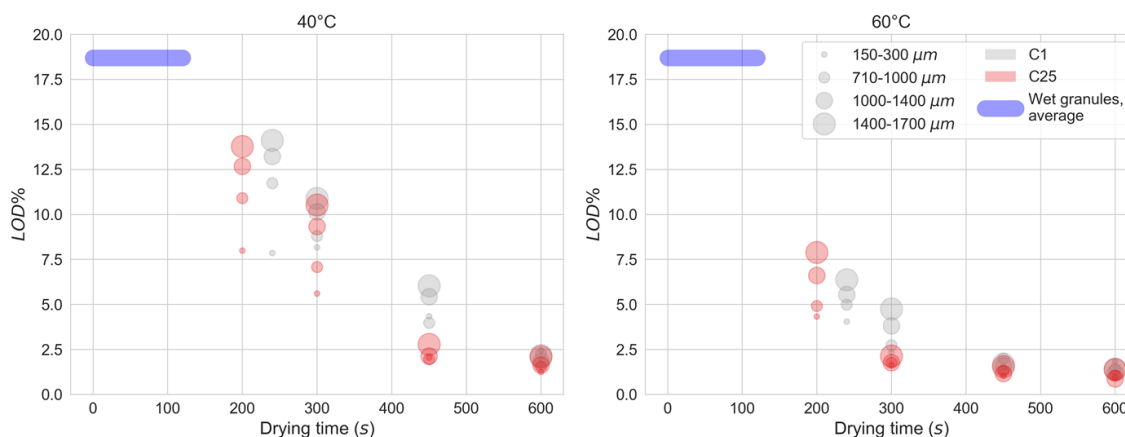


Figure 7.5: Residual moisture content of the granules produced on C1 and C25 in function of drying time at 40 °C (A) and 60 °C (B) for different size fractions (smaller size fractions are represented by smaller dots, whereas larger size fractions are represented by larger dots). The average moisture content of granules entering the drying cells during the filling phase was depicted by the blue bar.

### 7.3.2.2 GRANULE SIZE

#### 7.3.2.2.1 ConsiGma™-25

In this section, the effect of drying process settings on the final granule size (i.e., granules collected after the dry transfer line) was evaluated. From Section 7.3.1. it was clear that breakage and attrition was very limited during drying. Hence, the investigation of the effect of drying parameters on particle size of granules processed on the C25 mainly corresponds to investigating the effect of drying parameters on the breakage in the dry transfer line, taking into account that the degree of breakage and attrition in the wet transfer line was identical for each experiment (see Figure 7.4-A).

Figure 7.6 illustrates the overall moisture content and the fraction of fines and oversized granules for each experiment (Table 7.1) and, in addition, the corresponding GSD. Generally, the extent of breakage and attrition caused by the dry transfer line depended on the residual moisture content of the granules. A higher moisture content due to insufficient drying, resulted in more breakage in the dry transfer line as less solid bonds were formed. This was demonstrated for granules that were only dried for 200 or 300 s at a drying temperature of 40 °C. Fewer oversized granules and more fines were observed as these granules still contained 9.1 and 6.6 % moisture, respectively. A nearly identical GSD was observed for 450 and 600 s of drying, indicating a similar breakage behaviour, as these granules had a similar

residual moisture content, i.e., only 1 – 2 %. A drying temperature of 60 °C resulted in a more pronounced breakage only at the lowest drying time – with a higher amount of fines and lower amount of oversized granules – presumably because the overall moisture content was still higher (i.e., 4.9 %). As a moisture content between 1 and 2 % was observed for granules dried for 300 and 450 s, an almost identical GSD was measured. Surprisingly, granules were further broken to a greater extent when the most extreme drying condition – 600 s at 60°C – was used, resulting in slightly more fines (19.6 %) and less oversized granules (47.8 %). These granules contained less than 1 % of moisture.

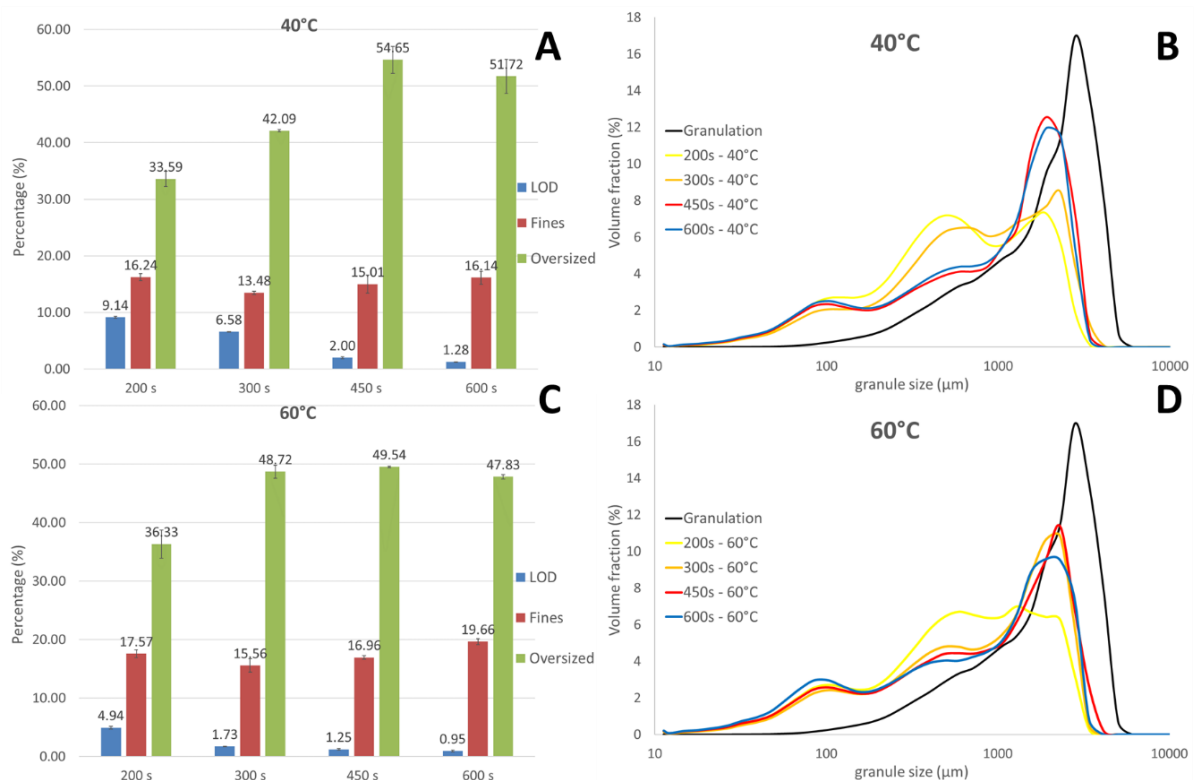


Figure 7.6: The fraction in fines and oversized granules and the corresponding overall moisture content after different drying times for granules collected after the conditioning unit at 40 (A) and 60°C (C). Granules size distributions to visualize the effect of drying time at 40 (B) and 60°C (D).

To understand these phenomena, an additional experiment was performed to illustrate the effect of granule residual moisture content on granule strength. For this experiment, granules obtained after the granulation module were intensively oven-dried at 70 °C. Figure 7.7 depicts the overall residual moisture content in function of friability (i.e., a measure for granule strength). Friability decreased at lower moisture content because more solid bridges were formed when liquid was evaporated from the granules. The lowest friability was obtained for

granules having a residual moisture content between 1 and 2.5 %. However, further liquid elimination weakened the granules again, indicating that a residual moisture of 1 – 2.5 % in granules provided some plasticity to endure mechanical stress. This is in accordance with the statements of Mezhericher et al. (32), where the author stated that drying-induced stress occurred more at higher temperature. At higher temperature, an accumulation of vapor might occur in the particle core during the second drying stage as the excess of vapor can possibly not easily escape through the pores towards the surface. This leads to a higher internal temperature and pressure gradient that might damage the granule microstructure, making the granules prone to mechanical stress which leads to more breakage (34). Hence, the increase in friability at residual moisture below 1 % can be explained since more liquid was evaporated and granules were subjected for a longer time to a high temperature (70°C was applied to induce an intensive drying), a higher temperature and pressure gradient was obtained, making the granules more prone to breakage. Evidently, this explains the additional breakage at 60 °C and 600 s as seen in Figure 7.6.

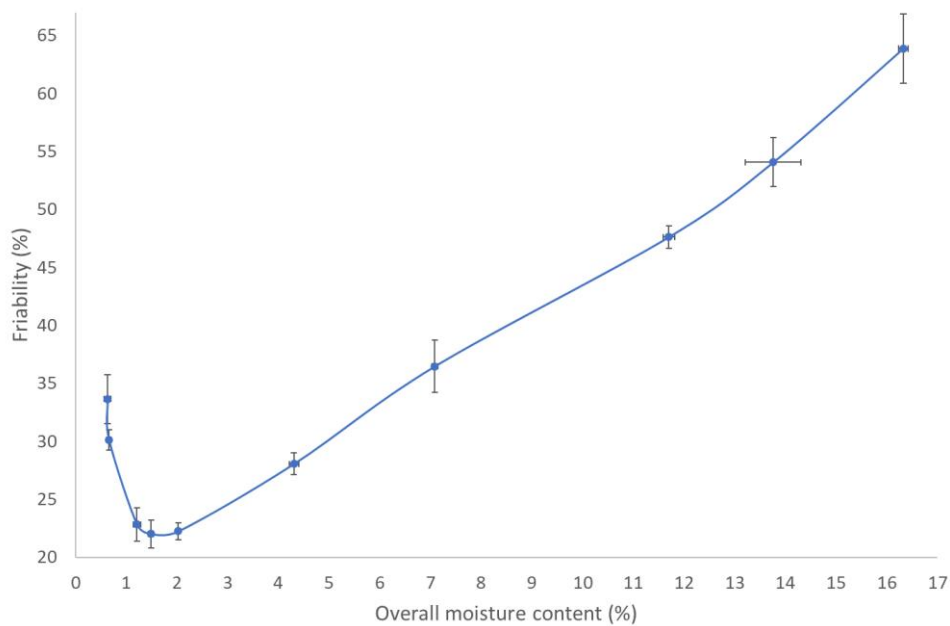


Figure 7.7: Friability as a function of overall residual moisture content.

De Leersnyder et al. (29) stated that drying air temperature had no effect on granule size. Conversely, in this study, a clear difference in GSD for granules dried at 40 and 60 °C was observed via a head-to-head comparison. On the one hand, a drying air temperature of 40 °C resulted in more breakage compared to a drying air temperature of 60 °C for the same drying

time of 300 s. This could be due to an insufficient drying at 40 °C within this period of 300 s as explained in the beginning of the section (Figure 7.8-A). On the other hand, even more breakage was observed with a drying air temperature of 60 °C after an extended drying time of 600 s as the resulting very dry granules (< 1 moisture content) were more prone to breakage (cf. breakage behaviour observed in Figure 7.7). This demonstrated that the final particle size primarily depended of the moisture content obtained after drying and, consequently, the final particle size was indirectly governed by the drying parameters. De Leersnyder et al. (29) compared the final GSD (collected after the conditioning unit) for granules processed with a horizontal and a vertical set-up. The vertical set-up also showed extensive breakage, although it was to a lesser extent compared to the horizontal set-up due to the absence of the wet transfer line, indicating that the breakage caused by the dry transfer line is present for both equipment. This emphasizes that an optimal drying process, granulation process and formulation need to be developed to minimize the breakage and attrition phenomena.

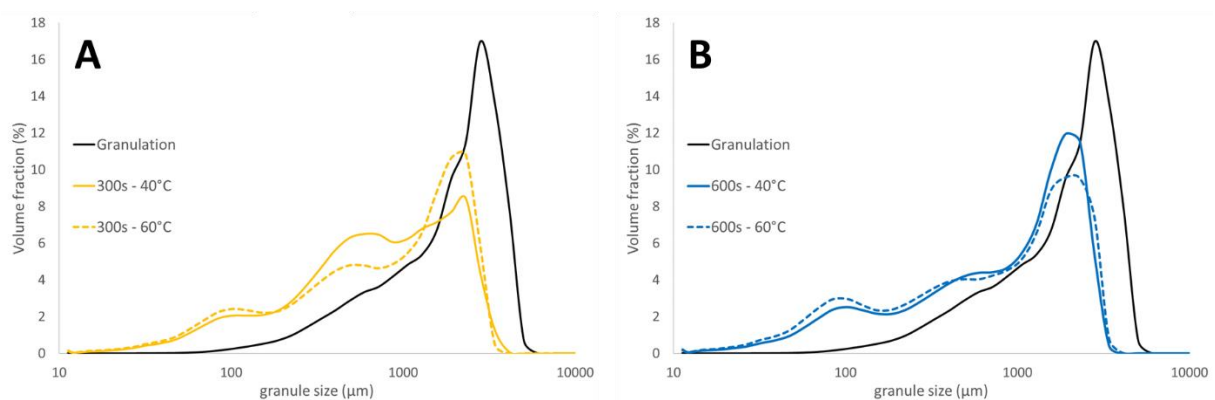


Figure 7.8: Granules size distribution to study the effect of drying air temperature on granule size after 300 (A) and 600 s (B) of drying.

#### 7.3.2.2.2 ConsiGma™-1

Granules were directly transferred by gravitation from the granulation module to the drying cell at the C1 equipment (Figure 7.1). Breakage due to the wet transfer line is therefore absent. Only a moderate change in the fraction in fines and oversized granules was observed after 240 s of drying (Fig 7.9-A), indicating that minor breakage and attrition occurred during the filling phase, similar to the filling phase at C25. By comparing the fines and oversized fraction at different time points at 40 and 60 °C, it is clear that drying air temperature and drying time did not have any relevant influence on granule size. This is also seen by examining the GSD



after 600 s drying at 40 and 60 °C, as a nearly identical GSD was observed. Similar to the drying process with the C25, minimal breakage and attrition phenomena were observed during the drying process.

As granules were manually removed from the drying cell, the impact of the dry transfer line is also missing. Therefore, a completely different GSD is seen at the end of the process between granules from C1 (Figure 7.9) and C25 (Figure 7.6). The unimodal GSD from the C1 are not comparable with the bimodal GSD from the C25. During formulation development and process optimisation, the final GSD obtained on the C25 equipment could therefore not be estimated based on the C1.

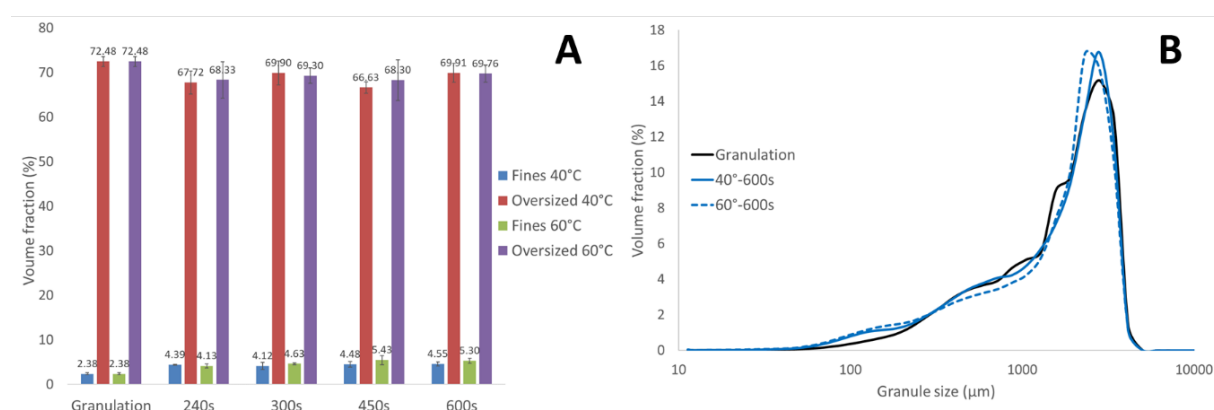


Figure 7.9: The fraction of fines and oversized granules after granulation and at different drying time points on the C1 (A). Granules size distribution after 600 s of drying at 40 and 60°C of drying air temperature (B).

## 7.4 CONCLUSIONS

In this study, it was possible to elucidate where and to what extent breakage and attrition occurred along the length of the C25 line. It was shown that breakage occurred in the wet transfer line because solid intra-granular bonds were not yet formed. Furthermore, breakage and attrition during drying were very limited, whereas the pneumatic transfer via the dry transfer line caused extensive breakage as the drying cells were powerfully emptied. Since fixed granulation parameters were applied on the same formulation, the extent of breakage presumably differs when different parameters and different raw materials are applied. However, it is suggested that similar breakage and attrition phenomena would occur at the studied locations, regardless of the formulation.

This study showed that the moisture content influenced the final granule size on C25, as it co-determines granule strength. It was found that an optimal moisture content range for granule strength exists, granules were found to be more prone to breakage when having a moisture content below and above the range of 1 – 3 % due to drying-induced thermal stresses and incomplete solid bond formation, respectively. Moreover, the current study also demonstrated that the residual moisture content was generally lower for identical process parameters for granules processed on C25, because heat was transferred by convection and conduction from the surrounding empty cells. The final particle size of granules processed on C1 differed substantially, making it difficult during process development to obtain a granule quality that is representative for the C25. Overall, this study provided an enhanced understanding in the breakage behaviour during fluid bed drying, which is important in process and formulation optimization and process control. Further, the obtained results are useful in the development of a generic drying model or a flowsheet model used for the simulation of granule size.

## 7.5 REFERENCES

1. Van Snick B, Holman J, Vanhoorne V, Kumar A, De Beer T, Remon JP, et al. Development of a continuous direct compression platform for low-dose drug products. *Int J Pharm* [Internet]. 2017;529(1–2):329–46. Available from: <http://dx.doi.org/10.1016/j.ijpharm.2017.07.003>
2. Gohel MC, Jogani PD. A review of co-processed directly compressible excipients. *J Pharm Pharm Sci*. 2005;8(1):76–93.
3. Leane M, Pitt K, Reynolds G, Anwar J, Charlton S, Crean A, et al. A proposal for a drug product Manufacturing Classification System (MCS) for oral solid dosage forms. Vol. 20, *Pharmaceutical Development and Technology*. 2015. p. 12–21.
4. Byrn S, Futran M, Thomas H, Jayjock E, Maron N, Meyer RF, et al. Achieving Continuous Manufacturing for Final Dosage Formation: Challenges and How to Meet Them. May 20–21, 2014 Continuous Symposium. *J Pharm Sci* [Internet]. 2015;104(3):792–802. Available from: <http://dx.doi.org/10.1002/jps.24247>
5. Vervaet C, Remon JP. Continuous granulation in the pharmaceutical industry. *Chem Eng Sci*. 2005;60(14):3949–57.
6. Portier C, Pandelaere K, Delaet U, Vigh T, Di Pretoro G, De Beer T, et al. Continuous twin screw granulation: A complex interplay between formulation properties, process settings and screw design. *Int J Pharm* [Internet]. 2020;576(December 2019):119004. Available from: <https://doi.org/10.1016/j.ijpharm.2019.119004>
7. Verstraeten M, Van Hauwermeiren D, Lee K, Turnbull N, Wilsdon D, am Ende M, et al. In-depth experimental analysis of pharmaceutical twin-screw wet granulation in view of detailed process understanding. *Int J Pharm* [Internet]. 2017;529(1–2):678–93. Available from: <http://dx.doi.org/10.1016/j.ijpharm.2017.07.045>
8. Vanhoorne V, Janssens L, Vercruyssen J, De Beer T, Remon JP, Vervaet C. Continuous twin screw granulation of controlled release formulations with various HPMC grades. *Int J Pharm* [Internet]. 2016;511(2):1048–57. Available from: <http://dx.doi.org/10.1016/j.ijpharm.2016.08.020>
9. Vercruyssen J, Córdoba Díaz D, Peeters E, Fonteyne M, Delaet U, Van Assche I, et al. Continuous twin screw granulation: Influence of process variables on granule and tablet quality. *Eur J Pharm Biopharm* [Internet]. 2012;82(1):205–11. Available from: <http://dx.doi.org/10.1016/j.ejpb.2012.05.010>
10. Dhenge RM, Cartwright JJ, Doughty DG, Hounslow MJ, Salman AD. Twin screw wet granulation: Effect of powder feed rate. *Adv Powder Technol* [Internet]. 2011;22(2):162–6. Available from: <http://dx.doi.org/10.1016/j.apt.2010.09.004>
11. Fonteyne M, Wickström H, Peeters E, Vercruyssen J, Ehlers H, Peters BH, et al. Influence of raw material properties upon critical quality attributes of continuously produced granules and tablets. *Eur J Pharm Biopharm* [Internet]. 2014;87(2):252–63. Available from: <http://dx.doi.org/10.1016/j.ejpb.2014.02.011>

12. Fonteyne M, Correia A, Plecker D, Vercruyssen J, Ili I, Zhou Q, et al. Impact of microcrystalline cellulose material attributes : A case study on continuous twin screw granulation. 2015;478:705–17.
13. Willecke N, Szepes A, Wunderlich M, Remon JP, Vervaet C, Beer T De. A novel approach to support formulation design on twin screw wet granulation technology : Understanding the impact of overarching excipient properties on drug product quality attributes. *Int J Pharm* [Internet]. 2018;545(1–2):128–43. Available from: <https://doi.org/10.1016/j.ijpharm.2018.04.017>
14. Willecke N, Szepes A, Wunderlich M, Remon JP, Vervaet C, Beer T De. Identifying overarching excipient properties towards an in-depth understanding of process and product performance for continuous twin-screw wet granulation. *Int J Pharm* [Internet]. 2017;522(1–2):234–47. Available from: <http://dx.doi.org/10.1016/j.ijpharm.2017.02.028>
15. Lute S V., Dhenge RM, Salman AD. Twin screw granulation: Effects of properties of primary powders. *Pharmaceutics*. 2018;10(2).
16. Yu S, Reynolds GK, Huang Z, De Matas M, Salman AD. Granulation of increasingly hydrophobic formulations using a twin screw granulator. *Int J Pharm* [Internet]. 2014;475(1–2):82–96. Available from: <http://dx.doi.org/10.1016/j.ijpharm.2014.08.015>
17. Portier C, Pandelaere K, Delaet U, Vigh T, Kumar A, Di Pretoro G, et al. Continuous twin screw granulation: Influence of process and formulation variables on granule quality attributes of model formulations. *Int J Pharm* [Internet]. 2020;576(December 2019):118981. Available from: <https://doi.org/10.1016/j.ijpharm.2019.118981>
18. Vandevivere L, Denduyver P, Portier C, Häusler O, Beer T De, Vervaet C. Influence of binder attributes on binder effectiveness in a continuous twin screw wet granulation process via wet and dry binder addition. *Int J Pharm* [Internet]. 2020;585(February):119466. Available from: <https://doi.org/10.1016/j.ijpharm.2020.119466>
19. Stauffer F, Ryckaert A, Van Hauwermeiren D, Funke A, Djuric D, Nopens I, et al. Heat Transfer Evaluation During Twin-Screw Wet Granulation in View of Detailed Process Understanding. *AAPS PharmSciTech*. 2019;20(7):1–13.
20. Dhenge RM, Cartwright JJ, Hounslow MJ, Salman AD. Twin screw granulation: Steps in granule growth. *Int J Pharm*. 2012 Nov;438(1–2):20–32.
21. Lute S V., Dhenge RM, Hounslow MJ, Salman AD. Twin screw granulation: Understanding the mechanism of granule formation along the barrel length. *Chem Eng Res Des*. 2016 Jun 1;110:43–53.
22. Hagrasy AS El, Litster JD. Granulation Rate Processes in the Kneading Elements of a Twin Screw Granulator Processes in the Kneading Elements of a Twin Screw Granulator. *AIChE J*. 2013;59(11):4100–15.
23. Van Hauwermeiren D, Verstraeten M, Doshi P, am Ende MT, Turnbull N, Lee K, et al. On the modelling of granule size distributions in twin-screw wet granulation: Calibration of a

- novel compartmental population balance model. *Powder Technol* [Internet]. 2019;341:116–25. Available from: <https://doi.org/10.1016/j.powtec.2018.05.025>
24. Vercruysse J, Delaet U, Van Assche I, Cappuyns P, Arata F, Caporicci G, et al. Stability and repeatability of a continuous twin screw granulation and drying system. *Eur J Pharm Biopharm* [Internet]. 2013;85(3 PART B):1031–8. Available from: <http://dx.doi.org/10.1016/j.ejpb.2013.05.002>
25. Vercruysse J, Peeters E, Fonteyne M, Cappuyns P, Delaet U, Van Assche I, et al. Use of a continuous twin screw granulation and drying system during formulation development and process optimization. *Eur J Pharm Biopharm* [Internet]. 2015;89:239–47. Available from: <http://dx.doi.org/10.1016/j.ejpb.2014.12.017>
26. Chablani L, Taylor MK, Mehrotra A, Rameas P, Stagner WC. Inline Real-Time Near-Infrared Granule Moisture Measurements of a Continuous Granulation – Drying – Milling Process. 2011;12(4):1050–5.
27. Fonteyne M, Gildemyn D, Peeters E, Mortier STFC, Vercruysse J, Gernaey K V., et al. Moisture and drug solid-state monitoring during a continuous drying process using empirical and mass balance models. *Eur J Pharm Biopharm* [Internet]. 2014;87(3):616–28. Available from: <http://dx.doi.org/10.1016/j.ejpb.2014.02.015>
28. Stauffer F, Vanhoorne V, Pilcer G, Chavez PF, Vervaet C, De Beer T. Managing API raw material variability in a continuous manufacturing line – Prediction of process robustness. *Int J Pharm*. 2019;569(July).
29. De Leersnyder F, Vanhoorne V, Bekaert H, Vercruysse J, Ghijs M, Bostijn N, et al. Breakage and drying behaviour of granules in a continuous fluid bed dryer: Influence of process parameters and wet granule transfer. *Eur J Pharm Sci* [Internet]. 2018;115(September 2017):223–32. Available from: <https://doi.org/10.1016/j.ejps.2018.01.037>
30. FDA. Guidance for Industry PAT: A Framework for Innovative Pharmaceutical Development, Manufacturing, and Quality Assurance. FDA Off Doc. 2004;(September):16.
31. Fonteyne M, Vercruysse J, Díaz DC, Gildemyn D, Vervaet C, Remon JP, et al. Real-time assessment of critical quality attributes of a continuous granulation process. *Pharm Dev Technol*. 2013 Feb;18(1):85–97.
32. Mezhericher M. Development of drying-induced stresses in pharmaceutical granules prepared in continuous production line. *Eur J Pharm Biopharm* [Internet]. 2014;88(3):866–78. Available from: <http://dx.doi.org/10.1016/j.ejpb.2014.08.003>
33. Ghijs M, Schäfer E, Kumar A, Cappuyns P, Van Assche I, De Leersnyder F, et al. Modeling of Semicontinuous Fluid Bed Drying of Pharmaceutical Granules With Respect to Granule Size. *J Pharm Sci*. 2019;108(6):2094–101.
34. Nešić S, Vodnik J. Kinetics of droplet evaporation. *Chem Eng Sci*. 1991;46(2):527–37.

**8 INVESTIGATING THE CELL-  
TO-CELL VARIABILITY IN A  
SEMI-CONTINUOUS FLUID  
BED DRYER**

**ABSTRACT**

The semi-continuous drying unit of a continuous from-powder-to-tablet manufacturing line (ConsiGma™ 25, GEA Pharma Systems) is a crucial intermediate process step to achieve the desired tablet quality. The goal of this study was to evaluate the cell-to-cell variability in the six-segmented fluid bed dryer of the ConsiGma™-25 system. In this study, six different experiments (varying drying temperature and drying time) were performed to evaluate the granule quality (moisture content per sieve fraction, overall moisture content and granule size) obtained from the six different cells. No significant difference in granule quality was observed for the different cells, indicating that the no cell-to-cell variability was observed. However, the drying air temperature for the cells which are positioned further from the inlet air was found to be slightly lower. It was concluded that a cell-to-cell variability exists due to the design of the dryer, but that it does not affect the granule quality when the air flow sufficient, the drying temperature was high enough and the drying time was long enough.

## 8.1 INTRODUCTION

Direct compression (DC) is the most desirable technique for continuous pharmaceutical manufacturing of solid-dosage forms. In case, DC is not applicable due to unfavourable powder properties (i.e., poor flowability and compatibility) of the Active Product Ingredient (API), granulation may be required as intermediate process step. Three different continuous granulation techniques can be distinguished: melt, dry (i.e., roller compaction) and wet granulation (1,2). Among the different continuous wet granulation processes currently available, twin-screw granulation (TSG) is the most evaluated process (3). As this technique makes use of a granulation liquid, an additional drying step is required. The main challenge of the drying process is to achieve sufficient drying in a reasonable amount of time (4).

Several integrated from powder-to-tablet lines for the continuous production of tablets via twin-screw granulation are available. Among these lines, a different drying set-up is used. Granules manufactured with QbCon® by L.B. Böhle are gravimetrically transported towards a moving fluid bed dryer (Figure 8.1-A). Therefore, less fines are formed during the drying process, true plug flow conditions are established, a first-in first-out principle is valid and a narrow residence time distribution is obtained. The GRANUCON® line of Lödige uses a linear fluid bed dryer (Figure 8.1-B) integrated with a screw to convey the granules towards the exit of the dryer. Hence, a narrow retention time distribution is obtained, leading to uniform drying conditions. Granules are pneumatically transported towards a fluid bed dryer in the MODCOS system by Glatt (Figure 8.1-C). This systems consists of a conventional fluid bed with several rotating inserts which split the fluid bed into segments. In addition, the rotating insert conveys each segment from the inlet towards the discharge of the dryer. The ConsiGma™ system by GEA Pharma Systems (Figure 8.1-D) consists of a six-segmented fluid bed dryer. Granules can either be transferred pneumatically (horizontal set-up) or gravimetrically (vertical set-up) to the dryer. In this process, the cells are consecutively filled and emptied. While one cell is filled for a set filling time, another is drying, discharging or empty. Hence, small packages of granules (key product) are dried in separate drying cells.



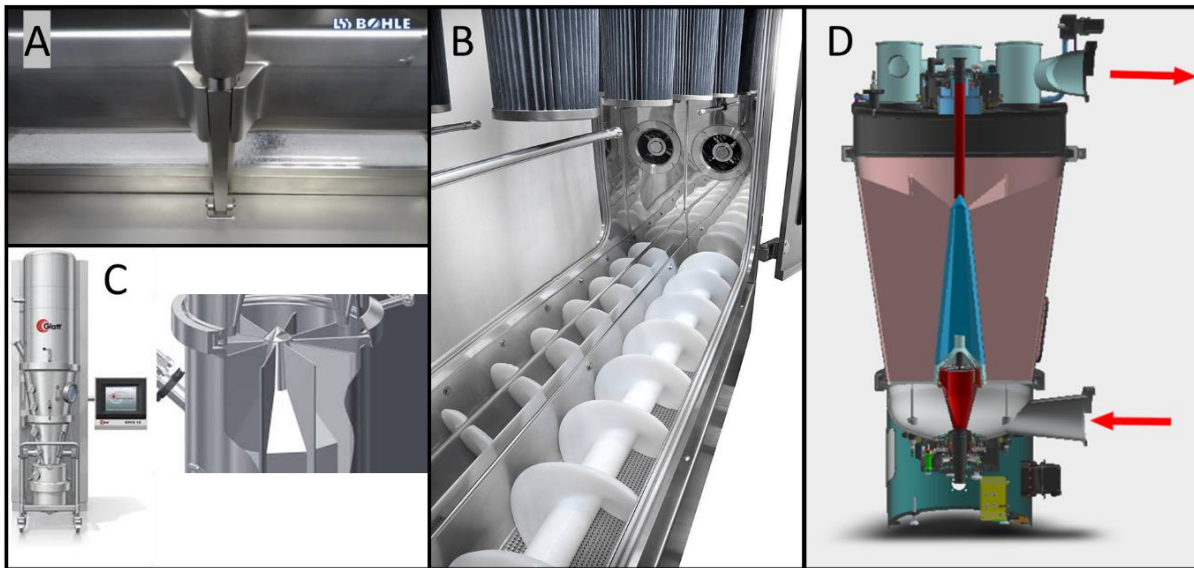


Figure 8.1: Drying unit of different integrated from powder-to-tablet lines: QbCon® by L.B. Bohle (A – Courtesy of Bohle), GRANUCON® by Lödige (B – Courtesy of Lödige), MODCOS system by Glatt (C – Courtesy of Glatt) and a cross-section view of GEA ConsiGma™-25 dryer (D – Courtesy of GEA).

Several authors have already performed investigations on the dryer unit of the ConsiGma™-25. Vercruyse et al. evaluated the stability and repeatability of the drying unit during a long production run (5). Further, the same author used a single cell of the segmented dryer unit to examine whether the granule quality was predictive for the granule quality obtained during full-scale manufacturing (6). De Leersnyder et al. investigated the influence of drying parameters on granule quality attributes and breakage behaviour with a horizontal and vertical set-up of the ConsiGma™-25 (7). Moreover, the influence of granule properties on drying stability (i.e., air flow deviations) was investigated by Stauffer et al (8). However, a cell-to-cell variability has never been investigated. Because, in contrast to the drying unit of the MODCOS, QbCon® and GRANUCON® line where all granules follow the same drying route, different batches of granule are dried in different cells in the ConsiGma-25™ dryer. For all cells, the same inlet air is used for fluidization. However, some cells are located slightly further away from the inlet, suggesting that the air might not evenly distributed over the different cells. Therefore, the cell-to-cell variability in the six-segmented cell was investigated. In this study, six different experiments (varying drying temperature and drying time) were performed to evaluate the granule quality (moisture content per sieve fraction, overall moisture content and granule size) obtained from the six different cells.

## 8.2 MATERIALS AND METHODS

### 8.2.1 MATERIALS

The formulation consisted of a low drug-loaded, poorly soluble and poorly wettable API (BCS class II), a large content of  $\alpha$ -lactose monohydrate (Pharmatose® 200, DFE Pharma, Goch, Germany), microcrystalline cellulose (MCC, Avicel® PH101, FMC biopolymer, Philadelphia, USA), hydroxypropyl methylcellulose (HPMC, Methocel® E5, Dow, Midland, USA), croscarmellose sodium (Ac-Di-Sol®, FMC, Philadelphia, USA) and sodium dodecyl sulphate (Kolliphor® SLS, BASF, Ludwigshafen, Germany).

### 8.2.2 METHODS

#### 8.2.2.1 GRANULATION MODULE

The powder mixture was first blended with a 20 L tumbling blender (Inversina-Bioengineering, Wald, Switzerland) for 15 minutes at 25 rpm. Thereafter, the pre-blend was transferred to the gravimetric loss-in-weight feeder (KT20, K-Tron Soder, Niederlenz, Switzerland). The screw configuration inside the granulator was composed of two kneading zones of six kneading elements ( $L/D = 1/4$ ) and two small chopper elements ( $L/D = 1/6$ ) inserted at the end of the screws. All elements were positioned in a forward stagger angle of  $60^\circ$  and the different kneading zones were separated by conveying elements. Two out-of-phase peristaltic pumps (Watson Marlow, Cornwall, UK) were used to gravimetrically dose demineralized water as granulation liquid into the granulator. Silicon tubes with an internal and external diameter of 1.6 and 4.0 mm respectively, were connected to 1.6 mm nozzles. The jacket of the granulator barrel was pre-heated and maintained at a temperature of  $25^\circ\text{C}$ . Process settings were kept constant during all experiments. A mass feed rate (MFR) of 10 kg/h, a screw speed of 675 rpm and a liquid-to-solid ratio of 23 % were applied.

#### 8.2.2.2 FLUID BED DRYER

Granules were pneumatically transferred to the six-segmented fluid bed dryer via the wet transfer line. The cells were consecutively filled and emptied. After completing a drying cycle, the rotating discharge valve allowed to transport the granules pneumatically to the granule conditioning unit. It has to be noted that samples were only collected when the number of

operational cells was constant as this eliminates the effect of the start-up phase. The number of operational cells may vary as this depends on the set drying time. For all experiments, an identical filling time of 120 s was applied, resulting in a cell load of  $\pm 333$  g. The drying air flow was set at 300 m<sup>3</sup>/h as this resulted in an adequate fluidisation. During all experiments, the temperature was monitored via a PT100 temperature sensor located at the bottom plate inside each of the six dryer cells as an indication of the product temperature. The drying time was varied at three levels, whereas the drying temperature was varied at two levels. An overview of the applied process settings for the different experiments is shown in Table 8.1. For all experiments, granules were collected from each cell. This resulted in 36 (i.e., 6 cells x 6 experiments) different granule samples. For each sample, the residual moisture content per sieve fraction, the overall moisture content and the granule size was determined. Prior to the start of the experiments, the cells were first preheated for 1 h at 40 or 60 °C.

*Table 8.1: Overview of the applied drying parameters.*

<b>Experiment number</b>	<b>Drying time (s)</b>	<b>Drying temperature (°C)</b>
<b>1</b>	300	40
<b>2</b>	450	40
<b>3</b>	600	40
<b>4</b>	300	60
<b>5</b>	450	60
<b>6</b>	600	60

## 8.2.3 GRANULE CHARACTERISATION

### 8.2.3.1 GRANULE SIZE DISTRIBUTION

Dynamic image analysis (QICPIC, Sympatec, Etten-Leur, The Netherlands) was performed to evaluate the granule size distribution of the dried granules. A representative sample of 80 g of granules was fed by a vibratory feeder towards a gravimetric feed tube where the granules were dispersed in front of the measurement window. Volume-based size distributions were calculated by the WINDOX 5 software (Sympatec, Etten-Leur, The Netherlands). Measurements were performed in triplicate. The size fraction smaller than 150  $\mu\text{m}$  was defined as the fines fraction, the fraction larger than 1000  $\mu\text{m}$  corresponded to oversized

granules and the fraction between 150 and 1000  $\mu\text{m}$  was the yield fraction (Figure 8.2-A). Moreover, five percentile-values were also determined: d10, d25, d50, d75 and d90 (Figure 8.2-B).

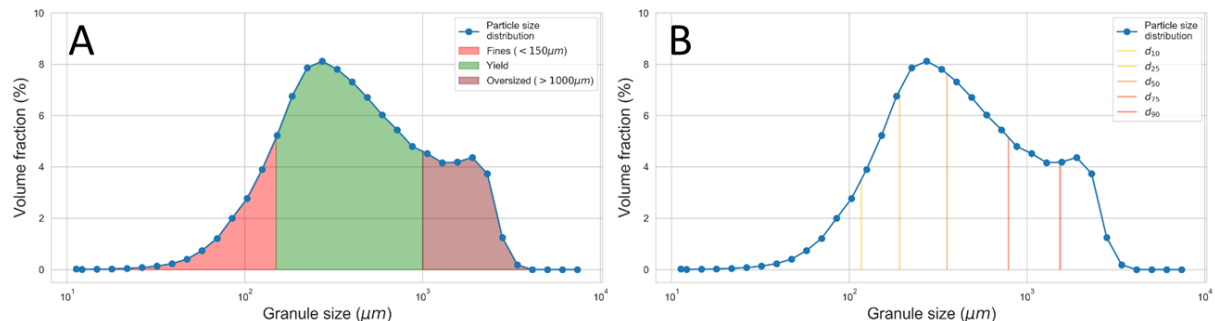


Figure 8.2: Overview of the different granules size responses: fraction of fines, yield and oversized (A) and percentile-values d10, d25, d50, d75 and d90 (B).

### 8.2.3.2 RESIDUAL MOISTURE CONTENT

First, granules were placed on a Retsch VE 1000 sieve shaker (Haan, Germany) using a series of sieves (150, 500, 850, 1000 and 2000  $\mu\text{m}$ ). Then, the overall residual moisture content and the residual moisture content per sieved granule fraction (i.e. > 2000, 1000–2000, 850–500, 150–500 and < 150  $\mu\text{m}$ ) was determined via loss-on-drying (LOD) using a Mettler LP16 moisture analyser (Mettler-Toledo, Zaventem, Belgium). A sample of approximately 3 g was dried at 105°C until its weight was constant for 30 s. At this point, the % LOD was recorded. Measurements were performed in triplicate.

### 8.2.3.3 STATISTICAL TEST

A Kruskal-Wallis statistical test was used to investigate whether there were significant differences in granule quality between the six cells. The null hypothesis ( $p\text{-value} > \alpha\text{-error}$ ) stated that the medians of a group (results for one cell) were all equal, whereas the alternative hypotheses ( $p\text{-value} < \alpha\text{-error}$ ) stated that at least one median was significantly different. A significance level of 0.05 was chosen, indicating a 5 % risk to reject the null hypothesis when it is actually true. Prior to the calculations, the results per group were first normalized.

## 8.3 RESULTS AND DISCUSSION

### 8.3.1 EMPTY CELL TEMPERATURE

A clean and empty dryer was preheated for one hour with an inlet air of 40 and 60 °C before the start of the experiments. The temperature measured in the six cells is shown in Figure 8.3. In both cases, the temperature in the dryer cell was lower than the inlet air temperature, as some energy was lost during the transfer to the cells. Moreover, it was seen that the lowest values were observed for cell 1 and cell 6. These cells are positioned further away from the air inlet (Figure 8.4), suggesting that more energy is lost during transport or that the air is not evenly distributed over the six cells.

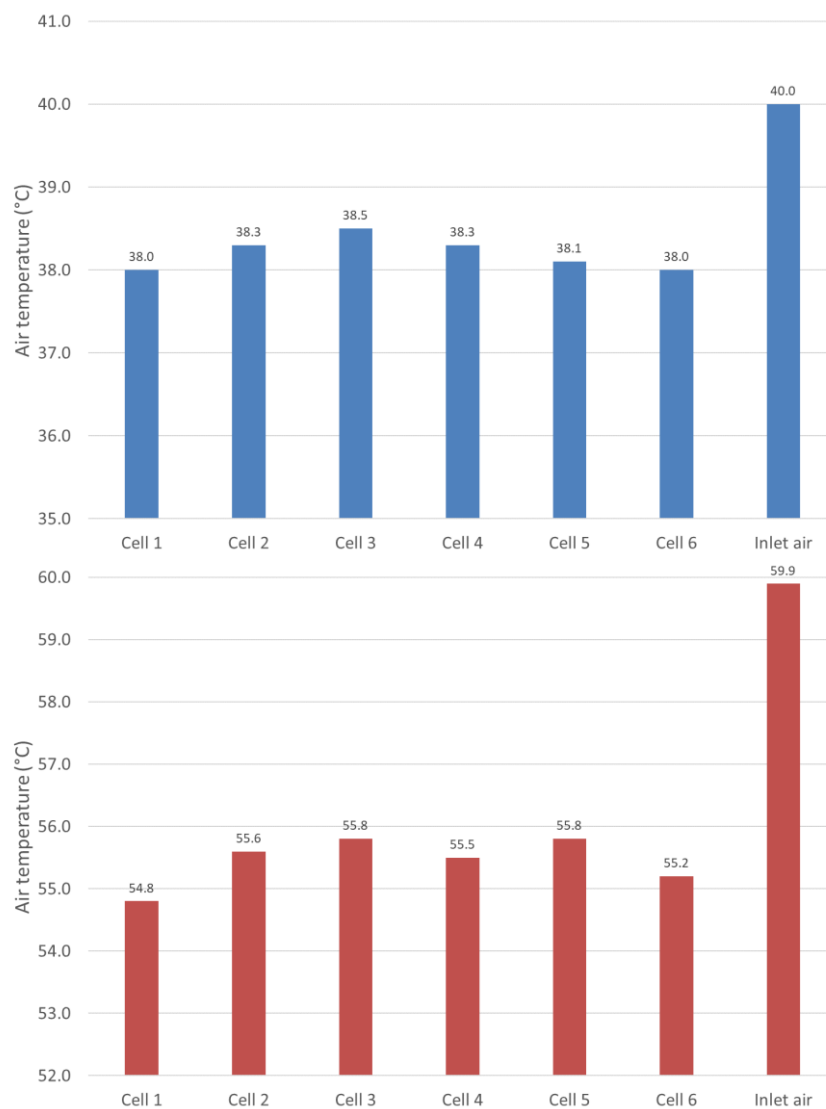


Figure 8.3: Temperature in the dryer during preheating at 40 °C (Top) and 60 °C (Bottom).

The results shown in Figure 8.3 were in accordance with the computational fluid dynamics (CFD) simulation of the ConsiGma™-25 dryer performed by Meyer et al. (9). The simulation showed that the air velocity was lower in cell 1 and 6 (Figure 8.4). Since the distance between those cells and the air inlet was larger, this indicated an uneven distribution of the drying air over the cells. Hence, these results suggest that a cell-to-cell variability might exist.

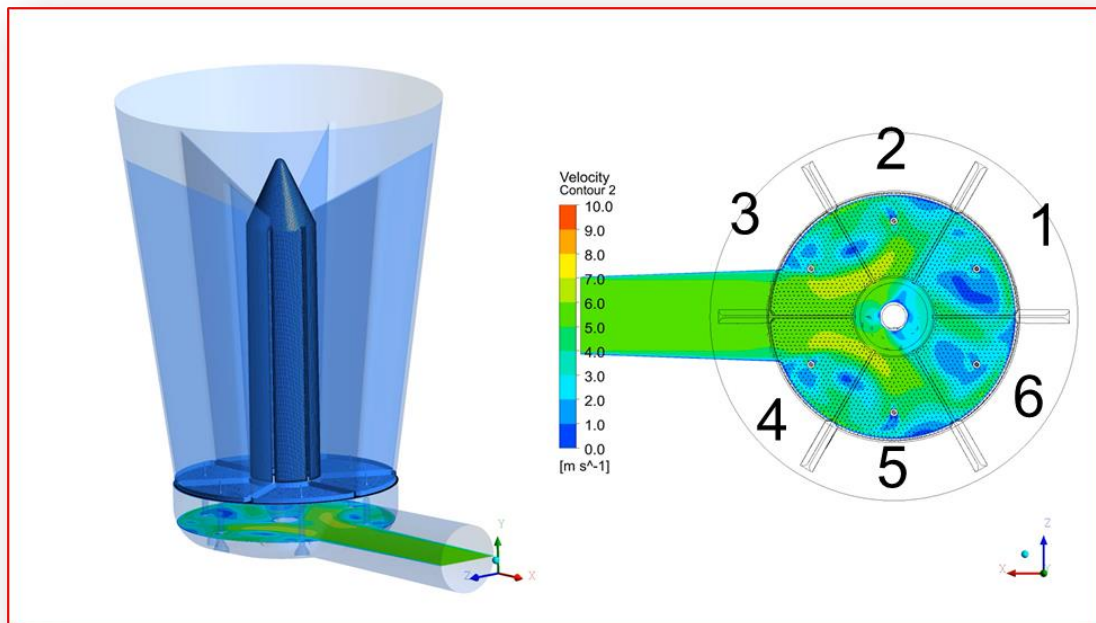


Figure 8.4: CFD simulation of the six-segmented dryer of the ConsiGma™-25 drying unit (9).

### 8.3.2 PARTICLE SIZE

A Kruskal-Wallis statistical test was performed for each percentile and for the fraction of fines, oversized and yield. Kruskal-Wallis is a non-parametric method to compare whether the medians of multiple independent samples are equal. A significant Kruskal-Wallis test indicates that at least one group is different from the others. Here, each group consisted of 18 samples: 6 experiments x 3 replicates. The variability within each group is graphically shown by the box-plot (Figure 8.5). The p-values represents the probability for the evidence against the null hypothesis. It was calculated for each response and it was seen that it was larger than 0.05, indicating that the differences between the medians are not statistically significant. Therefore, no cell-to-cell variability in granule size was observed.

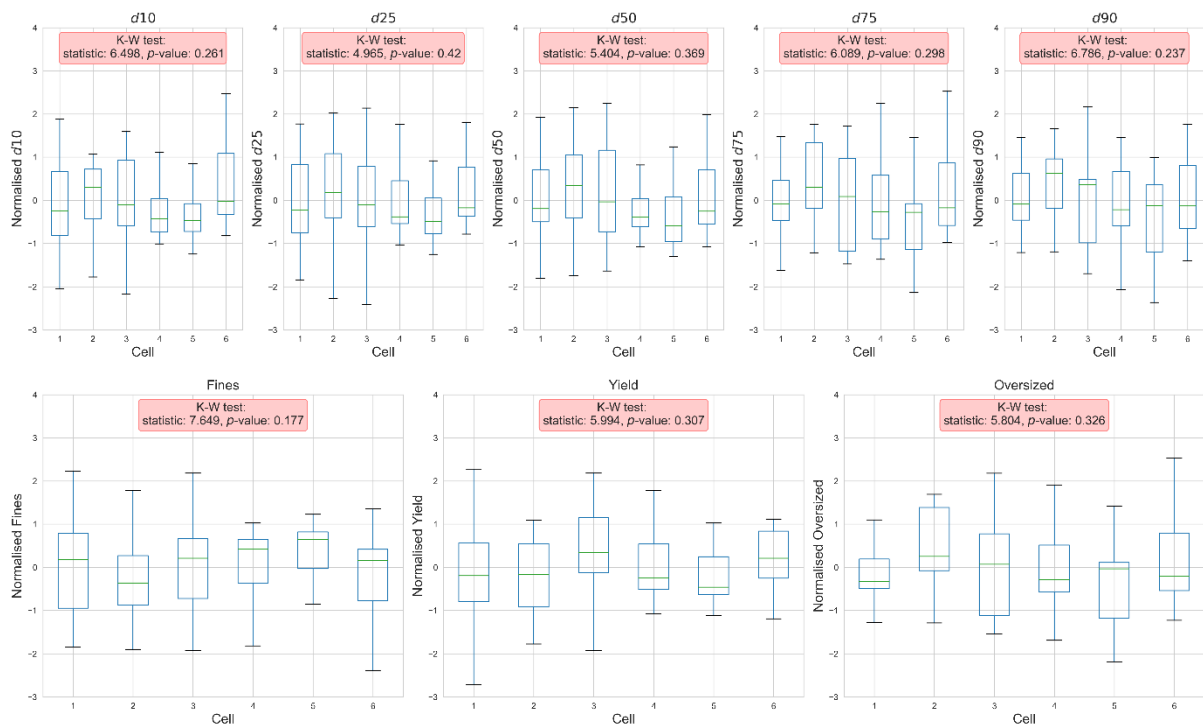


Figure 8.5: Boxplots of Kruskal-Wallis test for the different percentiles (top) and size fractions (bottom).

### 8.3.3 MOISTURE CONTENT

The drying profiles at 40 and 60 °C for each cell are illustrated in Figure 8.6A and Figure 8.6B, respectively. A clear effect of the drying temperature was seen as a fast decline in moisture content was observed at 60 °C. After 300 s, a plateau was already reached and additional drying only slightly decreased the moisture content to  $\pm 1.5$  %. Conversely, a less intensive drying was observed at 40 °C, resulting in a final moisture content after 600 s of  $\pm 2$  %. Moreover, larger granules dried slower than smaller size fractions since their surface-to-volume ratio is smaller (7). In general, very similar drying profiles were observed for all cells at 40 and 60 °C.

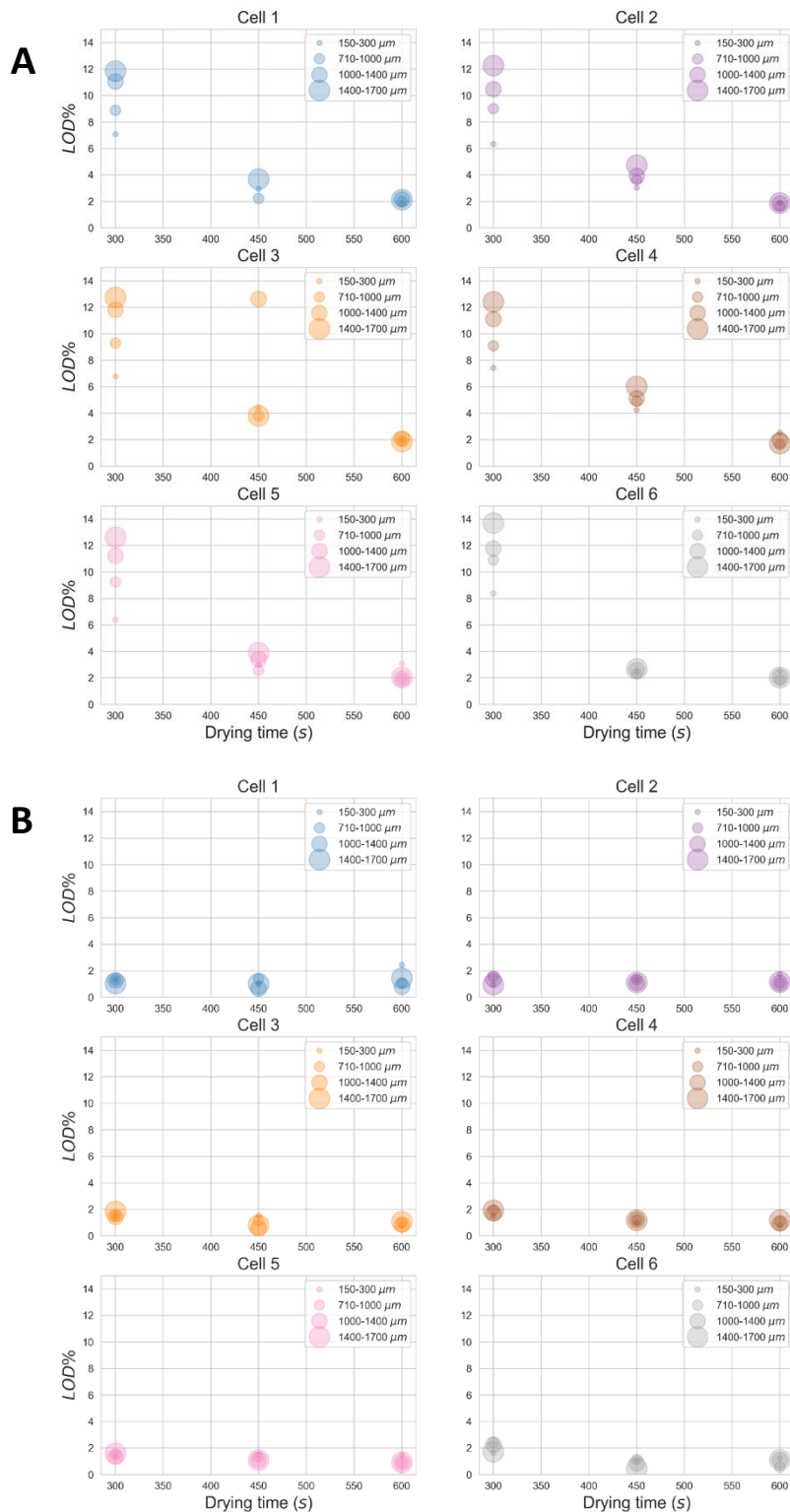


Figure 8.6: Residual moisture content of the granules as a function of drying time at 40 °C (A) and 60 °C (B) for different size fractions (smaller size fractions are represented by smaller dots, whereas larger size fractions are represented by larger dots) for all cells.

A Kruskal-Wallis statistical test was also performed for the different size fractions to investigate whether a certain cell resulted in a different drying behaviour. Figure 8.7 shows



that the p-value was greater than 0.05 for the moisture content of the different size fractions and for the overall moisture content, indicating that no cell-to-cell variability is observed. It has to be noted that only 2 (experiment 1 and 2) of the 6 experiments resulted in an overall moisture content larger than 3 %. Since 4 experiments (experiment 3-6) were sufficiently dried ( $LOD \leq 3\%$ ), very little differences in moisture content were observed between the cells. Therefore, a statistically significant effect is more difficult to obtain. So, although a cell-to-cell variability was observed in drying air temperature (Figure 8.3) and air partitioning in the different cells (Figure 8.4), this does not affect the final moisture content as the drying time, drying temperature and air flow were sufficient to obtain dry granules. However, it is possible that the uneven distribution of air over the cells affects the drying rate and thus the moisture content when granules are not sufficiently dried. As only two experiments resulted in a high moisture content, it was not sufficient to detect any cell-to-cell variability.

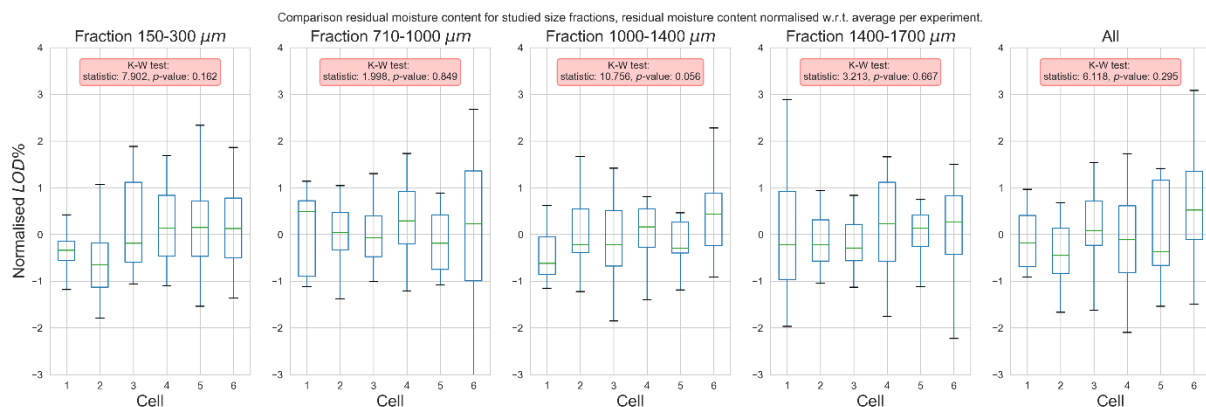


Figure 8.7: Boxplots of Kruskal-Wallis test for the residual moisture content in the different size fractions and the overall moisture content.

## 8.4 CONCLUSIONS

In this study, cell-to-cell variability was investigated for the drying unit of the ConsiGma™-25. Six experiments were performed by varying drying time and drying temperature. For each experiment, the granule size, residual moisture content for different size fractions and overall moisture content was measured for granules collected at the six different cells. No significant difference in granule quality was observed for the different cells, indicating that no cell-to-cell variability was observed. However, the drying air temperature for the cells which are positioned further from the inlet air was found to be slightly lower. It was concluded that a cell-to-cell variability exists due to the design of the dryer, but that it does not affect the

granule quality when the air flow sufficient, the drying temperature is high enough and the drying time is long enough. Hence, to fully understand the impact of cell-to-cell variability on granule quality attributes, only experiments should be selected which resulted in an insufficient drying performance (i.e., moisture content larger than 3 %). Further, the air velocity of the drying air should be experimentally determined for each cell to study the fluidization behaviour in each cell.

## 8.5 REFERENCES

1. Leane M, Pitt K, Reynolds G, Anwar J, Charlton S, Crean A, et al. A proposal for a drug product Manufacturing Classification System (MCS) for oral solid dosage forms. Vol. 20, *Pharmaceutical Development and Technology*. 2015. p. 12–21.
2. Gohel MC, Jogani PD. A review of co-processed directly compressible excipients. *J Pharm Pharm Sci*. 2005;8(1):76–93.
3. Vervaet C, Remon JP. Continuous granulation in the pharmaceutical industry. *Chem Eng Sci*. 2005;60(14):3949–57.
4. Byrn S, Futran M, Thomas H, Jayjock E, Maron N, Meyer RF, et al. Achieving Continuous Manufacturing for Final Dosage Formation: Challenges and How to Meet Them. May 20-21, 2014 Continuous Symposium. *J Pharm Sci [Internet]*. 2015;104(3):792–802. Available from: <http://dx.doi.org/10.1002/jps.24247>
5. Vercruyssen J, Delaet U, Van Assche I, Cappuyns P, Arata F, Caporicci G, et al. Stability and repeatability of a continuous twin screw granulation and drying system. *Eur J Pharm Biopharm [Internet]*. 2013;85(3 PART B):1031–8. Available from: <http://dx.doi.org/10.1016/j.ejpb.2013.05.002>
6. Vercruyssen J, Peeters E, Fonteyne M, Cappuyns P, Delaet U, Van Assche I, et al. Use of a continuous twin screw granulation and drying system during formulation development and process optimization. *Eur J Pharm Biopharm [Internet]*. 2015;89:239–47. Available from: <http://dx.doi.org/10.1016/j.ejpb.2014.12.017>
7. De Leersnyder F, Vanhoorne V, Bekaert H, Vercruyssen J, Ghijs M, Bostijn N, et al. Breakage and drying behaviour of granules in a continuous fluid bed dryer: Influence of process parameters and wet granule transfer. *Eur J Pharm Sci [Internet]*. 2018;115(September 2017):223–32. Available from: <https://doi.org/10.1016/j.ejps.2018.01.037>
8. Stauffer F, Vanhoorne V, Pilcer G, Chavez PF, Vervaet C, De Beer T. Managing API raw material variability in a continuous manufacturing line – Prediction of process robustness. *Int J Pharm*. 2019;569(July).

9. Meyer J., 2020. Model based control for pharmaceuticals from a mechanistic standpoint, IFPAC2020, 26 February, Washington DC.

**9 COMPARISON OF A PARTIAL  
LEAST SQUARES (PLS) MODEL  
WITH A MOVING F-TEST TO  
MONITOR BLEND  
UNIFORMITY IN A TABLET  
PRESS**

**ABSTRACT**

Monitoring the blend uniformity in the feed frame of a tablet press is important to guarantee the quality of the end product and allows real-time release. In this study, in-line NIR measurements were obtained from a NIR spectrometer mounted in the filling chamber of the feed frame, in close proximity to the die filling station. The blend homogeneity was evaluated by a quantitative Partial Least Squares (PLS) regression model and a qualitative moving F-test. The latter is a statistical method that evaluates the change in spectral variances between two consecutively collected blocks of spectra. In contrast to PLS, it is a maintenance free method. First, 15 batches of granules, varying in API concentration at 5 levels (i.e., 90, 95, 100, 105, 110 % relative to target) and varying in applied liquid-to-solid (L/S) ratio at 3 levels (i.e., 25, 28, 31 %) during twin-screw wet granulation were produced on a ConsiGma™-1 system. After drying and milling, the granules were tableted for 15 minutes on a Modul™ P tablet press, where in-line NIR measurements in the feed frame were acquired. The complete dataset was used to develop the PLS model, whereas only the experiments corresponding with an API content of 90, 100 and 110 % were used to determine the minimum block size to comply with the F-test  $\alpha$  and  $\beta$ -error and to find appropriate spectral regions to develop a sensitive F-test. Three different case studies were then performed to evaluate both techniques. It was seen that the moving F-test could detect inhomogeneity of the blend due to changes in API concentration. However, the API content might be off-target while a homogeneous powder bed is monitored. In contrast, via the traditional PLS regression calibration method the API content was continuously monitored as every second the API content is predicted by the PLS model.

## 9.1 INTRODUCTION

The production of tablets in a rotary tablet press is an inherently continuous process. Tablets are produced and ejected as long as the tablet press is fed with new incoming material (1). During this unit-operation, Process Analytical Technology (PAT) is indispensable for real-time measurement of the drug content and process control to guaranty quality of the end product. Ultimately, this might allow real time release of the tablets (1,2). Among the different PAT tools, near infrared spectroscopy (NIR) is an attractive PAT tool for the quantitative and qualitative analysis of tablets, as it is a rapid, simple, non-destructive and non-invasive technique (1,3).

Several studies have already used in-line NIR measurements to investigate blend uniformity in the feed frame of a rotary tablet press (2–8). In all studies, the NIR probes were installed in proximity to the die filling station because a representative sampling of the final tablet quality can be achieved there. Li et al. studied the effect of different factors such as integration time of the NIR spectrometer, paddle speed and averaging number (i.e., number of co-adds) on the effective sample size measured by NIR. Furthermore, the effect of sample size on the quality of the API prediction was investigated (2). In the study of Dalvi et al., polymer-coated ibuprofen pellets were tableted and quantitative predictions of the ibuprofen content in the feed frame were made. Subsequently, the predictions were compared to UV-assay results of the sampled tablets to study the observed delay (i.e., lead-lag time) in ibuprofen content changes (4). Wahl et al. performed not only a quantification of the API content, but a predictive model was also established for the two major excipients (7). Other studies were focussing on optimizing the spectral acquisition in the tablet press (3,5,8). NIR measurements were simultaneously executed in the feed chute and in the feed frame by Sierra-Vega et al. (5). This study showed that the feed frame is the most representative sampling location to evaluate blend uniformity. De Leersnyder et al. focussed on the design of the paddle wheel of the feed frame. Cutting notches inside the paddle wheel fingers had a positive effect on the predictive performance of the model, as spectral disturbances caused by the moving paddle wheel were avoided. The same study also investigated the effect of process parameters on the residence time distribution (RTD) inside the tablet press (8). In addition, an optimal positioning of the NIR probe in the feed frame was evaluated. The study

showed that NIR measurements from the bottom of the feed frame instead of the top aligned much better with off-line measured tablets (3).

Partial Least Squares (PLS)-regression is the most applied technique to monitor blend uniformity with NIR (9). Another approach is to evaluate changes in spectral variance of two consecutive blocks of NIR spectra. Therefore, a qualitative statistical method can be used: the moving F-test. A major advantage of this test is that the construction of a calibration model is not needed, which limits the consumption of material and makes it less labour-intensive. In addition, it is maintenance free and it is easily transferable to different equipment (9,10). The moving F-test was used by Besseling et al. to determine the endpoint of mixing when using tumbling blenders (10). Once the spectral variance did not change anymore, the blending process was considered as finished. Fonteyne et al. applied the moving F-test to evaluate the blend homogeneity of a binary mixture during continuous blending in a twin-screw granulator (9). However, the moving F-test has never been evaluated to monitor the blend homogeneity in the feed frame of a tablet press.

The objective of this study was to evaluate both a traditional, quantitative calibration model via PLS regression and a qualitative moving F-test to monitor blend uniformity (BU) of granules in the feed frame of a tablet press with NIR. First, the granules were manufactured via continuous twin-screw granulation (TSG). The liquid-to-solid (L/S) ratio was varied to obtain granules with different granule properties such as density and size. As NIR is also affected by these physical characteristics, their variability is consequently also to be trained into the models. Then, in-line NIR measurements were acquired during tableting of the different granules. After selecting optimal spectral ranges and the optimal block size for the traditional calibration method and the moving F-test, three case studies were performed to evaluate both blend uniformity determination methods.

## 9.2 MATERIALS AND METHODS

### 9.2.1 MATERIALS

A low drug-loaded formulation containing a poorly soluble API (BCS class II), an abundant amount of  $\alpha$ -lactose monohydrate (Pharmatose<sup>®</sup> 200M, DFE Pharma, Goch, Germany), microcrystalline cellulose (MCC, Avicel<sup>®</sup> PH101, FMC biopolymer, Philadelphia, USA),



hydroxypropyl methylcellulose (HPMC, Methocel® E5, Dow, Midland, USA), croscarmellose sodium (Ac-Di-Sol®, FMC, Philadelphia, USA), sodium dodecyl sulphate (Kolliphor® SLS, BASF, Ludwigshafen, Germany) and magnesium stearate (Ligamed MF-2-V, Peter Greven, Venlo, The Netherlands) was used in this study.

## 9.2.2 PREPARATION OF GRANULES

First, 5 preblends consisting of API (90, 95, 100, 105 and 110 %, relative to the target potency of 11.76 %),  $\alpha$ -lactose monohydrate, microcrystalline cellulose, hydroxypropyl methylcellulose, croscarmellose sodium and sodium dodecyl sulphate were blended using a 20 L Inversina tumbling mixer blender (Bioengineering, Wald, Switzerland). Then, granules were produced and dried using the ConsiGma™-1 system (GEA Pharma systems, Collette, Wommelgem, Belgium). The ConsiGma™-1 is a mobile laboratory unit consisting of a twin-screw wet granulation module and an integrated single fluid bed dryer. The powder premix is fed into the granulator barrel using a gravimetric twin-screw loss-in-weight feeder (DDSR20, Brabender, Duisburg, Germany). The granulator consists of two 25 mm diameter co-rotating screws with a length-to-diameter ratio of 20:1. Granules were produced using a 2x6 screw configuration composed of two kneading zones of six kneading elements each at 60° stagger angle. During granulation, the jacket of the granulator barrel was set at a temperature of 25°C. Granulation liquid is gravimetrically dosed into the screw chamber using two peristaltic pumps (Watson Marlow, Cornwall, UK) positioned out of phase and silicon tubes (internal and external diameter of 1.6 and 4.8 mm, respectively) connected to 1.6 mm nozzles. In the current study, demineralized water was used as granulation liquid. For each of the five blends, granules were produced with an L/S-ratio of 25, 28 and 31 %. Mass feed rate and screw speed were kept constant at 10 kg/h and 675 rpm, respectively. A filling time of 120 s was used for the drying cell, resulting in a cell load of about 333 g. The drying air flow was set at 70 m<sup>3</sup>/h to provide an adequate fluidisation, whereas the drying air temperature was set at 40 °C. The drying time was varied dependent on the applied L/S ratio, ensuring that granules having a moisture content between 1 and 2 % were always obtained. Subsequently, the dried granules were milled through a 1000  $\mu$ m grater screen with square impeller at 900 rpm using the co-mill (U10, Quadro, Ontario, Canada) incorporated in the ConsiGma™-25 line (GEA Pharma systems, Collette, Wommelgem, Belgium). A total of 15 different milled granule batches were hence obtained (Figure 9.1).



Figure 9.1: Schematic overview of the different granules: the relative amount of API to target varied at 5 levels (yellow), whereas the applied L/S ratio for each blend varied at three levels (blue).

### 9.2.3 PREPARATION OF TABLETS

One kg of the milled granules was blended with magnesium stearate and croscarmellose sodium for 5 minutes at 12 rpm before tableting. Tablets ( $\pm 85$  mg) were prepared on a Modul™ P tablet press (GEA Pharma Systems Courtoy, Halle, Belgium) equipped with 10 concave Euro B punches of 6 mm at a tableting speed of 30 rpm. An overfill cam of 6 mm was used, whereas a speed of 20 and 30 rpm for paddle 1 and paddle 2 was applied, respectively. As the granule bulk density varies between the differently prepared granule batches, the fill depth was adapted for each experiment in order to obtain a uniform tablet weight of 85 mg for each batch. A pre-compression force of  $\pm 1$  kN was used, whereas a main compression between 4 and 6 kN was applied depending on the granule properties. After 2 minutes of tableting start-up phase, to ensure complete filling of the feed frame, each tableting experiment was continued for another 15 minutes and tablets were collected for 5 seconds after 1, 3, 5, 7, 9, 11, 13 and 15 minutes (after the start-up phase) for off-line analysis (section 9.2.4).

### 9.2.4 API CONTENT IN GRANULE SIZE FRACTIONS AND TABLETS

An UV/VIS spectroscopy method was developed to determine the API content in the tablets and the API distribution over the different granule size fractions. The latter allows to detect whether segregation during tableting would impact the blend uniformity. Granules were placed on a Retsch VE 1000 sieve shaker (Haan, Germany) using a series of sieves (150, 310, 500, 710 and 1000  $\mu\text{m}$ ). Before the measurements, three tablets or 250 mg of the sieved granule fraction were crushed to powder. Subsequently it was mixed with acetonitrile to 50 mL for 24 h and centrifuged for 15 minutes at 4000 rpm (Heraeus Multifuge 3 S-R, Thermo scientific, USA). Then, the supernatant was removed and 1/100 diluted with acetonitrile before the API content was measured via UV absorbance at 251 nm. The 15 series of tablets (each having 8 time points) and the 15 batches of granules (each consisting of 5 granule size fractions (< 150, 150 – 310, 310 – 500, 500 – 710 and 710 – 1000  $\mu\text{m}$ )) were evaluated.

### 9.2.5 NIR SPECTROSCOPY

NIR spectra were collected in reflection mode using a diode array system SentroPAT FO (Sentronic, Dresden, Germany). This NIR spectrometer was coupled via a fibre-optic cable to a SentroProbe DLR RS NIR (Sentronic, Dresden, Germany) with a probe length of 200 mm and an illumination spot size of 5 mm. The probe was installed in the first chamber (i.e., filling chamber) of the feed frame, in close proximity to the die filling station. Notches (3mm depth, 30 mm width) in the paddle wheel fingers allowed a fixed distance of 1 mm between the probe and the paddle wheel fingers using a probe holding device equipped with a micrometer. This ensured a close contact between powder and the illumination spot of the probe, avoiding spectral disturbances fingers caused by the paddle wheel fingers, as demonstrated by De Leersnyder et al. (3). An integration time of 14 ms and an averaging number of 42 were used, resulting in a sampling volume of 42.5 mg (half a tablet). One spectrum per second was collected. Each spectrum covered a spectral range of 1150-2100 nm and had a spectral resolution of 1 nm. NIR spectral acquisition was started at timepoint zero of tableting, and a total of  $\pm 900$  spectra were collected for each tableting experiment.

### 9.2.6 MOVING F-TEST METHOD

#### 9.2.6.1 INTRODUCTION

The moving F-test evaluates the homoscedasticity (i.e., equality of variances) of two consecutive blocks of consecutively collected spectra. It is a qualitative approach, meaning that the actual concentration of the API is not predicted. Two blocks of spectra that each correspond to a different API concentration might have the same variance. The moving F-test is able to detect inhomogeneity of a blend due to changes in concentration, because this induces a change in variance within a block. The spectral variance within a block is calculated by Equation 9.1.

$$\sigma^2 = \frac{\sum_{j=1}^k \sum_{i=1}^n (x_{i,j} - \bar{x}_{i,j})^2}{(n - 1)} \quad [9.1]$$

Where k is the amount of wavelengths, n is the block size (i.e., amount of spectra),  $x_{i,j}$  is the spectral value for the  $i^{\text{th}}$  block and  $j^{\text{th}}$  wavelength and  $\bar{x}_{i,j} = \frac{1}{n} \sum_{i=1}^n x_{i,j}$  is the average spectral value within a column. For example, for a block size of 5: block n consist of [spectra x to x+4],

whereas block n+1 consists of [spectra x+5 to x+9]. Subsequently, an F-value is calculated by Equation 9.2.

$$F = \frac{\sigma_1^2}{\sigma_2^2} = \frac{\textit{largest sample variance}}{\textit{smallest sample variance}} \quad [9.2]$$

Where  $\sigma_1^2$  is the variance of the block with the largest variance and  $\sigma_2^2$  is the variance of the block with the smallest sample variance. Subsequently, a two-sided F-test is applied to evaluate the ratio of the variances:

If  $F < F_{crit}$ , the null hypothesis is valid:  $H_0$  = variance of the two blocks is equal.

If  $F > F_{crit}$ , the alternative hypothesis is valid:  $H_1$  = variance of the two blocks is not equal.

$F_{crit}$  is derived from the F-distribution tables and depends on the block size (i.e., sample size) and the chosen  $\alpha$ -error. The  $\alpha$ -error is the probability that  $H_0$  is rejected when it is actually true. In this study, it is the probability that a uniform blend is not considered as uniform. The  $\beta$ -error is the probability that  $H_0$  is not rejected when it should be rejected. In this study, it is the probability that a non-uniform blend is considered as uniform. The  $\beta$ -error depends on the block size, the  $\alpha$ -error and the sensitivity. The sensitivity depends on the spectral pre-processing that facilitates the distinction of spectra corresponding to a different API content. As the  $\alpha$ -error and  $\beta$ -error are related to each other, both errors need to be under control. In this study, the  $\alpha$ -error was set at 5 % and  $\beta$ -error was aimed to be lower than 5 %.

### 9.2.7 DATA ANALYSIS SOFTWARE

The moving F-test was performed using in-house developed scripts in the MATLAB software (R2016b, MathWorks, Natick, MA, USA).

For the development of the traditional calibration model for API content quantification in the tablet press feed frame, the SIMCA 16.0 (Umetrics, Umeå, Sweden) software was used. The in-line collected NIR spectra were standard normal variate (SNV) and first derivative pre-processed after optimal spectral range selection (see results section). To develop the PLS model, the X data matrix consisted of  $\pm 13\,500$  NIR spectra (3 (L/S ratio's) x 5 (API levels) x  $\pm 900$  spectra), whereas the Y data matrix was composed of the corresponding, theoretical API content. The theoretical concentration is a reference value that was used because it was neither possible to link a specific spectrum with the real assay values of tablets due to the

unknown lead-lag time nor to collect powder samples from the feed frame to obtain real assay values. Based on the goodness-of-prediction ( $Q^2$  value, being the cumulative percentage of model prediction calculated by cross-validation (Equation 9.3)), the number of PLS components was selected. Extra PLS components were added gradually until the goodness-of-prediction did not improve significantly. Cross-validation by leave-one-out was performed on the model, allowing the determination of the root mean square error of cross validation (RMSE<sub>cv</sub>) providing an indication of the predictive potential of the model (Equation 9.3).

$$RMSE_{cv} = \sqrt{\frac{\sum_{i=1}^n (y_i - \hat{y}_i)^2}{n}} \quad [9.3]$$

Where  $n$  is the total amount of spectra in the model,  $y_i$  is the theoretical concentration corresponding to a spectrum and  $\hat{y}_i$  is the concentration of a spectrum that is estimated by cross-validation (i.e., estimation of a concentration for object  $i$  by using a model that does not include object  $i$ ).

### 9.2.8 CASE STUDY

Three case studies were performed to evaluate the blend uniformity determination via the predicted API content derived from the PLS model and the F-values from the moving F-test. Moreover, the actual API content in the tablets was also assessed. For these case studies, either granules with an API content of 100 % or 110 % relative to target were produced with a L/S ratio of 28 %. During all three experiments, tablets were collected every minute for 5 seconds for UV-assay. Prior to the start of each case study, a complete filling of the feed frame was ensured (see section 9.2.3). A schematic illustration of the three case studies is shown in Figure 9.2. For the first case study, the tablet press feed tube was filled with 600 g granules of 100 % target concentration. Since granules consisting of 100 % were exclusively processed, the blend should be considered as uniform by both methods. The total time of production of tablets and the spectral acquisition thereof was 8 min. In the second case study, the tablet press feed tube was first filled with 500 g granules of 100 % target concentration. On top of that, 300 g granules of 110 % of target API concentration were added. Finally, the tablet press feed tube was further filled with 500 g granules at the target concentration of 100 %. This case study tested the two blend uniformity determination methods to detect the disturbance in blend uniformity. This case study took 25 minutes. At the start of the 3<sup>rd</sup> case study, only the

feed frame was filled with 300 g granules having a relative API content of 100 %. On top of the feed frame, the feed chute was exclusively filled with 600 g granules of 110 % relative to target. In contrast to the second case study, the aim of this case study was to evaluate the blend uniformity when the API concentration remained different from the target concentration. The case study took 21 min.

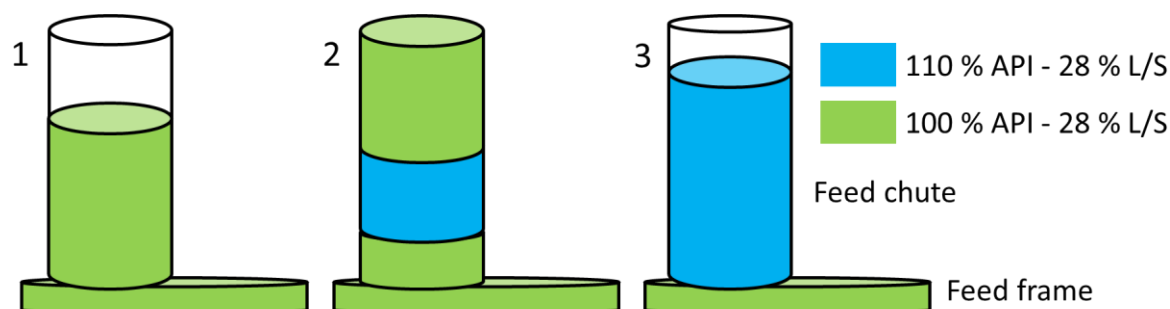


Figure 9.2: Schematic illustration of the set-up for each case study at the start of the experiment in the tablet press. Blue represents the granules of 110% relative to target API concentration, whereas green represents the granules of 100 % relative to target API concentration.

## 9.3 RESULTS AND DISCUSSION

### 9.3.1 ASSAY OF SIEVED GRANULES

In a previous study, the wetting stage (i.e., the nucleation phase) of the granulation process was investigated for the formulation under study. This study showed that a preferential wetting (i.e., a higher chance to be nucleated) of certain excipients occurred, resulting in an uneven repartition of API over the different size fractions (see chapter 4) (11). The API recovery in the smaller sieve fraction ( $< 500 \mu\text{m}$ ) was lower and this effect was independent of any process parameter. As the unequal API distribution over the different granule size fractions might impact the blend uniformity during tableting (e.g., when segregation occurs), it was also evaluated in this study for the milled granules.

Independently of the API fraction in the blend and the applied L/S ratio, similar results were obtained for all 15 batches of granules. Therefore, the API distribution over the different granule size fractions for the formulation containing 100 % of API relative to target and manufactured with an L/S ratio of 28 % is shown as representative example in Figure 9.3. The size fraction smaller than  $150 \mu\text{m}$  contained less API, whereas the other size fractions had an

API recovery just above 100 % relative to target. This indicates that granule segregation might impact the blend and content uniformity during tableting.

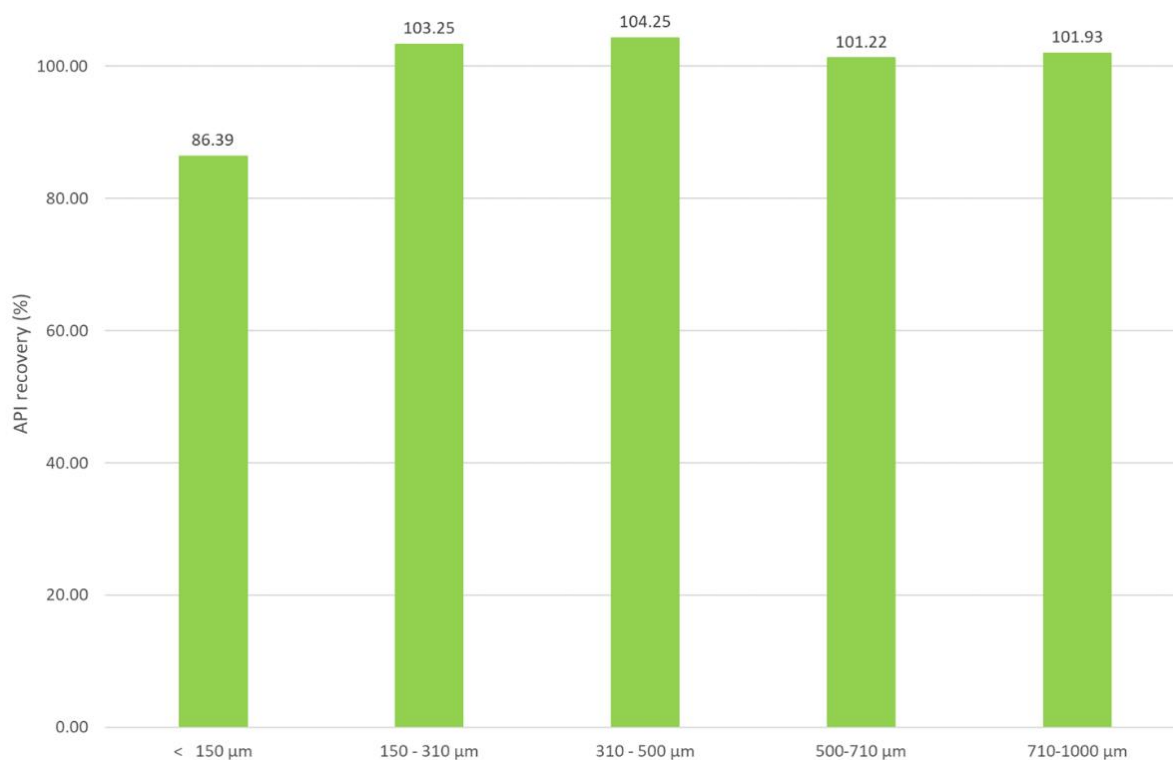


Figure 9.3: API recovery per size fraction for the milled granules (API content: 100% relative to target, L/S ratio = 28%).

### 9.3.2 ASSAY OF TABLETS

For each of the 15 batches of granules, an assay was also performed on the collected tablets at the different time points (1, 3, 5, 7, 9, 11, 13 and 15 min). The API recoveries in the collected tablets for three of the 15 granule batches, each corresponding with a different API content and processed with a different L/S ratio (25, 28 or 31 %), are shown as representative examples in Figure 9.4. It can be seen that the API recovery was close to the target recovery. In all three experiments, the API recovery fluctuated around the target concentration. These three representative examples showed that the API recovery did not increase or decrease in function of time, indicating that segregation was limited.

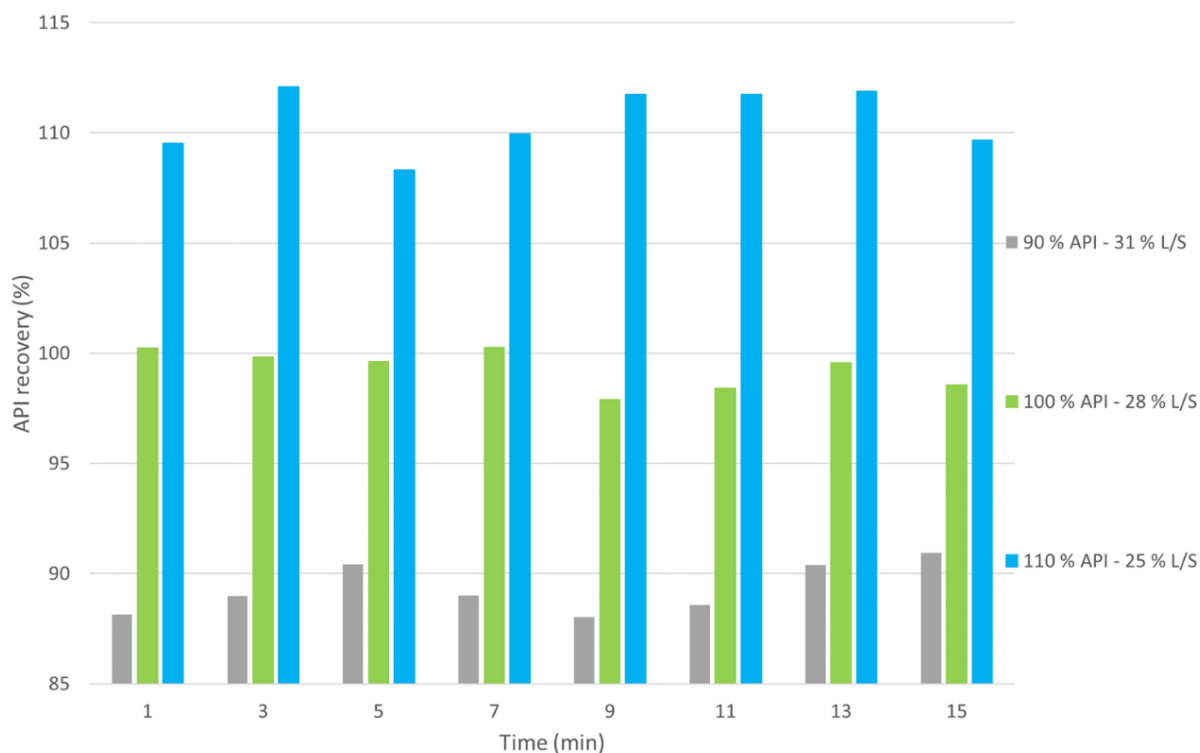


Figure 9.4: % API recovery for tablets at different time points for three representative experiments: 90 % API relative to target at 31 % L/S ratio (grey), 100 % API relative to target at 28 % L/S ratio (blue) and 110 % API relative to target at 25 % L/S ratio (orange).

### 9.3.3 PLS CALIBRATION

A quantitative PLS model was generated for in-line NIR predictions of the API concentration in the filling chamber of the feed frame of the used tablet press. The API concentration was varied at 5 levels (90, 95, 100, 105 and 110 % of the theoretical concentration) to develop the calibration model. Each formulation blend was granulated at 3 different levels of L/S ratio (25, 28 and 31 %) to include granule size and porosity/density as sources of variability. Thus, a total of 15 calibration formulation blends were obtained. First, SNV pre-processing was applied followed by Savitzky-Golay first-derivative transformation with 15 point segment size and second order polynomial fit in combination with the selection of the most optimal spectral regions. The most optimal spectral region, based on the lowest RMSEcv value, was found to be the entire spectrum without the regions of [1100-1140 nm] and [1871-1969 nm] as these regions corresponded with the very noisy edge of the spectrum and the strong NIR absorption band of water, respectively. Thus the selected spectral region was from [1141-1870 nm] and [1970-2100 nm]. The number of latent variables was increased until the goodness-of-prediction ( $Q^2$ , being the fraction of response variation that can be predicted by the model by



applying cross-validation) did not improve significantly to avoid potential overfitting. Four latent variables were chosen for this PLS model and it explained 60.69 % of the total variation in  $X (R_x^2)$  and 94 % of the total variance in  $Y (R_y^2)$ , whereas the  $Q^2$  was 94 %. The correlation between the theoretical and predicted concentration obtained after cross-validation is shown in Figure 9.5. As the theoretical concentration slightly differed from the actual concentration in the feed frame, as also shown in Figure 9.4, this inherently impairs the quantitative performance to some extent. Finally, the developed PLS model resulted in an RMSEcv of 0.93 %. As the model incorporates different sources of variability (size, density, moisture content), through which it became more robust but also less accurate. In addition, the API content was only varied at 5 levels with a difference of 5 %.

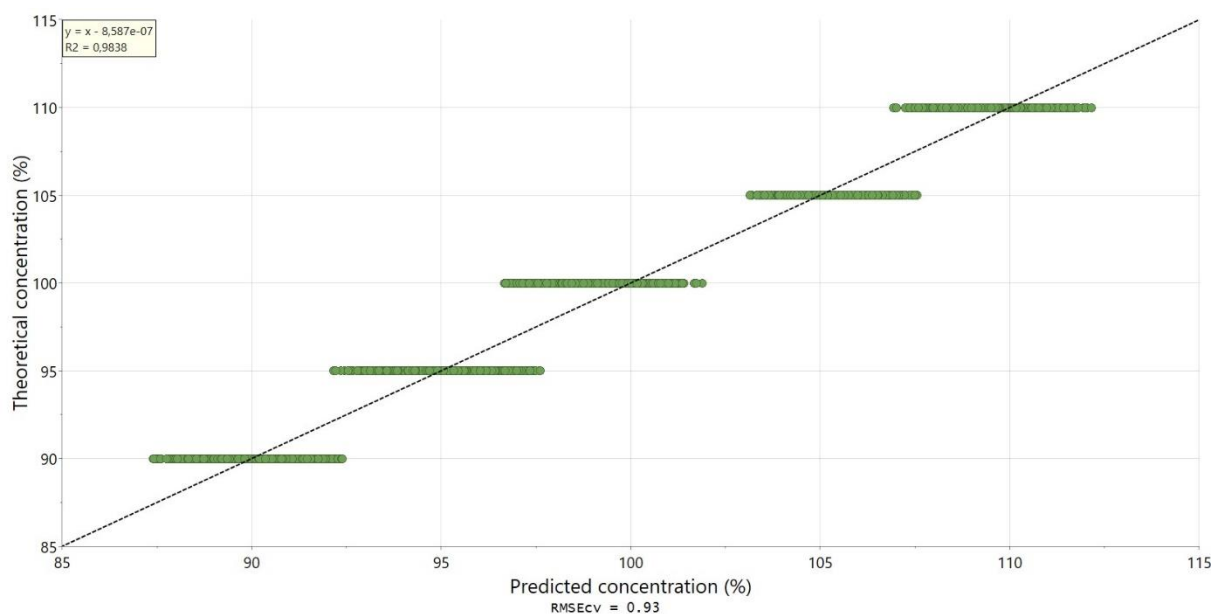


Figure 9.5: Observed versus predicted plot obtained after cross-validation using the complete dataset.

### 9.3.4 MOVING F-TEST

#### 9.3.4.1 CALCULATION OF THE NOISE-INDUCED SPECTRAL VARIANCE ( $s_{noise}^2$ )

The first step in the development of a moving F-test is to determine the noise-induced spectral variance. The noise-induced spectral variance ( $s_{noise}^2$ ) is the variance which is due to physical properties such as granule size, density and shape. In addition, as an overall moisture content between 1 and 2 % was obtained, the moisture content also slightly varied between different batches of granules and between different granule size fractions (i.e., smaller granules

typically have a lower moisture content (12)). Therefore, the variance in the spectra could also be due to a change in moisture content. Furthermore, the spectral variance of a single experiment can also be caused by small variations in API concentration during tableting. As shown by the assay of the tablets (Figure 9.4), the actual API concentration fluctuated around the target. The noise induced spectral variance was calculated from the three experiments (i.e., three granule batches each applying a different L/S ratio) corresponding with an API concentration of 100 % relative to target. This resulted in a matrix of 2700 (i.e., 3 x 900) spectra and k wavelengths, [2700 x k]. The noise induced spectral variance is the sum of the variances between all spectra at each wavelength (Equation 9.4). The noise induced spectral variance was calculated for differently selected spectral ranges in section 9.3.4.3.

$$S_{noise}^2 = \frac{\sum_{j=1}^k \sum_{i=1}^n (x_{i,j} - \bar{x}_{i,j})^2}{(n - 1)} \quad [9.4]$$

#### 9.3.4.2 CALCULATION OF THE API-INDUCED SPECTRAL VARIANCE ( $S_{API}^2$ )

Changes in API concentration evidently also cause spectral variance. The API-induced spectral variance ( $S_{API}^2$ ) was calculated with the aid of the collected spectra from the granule batches corresponding with an API concentration of 90 and 110 % relative to target. For both formulation blends, the 2700 (i.e., 3 x 900) spectra were averaged to erase the noise. Then, an arbitrary block size ( $B_{arb}$ ) was chosen, for example  $B_{arb} = 30$ . This resulted in the construction of thirty different blocks, whereby each block contained a different ratio of the 90 and 110 % averaged spectra. The first block consisted of 29 times the 90%-spectra and 1 time the 110%-spectrum, whereas the second block consisted of 28 times the 90%-spectra and 2 times the 110%-spectra. The thirtieth block consisted of 30 identical 110%-spectra. For each of the blocks, the mean content (Equation 9.5) and the relative standard deviation (RSD) (i.e., the API content variation) (Equation 9.6) were calculated. Clearly, the RSD of the thirtieth block was zero, as this block only consisted of 110%-spectra. Furthermore, the RSD value of the  $n^{th}$  and the  $30-n^{th}$  block were identical.

$$\bar{c} = \frac{(n_1 c_1 + n_2 c_2)}{(n_1 + n_2)} \quad [9.5]$$

$$RSD = \sqrt{\frac{(n_1 B_{arb} - n_1^2)(c_1 - c_2)^2}{B_{arb}(B_{arb} - 1)}} \quad [9.6]$$

Where  $c_1$  and  $c_2$  are the API percentages of the label claim and  $n_1$  and  $n_2$  are the amount of spectra in a block corresponding with  $c_1$  and  $c_2$ .

Further, the API-induced spectral variance was calculated for each block (Equation 9.7). Within each block, it is the sum of the variances at each wavelength which is induced by the change in composition. It was used to indicate the spectral difference which was attributed to the concentration difference.

$$s_{API}^2 = \frac{(n_1 B_{arb} - n_1^2)}{B_{arb}(B_{arb} - 1)} \sum_{j=1}^k (s_{1,j} - s_{2,j})^2 \quad [9.7]$$

With  $s_{1,j}$  and  $s_{2,j}$  are the  $j^{\text{th}}$  wavelength of the averaged spectrum of  $c_1$  and  $c_2$ , respectively.

The  $F_{API}$  value (Equation 9.8) is the ratio of the total spectral variance and the noise spectral variance. This value is needed to establish a sensitivity curve.  $s_{API}^2$  and  $F_{API}$  -values were calculated for differently selected spectral ranges in section 9.3.4.3.

$$F_{API} = \frac{s_{API}^2 + s_{noise}^2}{s_{noise}^2} = 1 + \left( \frac{s_{API}^2}{s_{noise}^2} \right) \quad [9.8]$$

#### 9.3.4.3 ESTABLISHMENT OF THE SENSITIVITY CURVE

A sensitivity curve was constructed by plotting the relationship between RSD and  $F_{API}$  for blocks 1 to 15, as a similar RSD and  $F_{API}$  are logically obtained for block 1+n and 30-n. Next, each  $F_{API}$  was compared to  $F_{crit}$  to verify if  $s_{API}^2$  was considered significantly different from  $s_{noise}^2$ . As mentioned before,  $F_{crit}$  is derived from the F-distribution tables, in this study the  $\alpha$ -error was set to 5 % (i.e., a significance level of 0.95), resulting in a small probability of falsely rejecting a homogeneous blend. For a two-sided F-test with a degree of freedom of 29 for numerator and denominator:  $F_{crit} = 2.10$ . Further, the parameter  $C_{sens}$  was calculated to determine the increase of  $F_{API}$  with increasing RSD.  $C_{sens}$  depends on the spectral pre-processing, the selected spectral ranges and the noise. It is independent of the block size and it can be used to optimize the sensitivity (Equation 9.9).

$$C_{sens} = \frac{\sum_{j=1}^k (s_{1,j} - s_{2,j})^2}{s_{noise}^2 (c_1 - c_2)^2} \quad [9.9]$$

In this study, different spectral ranges were assessed with the goal to find regions where the spectral difference between both averaged spectra was large and where the noise was limited. Spectral ranges were selected based on a comparison of the pre-processed averaged spectrum of the pure API and the pre-processed averaged spectrum of the three experiments (i.e., three granule batches each applying a different L/S ratio) with an API content at target (Figure 9.5). First, similar to the selected spectral range of the calibration model, the complete spectrum without [1100-1140 nm] and [1871-1969 nm] (full line) was selected. Then, mainly the ranges corresponding to API signals ([1505-1558 nm][1603-1871 nm][1969-2068 nm]) were selected (dashed line). Finally, only the range corresponding with the high-intensity peak of the API was selected, focussing on only 8 wavelengths [2028-2036] (dotted line). A sensitivity curve was developed for the different selected spectral ranges (Figure 9.6).

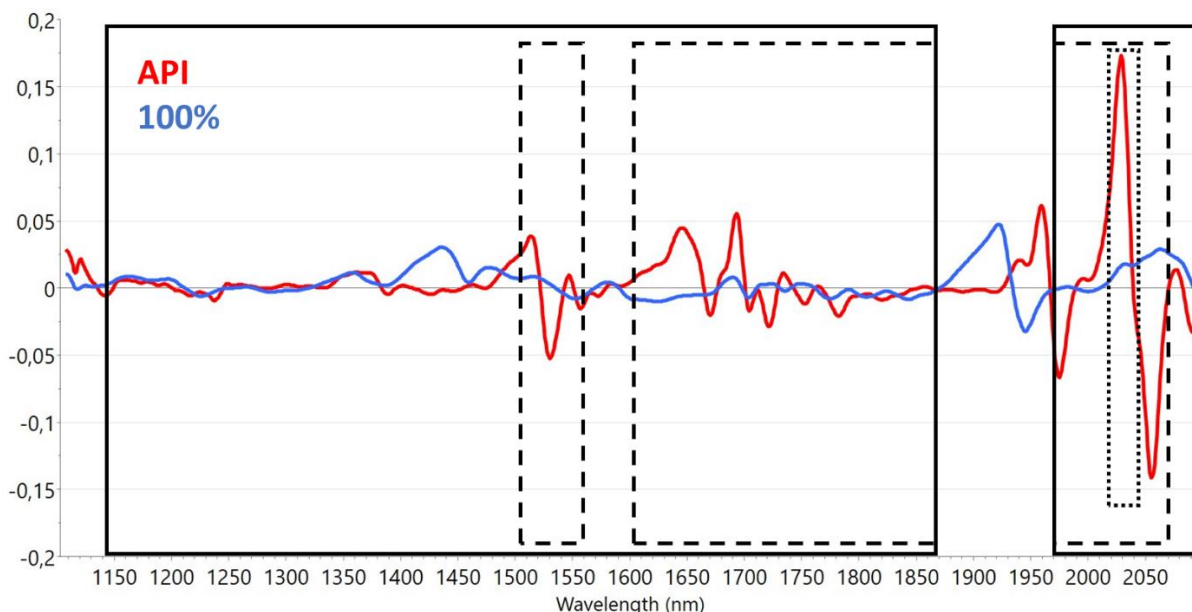


Figure 9.5: Pre-processed averaged spectrum of the pure API (red) and the 100%-experiments blue). Three spectral ranges were selected: (1) complete spectrum without [1100-1140 nm] (full line), (2) [1505-1558 nm][1603-1871 nm][1969-2068 nm] (dashed line) and (3) [2028-2036 nm] (dotted line).

The first ( $C_{sens} = 0.011$  and  $s_{noise}^2 = 2.41 \times 10^{-5}$ ) and second ( $C_{sens} = 0.013$  and  $s_{noise}^2 = 1.47 \times 10^{-5}$ ) selected spectral ranges showed that RSD at the intersection of the sensitivity curve with  $F_{crit}$  was  $\pm 10$  and  $\pm 9$  %, respectively. This demonstrated that the method became more sensitive (i.e., increase in  $c_{sens}$  and decrease in  $s_{noise}^2$ ) when mainly spectral regions were selected corresponding with the API signal (i.e., selection 2). However, in both cases, the sensitivity curve was not steep enough to intersect the  $F_{beta}$  ( $\beta = 5$  %), indicating insufficient power (Figure 9.6). The third spectral range [2028-2036] resulted in a steeper sensitivity curve ( $C_{sens}$  increased to 0.092) as the  $s_{noise}^2$  decreased ( $3.06 \times 10^{-7}$ ). This implied that the spectral difference between the averaged spectrum of 90 and 110 % was more pronounced. Consequently,  $s_{API}^2$  was already considered significantly different from  $s_{noise}^2$  when the block of 30 comprised only 1 different spectrum, meaning that the API induced spectral difference is greater than the noise induced spectral difference. Moreover, the intersection of the sensitivity curve and  $F_{beta}$  occurred at an RSD  $< 8.2$  % (Figure 9.6). According to the performance criteria of the harmonized unit-dose uniformity test (10), the probability to accept a blend with an RSD of 8.2 % as uniform should not exceed 5 %. Therefore, the RSD value corresponding with the intersection between the sensitivity curve and  $F_{beta}$  should not exceed 8.2 %. This was seen for the selection of the third spectral range. For further details the reader is referred to the study of Besseling et al. (10).

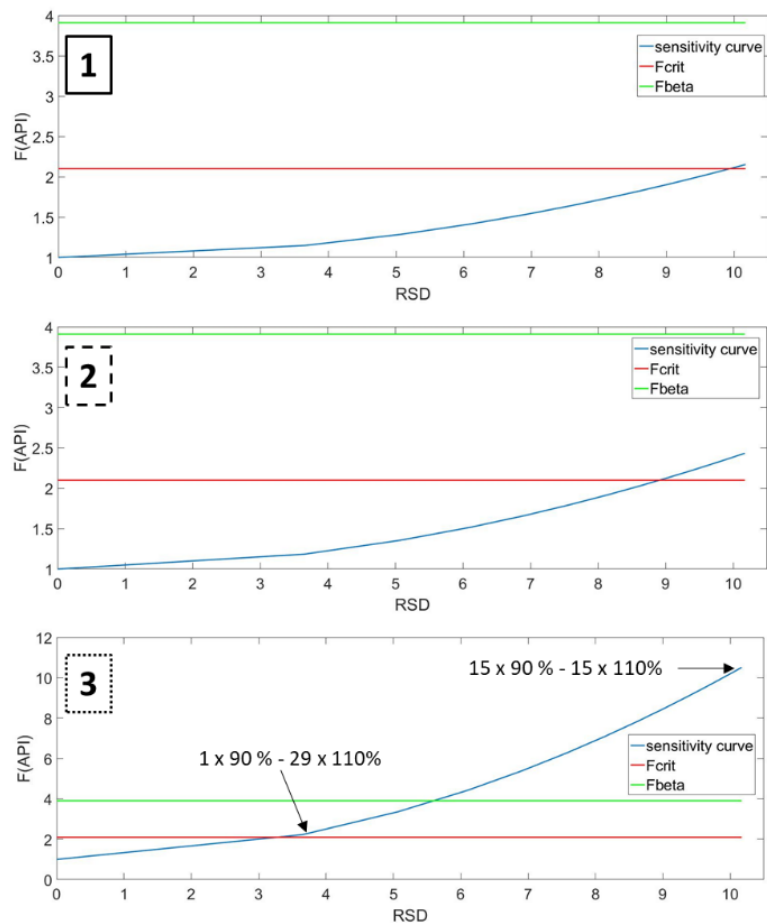


Figure 9.6: Sensitivity curves (blue) for the three selected spectral ranges to find the intersection with  $F_{crit}$  (red) and  $F_{beta}$  (green) with  $Barb=30$ . (1) Complete spectrum without [1100-1140 nm] (full line), (2) [1505-1558 nm][1603-1871 nm][1969-2068 nm] (dashed line) and (3) [2028-2036 nm] (dotted line).

#### 9.3.4.4 THE MINIMUM BLOCK SIZE

A minimum block size needed to be selected to assure a  $\beta \leq 0.05\%$ . Therefore, additional sensitivity plots were developed for block sizes consisting of 2 to 29 spectra for the selected spectral range: [2028-2036]. For all the different block sizes, the RSD corresponding with the intersection between the sensitivity curve and  $F_{crit}$  was plotted in Figure 9.7 (blue). The RSD at  $F_{crit}$  decreased for increasing block size because the  $F_{crit}$ -value decreased and the true variance is determined more accurately for increasing block size. As aforementioned the RSD at the intersection of the sensitivity curve and  $F_{beta}$  should not exceed 8.2 %. Hence, a maximum allowable RSD (Figure 9.7 – red) at  $F_{crit}$  was calculated for each studied block size by Equation 9.10.

$$RSD_{\alpha,\beta=5\%,n}^{max}(F_{crit}) = \sqrt{\frac{F_{crit}(\alpha, B) - 1}{F_{\beta=5\%}(\alpha, B) - 1}} * 8.2 \% \quad [9.10]$$

An intersection between the blue and red line was seen at block size 16, indicating that a minimum block size of 16 was needed to ensure that the RSD at  $F_{crit}$  was below 8.2 %. A smaller block sizes implies that the probability is not less than 5 % that a blend with an RSD of 8.2 % is considered as uniform. In this study, a block size of 20 was chosen because this even further decreases the probability for a  $\beta$ -error (type II-error). A higher block size would require more spectral data collection time to fill a block. For this two sided F-test a  $F_{crit}$  of 2.51 was derived from the F-distribution tables (degrees of freedom for numerator and denominator of 19).

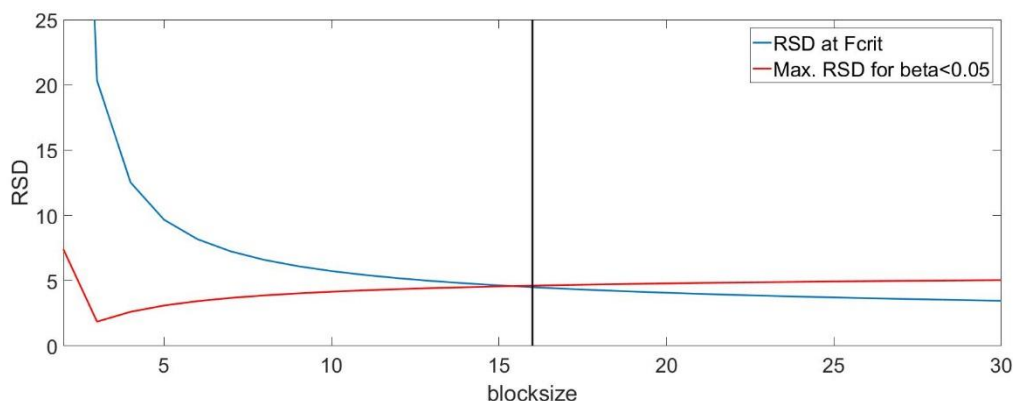


Figure 9.7: RSD at  $F_{crit}$  for block sizes of 2 to 30 spectra (blue) and the maximum allowable RSD to comply with a  $\beta$ -error of max 5 % (red). The intersection of both lines determines the minimum allowable block size.

### 9.3.5 CASE STUDIES

#### 9.3.5.1 CASE STUDY 1

For the first case study, the tablet press feed tube was exclusively filled with granules of 100 % target concentration (Figure 9.2). Figure 9.8 (Top) shows the NIR predictions derived from the PLS model at each time point (1 API concentration prediction per second) and the assay results of the tablets collected every minute, whereas Figure 9.8 (bottom) shows the calculated F values for each pair of consecutive blocks of spectra. The API content predictions varied from 98.3 to 102.8 %, whereby the predicted values fluctuated around the target concentration. The UV-based assay results of the tablets demonstrated API concentrations close to the target concentration. Although the API concentration prediction from a certain

NIR spectrum could not be correlated to a certain tablet, due to the unknown lead-lag time (i.e. NIR signal of the API that is ahead of time compared to the actual API content in tablets), the assay results were in accordance with the in-line NIR predictions.

The first F-value was obtained after 40 s because then the first two blocks of 20 spectra were obtained and the variances within each block could subsequently be compared. Unsurprisingly, the F-value was at all times lower than  $F_{crit}$  as the variance between the compared blocks was only due to noise because a uniform blend was tableted. At two time periods, indicated by the green squares on Figure 9.8 (bottom),  $F_{crit}$  was almost exceeded by the F-value due to an abrupt change in API content, also indicated by the PLS based predictions (top). However, the F-value remained lower than  $F_{crit}$ . Therefore, in this case study, the moving F-test and the PLS model were able to confirm the steady-state conditions during tableting of the content-uniform granule blend.



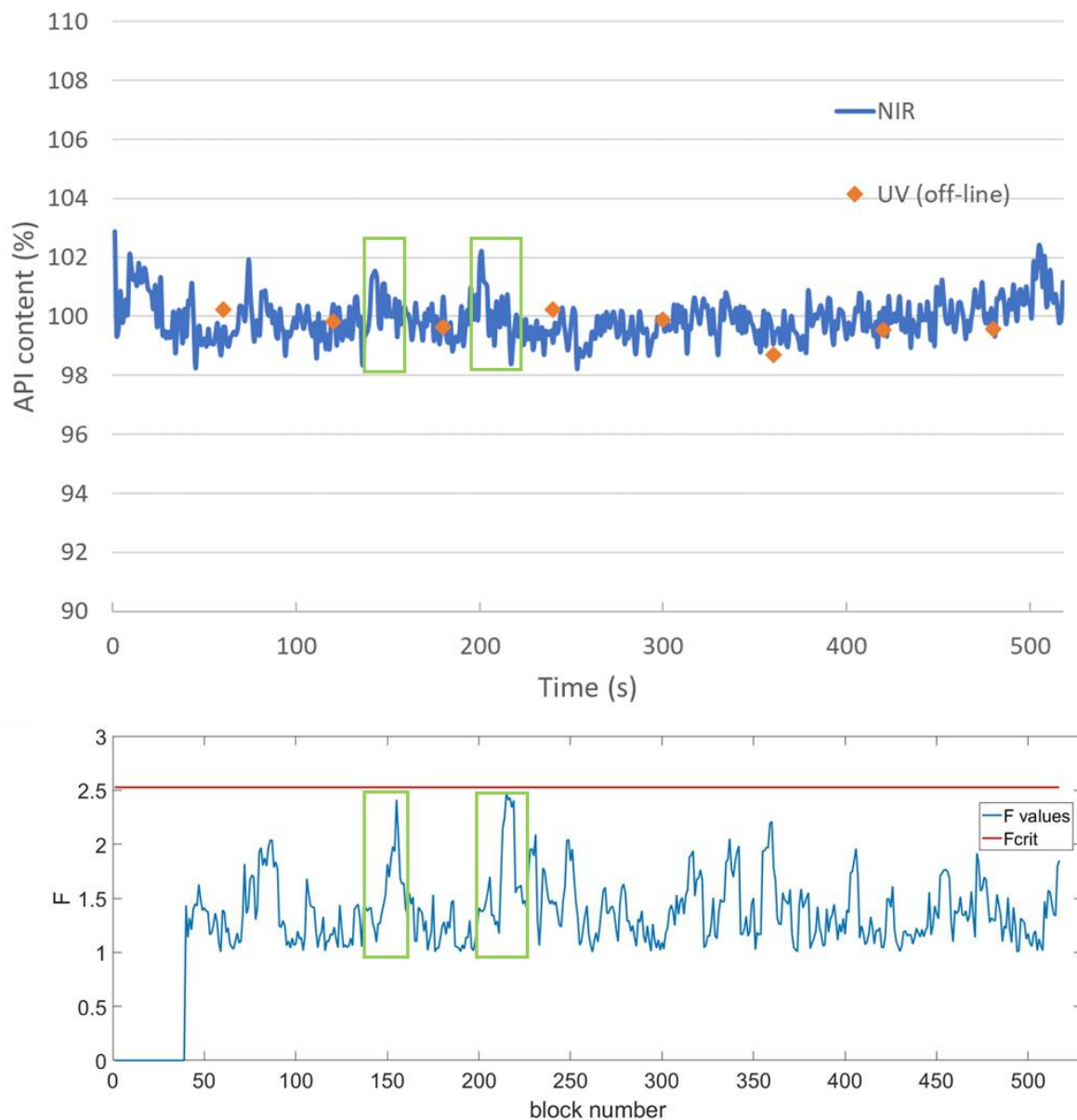


Figure 9.8: Case study 1: In-line NIR based predicted API content values at each second (blue) and the off-line UV based API content values of the tablets collected each minute (orange dots) as a reference (Top). The F-values of consecutive blocks of spectra (blue) plotted against the critical F-value (red) (Bottom).

### 9.3.5.2 CASE STUDY 2

In the second case study, the tablet press feed tube was first filled with granules of 100 % target concentration. On top of that, granules of 110 % of target API concentration were added. Finally, the tablet press feed tube was further filled with granules at the target concentration of 100 % (Figure 9.2). Similar as for case study 1, the NIR based predicted API content using the PLS regression model, the API content of the tablets as determined by off-

line UV-analysis and the F-values calculated by the moving F-test method on the in-line collected NIR data are shown in Figure 9.9. At the start of this experiment (depicted on the top and bottom of figure 9.9 as '1'), the feed frame consisted only of granules with the target API concentration (i.e., 100 %). Consequently and as expected, the NIR PLS based predictions fluctuated around the target of 100 % and the F-values did not exceed  $F_{crit}$ . During this tableting experiment, a mass throughput of 1.53 kg/h was obtained. Hence,  $\pm 140$  g of granules were tableted at time point 2 (i.e.,  $\pm 3.5$  minutes). At that point, the predicted API content suddenly increased as granules containing 110 % API relative to target entered the feed frame (as expected see Figure 9.2) and were consequently diluted with granules at target concentration. As a consequence, F-values exceeded  $F_{crit}$  because variances of consecutive block were significantly different. After a gradual increase in predicted API content, a gradual decrease was again observed at time point 3, also resulting in F-values larger than  $F_{crit}$ . In the fourth zone, F-values that exceeded  $F_{crit}$  succeeded each other rapidly. The predicted API content steeply increased and it was suggested that more and more granules containing 110 % of target entered the feed frame. A similar trend in NIR predictions was observed by De Leersnyder et al. when a low throughput was combined with a low paddle wheel speed during RTD studies (8). The authors believe that this can be explained by the preferential powder flow in and from the feed chute towards the filling chamber in the feed frame. As a plug flow is not present, first a smaller part of granules containing 110 % were mixed during time-period 2 and 3, followed by the larger remaining granules during time-period 4. Finally, the second layer of granules with 100 % API relative to target (Figure 9.2) entered the feed frame, causing dilution in the feed frame. Consequently, the predicted API content decreased in the fifth time period. Simultaneously,  $F_{crit}$  was constantly exceeded due to the intense mixing of the two types of granules. As a consequence of the intensive mixing, the predicted API content and the real API content of tablets did not reach 110 %. In general, a similar trend in API content was observed for the tablets after off-line UV analysis. A delay due to a lead-lag time was however observed. In this case-study, both the moving F-test and the PLS mode were able to alarm when the granule bed became inhomogeneous and when it remained inhomogeneous.

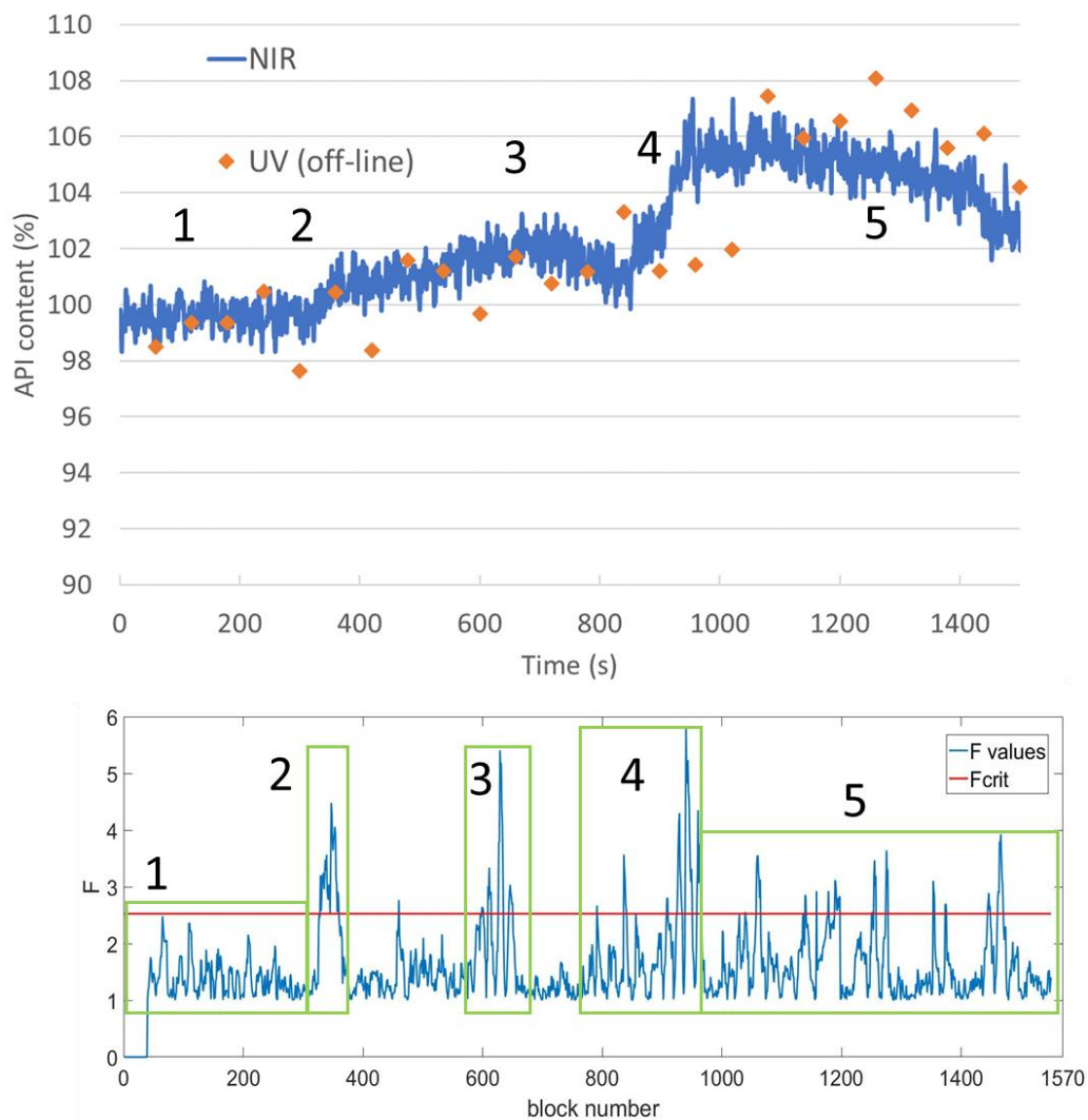


Figure 9.9: Case study 2: In-line NIR based predicted API content values at each second (blue) and the off-line UV based API content values of the tablets collected each minute (orange dots) as a reference (Top). The F-values of consecutive blocks of spectra (blue) plotted against the critical F-value (red) (Bottom).

### 9.3.5.3 CASE STUDY 3

In the last case study (see set-up in Figure 9.2), only the tablet press feed frame (filling and dosing chamber) was filled with granules of 100 % API relative to target. As a consequence, only during the first short time period of  $\pm 50$  seconds, a homogeneous granule bed was present in the feed frame. Immediately afterwards (Figure 9.10 – second time period), the F-value was already exceeded for the first time due to an increase in API content as the granules of 110 % API relative to target entered the feed frame. Although the feed frame still mainly contained the initial granules, the introduction of granules containing 110 % API was quickly

noticed because the inlet of the feed frame is in close proximity of the NIR probe. Subsequently, both types of granules (100 % and 110 % relative to target) were further mixed in the feed frame during the third time-period, resulting in an increase of the predicted API content and multiple F-values that exceeded  $F_{crit}$ . After  $\pm 840$  s (i.e., the start of time period 4 in Figure 9.10), the predicted API content reached a plateau and  $F_{crit}$  was not exceeded anymore, indicating that a homogeneous granule bed (granules containing 110 % relative to target) was again obtained in the feed frame.

The quantitative PLS model was able to show how much the API content was off-target, whereas the F-value was smaller than  $F_{crit}$  at the end of this experiment (while the API content was off-target). The qualitative moving F-test only alarmed for an inhomogeneous granule bed, but once a homogeneous blend was again obtained, the F-value remained smaller than  $F_{crit}$  although the API content was off-target. This is because the moving F-test only compared variances of blocks. As an example, the F-value of the first 20 spectra and the last 20 spectra of the case study was calculated:  $F\text{-value} = 1.29 < F_{crit} = 2.53$ . Although there was a spectral difference between both blocks of spectra, a low spectral variance was present in both blocks, resulting in an insignificant variance difference between both blocks. The incapability of the moving F-test to quantify a difference in average concentration can however be overcome in a continuous process by monitoring the logged data of the continuous loss in weight raw material feeders and understanding the RTD along the length of the manufacturing line.

In general, a comparable trend was observed for the in-line NIR based predicted API content and the off-line UV-based determined API content of the tablets. However, a small underprediction was observed for the predicted API contents during the steady state. This can be explained by the RMSEcv (i.e., 0.93 %) of the quantitative model, indicating the predictive error of the model.

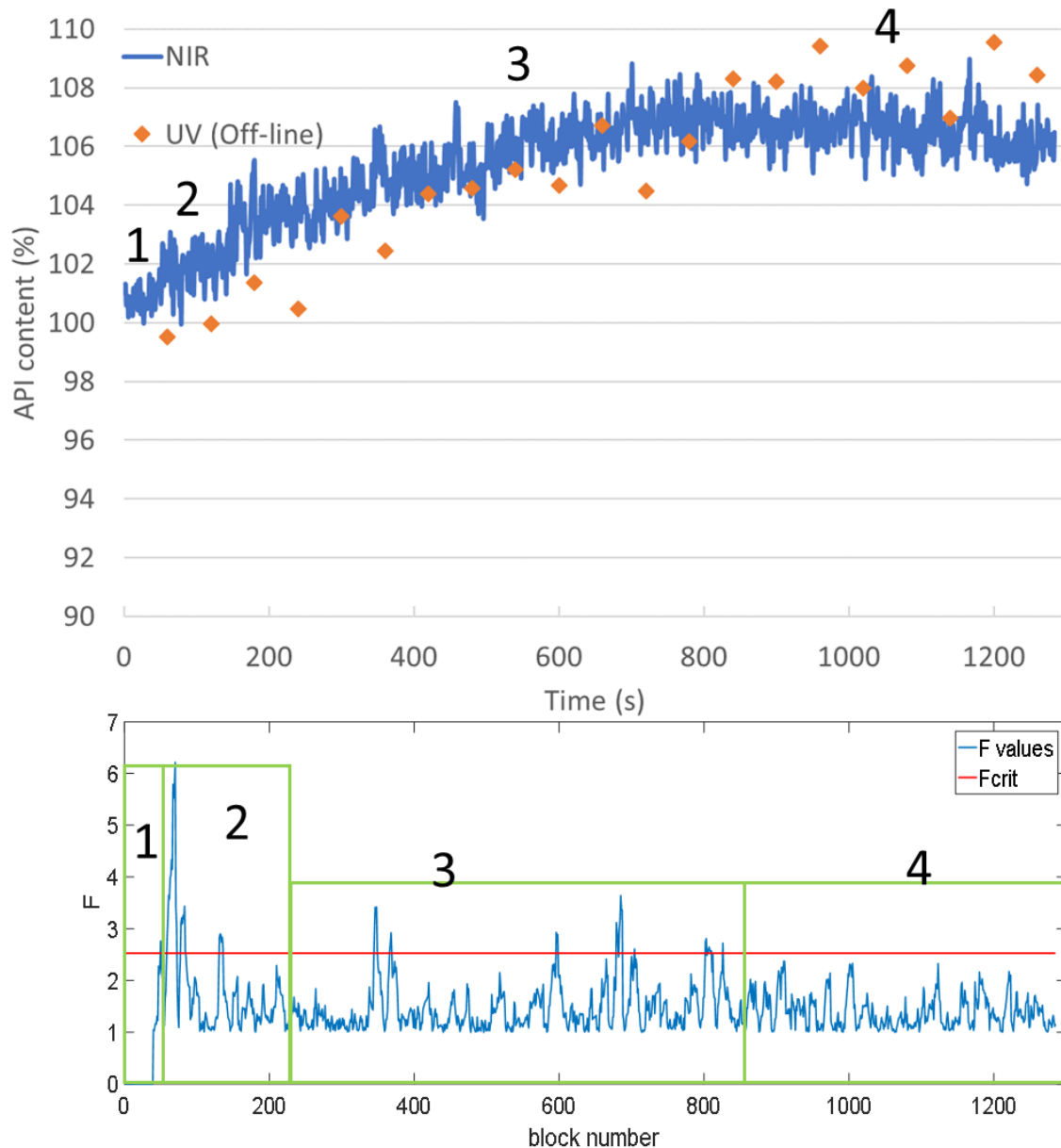


Figure 10: Case study 3: In-line NIR based predicted API content values at each second (blue) and the off-line UV based API content values of the tablets collected each minute (orange dots) as a reference (Top). The F-values of consecutive blocks of spectra (blue) plotted against the critical F-value (red) (Bottom).

## 9.4 CONCLUSIONS

In this study, a quantitative PLS regression model and a qualitative moving F-test were assessed and compared to monitor blend uniformity in the feed frame of the tablet press. Real-time predictions of the API concentration in the blend, based on the in-line NIR PLS model, were used for the quantitative approach, whereas a real-time comparison of the variances of consecutive blocks of NIR spectra (each block containing 20 spectra) was

performed for the moving F-test. It was seen that the moving F-test was sensitive to detect disturbances while focussing on a narrow spectral region. Consequently, the moving F-test was able to detect well inhomogeneities in the powder bed as a result from changes in API concentration. However, once the blend became homogenous again – although having an API concentration out of target - the moving F-test did not alarm, because the spectral variance difference between 2 blocks of spectra was non-significant. Conversely, the qualitative PLS model was able to predict the actual API concentration each second. As a conclusion, the moving F-test could be used as it was proven to be a sensitive method to detect blend homogeneity. In addition, less experimental effort is needed. The PLS model being a quantitative method provides more information (i.e., the actual API content) but also requires more experimental efforts.

### 9.5 ACKNOWLEDGEMENT

Sentronic (especially Sebastian Sowinski) and GEA Pharma Systems (especially Frederik Detobel) are also kindly acknowledged for the loan of the SentroPAT and the overfill cam, respectively.

## 9.6 REFERENCES

1. Peeters E, Tavares da Silva AF, Toiviainen M, Van Renterghem J, Vercruyssen J, Juuti M, et al. Assessment and prediction of tablet properties using transmission and backscattering Raman spectroscopy and transmission NIR spectroscopy. *Asian J Pharm Sci* [Internet]. 2016;11(4):547–58. Available from: <http://dx.doi.org/10.1016/j.ajps.2016.04.004>
2. Li Y, Anderson CA, Drennen JK, Airiau C, Igne B. Development of an In-Line Near-Infrared Method for Blend Content Uniformity Assessment in a Tablet Feed Frame. *Appl Spectrosc*. 2019;73(9):1028–40.
3. De Leersnyder F, Peeters E, Djalabi H, Vanhoorne V, Van Snick B, Hong K, et al. Development and validation of an in-line NIR spectroscopic method for continuous blend potency determination in the feed frame of a tablet press. *J Pharm Biomed Anal* [Internet]. 2018;151:274–83. Available from: <http://dx.doi.org/10.1016/j.jpba.2018.01.032>
4. Dalvi H, Langlet A, Colbert MJ, Cournoyer A, Guay JM, Abatzoglou N, et al. In-line monitoring of Ibuprofen during and after tablet compression using near-infrared spectroscopy. *Talanta* [Internet]. 2019;195(September 2018):87–96. Available from: <https://doi.org/10.1016/j.talanta.2018.11.034>
5. Sierra-Vega NO, Román-Ospino A, Scicolone J, Muzzio FJ, Romañach RJ, Méndez R. Assessment of blend uniformity in a continuous tablet manufacturing process. *Int J Pharm* [Internet]. 2019;560(February):322–33. Available from: <https://doi.org/10.1016/j.ijpharm.2019.01.073>
6. Järvinen K, Hoehe W, Järvinen M, Poutiainen S, Juuti M, Borchert S. In-line monitoring of the drug content of powder mixtures and tablets by near-infrared spectroscopy during the continuous direct compression tableting process. *Eur J Pharm Sci*. 2013;48(4–5):680–8.
7. Wahl PR, Fruhmann G, Sacher S, Straka G, Sowinski S, Khinast JG. PAT for tableting: Inline monitoring of API and excipients via NIR spectroscopy. *Eur J Pharm Biopharm* [Internet]. 2014;87(2):271–8. Available from: <http://dx.doi.org/10.1016/j.ejpb.2014.03.021>
8. De Leersnyder F, Vanhoorne V, Kumar A, Vervaet C, De Beer T. Evaluation of an in-line NIR spectroscopic method for the determination of the residence time in a tablet press. *Int J Pharm* [Internet]. 2019;565(January):358–66. Available from: <https://doi.org/10.1016/j.ijpharm.2019.05.006>
9. Fonteyne M, Vercruyssen J, De Leersnyder F, Besseling R, Gerich A, Oostra W, et al. Blend uniformity evaluation during continuous mixing in a twin screw granulator by in-line NIR using a moving F-test. *Anal Chim Acta* [Internet]. 2016;935:213–23. Available from: <http://dx.doi.org/10.1016/j.aca.2016.07.020>
10. Besseling R, Damen M, Tran T, Nguyen T, van den Dries K, Oostra W, et al. An efficient, maintenance free and approved method for spectroscopic control and monitoring of blend uniformity: The moving F-test. *J Pharm Biomed Anal* [Internet]. 2015;114:471–81. Available from: <http://dx.doi.org/10.1016/j.jpba.2015.06.019>

11. Stauffer F, Ryckaert A, Van Hauwermeiren D, Funke A, Djuric D, Nopens I, et al. Heat Transfer Evaluation During Twin-Screw Wet Granulation in View of Detailed Process Understanding. *AAPS PharmSciTech*. 2019;20(7):1–13.

12. De Leersnyder F, Vanhoorne V, Bekaert H, Vercruysse J, Ghijs M, Bostijn N, et al. Breakage and drying behaviour of granules in a continuous fluid bed dryer: Influence of process parameters and wet granule transfer. *Eur J Pharm Sci [Internet]*. 2018;115(September 2017):223–32. Available from: <https://doi.org/10.1016/j.ejps.2018.01.037>



**10 BROADER  
INTERNATIONAL CONTEXT,  
RELEVANCE AND FUTURE  
PERSPECTIVES**

## 10.1 BROADER INTERNATIONAL CONTEXT

The implementation of continuous manufacturing processes into the pharmaceutical industry demands a comprehensive knowledge, innovative technologies and equipment, and advanced control strategies. Therefore, the collaboration between academic institutions, pharmaceutical companies, regulators, equipment manufactures was initiated in several consortia. A few examples are given below:

The European Consortium for Continuous Pharmaceutical Manufacturing (ECCPM) is a collaboration between several pharmaceutical partners (AstraZeneca, Bayer, UCB, Roche, MSD, Boehringer Ingelheim), equipment/technology providers (Siemens, GEA Pharma Systems, Automatic, Maag, ...), universities (Ghent University, Graz University of Technology, University of Eastern Finland, Heinrich Heine University Düsseldorf) and the Research Centre Pharmaceutical Engineering (RCPE, Graz, Austria). The consortium was founded to serve as a platform for industrial companies and universities to share their know-how to address challenges when transferring a continuous manufacturing concept from R&D to commercial scale (1).

The Center of Structured Organic Particulate Systems (C-SOPS) is a multi-university consortium between Rutgers University, Purdue University, New Jersey Institute of Technology and the University of Puerto Rico created in 2006. The consortium works closely with industrial partners (including technology suppliers, technology integrators and pharmaceutical companies) and regulatory authorities. The focus is to improve the way pharmaceuticals, foods and agriculture products are manufactured (2).

The Centre of Excellence in Sustainable Pharmaceutical Engineering (CESPE) is a multidisciplinary innovation accelerator. This consortium is focussing on the development, design and optimisation of drug substance and drug product production platforms. CESPE consists of several research groups in Ghent: Ghent University's Faculty of Pharmaceutical Sciences, the Faculty of Bioscience Engineering and the Tech Lane Ghent Science Park. Soon, the consortium will start the alliance with industrial partners (3).

## 10.2 RELEVANCE

Among the different pharmaceutical dosage forms, tablets are still by far the most dominant as they account for more than 80 % of all pharmaceutical products. This dosage form is desirable for the pharmaceutical industry and for the patients due to an accurate dosing, the ease of manufacturing, the long shelf life, the low costs, tamper-proofness in comparison to capsules, the ease of transportation, the convenience of administration and the possibility to cover any unpleasant tastes (4,5). As a consequence, the global oral solid dosage pharmaceutical formulation market was estimated in 2017 at 493 billion dollar (6). However, the profits that are made in the pharmaceutical industry are not a result of innovative manufacturing techniques. In 2003, The Wall Street Journal revealed that: “The pharmaceutical industry has a little secret: Even as it invents futuristic new drugs, its manufacturing techniques lag far behind those of potato-chip and laundry-soap makers” (7). And, almost a decade later, FDA director Janet Woodcock mentioned that: “Manufacturing experts from the 1950’s would easily recognize the pharmaceutical manufacturing processes of today. It is predicted that manufacturing will change in the next 25 years as current manufacturing practices are abandoned in favour of cleaner, flexible, more efficient continuous manufacturing”, indicating that the pharmaceutical industry is rather old-fashioned. Hence, one may ask why a slow transition in innovation is observed in pharmaceutical manufacturing.

### *The slow transition towards continuous manufacturing*

The pharmaceutical industry has been hesitant to change the traditional batch manufacturing due to several reasons. For decades, it could make high profits from the patent-protected blockbuster drugs, making it not needed to improve the manufacturing efficiency (8). Further, the rigid regulatory system demands a resubmission when changes are made to the manufacturing process. Even though a small change could be cost-saving, the submission for a change is not easy to obtain because it requires time, fees to submit changes and administrative paperwork, making it reluctant for changes. In addition, as a change also might result in a production delay, the industry rather continued with the use of old and inefficient processes (7,9). Moreover, the pharmaceutical industry invested in the last decades in batch

process equipment, the high investments costs for novel equipment also hampers the transition.

### *Why a transition towards continuous manufacturing occurred*

The pharmaceutical industry had to rethink their manufacturing approach in 21th century as they faced many challenges:

More and more blockbuster drugs reached the end of the patent protection. Once the patents expire, the production of generic drugs begins and a decrease in their market share typically occurs, making the blockbuster less lucrative. As blockbuster drugs generally treat diseases with a high number of patients, the development of new drugs focussing on similar treatments would only increase the competition. As a consequence, the pharmaceutical industry had changed their strategy and it was gradually focussing on oral solids that treat a specific group of diseases. This would reduce the competition and thereby increase the profits. However, the manufacturing of these drugs would demand another approach of manufacturing as smaller volumes need to be produced and less manufacturing errors are desired due to the costly API (10,11).

Several economic factors forced the pharmaceutical industry to save money. (i) The total costs, from a laboratory idea to commercialization of the drug product, has increased and is estimated to be over 2 billion dollar. (ii) The number of new drug products reaching the market has decreased although the investments in R&D were increased (12). (iii) Governments targeted the pharmaceutical industry to regulate the drug prices in order to reduce the public expenditure on pharmaceutical products, especially as the cost increased with the aging populations (13).

Further, as already mentioned, the pharmaceutical industry has been hesitant for innovation due to the rigid regulatory system. However, the mindset of the regulatory agencies has also changed, because they are aware that inefficient manufacturing can lead to drug shortages or product recalls which is highly unfavourable from a public health perspective (14,15). A textbook example was seen in The Netherlands: a shortage of an anti-conception drugs occurred as four out of seven manufacturers were not able to adequately produce the drug product (16).

*Advantages of the transition towards continuous manufacturing*

Previous paragraphs clearly explained that the need to modernize the pharmaceutical industry emerged. Therefore, continuous manufacturing arose as an alternative for the traditional batch manufacturing since it has multiple advantages for the pharmaceutical industry and the society:

- The operating time of a continuous manufacturing process determines the production volume rather than the dimensions of the equipment. Hence, it is a flexible production approach that is able to adapt to the market demands. This is especially favourable in case of pandemics or drug shortages (17).
- The same equipment size can be used during development and commercial manufacturing. Therefore, scale-up studies can be avoided which saves time and consumption of valuable API during process development (17). Further, this also reduces the development time which results in a longer monopoly for the company before the patent expires, leading to an economic advantage (18).
- All unit operations are integrated into a continuous manufacturing line, whereby all intermediate products are transferred from one unit operation to another. Hence, storage and testing of intermediate products is avoided, resulting in a much shorter processing time and a shorter time-to-market (18).
- Generally, continuous manufacturing requires less floor space as the equipment is smaller and storage of the intermediate product is not needed. The use of solvents is also reduced during off-line analyses of the intermediate and final product. In addition, a smaller part of a material is discarded when productions are out-of-specification in contrast to batch manufacturing where the complete batch is at risk, reducing the amount of waste. Consequently, continuous manufacturing results in reduced environmental footprint (19–21).
- Overall, increased improvements in manufacturing efficiency can be translated in the form of more affordable pharmaceuticals. Or the savings due to continuous manufacturing could be also used for the discovery of new drug products (9,22).

- The amount of errors due to human interventions is minimized as transfer, storage and testing of the intermediate products is not needed (19).

The aim of this research was to obtain an enhanced process understanding of several unit operations of a continuous from-powder-to-tablet line, ConsiGma™-25. Investigating the impact of process parameters, formulation properties and the different unit operations on the quality attributes of the intermediate products could help and accelerate the adoption of the continuous manufacturing line. Ultimately, aforementioned list of benefits could become more and more a reality, which is favourable for our society.

### 10.3 FUTURE PERSPECTIVES

#### 10.3.1 TWIN-SCREW GRANULATION MODULE

A TPLS model was developed in chapter 6 to obtain an enhanced process understanding for twin-screw granulation (TSG). The predictive ability was also tested as a support during process and formulation development. It was seen that there were several challenges as the current approach is a linear model, possible extensions could be looking into non-linear relationships to improve the accuracy of the predictions.

Further, the TPLS model was able to indicate the most influencing raw material properties upon granule quality. This allows to finetune the raw material database that was constructed for TSG by removing irrelevant properties. In a next step, the modified database could be tested to find a surrogate component for a new API. A surrogate component is defined as a component with similar raw material properties as the new API. Ultimately, this would be very helpful during process and formulation development as limited amount of new API is available.

The TPLS model was one way to predict granule quality. Another approach is to develop a generic mechanistic model for the prediction of the granule quality. A first attempt was already performed by Van Hauwermeiren et al. (23). This study used Population Balance Models (PBMs) as suitable framework to allow the prediction of the dynamic granule size distribution (GSD). In a next step, the input of different process settings (L/S ratio, mass feed rate and screw speed) for different blend properties have to be evaluated to develop the

generic model for several granule responses such as granule size, porosity, etc. Ultimately, this would allow to predict optimal operational settings for new formulations.

### 10.3.2 Drying unit

A more enhanced understanding of the six-segmented fluid-bed dryer was obtained in chapter 7 and 8. But, ultimately, the main goal is to achieve a generic mechanistic dryer model. Ghijs et al. already successfully modelled single granule drying kinetics at constant filling time and throughput (24). However, the semi-continuous drying process is a very complex process. During the filling phase and drying phase of a certain cell, the air humidity and drying air temperature changes and this alters the drying behaviour of granules entering at other time points. In addition, breakage and attrition phenomena of granules during drying, although this might be limited, will also change the drying behaviour as it was reported that the drying rate depends on the granule size.

Due to the design of the drying unit of the ConsiGma™-25, it is possible that the distribution of drying air over the different cells and the air flow rate in the different cells might vary. This might impact the fluidisation patterns and as a consequence also the drying behaviour. So far, fluidisation patterns are not taken into account for the mechanistic model. More process knowledge is required. On the one hand, as a first step, the fluidization can be experimentally visualized through the transparent drying cell of the ConsiGma™-1. The effect of the granule size and the position of the granules in the cell on fluidization can be studied. On the other hand, fluidization can also be described by numerical models such as Computational Fluid Dynamics (CFD). In addition, it is also interesting to revise the DoE that was used in chapter 8 to evaluate cell-to-cell. Focussing on granule that are not sufficiently dried might allow to observe differences in moisture content for the different cells.

In addition, as the drying behaviour may not only be influenced by the initial granule properties and the applied process setting, it is also important to investigate the effect of formulation properties. Therefore, after a raw material characterization, similar granules (i.e., similar granule size distribution and porosity) can be produced for different formulations. Subsequently, the granules can be dried at different drying parameters to develop drying profiles. Hence, this would allow to determine the raw material properties having an impact on drying.

One may argue whether the dryer design is optimal for the drying process. It is certainly an additional challenge for the development of a generic mechanistic model. Therefore, it might be interesting in the field of pharmaceutical engineering to investigate the optimization of a drying design.

### 10.3.3 TABLET PRESS

Chapter 9 in this dissertation discussed the implementation of near infrared (NIR) inside the feed frame of the Modul™P tablet press to monitor API concentration of the circulating powder blend. In this study, NIR predictions of the API content in the feed frame differed from the actual API content in tablets collected downstream due to a lead-lag time. The lead-lag time is indispensable to link in-line NIR blend potency measurements to the actual API content in the tablets. This could be extremely helpful to support real-time release (RTR), as the in-line feed frame monitoring of blend potency could determine the time-period in which tablets need to be diverted. However, this phenomenon is not well understood. Therefore, research need to be performed to study the effect of process parameters (such as paddle speed, turret speed, overfill level, paddle speed ratio, type of paddle, etc.) upon lead-lag time.

In addition, in chapter 9, the profile of the NIR predictions was explained by the complex powder flow in and from the feed chute towards the filling chamber in the feed frame. More research needs to be performed to gain an enhanced knowledge of the flow behaviour, the mixing behaviour and the existence of dead-spots. Several approaches can be used for enhanced understanding. The addition of coloured powder could be helpful to visualize dead-spots in feed chute and the preferential flow from feed chute toward feed frame. Moreover, a custom-made transparent feed frame can be used to study the mixing in the feed frame and to indicate dead-spots in one of the chambers. On the other hand, modelling frameworks such as the discrete-element method (DEM) can be used to model the powder flow during tableting.



## 10.4 REFERENCES

1. European Consortium for Continuous Pharmaceutical Manufacturing [Internet]. Available from: <http://www.eccpm.com/>
2. Center of Structured Organic Particulate Systems [Internet]. Available from: <https://www.csops.org/about-us-1>
3. CESPE [Internet]. Available from: <https://www.cespe.be/>
4. Gohel MC, Jogani PD. A review of co-processed directly compressible excipients. *J Pharm Pharm Sci.* 2005;8(1):76–93.
5. Armstrong N. Encyclopedia of Pharmaceutical Technology: Tablet Testing. In: Swarbrick J, editor. *Encycl Pharm Technol.* Pinehurst, North Carolina, USA; 2007. p. 3653–63.
6. Oral Solid Dosage Pharmaceutical Formulation Market: Oral Solid Dosage Pharmaceutical Formulation Market: Emerging Markets of Latin America, APEJ and MEA to Collectively Hold over 45% Market Value Share: Global Industry Analysis 2012 - 2016 and Opportunit [Internet]. 2017. Available from: <https://www.futuremarketinsights.com/reports/oral-solid-dosage-pharmaceutical-formulation-market>
7. Abboud L, Hensley S. Factory Shift: New Prescription For Drug Makers: Update the Plants; After Years of Neglect, Industry Focuses on Manufacturing; FDA Acts as a Catalyst; The Three-Story Blender. *The Wall Street Journal.* 2003 Sep 3;A.1.
8. Ubel P. Is The Golden Era Of Pharmaceutical Profits Over? [Internet]. Available from: <https://www.forbes.com/sites/peterubel/2016/07/29/is-the-golden-era-of-pharmaceutical-profits-over/?sh=2fb3e8f47207>
9. Suresh P, Basu PK. Improving pharmaceutical product development and manufacturing: Impact on cost of drug development and cost of goods sold of pharmaceuticals. *J Pharm Innov.* 2008;3(3):175–87.
10. Srai JS, Badman C, Krumme M, Futran M, Johnston C. Future supply chains enabled by continuous processing-opportunities and challenges May 20-21, 2014 continuous manufacturing symposium. *J Pharm Sci* [Internet]. 2015;104(3):840–9. Available from: <http://dx.doi.org/10.1002/jps.24343>
11. Wright T. The Future of Oral Solids [Internet]. Available from: [https://www.contractpharma.com/issues/2017-03-01/view%7B\\_%7Deditorials/the-future-of-oral-solids/53369](https://www.contractpharma.com/issues/2017-03-01/view%7B_%7Deditorials/the-future-of-oral-solids/53369)
12. Basu P, Joglekar G, Rai S, Suresh P, Vernon J. Analysis of manufacturing costs in pharmaceutical companies. *J Pharm Innov.* 2008;3(1):30–40.
13. Ess Si, Schneeweiss S, Szucs TD. European healthcare policies for controlling drug expenditure. *Pharmacoeconomics.* 2003;21:89–103.

14. Mazer-Amirshahi M. Drug shortage crisis puts public health at risk. Available from: <https://theconversation.com/drug-shortage-crisis-puts-public-health-at-risk-34901>
15. O'Connor TF, Yu LX, Lee SL. Emerging technology: A key enabler for modernizing pharmaceutical manufacturing and advancing product quality. *Int J Pharm* [Internet]. 2016;509(1–2):492–8. Available from: <http://dx.doi.org/10.1016/j.ijpharm.2016.05.058>
16. Vleugels A. Tekort aan anticonceptiepil ontstond door pech op pech op pech [Internet]. 2018. Available from: <https://nos.nl/op3/artikel/2250224-tekort-aan-anticonceptiepil-ontstond-door-pech-op-pech-op-pech.html>
17. Ierapetritou M, Muzzio F, Reklaitis G. Perspectives on the Continuous Manufacturing of Powder-Based Pharmaceutical Processes. *AIChE J*. 2016;62(6):1846–62.
18. Fonteyne M, Vercruyssen J, De Leersnyder F, Van Snick B, Vervaeke C, Remon JP, et al. Process Analytical Technology for continuous manufacturing of solid-dosage forms. *TrAC - Trends Anal Chem* [Internet]. 2015;67:159–66. Available from: <http://dx.doi.org/10.1016/j.trac.2015.01.011>
19. Vanhoorne V, Vervaeke C. Recent progress in continuous manufacturing of oral solid dosage forms. *Int J Pharm* [Internet]. 2020;579(December 2019):119194. Available from: <https://doi.org/10.1016/j.ijpharm.2020.119194>
20. Lee SL, O'Connor TF, Yang X, Cruz CN, Chatterjee S, Madurawe RD, et al. Modernizing Pharmaceutical Manufacturing: from Batch to Continuous Production. *J Pharm Innov*. 2015;10(3):191–9.
21. De Soete W, Dewulf J, Cappuyns P, Van Der Vorst G, Heirman B, Aelterman W, et al. Exergetic sustainability assessment of batch versus continuous wet granulation based pharmaceutical tablet manufacturing: A cohesive analysis at three different levels. Vol. 15, *Green Chemistry*. 2013. p. 3039–48.
22. Vernon JA, Hughen WK, Trujillo AJ, Trujillo AJ. Pharmaceutical Manufacturing Efficiency, Drug Prices, and Public Health: Examining the Causal Links. *Drug Inf J*. 2007;41(2):229–39.
23. Van Hauwermeiren D, Verstraeten M, Doshi P, am Ende MT, Turnbull N, Lee K, et al. On the modelling of granule size distributions in twin-screw wet granulation: Calibration of a novel compartmental population balance model. *Powder Technol* [Internet]. 2019;341:116–25. Available from: <https://doi.org/10.1016/j.powtec.2018.05.025>
24. Ghijs M, Schäfer E, Kumar A, Cappuyns P, Van Assche I, De Leersnyder F, et al. Modeling of Semicontinuous Fluid Bed Drying of Pharmaceutical Granules With Respect to Granule Size. *J Pharm Sci*. 2019;108(6):2094–101.

# **11 SUMMARY AND GENERAL CONCLUSIONS**

For decades, the manufacturing of pharmaceutical solid-dosage forms relied on batch-wise processes. However, batch-wise manufacturing is related with off-line quality testing, which is time-consuming, destructive and labour-intensive, a varying product quality, high productions costs and several other issues. Hence, the interest in the transition from batch towards continuous pharmaceutical manufacturing has increased. However, a thorough knowledge and understanding of the continuous manufacturing process is needed to truly benefit from the advantages of continuous manufacturing. The advantages, the challenges and the rationale of the transition towards continuous manufacturing in the pharmaceutical industry as well as the different continuous manufacturing techniques were discussed in detail in **chapter 1**. The objectives of this dissertation were outlined in **chapter 2**.

In **chapter 3**, the use of a compartmental set-up allowed to study the evolution of granule quality attributes and heat exchanges along the length of the granulator barrel. Granule size, mechanical energy, barrel temperature and granule temperature (measured using an in-line implemented infra-red camera) were measured to evaluate heat transfer occurring at the different compartments and to relate them to granulation mechanisms. Collected data identified wetting enthalpy and friction forces as the main sources of heat along the granulator length. Wetting occurred in the wetting zone and generated temperature increase depending on liquid-to-solid ratio and powder wettability. In the kneading zones, granule temperature increase was proportional to mechanical energy. While it is usually admitted that granule consolidation and reshaping are the consequence of the high shear experienced by the granules, it was highlighted that most of the mechanical energy is converted into thermal energy with no correlation between friction forces and granule size distribution. Combined mass and energy balance of the granulation process are therefore necessary to capture the interaction between granule properties and physico-chemical and mechanical phenomena occurring in each compartment.

In twin-screw wet granulation, wetting is physically separated from granule consolidation, growth, breakage and attrition. Hence, the study in **chapter 4** used this particularity to investigate the wetting step in such a way that the fundamental mechanisms governing the wetting can be understood. Granules obtained after the wetting zone were analysed for granule size distribution, API distribution over the different size fractions and granule temperature. It was found that “wetting efficiency” (i.e., fraction of powder being nucleated

during the wetting stage) could be predicted using an energy balance based on in-line measurement of the granule temperature. Wetting efficiency could moreover be linked to final granule size distribution at the outlet of the granulator. It was demonstrated that granule growth and consolidation could only be achieved when complete wetting was achieved in the wetting zone of the granulator. This study suggested a methodology based on in-line temperature measurements to quickly determine wetting efficiency. The described methodology could therefore be used as a tool to gain more fundamental understanding of the wetting stage during twin-screw granulation as well as to define suitable formulation and process ranges for further granulation process development.

The potential of torque as an in-process control to monitor the granule size in twin-screw wet granulation was investigated in **chapter 5**. An experimental set-up allowing the collection of granules at four different locations (i.e., in the wetting zone, after the first and second kneading zone and at the end of the granulation barrel) of the granulator screws was used to determine the change in granule size along the length of the barrel and the contribution of each compartment to the overall torque. A D-optimal Design of Experiments was performed to evaluate the influence of screw speed, mass feed rate and liquid-to-solid ratio upon those responses. Herewith, the correlation between granule size change (expressed as the fine fraction  $< 150 \mu\text{m}$  and the oversized fraction  $> 2000 \mu\text{m}$ ) and the increase in torque was investigated at each location. No correlation was observed between changes in the granule size and torque in the wetting zone, after the second kneading zone and at the end of the granulator. The only observed correlation was between the granule size and torque increase after the first kneading zone because the torque increase was an indication of the degree in granule growth which was consistently observed with all applied granulation process parameters. Moreover, a higher torque increase in these locations was correlated to a higher granule temperature, suggesting that the energy put into the granulator by the applied process settings was partly used to heat up the material being processed. The study showed that torque could not be used as an IPC to monitor and control the wet granule size in a TSG process.

In **chapter 6**, a TPLS model was developed to link raw material properties, the ratios in which these raw materials were combined and the applied process parameters for the twin-screw wet granulation process with the granule quality attributes. A raw material property database

including dry (size, flow, etc.) and wet (solubility, contact angle, etc.) properties was first established for Active Pharmaceutical Ingredients (APIs) and excipients. Hereafter 10 different formulations consisting of an API, a filler and a binder were selected and the API content was varied at three levels (10, 40 and 70 %) for each formulation. A total of 30 powder mixtures were subsequently granulated under different twin-screw granulation process parameters. Finally, granule quality attributes (i.e., friability, fines and oversized size fraction and angle of repose) were determined for all granules after oven-drying. TPLS highlighted L/S ratio as the most influencing process setting and dissolution rate, solubility, compressibility, density and water binding capacity as the most influencing raw material properties upon granule quality. In addition, the predictive ability of the TPLS model was used to find a suitable formulation composition and combination of twin-screw granulation process settings for a new API leading to desired granule quality attributes. In a next step, these predicted granule quality attributes were compared to the experimental values. Although the predictions were not optimal for the entire examined twin-screw granulation process parameter space, it was possible to predict a suitable combination of process settings and formulation properties for the new API resulting in the desired granule quality attributes. As TPLS is a self-learning, data-driven platform, the inclusion of more data would improve the predictive ability. Overall, this study helped to better understand the link between raw material properties, formulation composition and process settings on granule quality attributes. In addition, as TPLS can provide a reasonable starting point for formulation and process development for new APIs, it can reduce the experimental development efforts and consequently the consumption of expensive (and often limited available) new API.

The major goal of **chapter 7** was to investigate the breakage and attrition phenomena during transport of wet and dry granules (i.e., before and after semi-continuous drying), during filling of a drying cell and during fluid bed drying on a ConsiGma™-25 system (C25). Therefore, the granule size distribution (GSD) was determined at 8 different locations of the continuous manufacturing line. Pneumatic transport of the wet granules after twin-screw granulation towards the semi-continuous dryer via the wet transfer line induced extensive breakage. Hereafter, the turbulent filling phase of the fluid bed drying cells caused further moderate breakage and attrition, while additional breakage during drying was limited. Subsequently, the dry transfer line connecting the semi-continuous dryer with the conditioning unit, was

responsible for additional extensive breakage and attrition. Additionally, the influence of drying air temperature and drying time was assessed. For this purpose, granule size and residual moisture content per size fraction were characterised for granules processed with a commercial-scale ConsiGma™-25 system as well as those produced with the R&D-scale ConsiGma™-1 (C1) system. A higher drying rate was observed for granules dried with the C25 system in comparison to granules dried with the C1 system, presumably because of heat being transferred by convection and conduction from the surrounding empty cells. Furthermore, for C25, the final GSD was governed by the moisture content of the granules. Both, higher (> 3%) and very low moisture content (< 1%) resulted in more breakage and attrition in the dry transfer line. As the final GSD after drying for granules processed with C1 differed significantly from those processed on C25, it is challenging during process and formulation development to produce granules with the C1 that results in a representative GSD for the C25 process.

Cell-to-cell variability was investigated for the drying unit of the ConsiGma™-25 in **chapter 8**. Six experiments were performed by varying drying time and drying temperature. For each experiment, the granule size, residual moisture content for different size fractions and overall moisture content was measured for granules collected at the six different cells. No significant difference in granule quality was observed for the different cells, indicating that the no cell-to-cell variability was observed. However, the drying air temperature for the cells which are positioned further from the inlet air was found to be slightly lower. It was concluded that a cell-to-cell variability exists due to the design of the dryer, but that it does not affect the granule quality when the air flow sufficient, the drying temperature was high enough and the drying time was long enough. Hence, to fully understand the cell-to-cell variability, only experiments should be selected which resulted in an insufficient drying performance (i.e., moisture content larger than 3 %).

In **chapter 9**, in-line NIR measurements were obtained from a NIR spectrometer mounted in the filling chamber of the feed frame, in close proximity to the die filling station. The blend homogeneity was evaluated by a quantitative Partial Least Squares (PLS) regression model and a qualitative moving F-test. First, 15 batches of granules, varying in API concentration at 5 levels (i.e., 90, 95, 100, 105, 110 % relative to target) and varying in applied liquid-to-solid (L/S) ratio at 3 levels (i.e., 25, 28, 31 %) during twin-screw wet granulation were produced on a ConsiGma™-1 system. After drying and milling, the granules were tableted for 15 minutes on

a Modul<sup>™</sup> P tablet press, where in-line NIR measurements in the feed frame were acquired. The complete dataset was used to develop the PLS model, whereas only the experiments corresponding with an API content of 90, 100 and 110 % were used to determine the minimum block size to comply with the F-test  $\alpha$  and  $\beta$ -error and to find appropriate spectral regions to develop a sensitive F-test. Three different case studies were then performed to evaluate both techniques. It was seen that the moving F-test could detect inhomogeneity of the blend due to changes in API concentration. However, the API content might be off-target while a homogeneous powder bed was monitored. In contrast, via the traditional PLS regression calibration method the API content was continuously monitored as every second the API content was predicted by the PLS model.



# **Samenvatting**

Vaste farmaceutische doseervormen werden decennialang geproduceerd via batchprocessen. Deze batchgewijze productie wordt echter gecombineerd met *offline* kwaliteitstesten die tijdrovend, destructief en arbeidsintensief zijn. Verder is de batchgewijze productie gelinkt met een variërende productkwaliteit, hoge productiekosten en tal van andere problemen. Daarom is de interesse in de transitie van een batchgewijze naar een continue productie van vaste farmaceutische doseervormen gestegen. Een grondige kennis en begrip van het continue productieproces is echter nodig om ten volle van de voordelen van continue productie te kunnen profiteren. De voordelen, de uitdagingen en de redenen van de transitie naar een continue productie in de farmaceutische industrie, alsook de verschillende continue productietechnieken werden in detail besproken in **hoofdstuk 1**. De objectieven van dit proefschrift werden beschreven in **hoofdstuk 2**.

In **hoofdstuk 3** liet het gebruik van een compartimentele opstelling toe om de evolutie van de kwaliteitseigenschappen van de granulen en warmte-uitwisselingen over de lengte van de granulator te bestuderen. De granulegrootte, de mechanische energie, de temperatuur van het omhulsel van de granulator en temperatuur van de granulen (door gebruik te maken van een warmtebeeldsysteem) werden ook gemeten op de verschillende locaties over de lengte van de granulator om de warmte-uitwisselingen op de verschillende locaties te kunnen evalueren en om deze te linken aan het mechanisme van het granulatieproces. De verkregen resultaten toonden aan dat de bevochtigingsenthalpie en de wrijvingskrachten de grootste oorzaken waren van de warmte-uitwisseling. De bevochtiging van het poederbed gebeurde in de bevochtigingszone en dit veroorzaakte een temperatuurstijging van het bevochtigde materiaal dat afhing van de hoeveelheid vloeistof en de bevochtigbaarheid van het poeder. De temperatuurstijging in de kneedzones was in verhouding met de desbetreffende wrijvingskrachten. Terwijl er normaliter werd aangenomen dat de consolidatie en vervorming van de granulen de gevolgen waren van de hoge schuifspanning in de kneedzones, werd er aangetoond dat de meeste wrijvingskrachten werden omgezet in warmte waardoor er geen correlatie werd gezien tussen wrijvingskrachten en de granulegroottedistributie (GSD). Een gecombineerde massa- en energiebalans van het granulatieproces is daarom nodig om de interactie tussen de lokale granule-eigenschappen, de fysicochemische en mechanische fenomenen te onderzoeken op iedere locatie.

De bevochtiging van het poeder is tijdens dubbelschroef vochtige granulatie fysiek afgezonderd van de consolidatie, de groei, het afbreken en de attritie van granulen. Dit bijzonder gegeven werd in **hoofdstuk 4** gebruikt om de bevochtigingsstap te onderzoeken opdat het fundamenteel mechanisme van de bevochtigingsstap beter begrepen kon worden. De granulen werden gecollecteerd na de bevochtigingszone zodat de grootte van de granulen, de verdeling van het *Actief Farmaceutisch Ingrediënt* (API) in de verschillende groottefracties en de temperatuur van de granulen bepaald konden worden. Er werd gevonden dat de “bevochtigingsefficiëntie” (zijnde de poederfractie die na de bevochtigingsfase tot een vochtige kern behoort) voorspeld kon worden door middel van een energiebalans die tot stand komt door de *in-line* meting van de temperatuur van de granulen. De bevochtigingsefficiëntie kon verder gelinkt worden met de finale grootteverdeling van de granulen aan de uitgang van de granulator. Er werd aangetoond dat de groei en consolidatie van de granulen enkel bereikt kon worden wanneer er een volledige bevochtiging werd bereikt in de bevochtigingszone van de granulator. Deze studie stelde een methode voor om snel de bevochtigingsefficiëntie te bepalen op basis van een *in-line* temperatuurmeting van de granulen. Deze methode kon daarom gebruikt worden om de bevochtigingsfase tijdens dubbelschroef vochtige granulatie fundamenteel beter te begrijpen. Daarenboven kan het ook helpen om een geschikte formulatie en geschikte procescondities te bepalen tijdens de procesontwikkeling.

De mogelijkheid van torque als in-proces control (IPC) om de granulegrootte te monitoren tijdens dubbelschroef vochtige granulatie werd onderzocht in **hoofdstuk 5**. Een experimentele opstelling die het mogelijk maakte om de granulen op vier verschillende locaties (met name in de bevochtigingszone, na de eerste en tweede kneedzone en op het einde van de granulator) van de granulatieschroeven te verzamelen, werd gebruikt om de verandering in granulegrootte over de lengte van de granulator en de bijdrage van elk compartiment aan de totale hoeveelheid torque te bepalen. Er werd een D-optimal Design of Experiments (DoE) uitgevoerd om de invloed van de schroefsnelheid, de massa-toevoersnelheid en de vloeistof-tot-vaste-stof-verhouding (L/S ratio) te evalueren. Hiermee werd de correlatie tussen de verandering in granulegrootte (uitgedrukt als de fijne fractie < 150  $\mu\text{m}$  en de grove fractie > 2000  $\mu\text{m}$ ) en de toename in torque op elke locatie onderzocht. Er werd geen correlatie waargenomen tussen de verandering in granulegrootte en torque in de bevochtigingszone, na de tweede kneedzone en aan het einde van de granulator. Er werd enkel een correlatie

waargenomen tussen de granulegrootte en de toename in torque na de eerste kneedzone, omdat de toename in torque een indicatie was van de granulegroei. Deze groei werd consistent waargenomen bij alle toegepaste parameters van het granulatieproces. Bovendien werd een hogere toename in torque op deze locaties gecorreleerd met een hogere temperatuur van de granulen, wat suggereert dat de energie die in de granulator werd gebracht door de toegepaste procesinstellingen, gedeeltelijk werd gebruikt om het te verwerken materiaal op te warmen. De studie toonde aan dat torque niet kan worden gebruikt als IPC om de natte granulegrootte in een dubbelschroef vochtige granulatie proces te monitoren en te controleren.

In **hoofdstuk 6** werd een TPLS-model ontwikkeld om de eigenschappen van de grondstoffen, de verhoudingen waarin deze grondstoffen werden gecombineerd en de toegepaste procesparameters bij dubbelschroef vochtige granulatie te linken aan kwaliteitseigenschappen van de granulen. Er werd eerst een databank tot stand gebracht met zowel droge (partikelgrootte, vloeieigenschappen, enz.) als natte (oplosbaarheid, contacthoek, enz.) eigenschappen van de APIs en excipiënten. Hierna werden 10 verschillende formulaties bestaande uit een API, een vulmiddel en een bindmiddel geselecteerd en werd het API-gehalte vervolgens nog voor elke formulatie gevarieerd op drie niveaus (10, 40 en 70 %). Een totaal van 30 poedermengsels werd gegranuleerd met verschillende dubbelschroef vochtige granulatieparameters. Ten slotte werden de kwaliteitskenmerken van de granulen (met name de broosheid, de fractie fijne partikels en te grove deeltjes en de rusthoek) bepaald voor alle granulen na drogen in de oven. TPLS maakte het mogelijk om enerzijds de meest invloedrijke procesparameter op de kwaliteit van de granulen te benadrukken, namelijk de L/S-ratio. En anderzijds was het ook mogelijk om de meest invloedrijke grondstofeigenschappen op de kwaliteit van de granulen aan te duiden, zijnde oplossnelheid, oplosbaarheid, samendrukbaarheid, dichtheid en het waterbindend vermogen. Bovendien werd het voorspellend vermogen van het TPLS-model gebruikt om een geschikte formulatiesamenstelling en bijhorende procesparameters voor het dubbelschroef vochtige granulatieproces te vinden voor een nieuwe API die resulteren in de gewenste granulekwaliteit. In een volgende stap werden deze voorspelde kwaliteitseigenschappen van de granulen vergeleken met de experimenteel bepaalde waarden. Hoewel de voorspellingen niet optimaal waren voor het gehele bereik van de onderzochte procesparameters van het

granulatieproces, was het mogelijk om een geschikte combinatie van procesinstellingen en formulatie-eigenschappen voor het nieuwe API te voorspellen die resulteerden in de gewenste granulekwaliteit. Aangezien TPLS een zelflerend, data-gedreven platform is, zou het includeren van meer data het voorspellend vermogen verbeteren. In het algemeen heeft deze studie geholpen om het verband tussen de grondstofeigenschappen, de formulatiesamenstelling en de procesparameters op de granulekwaliteit beter te begrijpen. Aangezien TPLS bovendien een aanvaardbaar vertrekpunt kan bieden tijdens formulatie- en procesontwikkeling voor nieuwe APIs, kan het de experimentele inspanningen tijdens de ontwikkeling en bijgevolg het verbruik van dure (en vaak beperkt beschikbare) nieuwe APIs verminderen.

Het voornaamste doel van **hoofdstuk 7** was om het breek- en attritiegedrag tijdens transport van de natte en droge granulen (zijnde voor en na het semi-continu droogproces), tijdens het vullen van een droogcel en tijdens het wervelbeddrogen van het ConsiGma™-25 (C25) systeem te onderzoeken. Daarom werd de GSD op 8 verschillende plaatsen van de continue productielijn bepaald. Het pneumatisch transport, die de natte granulen na dubbelschroef vochtige granulatie richting de semi-continue droger brengen door middel van de natte transferlijn, veroorzaakte veel afbraak. De turbulente vulfase van de droogcel zorgde verder voor een geringe afbraak en attritie van de granulen, terwijl verdere afbraak en attritie minimaal was tijdens het droogproces op zich. De droge transferlijn, die de semi-continue droger verbindt met de conditioneereenheid, was verantwoordelijk voor een bijkomende en intensieve afbraak en attritie. Daarenboven werd de invloed van de droogtemperatuur en droogtijd onderzocht. Daarvoor werd de grootte van de granulen en het residueel vochtgehalte per groottefractie bepaald voor granulen vervaardigd met het commerciële ConsiGma™-25 (C25) systeem en het R&D-systeem: ConsiGma™-1 (C1). Een hogere droogsnelheid werd waargenomen voor granulen die gedroogd werden met het C25 systeem in vergelijking met de granulen die gedroogd werden met het C1 systeem. Waarschijnlijk werd er warmte van de omliggende, lege cellen getransfereerd via convectie en conductie naar de actieve droogcel bij het C25 systeem. Verder werd de finale GSD met het C25 systeem bepaald door het vochtgehalte in de granulen. Zowel een hoog (> 3 %) als een zeer laag vochtgehalte (< 1 %) resulteerde in meer afbraak en attritie in de droge transferlijn. Aangezien de finale GSD voor de granulen gedroogd met de C1 significant verschilde van deze verwerkt met de C25, is

het een uitdaging om met behulp van het C1 systeem tijdens de ontwikkeling van het proces en de formulatie granulen te bekomen die een GSD hebben die representatief zijn voor de C25.

De cel-tot-cel variabiliteit werd in **hoofdstuk 8** onderzocht voor de droogeenheid van de ConsiGma™-25. Zes experimenten werden uitgevoerd door de droogtijd en droogtemperatuur te laten variëren. Voor elk experiment werd de granulegrootte, het residueel vochtgehalte in verschillende groottefracties en het algemene vochtgehalte gemeten voor de granulen die gecollecteerd werden uit de zes verschillende cellen. Er werd geen significant verschil in kwaliteit waargenomen tussen de granulen uit verschillende cellen, wat aangeeft dat er geen cel-tot-cel-variabiliteit werd waargenomen. De temperatuur van de drooglucht in de cellen die verder van de inkomende lucht zijn gepositioneerd bleek echter iets lager te zijn. Dit geeft aan dat er een cel-tot-cel variabiliteit bestaat door het ontwerp van de droger, maar dat dit geen invloed heeft op de kwaliteit van de granulen indien de luchtstroom voldoende was, de droogtemperatuur hoog genoeg was en de droogtijd lang genoeg was. Daarom moet er om de cel-tot-cel-variabiliteit volledig te begrijpen, uitsluitend experimenten worden geselecteerd die resulteerden in een droogproces dat onvoldoende droogde (zijnde in granulen met in een vochtgehalte van meer dan 3 %).

In **hoofdstuk 9** werden *in-line* nabij infrarood (NIR) metingen uitgevoerd met een NIR-spectrometer die in de vulkamer, in nabijheid van het vulstation van de matrijs, was geïnstalleerd. De homogeniteit van het poedermengsel werd geëvalueerd door een kwantitatief *Partial Least Squares* (PLS) regressiemodel en een kwalitatieve *moving* F-test. Eerst werden 15 verschillende batches van granulen, variërend in API-concentratie op 5 niveaus (met name 90, 95, 100, 105 en 110 % relatief ten opzichte van de streefwaarde) en variërend in toegepaste L/S ratio op 3 niveaus (met name 25, 28 en 31 %) tijdens dubbelschroef vochtige granulatie geproduceerd op een ConsiGma™ -1 systeem. Na drogen en malen werden de granulen 15 minuten getabletteerd op een Modul™ P-tabletters, waar *in-line* NIR-metingen in het voedingssysteem werden verkregen. De volledige dataset werd gebruikt om het PLS-model te ontwikkelen, terwijl alleen de experimenten die overeenkomen met een API-gehalte van 90, 100 en 110 % werden gebruikt om de minimale blok grootte te bepalen om te voldoen aan de  $\alpha$ - en  $\beta$ -fout van de F-test, en om geschikte spectrale gebieden te vinden zodat een gevoelige F-test kon ontwikkeld worden. Vervolgens werden drie

verschillende casestudies uitgevoerd om beide technieken te evalueren. Er werd gezien dat de *moving* F-test inhomogeniteit van het mengsel kon detecteren als gevolg van veranderingen in de API-concentratie. Het API-gehalte kon echter afwijken terwijl een homogeen poederbed wordt bewaakt. Daarentegen werd via de traditionele PLS-regressie kalibratiemethode het API-gehalte continu gemonitord aangezien elke seconde het API-gehalte werd voorspeld door het PLS-model.

# Acknowledgement

The authors would like to acknowledge Bayer AG for funding this dissertation.



# Curriculum vitae

## PERSONAL INFORMATION

Surname: Ryckaert

First names: Alexander Jean Christine

Date of birth: June 8<sup>th</sup> , 1991

Place of birth: Ghent

Nationality: Belgian

E-mail: AlexanderJ.Ryckaert@ugent.be, Alexander.Ryckaert@gmail.com

## EDUCATION

2016 – present: PhD in Pharmaceutical Sciences, Laboratory of Pharmaceutical Process Analytical Technology, Ghent University, Belgium

2014 – 2015: Master of Science in Industrial Pharmacy, Ghent University, Belgium

2012 – 2014: Master of Science in Drug Development, Ghent University, Belgium

2009 – 2012: Bachelor of Science in Pharmaceutical Sciences, Ghent University, Belgium

2003 – 2009: Degree Sciences – Mathematics, Koninklijk Atheneum, Mariakerke, Belgium

## LANGUAGE SKILLS

Native language: Dutch

Other languages: English, French

## RESEARCH EXPERIENCE

2016 – present: PhD research: “Towards an enhanced process understanding for a continuous pharmaceutical manufacturing process of tablets based on twin-screw wet granulation”  
Promoter: Prof. Thomas De Beer  
Laboratory of Pharmaceutical Process Analytical Technology, Ghent University, Belgium

September 2015 – Trainee Industrial Pharmacist  
February 2016: Department of Process Science and Technical Operations  
Baxalta, Lessines, Belgium

September – Master thesis: “Unraveling nanotoxicity: the influence of quantum dot  
December 2014: coating on autophagy”  
Promoter: Prof. S. De Smedt  
Laboratory of general biochemistry and physical pharmacy, Ghent University, Belgium

February – June Master thesis: “Synthesis and characterization of polypeptide-based  
2013: architectures”  
Promoter: J. Demeester  
Centro de Investigación Príncipe Felipe, Valencia, Spain / Laboratory of general biochemistry and physical pharmacy, Ghent University, Belgium

## PUBLICATIONS IN PEER REVIEWED JOURNALS

Stauffer F.\*, Ryckaert A.\*, Van Hauwermeiren D., Funke A., Djuric D., Nopens I., De Beer T., Heat Transfer Evaluation During Twin-Screw Wet Granulation in View of Detailed Process Understanding, AAPS PharmSciTech, 2019;20(7):1–13.

F. Stauffer\*, A. Ryckaert\*, V. Vanhoorne, D. Van Hauwermeiren, A. Funke, D. Djuric, C. Vervaet, I. Nopens, T. De Beer, In-line temperature measurement to improve the understanding of the wetting phase in twin-screw wet granulation and its use in process development, International Journal of Pharmaceutics, Volume 584, 2020, 119451.

N. Bostijn, J. Dhondt, **A. Ryckaert**, E. Szabó, W. Dhondt, B. Van Snick, V. Vanhoorne, C. Vervaet, T. De Beer., A multivariate approach to predict the volumetric and gravimetric feeding behavior of a low feed rate feeder based on raw material properties, *International Journal of Pharmaceutics*, 557 (2019) 342-353.

To be published:

**A. Ryckaert\***, **F. Stauffer\***, V. Vanhoorne, A. Funke, D. Djuric, C. Vervaet, T. De Beer., Evaluation of torque as an in-process control for granule size during twin-screw wet granulation.

**A. Ryckaert\***, **D. Van Hauwermeiren\***, J. Dhondt, A. De Man, A. Funke, D. Djuric, C. Vervaet, T. De Beer., TPLS as predictive platform for twin-screw granulation process and formulation development.

**A. Ryckaert**, M. Ghijs, C. Portier, A. Funke, D. Djuric, C. Vervaet, T. De Beer., The influence of equipment design and process parameters on granule breakage in a semi-continuous fluid bed dryer after continuous twin-screw granulation.

**A. Ryckaert**, M. Ghijs, A. Funke, D. Djuric, C. Vervaet, T. De Beer., Comparison a Partial Least Squares (PLS) model with a moving F-test to monitor blend uniformity in a tablet press.

## PRESENTATIONS AT CONFERENCES

### *Oral presentations*

- The Use of T-PLS to investigate the impact of raw material properties on granule quality attributes obtained after continuous twin-screw wet granulation  
**A. Ryckaert**, D. Van Hauwermeiren, A. Funke, D. Djuric, C. Vervaet, T. De Beer  
*2019 AIChE Annual Meeting, Orlando, Florida, USA, 10 November – 15 November 2019.*
- The use of TPLS for continuous twin-screw wet granulation  
**A. Ryckaert**, D. Van Hauwermeiren, A. Funke, D. Djuric, C. Vervaet, T. De Beer  
*13<sup>th</sup> PSSRC annual symposium, Dusseldorf, Germany, 12 – 13 September 2019.*
- Investigating wetting behaviour during twin-screw wet granulation  
**A. Ryckaert**, F. Stauffer, A. Funke, D. Djuric, C. Vervaet, T. De Beer  
*20th Forum of Pharmaceutical Sciences, Brussels, Belgium, May 20th 2019.*

- Investigating wetting behaviour during twin-screw wet granulation  
**A. Ryckaert**, F. Stauffer, A. Funke, D. Djuric, C. Vervaet, T. De Beer  
*12<sup>th</sup> PSSRC annual symposium, Leuven, Belgium, 18 – 19 September 2018.*

*Poster presentations*

- The use of TPLS for continuous twin-screw wet granulation  
**A. Ryckaert**, D. Van Hauwermeiren, A. Funke, D. Djuric, C. Vervaet, T. De Beer  
*2<sup>nd</sup> APV Continuous Manufacturing conference, Freiburg, Germany, 18 – 19 February 2020.*
- **Visualisation of the wetting phase during twin-screw granulation via thermal imaging for improved process understanding and process development**  
**A. Ryckaert**, F. Stauffer, A. Funke, D. Djuric, C. Vervaet, T. De Beer  
*1<sup>st</sup> APV Continuous Manufacturing conference, Antwerp, Belgium, 19 – 20 February 2019.*
- **Evaluation of torque as an in-process control for granule size during twin-screw wet granulation**  
**A. Ryckaert**, F. Stauffer, A. Funke, D. Djuric, C. Vervaet, T. De Beer  
*11<sup>th</sup> World Meeting on Pharmaceutics, Biopharmaceutics and Pharmaceutical Technology, Granada, Spain, 19 – 22 March 2018.*

**ATTENDED COURSES, CONFERENCES AND WORKSHOPS**

- 8th International Granulation Workshop, Sheffield, United Kingdom, June 28-30, 2017.
- The next generation pharma skills you will need in view of continuous manufacturing, Ghent University, Ghent, Belgium, 11 – 13 October 2017.
- Advanced Chemometric Course Dr. Salvador Garcia Munoz, Ghent, June 2019.
- Doctoral School on Advanced Academic English Writing skills Life Sciences and Medicine, Ghent 2018.
- Training on Multivariate Data Analysis & Design of Experiments Prof. Dr. Thomas De Beer, Ghent, Belgium, January 2016.
- Getting Started with High-Performance Computing (Phyton course), 27 – 29 May 2019.

- Dynamic vapour sorption and inversed gas chromatography Training Course (SMS), Leuven, Belgium, September 2017.
- Introduction to Matlab & hyperspectral imaging (Prof. Dr. José Amigo – University of Copenhagen), Ghent, Belgium, 14 – 20 January 2019.
- Operator Training, GEA Tableting Technology Center, Halle, Belgium, 12 – 14 March, 2019.